Contents

International Commission for Optics (ICO)

The International Commission for Optics (ICO) is a Category 1 Full Member of the International Science Council (ISC). With sixty members, which are 53 Territorial Committees (13 Associate Members) and 7 International Organizations, the ICO mission is to promote optics and photonics worldwide, with an especial emphasis in developing countries. It was created in 1947 as an Affiliated Commission of the International Union of Pure and Applied Physics (IUPAP). The first official meeting of ICO took place 12-17 July 1948. The ICO Bureau consists of the President, the Past-President, the Secretary General and the Associate Secretary, the Treasurer, and fifteen Vice-Presidents, (eight elected) of whom at least two are from industry. The bureau meets in person every year to discuss and make proposals to the General Assembly, which is the governing body of the organization and gathers every three years during the ICO worldwide congress.

The ICO Executive Committee (EXECOM) is in charge of day by day organisation between the meetings of the ICO Bureau. It is made up of the following members of the ICO Bureau: the President, the Past-President, The Secretary General, the Treasurer and the Associate Secretary.

ICO Executives

President: Prof John C Howell (Chapman College, USA)
Past President: Prof Roberta Ramponi (Politecnico di Milano, Italy)
Secretary General: Prof Humberto Michinel (Universidade de Vigo, Spain)
Treasurer: Prof Joseph Niemela (Abdus Salam ICTP, Italy)
Associate Secretary: Prof Adrian Podoleanu (University of Kent, UK)

Vice Presidents, Elected

Prof Jürgen Czarske (Technische Universität Dresden, Germany)
Prof Pietro Ferraro (CNR-ISASI, Italy)
Prof Qihaung Gong (Peking University, China)
Prof Natalya Kunikova(South Ural State University, Russia)
Prof Kaouru Minoshima (University of Electro-Communications, Japan)
Prof Sara Otero (Radiantis, Spain)
Prof Leszek Sirko (Polish Academy of Sciences, Poland)
Prof Nathalie Westbrrok (Institute d'Optique, France)

Vice Presidents, Appointed

Prof Gert von Bally (International Society OWLS)
Prof Kent D Choquette (IEEE Photonics Society)
Dr Yaseera Ismail (OPTICA)
Prof Carmiña Londoño (SPIE)
Prof Gilles Paulliat (EOS)
Prof Eric Rosas (RIAO)
Prof Ahmadou Wagué (LAM Network)
Prof Carmen Cisneros (IUPAP Delegate)

Optics and Photonics in Africa (OPA)

The International Commission for Optics (ICO), Optics and Photonics in Africa Conference (`www.opa2023.com`), which brings together the international scientific community in an inspiring location to share the latest advances in the field of optics and photonics and establish new international collaborations. The target audience is emerging and established researchers on the African Continent and internationally. Apart from South Africa, there is a strong focus of the participation of students originating from Ghana, Kenya, Morocco, Senegal, Cameroon, Nigeria, Egypt and Tunisia.

OPA2023 focuses on presenting the latest research and findings related to various fields, including Applied Optics and Photonics, Biomedical optics, Fiber & Integrated Photonics, Green Photonics, Lasers & Light Sources, LIDAR and Photogrammetry, Light-matter Interaction, Nanophotonics, Nonlinear & Quantum Optics, Optical Instrumentation, Optical Metrology, Optical Materials, Photovoltaic Systems, Photonics for Aerospace and Spectroscopy. The aim of the conference is to foster networks and encourage meaningful impact in the lives of researchers working in optics and photonics.

Local Organising Committee

Dr. Yaseera Ismail (Chair & OPTICA Vice President on the ICO and School of Chemistry and Physics, University of KwaZulu-Natal)
Dr. Patience Mthunzi Kufa (NLC-CSIR) (Co-Chair)
Dr. Christine Steenkamp (Physics, Stellenbosch University)
Dr. Angela Dudley (University of Witwatersrand)
Prof. Heidi Abrahamse (Laser Centre, University of Johannesburg)
Prof. Mathew Moodley (School of Chemistry and Physics, University of KwaZulu-Natal)
Prof. Francesco Petruccione (NITHECS & Stellenbosch University)
Prof. Malik Maaza (UNISA & iThemba LABS/NRF)

Advisory Committee

J C Howell (Chapman College, USA)
H Michinel (Universidade de Vigo, Spain)
R Ramponi (Politécnico di Milano, Italy)
J Niemela (ICTP, Italy)
A Podoleanu (University of Kent, UK)
J Czarske (TU Dresden, Germany)
P Ferraro (CNR, Italy)
Q Gong (Peking University, China)
N Kundikova (South Ural St. University, Russia)
K Minoshima (Univ. Electrocommunications, Japan)
S Otero (Radiantis, Spain)
L Sirko (Polish Academy of Sciences, Poland)
N Westbrook (Institute d'Optique, France)

International Representative

G von Bally (Optics Within Life Sciences)
K D Choquette (IEEE Photonics)
C Londoño (SPIE)
G Pauliat (European Optical Society)
E Rosas (Iberoamerican Optics Network- RIAO)
A Wagué (African Laser Network – LAM)
C Cisneros (IUPAP)

Program

PL: Plenary Lecture (45 minutes), IT: Invited Talk (25 minutes), CT: Contributed Talk (20 minutes) and ST: Student Talk (15 minutes).

Monday, 6 November 2023

7:30–9:00		Conference Registration (Venue: Imvubu)	
9:00–9:10		Welcome remarks: OPA Chair: Dr Yaseera Ismail (Venue: Imvubu)	
9:10–10:40		Plenary Session - Chair: Prof John Howell	
9:10–9:55	PL	**Prof Michal Lipson** Columbia University, USA	The Revolution of Silicon Photonics
9:55–10:40	PL	**Prof Sonja Franke-Arnold** Glasgow University, UK	Polarization textures of light - Spin textures of atoms
10:40–11:00		Coffee	
11:00–12:45		Session 1: Nonlinear and Quantum Optics	
		Venue: Imvubu and Chair: Dr Yaseera Ismail	
11:00-11:25	IT	**Prof Roberta Ramponi** Politecnico di Milano and IFN-CNR, Italy	Laser and Ion Beam Writing for Quantum Photonic Devices in Diamond
11:25–11:50	IT	**Dr Christine Steenkamp** Stellenbosch University, South Africa	Trapping ytterbium isotopes for unsharp quantum measurements
11:50–12:10	CT	**Prof Ilya Sinayskiy** University of KwaZulu-Natal, South Africa	Open Quantum Walks and Open Quantum Brownian Motions
12:10–12:30	CT	**Dr Chané Moodley** QLab, Raphta	Quantum ghost imaging: Back to basics
12:30–12:45	ST	**Neelan Gounden** University of Witwatersrand, South Africa	Twisting the uncertainty principle
11:00–12:45		Session 2: Lasers, Imaging and Spectroscopy	
		Venue: Ibubezi and Chair: Prof Maalik Maaza	
11:00-11:25	IT	**Dr Pieter Neetling** University of Stellenbosch, South Africa	Time-domain ptychography: Principles and application
11:25–11:45	CT	**Prof Luis Plaja** Universidad de Salamanca,Spain	Topological high-harmonic spectroscopy: observing matter response from the topology of the harmonic field.
11:45–12:05	CT	**Prof Edwin Fohtung** Rensselaer Polytechnic Institute, USA	Coherent diffraction imaging with structured x-ray photons

12:05–12:20	ST	**Eugene Egbert Fouche** Stellenbosch University, South Africa	Polarization-Sensitive Fourier Ptychographic Microscopy for Large Area, High-Resolution Birefringence Imaging
12:20–12:45	IT	**Prof Tjaart Krüger** University of Pretoria,South Africa	Real-time feedback-driven single-particle tracking
12:45–14:00		**Lunch - Ingwenyama Resort Restaurant**	
14:00–15:30		**Plenary Session - Chair: Prof Humberto Michinel (Venue: Imvubu)**	
14:00–14:45	PL	**Prof Carlos Hernández García** Universidad de Salamanca, Spain	Short Wavelength Structured Light for Attosecond Science
14:45–15:30	PL	**Prof Kaouru Minoshima** University of Electro-Communications, Japan	Versatile control of optical waves with optical frequency combs enables broad applications
15:30–16:00		**Coffee**	
15:45–17:15		**Poster session**	
17:30–18:00		**Cocktail Welcome Social**	
18:00–22:00		**Ice Breaker-Food Truck Dinner**	

Tuesday, 7 November 2023

Time	Type	Speaker	Title
9:00–10:30		**Plenary Session - Chair: Prof Kaouru Minoshima (Venue: Imvubu)**	
9:00–9:45	PL	**Prof Alexander Gaeta** Columbia University, USA	Non-linear Optics for all
9:45–10:30	PL	**Prof Maalik Maaza** iThemba LABS, South Africa	On the trapping of cold neutrons in nano-scaled Fabry-Perot resonating cavities and neutron lifetime considerations
10:30–11:00		**Coffee**	
11:00–12:45		**Session 3: Nanophotonics**	
		Venue: Imvubu and Chair: Prof Mathew Moodley	
11:00–11:25	IT	**Prof Yidong Huang** Tsinghua University, China	Future Perception Technology based on Nano-optoelectronics
11:25–11:50	IT	**Dr Oliver Jermaine Myers** Clemson University, USA	Functionalizing Bistable/Multi-stable CFRP Laminate Structures
11:50–12:10	CT	**Dr Mahmood Akbari** University of South Africa, South Africa	Optical properties of rare earth metal, Tb, dopped in cubic ceria nanoparticles
12:10–12:30	CT	**Prof Wenjing Liu** Peking University	Magnetically dressed CrSBr exciton-polariton in ultrastrong coupling regime
12:30–12:45	ST	**Shiva Shafiei Khosroshahi** University of South Africa, South Africa	Optical properties of nano-scaled silver iodide by pulsed laser ablation in liquid for cloud seeding
11:00–12:45		**Session 4: Biophotonics and Biomedical Opitcs**	
		Venue: Ibubezi and Chair: Prof Heidi Abrahamse	
11:00-11:25	IT	**Dr Patience Mthunzi-Kufa** CSIR, South Africa	Biophotonics and artificial intelligence for improved Diagnostics: Applications in Health, Pharmaceutical's and Agriculture
11:25–11:50	IT	**Prof Nathalie Westbrook** Universite Paris-Saclay	Biomechanics using optical tweezers
11:50-12:10	CT	**Dr Kelvin Mpofu** CSIR, South Africa	Quantum enhancement in the limit of detection measurement of a phase-based plasmonic biosensor with loss
12:10-12:30	CT	**Prof Blassan George** University of Johannesburg, South Africa	Phytochemicals and medicinal plants in photodynamic therapy of cancer
12:30–12:45	ST	**Daniella Da Silva** University of Johannesburg, South Africa	The Dose–Response Relationship of Photobiomodulation Therapy on Adipose-derived Stem Cells into Osteoblast-like Cells
12:45–14:00		**Lunch - Ingwenyama Resort Restaurant**	
14:00–14:45		**Plenary Session - Chair: Prof Roberta Ramponi (Venue: Imvubu)**	

Time	Type	Speaker	Title
14:00–14:45	PL	**Prof Anna Chiara De Luca** Institute of Endocrinology and Experimental Oncology IEOS	Raman and SERS-bases biosensors for biomedical applications
14:45-15:15		Coffee	
15:00-18:00		ICO Bureau Members Meeting - Venue: Country Boutique Hotel	
15:15–16:40		Session 5: Nanophotonics	
		Venue: Imvubu and Chair: Prof Maalik Maaza	
15:15–15:40	IT	**Prof Zhexuan Wang** Tsinghua University, China	Electron emission from graphene-hBN-graphene heterostructure
15:40–16:00	CT	**Dr Boitumelo Mabakachaba** University of the Western Cape/ iThemba LABS, South Africa	Influence of 2 MeV Proton irradiation on Vanadium dioxide(VO2)'s optical and electrical characteristics
16:00–16:20	CT	**Prof Yan Li** Peking University, China	Multiple single-photon chiral edge states generated in the fractal photonic anomalous Floquet topological insulator
16:20–16:40	CT	**Prof Site Zhang** Changchun Institute of Optics, Fine Mechanics and Physics, China	Accurate and fast calculation of wavefront modulation caused by multilayered surfaces
15:15–17:00		Session 6: Biophotonics and Biomedical Optics	
		Venue: Ibubezi and Chair: Dr Patience Mthunzi-Kufa	
15:15–15:40	IT	**Prof Heidi Abrahamse** University of Johannesburg, South Africa	Effective multicomponent drug synthesis for Photodynamic therapy in cancer treatment
15:40-16:05	IT	**Dr Martin Kroll** TU Dresden, Germany	Novel lensless fiber endoscopy by additive and subtractive femtosecond laser based manufacturing for biomedicine
16:05-16:25	CT	**Dr Masixole Lugongolo** CSIR, South Africa	Optical biosensors for the detection of human immunodeficiency virus
16:25–16:45	CT	**Dr Anine Crous** University of Johannesburg, South Africa	Unveiling the Potential: Targeting Cancer Stem Cells with Nano-Photodynamic Therapy
16:45–17:00	ST	**Glory Kah** University of Johannesburg, South Africa	Photodynamic therapy of melanoma induced by biogenic metallic silver nanoparticles chromophore
18:00-22:00		Potjie Dinner - Ingwenyama Resort Restaurant	
18:30-22:00		ICO and COS VIP Dinner - Country Boutique Hotel	

Wednesday, 8 November 2023

9:00–10:30		Plenary Session - Chair Prof Qihaung Gong (Venue: Imvubu)	
9:00–9:45	PL	**Prof Andrew Forbes** University of Witwatersrand, South Africa	Tailoring distortion-free light
9:45–10:30	PL	**Prof Xu Liu** Zhejiang University, China	Multibeam parallel laser direct writing and 3D nanofabrication
10:30–11:00		Coffee	
11:00–11:25	IT	**Prof Bo Gu** BOS, USA	Artificial Intelligence in Photonics
11:25–13:00		Student Engagement Session- Chair: Ms Kari Apter (Venue: Imvubu)	
11:25–11:40	IT	**Dr Yaseera Ismail** University of KwaZulu-Natal, South Africa	Overview of the South African Quantum Initiative
11:40–11:55	IT	**Prof John Howell** Chapman University, USA	International Commission for Optics Activities
11:55–12:10	IT	**Prof Bo Gu** The Chinese Optical Society, China	Activities of the Chinese Optical Society
12:10–12:25	IT	**Dr Carmina Londono** Retired, National Science Foundation USA	SPIE International Outreach Initiatives
12:25–12:40	IT	**Prof Michal Lipson** Columbia University, USA	Opportunities through Optica
12:40-13:00		Scientific Societies Panel Discussion Q&A	
13:00–14:30		Lunch - Ingwenyama Resort Restaurant	
15:30		Excursion - Game Drive (Kruger National Park)	
20:00		Conference Dinner - Bush Braai in the Kruger National Park	

Thursday, 9 November 2023

9:00–9:45		Keynote on Science in South Africa - Chair: Dr Yaseera Ismail (Venue: Imvubu)	
9:00–9:45	PL	**Dr Phil Mjwara** Director General of Department of Science and Technology, South Africa	Optics and Photonics Landscape in South Africa
9:45–10:30		Plenary Session - Chair: Dr Christine Steenkamp (Venue: Imvubu)	
9:45–10:30	PL	**Prof Francesco Petruccione** Stellenbosch University, South Africa	TBA
10:30–11:00		Coffee	
11:00–12:30		Session 7: Applied Optics and Photonics	
		Venue: Imvubu and Chair: Dr Christine Steenkamp	
11:00–11:25	IT	**Prof Humberto Michinel** Universidade de Vigo, Spain	Vortex Crystals in Self-Trapped Optical Beams
11:25–11:45	CT	**Prof Yunquan Liu** Peking University, China	Attosecond Physics with Sculptured Circular Light Fields
11:45–12:00	ST	**Sachleen Singh** University of Witwatersrand, South Africa	Fixing light with light
12:00–12:15	ST	**Steven Gamuchirai Makoni** University of Witwatersrand, South Africa	Modelling OAM crosstalk due to tilt and displacement with neural networks
12:15–12:30	ST	**Mwezi Koni** University of Witwatersrand, South Africa	Deutsch-Josza Algorithm on Optical Vector Matrix Multipliers
11:00–12:40		Session 8: Applications of RADARS, LIDARS and Spectrometers	
		Venue: Ibubezi and Chair: Dr Carmina Londono	
11:00–11:25	IT	**Prof John Howell** Chapman University, USA	Super RADAR
11:25–11:50	IT	**Prof Sivakumar Venkataraman** UKZN, South Africa	Characterization of the atmospheric aerosol optical properties using Laser and Optics, especially in South Africa
11:50–12:10	CT	**Prof Yue Li** Changchun Institute of Optics, Fine Mechanics and Physics, China	Development and In-Orbit Calibration of the New-Generation Solar Irradiance Spectrometer
12:10–12:25	ST	**Michael Lovemore** University of Pretoria, South Africa	Beam quality optimization to improve single-molecule spectroscopy signals
12:25–12:40	ST	**Fortune Iga** University of Witwatersrand, South Africa	Development of a Cost Effective Fibre-based FSO System
12:40–14:00		Lunch - Ingwenyame Resort Restaurant	
14:00–15:30		Plenary Session - Chair: Prof Ahmadou Wague (Venue: Imvubu)	

14:00–14:45	PL	**Dr Xeujen Zhang** Changchun Institute of Optics, Fine Mechanics and Physics, China	Manufacturing and Application of Freeform Optical Systems for Space Telescopes
14:45–15:30	PL	**Prof Zouheir Sekkat** University of Rabat, Morocco	Smart Molecular Machines in Polymers: Light induced Nonlinear Optical Effects and Mass Motions and Mechanics
15:30–16:00		**Coffee**	
16:00–17:20		**Session 9: Applied Optics and Photonics**	
		Venue: Imvubu and Chair: Prof Nathalie Westbrook	
16:00–16:25	IT	**Prof Ahmadou Wague** Université Cheikh Abta Diop, Senegal	Contributions of The African Laser Atomic Molecular and optical sciences Network (LAM) for the development of optical sciences in Africa
16:25–16:45	CT	**Prof Xiaodi Tan** Fujian Normal University, China	High Density Holographic Data Storage using Polarization Multiplexing
16:45–17:05	CT	**Prof Rasha Khafagy** Ain Shams University, Egypt	TBA
17:05–17:20		**Closing - End of Conference (Venue: Imvubu)**	
18:00-22:00		**Dinner - Ingwenyama Resort Restaurant**	

List of Abstracts – Talks

Plenary Sessions

Polarization textures of light - Spin textures of atoms

Prof Sonja Franke-Arnold   University of Glasgow, UK

Over the last decades we have gained unprecedented control over light, allowing us to shape its phase and polarisation structures and explore its topologies. Vector light is correlated in its polarisation and spatial degree of freedom, resulting in unexpected features, including effects of geometric phases, the generation of polarisation components along the propagation direction for strongly focused light, and access to the vectorial nature of light-matter interactions. In this talk I will illustrate a kaleidoscope of effects arising from the latter: an atom state interferometer that allows the generation of atomic spin alignments, promising applications in magnetometry and inertial sensing, and the first direct observation of longitudinal electric fields based on spectroscopy in THz magnetic fields.

Bio:
Prof Sonja Franke-Arnold holds the Chair of Quantum Optics in the School of Physics and Astronomy at the University of Glasgow and is an elected Fellow of the Institute of Physics with over 25 years' of experience in atom and quantum optics. She is fascinated by the nature of light, especially its topological structures and its interaction with atoms. Her team has developed this work towards applications in funded collaborations with optical and bio-medical companies.

List of Abstracts – Talks

The Revolution of Silicon Photonics

Prof Michal Lipson   Columbia University, USA

We are now experiencing a revolution in optical technologies, where one can print and control massive optical circuits, on a microelectronic chip. This revolution is enabling a whole range of applications that are in need for scalable optical technologies and its opening the door to areas that only a decade ago were unimaginable. In the past decade the photonic community witnessed a complete transformation of optics. We went from being able to miniaturize a handful of devices to being able to define and control the flow of light using thousands of monolithically integrated optical components – all on a silicon chip. The main drive for silicon photonics is the ability to transmit and manipulate ultra-high bandwidth with low power dissipation. Today there are hundreds of products being developed and commercialized towards this goal. The field of silicon photonics is rapidly evolving and is now enabling completely new applications, ranging from Lidar to biomedical devices. This is partly due to the development of novel chip-scale technologies, novel devices and novel materials compatible with silicon photonics. Many of these technologies and devices can manipulate light across the whole VIS, IR and the Mid IR spectrum. I will discuss these emerging applications, as well as the advancement brought by these novel devices and materials. The key challenges of the field relate to the scalability of the systems in bandwidth, size and power. Some of these challenges are fundamental and require innovations that break traditional tradeoffs. Novel approaches for switching, modulating and amplifying light have emerged that can open the door to applications that rely on such scalable systems. I will describe the challenges of the field and some of the recent innovations that can potentially address these challenges.

Bio:

2023 Optica President Michal Lipson is the Eugene Higgins Professor at Columbia University, US. She completed her B.S., MS and Ph.D. degrees in Physics at The Technion – Israel Institute of Technology in 1998. Following a Postdoctoral position in MIT, US, in the Material Science department, in 2001 she joined the School of Electrical and Computer Engineering at Cornell University, US, and was named the Given Foundation Professor of Engineering at the School of Electrical and Computer Engineering in 2012. In 2015 she joined the electrical engineering department at Columbia University. Lipson is one of the pioneers of the field of silicon photonics. Lipson pioneered critical building blocks in the field of Silicon Photonics, recognized as one of the most promising directions for solving the major bottlenecks in microelectronics. In 2004 she showed the ability to tailor the electro-optic properties of silicon (Almeida, et

al., Nature 2004 with more than 1300 citations
and Xu et al Nature 2005 with more than 2000
citations) which represent critical advances that
led to the explosion of silicon photonics research and development. The number of publications related to silicon photonic devices and systems is now more than 50,000 a year. A large fraction of these publications are based on Lipson's original papers. Today more than one thousand papers published yearly involve devices and circuits based on Lipson's original modulators, as well as on other silicon photonics devices demonstrated by her group including slot waveguides (Almeida et al, Optics Letters 2004 with more than 1500 citations) and inverse tapers (Almeida et al, Optics Letters, 2003 with more than 80 citations). The growth of the field of silicon photonics has been evident in industry with an increasing number of companies developing silicon photonics products (IBM and Intel, HP Aurrion, Melannox, Apic, Luxtera, etc). Lipson's work has been cited in top high-impact journals such as Nature, Nature Photonics, Nature Physics, IEEE Photonics Technology Letters, Nanoletters, Lab on a Chip, Physical Review Letters and IEEE Journal of Lightwave Technologies. Her papers (over 200 refereed journal publications) have been cited more than 32,000 times. Her h-index (measurement of productivity and impact of the published work) of 90 is also indicative of the impact that her work has had on the scientific community. Lipson has delivered hundreds of invited, keynote and plenary lectures in all the major conferences in optics and related fields. She has over 30 patents and approximately half of them have been licensed to industry. In 2010 in recognition of her work in silicon photonics she was awarded the MacArthur Fellow. She was also awarded the Blavatnik award in 2010, She received the R. W. Wood prize in 2016 and has been named by Thomson Reuters as a top 1% highly cited researcher in the field of Physics since 2014.

Short Wavelength Structured Light for Attosecond Science

Prof Carlos Hernández-García   Grupo de Investigación en Aplicaciones del Láser y Fotónica, Departamento de Física Aplicada, Universidad de Salamanca, E-37008, Salamanca, Spain

The development of structured ultrafast laser sources is a key ingredient to advance our knowledge about the fundamental dynamics of electronic and spin processes in matter. It has been widely recognized the relevance of ultrafast sources structured in their spin angular momentum (associated to the polarization of light) and orbital angular momentum (associated with the transverse phase profile, or vorticity of a light beam) to study chiral systems and magnetic materials in their fundamental temporal and spatial scales. The possibility to generate structured ultrafast laser pulses in the shortest time scales known, as attosecond pulses, has been triggered by substantial developments in nonlinear optics during the last years. In particular, thanks to the highly nonlinear process of high harmonic generation (HHG), where an intense infrared driving beam is up converted into the EUV extreme-ultraviolet (EUV)/soft x-rays, structured attosecond pulses can be nowadays. In this talk we will review several works that have boosted the field of ultrafast structured EUV pulses and attosecond science during the last decade [1-6]. We will focus not only in the ability to tailor the angular momentum properties of high harmonics and attosecond pulses, but also on how through the angular momentum of the infrared driving beam we can harness the spatiotemporal properties of the attosecond pulses being emitted.

[1] C. Hernández-García, A. Picón, J. San Román, and L. Plaja, Physical Review Letters 111, 083602 (2013).
[2] L. Rego, K. Dorney, N. Brooks, Q. Nguyen, C. Liao, J. San Román, D. Couch, A. Liu, E. Pisanty, M. Lewenstein, L. Plaja, H. Kapteyn, M. Murnane, C. Hernández-García, Science 364, eaaw9486 (2019).
[3] L. Rego, N. J. Brooks, Q. L. D. Nguyen, J. San Román, I. Binnie, L. Plaja, H. C. Kapteyn, M. M. Murnane, C. Hernández-García, Science Advances 8, eabj7380 (2022).
[4] C. Hernández-García, A. Turpin, J. San Román, A. Picón, R. Drevinskas, A. Cerkauskaite, P. G. Kazansky, C. G. Durfee, and I. J. Sola, Optica, 4, 520 (2017).
[5] A. de las Heras, A. Pandey, J. San Román, J. Serrano, E. Baynard, G. Dovillaire, M. Pittman, C. Durfee, L. Plaja, S. Kazamias, O. Guilbaud, C. Hernández-García, Optica 9, 71-79 (2022).
[6] M. Luttmann, M. Vimal, M. Guer, J.-F. Hergott, A. Z. Khoury, C. Hernández-García, E. Pisanty, T. Ruchon. Science Advances 9, eadf3486 (2023).

Bio:
Associate Professor at Universidad de Salamanca (Spain), in the Research Group in Photonics and Laser Applications (ALF-USAL). Principal Investigator of the ERC Starting Grant, ATTOSTRUCTURA "Structured attosecond pulses for ultrafast nanoscience", Carlos' interests cover nonlinear optics and ultrafast phenomena, focusing in the ability to generate structured laser pulses for their application in attosecond science. Recipient of the EPS-QEOD Fresnel Prize in 2019 for fundamental aspects and the IUPAP Young Scientist Prize In Atomic, Molecular And Optical Physics 2021.

Versatile control of optical waves with optical frequency combs enables broad applications

Prof Kaoru Minoshima   The University of Electro-Communications, Japan

Optical frequency comb technology has been successfully used as an "ultraprecise frequency ruler," revolutionizing various fields of science and technology through absolute optical frequency measurements. However, numerous potential application fields remain unexplored for the comb. Optical frequency comb can be used as a tool for high-precision and versatile control of the full properties of optical waves as an "optical synthesizer". It provides multi-dimensionality, ultra-wide dynamic range, together with great controllability, making it highly attractive for a broad range of applications. In this talk, I will introduce several examples of new technologies enabled by fully utilizing the comb's properties, particularly optical phase controllability. These examples include highly functional spectroscopy, optical information processing, imaging, and quantum optics.

Bio:

Kaoru Minoshima is a Professor and vice-President of the University of Electro-Communications (UEC), Tokyo, Japan. She received her Ph.D. degrees from the University of Tokyo, and worked at the National Institute of Advanced Industrial Science and Technology (AIST) until 2013. She was also visiting at the University of Bordeaux I (1996), and MIT (2000-2001). She was 2019 MIT Hermann Anton Haus Lecturer. Her areas of research are optical frequency combs, ultrafast optical science and technology, and optical metrology. She has served as the CLEO Subcommittee Chair (2004-2005), where she built a new subcommittee for Optical Metrology, Program Co-Chair (2009), General Co-Chair (2011), and member of Steering Committee (2021-present). She is currently a LASE Symposium Chair of Photonics West. She is a vice-President of ICO, a member of the Science Council of Japan, a director of Laser Society of Japan (LSJ), and a Fellow of Optica, the Japan Society of Applied Physics (JSAP), and LSJ.
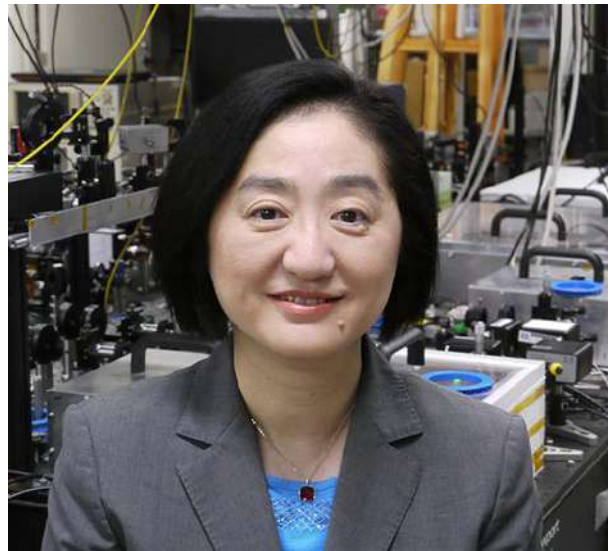
Tailoring distortion-free light

Prof Andrew Forbes   School of Physics, University of the Witwatersrand, Johannesburg, andrew.forbes@wits.ac.za

Light can be tailored in its many degrees of freedom for so-called structured light. This opens many exciting avenues in seeing smaller in imaging, enhanced precision in manufacturing, and in optical communication and information processing, where the many forms of structured light can be used as an information alphabet. Unfortunately light gets distorted when passing through noisy channels, negative the benefits of its initial structure. Here we explore how to find degrees of freedom and forms of structured light that are invariant to noisy channels, and show near distortion-free transport of light even in highly distorted media.

Bio:

Andrew is presently a Distinguished Professor within the School of Physics at the University of Witwatersrand (South Africa) where in 2015 he established a new laboratory for Structured Light. He is a Fellow of SPIE, Optica, the South African Institute of Physics (SAIP), an elected member of the Academy of Science of South Africa and editor-in-chief of the IoP's Journal of Optics. Andrew has won several awards for his research, including the NSTF national award for his contributions to photonics in South Africa (2015), the Georg Forster prize from the Alexander von Humboldt Foundation for outstanding contributions to photonics (2020), the SAIP Gold Medal (2020), the highest award for physics in South Africa, making him the youngest winner to date, the Sang Soo Lee award from Optica and the Korean Optical Society (2022) and the TWAS prize for Physics (2024).

Nonlinear Photonics for All

Prof Alexander Gaeta   Columbia University, USA

The developments of chip-based photonics over
the past two decades have made nonlinear optics widely accessible to the academic and commercial communities. I will describe these recent advances and several different types of nonlinear photonic devices that can be realized with only milliwatt-level lasers.

Bio:

Gaeta received his BS, MS, and PhD degrees in Optics from the University of Rochester. Gaeta joined Columbia Engineering as the David M. Rickey Professor of Applied Physics and Materials Science in 2015. Prior to that, Gaeta was the Samuel B. Eckert Professor of Engineering at Cornell University and was Chair of the School of Applied and Engineering Physics from 2011 – 2014. He has published more than 300 journal articles in quantum and nonlinear photonics. He served as the founding Editor-in-Chief of the journal Optica from 2014-2020 and Chair of the Optica Publications Council in 2022. He co-founded Xscape Photonics, Inc. in 2022 and is currently serving as the CEO. He is a Fellow of the Optica, APS, and IEEE, and a Thomson Reuters Highly Cited Researcher, and was awarded the 2019 Charles H. Townes Medal from Optica.

Multibeam parallel laser direct writing and 3D nanofabrication

Prof Xu Liu   Zhejiang University, China

3D nanofabrication is a n important technique in current nanophotonics and future integrated industry, optoelectronic industry, nanomaterial technical industry. The high precision photolithographer, e-bam lithographer are the major nano-manufacture techniques for these fields, but they all have their limit of the 3D nanofabrication. Laser direct writing is a convenient technique for 3D manufacture, but limit on the wavelength of the laser, it is hard to shrink down to nanometer, except using EUV laser. In the practical application, we need large size sample with nano-resolution structure, it always takes extremely long time to fabricate the sample especially for the scanning type nanofabrication techniques. Here we present our development of laser 3D nano fabrication technique, it profit the high flexible spatial modulation ability of laser beam, and is easy handle without critical vacuum requirement technique. In laser writing technique, the resolution is depended on the diffraction limit, to reach 3D nano fabrication ability with visible laser beam, it is very important to introduced nonlinear effect. Our high throughput 3D laser nanofabrication technique used two photon or two step absorption effect in the special laser nonlinear photo resist, this can get sub diffraction writing, but it still depends on laser wavelength. We introduce Peripheral Photoinhibition (called PPI) technique to arrive super high resolution laser priting, by using a solid focus spot to creat two photon or two step absorption exposition in the photoresist and using another laser with donnut spot to inhibit the expostion, the two beams are well aligned with same beam axes, in result to arrived super tinny spot expotion[1]. We have developed high throughput laser direct writing 3D nano fabrication technique, it promises us to produce arbitral complicate 3D structure with less than 50-100nm scale. It can be used to produce optical grating, microlens array, optical waveguide, because our photoresist can be optical transparent in the visible and near infrared range. It is sure, it can be used to produce different microfluid devices. The 3D nano fabrication ability create a lot of possibility.

Cao, C.; Kuang, C.; Liu, X.. Dip-In Photoresist for Photoinhibited Two-Photon Lithography to Realize High-Precision Direct Laser Writing on Wafer , ACS Applied Materials Interfaces 2022, 14 (27), 31332

Bio:

Yangtze River Scholarship Chair Professor in the College of Optical Science and Engineering of Zhejiang University in Hangzhou, China. His research fields are: Thin film optics and coatings techniques, Projection display, 3D display, Optical imaging and instrumentation. Currently, he is the Director of State Key Laboratory of Modern Optical Instrumentation. He is the author and co-author of more than 200 journal papers and 80 patents. He is fellow of Optica, SPIE and COS.

On the trapping of cold neutrons in nano-scaled Fabry-Perot resonating cavities neutron lifetime considerations

Prof Maalik Maaza   iThemba LABS-National Research Foundation of South Africa

Relatively to the atomic constituents' counterparts, the neutron is singular as it is sensitive to the four fundamental interactions namely strong, weak, electromagnetic, and gravitational. This multi sensitivity makes neutron wave-matter optics a particularly versatile tool for testing quantum mechanics specifically and fundamental physics concepts in general. The lifetime of a free neutron defined via its beta-decay $\langle \tau n \rangle$ is of a pivotal importance within the standard model & cosmology. Indeed, the precision on the neutron lifetime is of a paramount importance as it regulates the precision of the 1st element of the Cabibbo–Kobayashi–Maskawa matrix, central to the standard model. The two major methods used to measure $\langle n \rangle$ while trapping free neutrons, namely, the beam and the bottle methods give different neutron lifetime values; $\langle \tau n \rangle$Beam 888.0 ± 2.0 s , that obtained by the bottle technique is smaller; of about $\langle n \rangle$ Bottle 879.4 ± 0.6 s. In addition of the persistent difference of 10 s persists for years, even if the two methods have been modified to enhance the experimental accuracy. This latter was shown to be enhanced if one could trap cold neutrons in nanostructured Fabry-Perot resonators. This contribution reports on the de Broglie wave-matter quantum duality coupled to the Fermi total reflection phenomenon in addition to the tunneling & trapping of cold neutrons in such nano-resonating cavities. This quantum mechanics trapping driven phenomenon allows trapping times of cold neutrons with a precision governed by the Heisenberg uncertainty of about 10^{-12} s [1].

1. M. Maaza, Journal of Neutron Research -1 (2023) 1–16 1 DOI 10.3233/JNR-220015

Bio:
Prof. M. Maaza is a native of North Africa, holds a PhD from the University of Paris-VI, is the current incumbent, in South Africa, of the UNESCO UNISA-ITLABS-NRF Africa Chair in Nanosciences. He is a joint staff of the University of South Africa and the National Research Foundation of South Africa. He is a fellow of various Academies, including the African Academy of Science, the European Academy of Arts Sciences as well as the National Academy of Science of India, the Islamic Academy of Sciences the Royal Society of Chemistry-London. Prof. M. Maaza has been bestowed several awards accolade among which; the African Union Nkwame Nkrumah award for Excellence in Science Technology the Galileo-Galilei award by the International Commission for Optics (ICO).

Raman and SERS-bases biosensors for biomedical applications

Prof Anna Chiara De Luca   Institute of Experimental Endocrinology and Oncology "G. Salvatore", IEOS, second unit, National Research Council of Italy (CNR), Via P. Castellino 111, 80131 Naples, Italy. *annachiara.deluca@cnr.it

Raman-based microscopy, as well as, Surface-enhanced Raman scattering (SERS) has received increasing research interest due to its excellent resolution, high sensitivity and rapid detection of low concentration analytes, particularly in biomedicine. Herein, I will provide an overview of recent developments and applications of Raman microscopy, SERS-based nanosensors and nanoreporters developed in our laboratory for use in imaging, biochemical monitoring, medical diagnostics, and therapy. A disease, such as cancer, induces changes in the molecular composition of the affected cell (an increased nucleus-to-cytoplasm ratio, disordered chromatin, higher metabolic activity, and changes in lipid and protein levels) and therefore, these changes are reflected in the Raman spectra. I will demonstrate that Raman-based approaches bear significant benefits for the identification, classification and follow up of cancer cells, in in-vitro experiments and preclinical studies, providing label-free biochemical information [1]. Furthermore, it will be presented the development of an advanced Raman-based device and its integration/correlation with digital holography for the imaging cancer cells with significantly shorter spectrum/image acquisition times and identification of new parameters for classification of cancer cells, thus allowing a higher sample throughput necessary for clinical applications [2]. The application of Raman imaging approaches for localizing and following the internalization kinetics and transport of nanovectors in cancer cells, without chemical/charge alteration of the nanovectors surface itself will be provided [3]. The design and fabrication of different types of plasmonics-active nanostructures, including fiber SERS sensors, will be discussed [4,5]. The applications of the SERS nanosensors for protein detection, local quantification and controlled release of drugs in living cancer cells will be presented.

[1] S. Managò, C.Valente, P. Mirabelli, D. Circolo, F. Basile, D. Corda, A. C. De Luca, Sci. Rep. 6, 24821 (2016).

[2] M. Mangini, M. A. Ferrara, G. Zito, S. Managò, A. Luini, A. C. De Luca, G. Coppola, Front Bioeng. Biotech. 11, 1057216 (2023).

[3] S. Managò, C. Tramontano, D. Delle Cave, G. Chianese, G. Zito, L. De Stefano, M.Terracciano, E. Lonardo, A.C. De Luca, I. Rea, Small, 17, 2101711 (2021).

[4] A.C. De Luca, P. Reader-Harris, M.Mazilu, S. Mariggio, D. Corda, A. Di Falco, ACS Nano, 8, 2575-2583 (2014).

[5] S Spaziani, G Quero, S Managò, G Zito, D Terracciano, PE Macchia, F Galeotti, M Pisco, A.C De Luca, A Cusano Biosens Bioelectr 233, 115322 (2023).

Bio:

Anna Chiara obtained a master's degree in Physics (2004), followed by a PhD thesis in the field of Biophotonics at Department of Physics, University of Naples "Federico II" (2008). In 2009, she joined Prof. K. Dholakia group at University of St Andrews as post-doctoral research fellow. Since February 2012, she joined National Research Council of Italy (CNR) and the same year she has been appointed a tenured Research Fellow by the CNR. She is currently senior researcher at IEOS, CNR and her research activity is focused on the development of new tools enabling enhanced Raman Spectroscopy for cancer cell imaging and biomarker identifications and sensing. In 2015 she became member of the Euro-bioimaging ERIC infrastructure (EuBi) - Advanced Light Microscopy Italian Node (ALM) in Naples as scientific advisor. Since 2020, she is manager the Joint Research Unit for the development and managing of the research activities of the 4 AML Italian nodes of EuBi. She received several awards including the special "Young Scientist Award" from the CNR for her work in Biomedical Imaging received in the 2016. She has published more than 80 papers in reputed journals. She has been recognized with numerous prestigious research grants, including the Grant from PNRR - Research Infrastructure (National Recovery and Resilience Plan of Italian Ministry of Research and University), AIRC (Italian Association for Cancer Research), Italian "Future in Science" grant (FIRB), PON from Italian Ministry of Research and University, POR from Campania Region, Grant from Ministry of Health and @CNR grant.

Smart Molecular Machines in Polymers: Light induced Nonlinear Optical Effects and Mass Motions and Mechanics

Prof Zouheir Sekkat   Mohammed V University, Morocco

In this talk, I will give a brief overview of the main directions of research in Optics and Photonics in the world, and I will discuss capacity building in Africa (Morocco), with focus on applied research in the fields of renewable energies and agriculture. Research, encompassing photonic and smart materials and plasmonics will also be discussed.

Bio:

Zouheir Sekkat is Full Professor at the Department of Chemistry of the Faculty of Sciences of Mohammed V University in Rabat (UM5R), and the director of the Optics and Photonics Centre of the Moroccan Foundation for Science, Innovation and Research (MAScIR) of the University Mohammed VI Polytechnic at Benguerir (UM6P). Sekkat completed his Master, in 1988, and PhD, in 1992, and Habilitation, in 1998, degrees, all from Paris-Sud University, Orsay. Sekkat did postdoctoral research stays Max-Planck Institute for Polymer Research in Germany, and at CPIMA jointly between the University of California-Davis and IBM Almaden at San Jose, and Stanford University. In 1999 Sekkat joined Osaka Univeristy (Handai) as an Associate Professor of Applied Physics; and then he was appointed as a full professor of Handai by the cross-appointment program between Handai and UM5R. He is an author and coauthor of more than 200 peer-reviewed papers. He pioneered interfacing smart materials with optics, and his total number of citations exceeds 7000 and his actual h index is 44. Sekkat received several prizes and recognitions, including nomination as one of the first members of the Hassan II academy of sciences and technology, and the Elsevier prize for the most cited paper of Morocco, and the distinction prize of the Moroccan ministry of research. He is often invited to give invited and keynote talks at international conferences, and he organized several national and international conferences, and is the actual chair of the annual conference on Molecular and Nano-Photonic Machines of SPIE in San Diego, USA. He is fellow of the African Academy of Sciences (AAS) and Optica (former OSA) and SPIE. Sekkat built a laboratory of, and develops and promotes, optics and photonics in Morocco and Africa.

Invited Talks

Laser and Ion Beam Writing for Quantum Photonic Devices in Diamond

Prof Roberta Ramponi   IFN-CNR Milano, p. Leonardo da Vinci 32, 20133 Milano, Italy

The nitrogen-vacancy (NV) center is a defect in which two adjacent sites in diamond's tetrahedral lattice of carbon atoms are replaced. One site contains a nitrogen atom instead of carbon while the other is vacant. In its negatively charged state, the NV center gains an extra electron from the lattice, forming a ground state spin system which can be polarized with 532-nm light, even at room temperature. One of the spin states fluoresces much more brightly than the others so that fluorescence can be used for spin-state readout. At the same time, the NV's electron spin states are sensitive to magnetic and electric fields through the Zeeman and Stark effects, respectively. These properties make NVs in diamond very attractive both as an integrated and scalable platform for quantum information systems and for high sensitivity electromagnetic field quantum sensors. An integrated optics platform in diamond is essential for both quantum information systems and quantum enabled electric and magnetic field sensing, where the NV is used as an optically detecting atomic probe. This is because of the ultimate stability and integration provided by monolithic waveguides, in addition to the potential for enhanced optical interaction with NVs. Another promising quantum emitter in diamond is the Silicon vacancy (SiV), which has a narrow zero phonon line and a large Debye-Waller factor, making it suitable as a single photon source for quantum optics. For the first time, 3D laser microprocessing is combined with ion implantation nanofabrication to exploit the advantages of both techniques to achieve integrated high quality quantum emitters and buried optical waveguides in diamond. On one side, femtosecond laser micromachining has proved to be very efficient in the fabrication of a full portfolio of components in diamond chips, in particular waveguides, microchannels and NV quantum emitters in an intrinsically 3D geometry [1], thus allowing the realization of integrated quantum circuits and microfluidic components very promising for both quantum sensing and quantum information. A further advantage of this fabrication technique is that it provides large mode-field diameters, well matching fiber optic technology. On the other side, ion implantation can be used to form NV quantum emitters at nanometric depths at the end facets of laser written 3D optical waveguides. This hybrid fabrication scheme enables development of two-dimensional quantum sensing arrays, facilitating spatially and temporally correlated magnetometry. This innovative method is also applied to implant SiV in laser written photonic circuits, to engineer light at the single photon level, which could enable next generation quantum computation systems in diamond [2].

[1] A. N. Giakoumaki, G. Coccia, V. Bharadwa, J. P. Hadden, A. J. Bennett, B. Sotillo, R. Yoshizaki, P. Olivero, O. Jedrkiewicz, R. Ramponi, S. M. Pietralunga, M. Bollani, A. Bifone, P. E. Barclay, A. Kubanek and S. M. Eaton, "Quantum technologies in diamond enabled by laser processing", Appl. Phys. Lett. 120, 020502 (2022).
[2] M. K. Koch, M. Hoese, V. Bharadwaj, J. Lang, J. P. Hadden, R. Ramponi, F. Jelezko, S. M. Eaton, and A. Kubanek, "Super-Poissonian Light Statistics from Individual Silicon Vacancy Centers Coupled to a Laser-Written Diamond Waveguide", ACS Photonics 9(10), pp. 3366–3373 (2022).

Trapping ytterbium isotopes for unsharp quantum measurements

Dr Christine Steenkamp   Stellenbosch University, South Africa

Quantum technology enabling applications such as quantum communication, quantum key distribution and quantum computing is a fast-growing field of increasing industrial importance. Trapped ions have been successfully used to reach important milestones in the field of quantum computing as trapped ions can fulfill the criteria of scalability, easy initialization, useful coherence times, control mechanisms suitable to realize quantum gates, qubit-specific measurements, and the potential to be miniaturized and integrated with opto-electronics [1]. An inherent property of quantum systems is that measurements affect the state of the system. This precludes experimental real-time monitoring of quantum systems. However, unsharp measurements yield information on the state of a target system with minimal disturbance of its state by making measurements on an auxiliary system that is weakly entangled with the target [2]. In theoretical studies, unsharp measurements have been applied to state monitoring [3] and feedback control [4]. Unsharp measurements allow the realization of quantum simulators that makes it possible to study complex systems that cannot be simulated by classical computers, such as many-body systems in solid state materials, chemistry, and quantum biology [5]. However, experimental work in this field is limited. We report on an ongoing project to trap, selectively manipulate, and entangle two isotopes of ytterbium (171Yb and 174Yb) in a Paul trap, with the long-term goal to demonstrate entanglement and unsharp measurements in this experiment. Using two isotopes of the same element, 171Yb and 174Yb, reduces the equipment cost of the system whilst allowing species-specific single ion addressing. Unsharp measurement using ytterbium ions has to our knowledge not been demonstrated yet.

[1] H. Häffner, C.F. Roos and R. Blatt, "Quantum computing with trapped ions", Physics Reports 469, 155-203 (2008).
[2] S.K. Choudhary, T. Konrad, H. Uys, "Implementation schemes for unsharp measurements with trapped ions", Physical Review A 87, 012131 (2013).
[3] T. Konrad and H. Uys, "Maintaining quantum coherence in the presence of noise through state monitoring", Phys. Rev. A. 85, 012102 (2012).
[4] P.J.W du Toit, S.C. Burd, T. Konrad, H. Uys, Real-time state estimation and feedback control of an oscillating qubit via self-fulfilling prophecy (SFP), METROLOGIA 56(1), 104003 (2019).
[5] R. Blatt and C.F. Roos, "Quantum simulations with trapped ions", Nature Physics, 8(4), 277-284 (2012).

Time-domain ptychography: Principles and application

Dr Pieter Neetling

Laser Research Institute, University of Stellenbosch, South Africa

The ability to arbitrarily shape and tailor ultrashort laser pulses in time has opened interesting avenues of research, from coherent control of chemical reactions to materials processing. Borrowing from the concepts of lensless diffractive imaging (ptychographic imaging) we developed a temporal analogue, which allows for the measurement of a temporal objects, with a temporal resolution better than the duration of the temporal probe. The ability to measure both the amplitude and phase with this increased resolution, leads to improved control over the laser pulse, from compressing the laser pulse to its Fourier limit, to shaping the laser pulse for various spectroscopic applications. In this talk I will highlight the underlying principles of time-domain ptychography and showcase some examples from our laboratory, specifically where we have shown improvements in the signal to background obtained in nonlinear microscopy and nonlinear spectroscopy by compressing our laser pulses using a modified time-domain ptychography algorithm. I will end off by giving a preview of our current research, showcasing where the research is headed and what is possible.

Real-time feedback-driven single-particle tracking

Prof Tjaart Krüger   Department of Physics, University of Pretoria, South Africa

The ability to use light to detect individual molecules and observe their dynamical behaviour has revolutionised life sciences during the past three decades. State-of-the-art techniques provide nanometre-scale spatial resolution at a time resolution of 1 ms or shorter. Single-particle tracking (SPT) is an important single-molecule microscopy technique that allows direct access to the dynamics of individual freely diffusing molecules and particles in live cells. The conventional approach to SPT involves the acquisition of a sequence of images of fluorescent particles, determining their positions in each frame, and linking those into a trajectory for further analysis. Such image-based SPT can achieve excellent 3D spatial resolution (10–20 nm), but the time of resolution is limited to 30–100 ms. Real-time feedback-driven SPT offers a marked improvement in spatiotemporal resolution and an extended tracking time and tracking region compared to image-based SPT. It also enables concurrent spectroscopic measurements to be made on the tracked molecules, allowing single-molecule spectroscopy (SMS) to be performed non-invasively on freely diffusing biomolecules, thus representing an important steppingstone towards in vivo SMS. In this presentation, I will explain the principles of real-time SPT, compare the performance of different methods, and illustrate the first results obtained in our laboratory on single freely diffusing plant light-harvesting complexes.

Future Perception Technology based on Nano-optoelectronics

Prof Yidong Haung   Tsinghua University, China

With the trend of the intelligent society, more dimensions and ultra-high precision of integrated sensors are required for the next generation of perceptual technology. In this work, spectral imaging as a new information dimension, and phonons as a new information carrier are explored based on manipulating light (photons) and mechanical motion (phonons) in periodic micro/nano structures. Accordingly, ultraspectral imaging chip, phonon lasing sensors and on-chip mechanical exceptional points are achieved, which pave the way for a new information dimension and a new information carrier of intelligent on-chip sensors. Traditional spectral analysis principles such as prism dispersion, grating diffraction or Fourier transform, are impossible to get dynamic spectral imaging of a target in real time. We demonstrated a one-shot miniaturized ultraspectral camera [1-3] fitting thousands of micro-spectrometers on a CMOS image sensor chip to realize real-time on-chip spectral imaging. we realize the fast reconstruction of spectral images and eliminate the mosaic effect by using the reconstruction algorithm ADMM-net [4]. The performance of image detail reconstruction using ADMM-net is significantly better than that using traditional point-by-point CVX spectral reconstruction algorithm, effectively eliminating the mosaic phenomenon in the spectral image. Here, the single reconstruction using ADMM-net takes only 18 milliseconds, which achieves about 5 orders of magnitude improvement compared with point-by-point spectral reconstruction. Furthermore, real-time spectral imaging of the outdoor driving scene was realized by using ADMM-net. This study provides an integrated on-chip platform for investigating the related physics of mechanical EPs, such as non-Hermitian phenomena, nonlinear effects, and phononic topology, and also suggests possible solutions to technical obstacles in applications such as ultrasensitive sensing and precision measurement of physical quantities.

Functionalizing Bistable/Multi-stable CFRP Laminate Structures

Dr Oliver J. Myers   Clemson University, USA

An emerging research area in the field of composite materials focuses on Bistable/Multi-stable Composites. These composites have two or more stable shapes, which include snap through/snap back phenomenon between the shapes, which makes it a suitable material for using in "Adaptive Structures". Bistable composites are unsymmetric laminated CFRP that exhibits bistability because of the unsymmetric laminate stacking sequence about the middle surface. In the combination of symmetric and unsymmetric laminates, various standard geometries are split into smaller geometries, each of those smaller geometries are made into symmetric or unsymmetric laminates and different combinations of those symmetric and unsymmetric laminates are studied, to find out the various bistable shapes that are possible in each standard geometry. Numerical simulations and experiments are conducted to determine design constraints for sizes and alternative geometries of bistable laminates. Additionally, much study is necessary to functionlize bistable/multistable laminates for SHM/NDE, morphing structures, particularly incorporating mounting fixtures (boundary conditions) and thicker bistable structures for strength and impact mitigation. Continued research examines the mechanics of delamination and ply variation on the sensing ability for magnetostrictive materials embedded in a carbon fiber reinforced polymer laminate. Analytical models are used to determine how delamination and ply variation affect the mechanical state and magnetic properties of the embedded terfenol-d particles. Numerical models are also used to simulate the effect of delamination and ply variation on the mechanical state. For the analytical method, the mechanical properties observed are the net strain and stress in a local particle section resulting from magnetostriction. The analytical method reveals that the effect of a delamination is to reduce the resistance to particle actuation in a local area, which allows for variation in stress and magnetostriction magnitudes in damaged areas vs. non-damaged areas. This variation in the mechanical state subsequently affects the magnetic permeability, which changes the reluctance in the local particle layer. These results are compared to a numerical model of Terfenol-d embedded in carbon fiber reinforced polymer laminate, which reveal a drop in stress and increase in magnetostriction in the delamination region. Finally, these results are projected to experimental results from health monitoring scans of carbon fiber reinforced polymer laminates with varied ply count with delamination.

Biophotonics and artificial intelligence for improved Diagnostics: Applications in Health, Pharmaceutical's and Agriculture

Dr Patience Mthunzi-Kufa   CSIR-National Laser Centre, South Africa

A lot of individuals residing in resource limited settings where timely access to medical care is a challenge and healthcare infrastructure is usually poor have no access to laboratory facilities. Disease diagnosis in such sites is dependent on the presence of point-of-care (POC) devices. These POC diagnostics play a key role in ensuring rapid patient care because they are simple to use, inexpensive, portable, instrument independent and do not require a trained technician to operate. To date, optical spectroscopy has become the most important and promising approach in every field of medical, analytical, life, food, and pharmaceutical sciences. However, most currently available spectrometers are bulky and cannot be easily integrated in miniaturized devices. In this work, different biophotonics techniques, artificial intelligence and machine learning models are used to expedite POC diagnostic apparatus for different pathogens, non-communicable diseases, substandard drugs and towards application in food safety as well as security.

Biomechanics using optical tweezers

Prof Nathalie Westbrook   Universite Paris-Saclay, France

Mechanical response is involved in many biological phenomenon, such as cell migration, blood pressure, embryonnic development, muscle action. Its deregulation is involved in pathologies such as cancer or thrombosis. Optical tweezers, based on the mechanical action of a focused laser beam on a dielectric object, provide a non invasive tool to study mechanical behaviour of cells or organelles, in a range of force between 1-100pN. I will describe two applications of optical tweezers to biomechanics performed in our lab. In the first one, we combine force and fluorescence microscopy to understand the connection between a force applied on a cell membrane and the internal molecular force involved, to get insights on cancer cell migration or reconstruction of neuronal connection after an injury. The second application tests the rigidity of blood clots in search of a diagnosis for hypercoagulability and thrombosis.

Electron emission from graphene-hBN-graphene heterostructure

Prof Zhexuan Wang   Tsinghua University, China

The low energy electron sources with accelerating voltage less than 1kV shows desirable properties for electron microscopy [1]. The short penetration depth of electron leads to high spatial resolution and high image contrast. And semiconductor and insulator materials can be detected directly due to the reduction of radiation damage and charging effects [2-4]. In this work, we propose and realize the low-voltage electron source based on planar graphene-hBN-graphene heterostructure (GBGH). By applying the external electric field strength of only 4×10^4V/m^2 , the maximum emission current density reaches $7mA/cm^2$. Tunable emission behaviors are observed and the emission I-V curve from GBGH is well explained according to the Fowler-Nordheim tunneling equation. We realize the low-voltage planar electron sources based on GBGH. The electric properties of GBGH is studied by first-principle calculation and the existence of tunneling junction in the static band structure of GBGH is verified. The electron sources is drived with an extremely low extracting voltage of 20 V and driving voltage of about 24 V experimentally, corresponding to the external electric field strength of only 4×10^4V/m. Steady electron emission of over 1nA and operating duration of 100s is observed from 59.29m^2 stacking area in our experiments, and thus the maximum detected current density is $7mA/cm^2$. The easy-fabrication and miniature on-chip electron sources with extremely low driving voltage will establish the promising prospect of the development of next-generation free electron devices.

[1] Brodusch, N., H. Demers, and R. Gauvin, Field Emission Scanning Electron Microscopy: New Perspectives for Materials Characterization. 2018.
[2] Ul-Hamid, A., A Beginners' Guide to Scanning Electron Microscopy. 2018.
[3] Bell, D. and N. Erdman, Low Voltage Electron Microscopy: Principles and Applications. 2013.
[4] Zewail, A.H., Four-Dimensional Electron Microscopy. Science, 2010. 328(5975): p. 187-193.

Artificial intelligence in photonics

Prof Bo Gu   Boston Photonics, USA

Artificial intelligence (AI) is the most important new methodology in scientific research since adoption of quantum mechanics and it is providing exciting results in multiple fields of science and technology. Recently artificial intelligence has been used in photonics fields. We will review the current status and recent progress in this fast growing research area with an emphasis on the laser processing and micro machining fields.

[1] S. Russell and P. Norving, Artificial Intelligence: a Modern Approach. Pearson; 3rd Ed., 2010.
[2] S. Dutta, "An overview on the evolution and adoption of deep learning applications used in the industry," Wiley Interdisciplinary Reviews-Data Mining and Knowledge Discovery, e1257, vol. 8, 4, 2018

Vortex Crystals in Self-Trapped Optical Beams

Prof Humberto Michinel IFCAE. Instituto de Física e Ciencias Aeroespaciais. Universidade de Vigo, Spain

In the present work, we introduce self-trapped vortex soliton crystals that are formed in two-dimensional coherent beams propagating in optical media with competing nonlinearities, where focusing effects are dominant at intermediate powers and self-defocusing increase at higher intensities yielding a cubic-quintic (CQ) dependence of the refractive index with the amplitude of the wavefunction. This type of optical nonlinearity can be achieved, for instance, by appropriately preparing a quantum state within a cold gas of Rb atoms, [1, 2]. We introduce a new type of stable nonlinear waves that take the form of regular vortex patterns hosted in self-focused coherent light beams that propagate without distortion in cubic-quintic nonlinear optical materials.

[1] H. Michinel, M. J. Paz-Alonso and V. M. Pérez-García, Phys. Rev. Lett. 96, 023903 (2006).
[2] Zhenkun Wu, et. al, Phys. Rev. A. 88, 063828 (2013).

Super Radar

Prof John Howell   Chapman University, USA

Radar is used in a wide array of applications including archaeology, agriculture, transportation, navigation, law enforcement, noninvasive medical diagnostics, climate change monitoring, natural disaster mapping, defense etc. Range resolution in radar is the ability to determine the distance between two objects along the same line-of-sight when performing remote sensing. The prevailing thought is that radar range resolution is inextricably linked to the inverse bandwidth of a pulse or to the wavelength of the electromagnetic wave owing to the coherent nature of the interfering wavefronts. We quote, "Wave theory indicates that the best vertical resolution that can be achieved is one quarter of the dominant wavelength. Within that vertical distance any reflections will interfere in a constructive manner and result in a single, observed reflection" (originally stated in [1] and quoted in [2]). The desire for better range resolution has driven scientists and engineers to ever-higher frequencies radar. Unfortunately, propagation distance in the air, in the ground or in water decreases as the frequency of the radar increases. This means that using existing understanding an archaeologist can only peer a few centimeters below the surface to obtain sufficient resolution to observe a coin. We show how to improve range resolution by several orders of magnitude. With our existing system, we can observe objects 10's of meters underground with sub-mm resolution.

[1] Robert E Sheriff, "Limitations on resolution of seismic reflections and geologic detail derivable from them: Section 1. fundamentals of stratigraphic interpretation of seismic data," (1977).
[2] Adrian Neal, "Ground-penetrating radar and its use in sedimentology: principles, problems and progress," Earth-science reviews 66, 261–330 (2004).

Characterization of the atmospheric aerosol optical properties using Laser and Optics, especially in South Africa.

Prof Sivakumar Venkataraman   University of KwaZulu-Natal,South Africa

I shall provide a brief overview of the aerosol measurements using LiDAR, Sun-Photometer, Balloon Borne particle counter, LiDAR in Space (Calipso) over South Africa region. I may also showcase some of the observational results obtained from our recent campaign measurements in Kruger National Park during August to November 2022, named Biomass Burning Aerosol Campaign (BiBAC) together with French partners. The impact and traces of aerosol transport from other continents into South Africa region also be demonstrated using Space-Borne LiDAR and Aerosol network (Aeronet).

Contributions of The African Laser Atomic Molecular and optical sciences Network (LAM) for the development of optical sciences in Africa

Prof Ahmadou Wague   Université Cheikh Abta Diop, Senegal

Here, through the activities of the Atom Laser lab at Cheikh Anta Diop University of Dakar Senegal, and the activities of African Laser Molecular and Optical Sciences Network(LAM Network), we consider , Laser induced absorption and fluorescence spectroscopy together with laser induced breakdown spectroscopy and X-ray fluorescence spectroscopy for environmental monitoring and medical diagnostic and Therapy at atomic scale.

List of Posters

PO1: Entanglement-based technique robust against the effects of atmospheric turbulence by exploiting spatial coherence properties.

Marie Louise Umuhire, *University of KwaZulu-Natal*

PO2: Optical Emission Spectroscopy Measurements of Electron Density in a Laser Induced CNiCo Plasma

Ursula Monica Pillay, *University of KwaZulu-Natal*

PO3: Optical emission spectroscopy study on laser induced CNiY plasmas at room temperature

Bala Saraswathi Amirthapandian, *University of KwaZulu-Natal*

PO4: Stark Spectroscopy of Plant Photosystem I's Red Pigments

Michael Lovemore, *University of Pretoria*

PO5: Synthesis and characterisation of high-temperature Boron nanostructures and computational modelling

Sadiq Nafiu Aliyu , *University of KwaZulu-Natal*

PO6: Physics-Informed Neural Networks for Quantum Optics

Shivani Mahashakti Pillay, *University of KwaZulu-Natal*

PO7: Quantum Simulation of Fokker-Plank Equations for Q Functions of Quantum Optical Systems

Ian Joel David, *University of KwaZulu-Natal*

PO8: Fourier Ptychographic Microscopy for Large Area, High-Resolution Imaging

Eugene Egbert Fouche, *Stellenbosch University*

PO9: High-resolution phase-sensitive coherent anti-Stokes Raman scattering spectroscopy by time-domain ptychographye

Jan Anthonie de Beer, *Stellenbosch University, South Africa*

P1O: Exploring metallic nanoparticles for enhanced multiplexed SERS for diagnostics

Lungile Thwala, *CSIR, South Africa*

P11: Determination of cadmium in cocoa beans using laser-induced breakdown spectroscopy

Leila Raquel Pincay Abadiano, *Escuela Politécnica Nacional, Ecuador*

P12: Optical properties of biosynthesized nanoscaled Eu2O3 for red luminescence and potential antidiabetic applications

Hamza Mohamed, *University of South Africa, South Africa*

P13: Stokes reconstruction of Chiral fields

Light Mkhumbuza, *University of Witwatersrand, South Africa*

P14: Monitoring the metabolics of single yeast cells through fluorescence microscopy using integrated optical tweezers and microfluidic setup

Le Roi Alexander Du Plessis, *Stellenbosch University, South Africa*

P15: Photobiomodulation promotes wound healing in a diabetic cellular model

Dimakatso B. Gumede, *University of Johannesburg, South Africa*

P16: Photobiomodulation at 830 nm Promotes Cellular Viability and Reduces Cell Death in Fibroblast Diabetic Hypoxic Wounded Cells

Patricia Kasowanjete, *University of Johannesburg, South Africa*

P17: Preparation and in vitro evaluation of the anticancer photodynamic therapy efficacies of ionic phthalocyanine derivatives and their nanoparticle conjugates

Lindokuhle Cindy Nene, *University of Johannesburg, South Africa*

P18: Photobiomodulation at 830 nm modulates NF-B and apoptosis in wounded and diabetic wounded fibroblast cells

Tintswalo Nomsa Mgwenya, *University of Johannesburg, South Africa*

P19: Enhancement of Raman Spectroscopy on SARS-CoV-2 detection using machine learning

Nkgaphe Tsebesebe, *CSIR, South Africa*

P20: Determining the physical properties of a perturbed optically trapped particle using Mie scattering

Anneke Erasmus, *Stellenbosch University, South Africa*

P21: Photo-thermal effects of Citrate Gold Nanoparticle on Lung Cancer

Kave Moloudi, *University of Johannesburg, South Africa*

P22: Dose response cytotoxicity studies with naturally derived photosensitizers against cancer cells

Nosipho Fakudze, *University of Johannesburg, South Africa*

P23: Curcumin-based Nanoconjugates and their promising approaches to cancer treatment

Lufuno Gracious Nemakhavhani, *University of Johannesburg, South Africa*

P24: Optimisation of ADSC Seeding Density for use in 3D Culture with Photobiomodulation: A Pilot Study

Brendon Roets, *University of Johannesburg, South Africa*

P25: Synthesis of Graphene Oxide-Gold Nanorods Nanocomposite-Porphyrin Conjugate for Improved Dual Cancer Phototherapy Performance

Thabang Calvin Lebepe, *University of Johannesburg, South Africa*

P26: Comparative study of tetrapyrrolic photosensitizer mediated phototherapy against breast cancer cell subtypes

Paromita Sarbadhikary, *University of Johannesburg, South Africa*

P27: Curcumin-loaded solid lipid nanoparticles mediated photodynamic therapy-induced apoptosis in human lung cancer cells

Jose Merlin Jayaraj, *University of Johannesburg, South Africa*

P28: WiFoO: Democratizing Long-Range Free Space Optics Using 802.11 Over Optical

Mikaeel Dindar, *University of Witwatersrand, South Africa*

P29: Synergistic anticancer effects of gold nanoparticle-herceptinhypocrellin B conjugates in human breast cancer cells

Sheeja Sheela Rajan, *University of Johannesburg, South Africa*

P30: Photobiomodulation for enhanced neural embryoid body formation of Stem cells

Precious Earldom Mulaudzi, *University of Johannesburg, South Africa*

P31: Ag-H2O Nanofluids Synthesized via Pulsed Laser Liquid-Solid Interaction for Enhanced Photonics Integrated Circuit Cooling

Snenkosi Welcome Dlamini, *University of South Africa, South Africa*

P32: The UV-VIS spectrum of conjugated metal nanoparticles with some purposed COVID-19 drugs: a DFT study

Razieh Morad, *University of South Africa, South Africa*

P33: Nanofluid by pulsed laser ablation in liquid: Parameter influence

Meisam Aligholami, *University of South Africa, South Africa*

P34: Surface Enhanced Raman Spectroscopy and SERS/Drop-Coating Deposition Raman as Feasible Mechanisms for Detecting Dopants in Complex Matrices

Moses Juma, *University of South Africa, South Africa*

P35: Silver-Based Nanostructured Surface-Enhanced Raman Spectroscopy Technique for Enhancing Dexamethasone Detection

Nancy Mwikali Mwenze, *University of South Africa, South Africa*

P36: Biomimicry Highly reflecting material for radiative cooling

Nandipha L. Botha, *University of South Africa, South Africa*

P37: Development and In-Orbit Calibration of the New-Generation Solar Irradiance Spectrometer

Hui Wang, *Changchun Institute of Optics, Fine Mechanics and Physics, China*

List of Delegates

Prof Heidi Abrahamse	University of Johannesburg, South Africa
Dr Mahmood Akbari	ithemba Lab, South Africa
Mr Meisam Aligholami	ithemba Lab, South Africa
Mr Sadiq Aliyu	University of KwaZulu-Natal, South Africa
Ms Kari Apter	Optica, USA
Dr Nandipha Botha	ithemba Lab, South Africa
Dr Anine Crous	University of Johannesburg, South Africa
Prof Zhe Cui	Peking University, China
Ms Daniella Da Silva	University of Johannesburg, South Africa
Mr Ian Joel David	University of KwaZulu-Natal, South Africa
Mr Anthonie de Beer	Stellenbosch University, South Africa
Prof Anna Chiara De Luca	Institute of Endocrinology and Experimental Oncology IEOS, Italy
Mr Mikaeel Dindar	University of the Witwatersrand, South Africa
Snenkosi Dlamini	ithemba Lab, South Africa
Le Roi Du Plessis	Stellenbosch University, South Africa
Ms Anneke Erasmus	Stellenbosch University, South Africa
Ms Nosipho Fakudze	University of Johannesburg, South Africa
Prof Edwin Fohtung	Rensselar Polytechnic Institute, USA
Prof Andrew Forbes	University of the Witwatersrand, South Africa
Mr Eugene Fouche	Stellenbosch University, South Africa
Prof Sonja Franke-Arnold	University of Glasgow, UK
Prof Alex Gaeta	Columbia University, USA
Mr Bibin Mohan George	Mangosuthu University of Technology, South Africa
Prof Blassan George	University of Johannesburg, South Africa
Prof Qihuang Gong	Peking University, China
Mr Neelan Gounden	University of the Witwatersrand, South Africa
Prof Bo Gu	The Chinese Optical Society, China
Ms Dimakatso Gumede	University of Johannesburg, South Africa

Prof Carlos Hernández-García	Universidad de Salamanca, Spain
Prof John Howell	Chapman University, USA
Prof Yidong Huang	Tsinghua University, China
Mr Fortune Iga	University of the Witwatersrand, South Africa
Dr Yaseera Ismail	University of KwaZulu-Natal, South Africa
Dr Jose Merlin Jayaraj	University of Johannesburg, South Africa
Dr Moses Juma	ithemba Lab, South Africa
Ms Glory Kah	University of Johannesburg, South Africa
Ms Patricia Adrinah Kasowanjete	University of Johannesburg, South Africa
Prof Rasha Khafagy	Ain Shams University, Egypt
Ms Shiva Shafiei Khosroshahi	ithemba Lab, South Africa
Mr Mwezi Koni	University of the Witwatersrand, South Africa
Dr Martin Kroll	TU Dresden, Germany
Prof Tjaart Krüger	University of Pretoria, South Africa
Dr Thabang Lebepe	University of Johannesburg, South Africa
Prof Yan Li	Peking University, China
Prof Yue Li	Changchun Institute of Optics, Fine Mechanics and Physics, China
Prof Yun Li	Peking University, China
Prof Michal Lipson	Columbia University, USA
Prof Wenjing Liu	Peking University, China
Prof Xu Liu	Zhejiang University, China
Prof Yunquan Liu	Peking University, China
Dr Carmiña Londoño	Former National Science Foundation, USA
Mr Michael Lovemore	Univeristy of Pretoria, South Africa
Dr Masixole Lugongolo	CSIR, South Africa
Prof Maalik Maaza	ithemba Lab, South Africa
Ms Boitumelo Mabakachaba	iThemba Labs, South Africa
Mr Steven Makoni	Witwatersrand University, South Africa
Ms Tintswalo Mgwenya	University of Johannesburg, South Africa
Prof Humberto Michinel	Universidade de Vigo, Spain
Prof Kaoru Minoshima	University of Electro-Communications, Japan
Mr Light Mkhumbuza	University of the Witwatersrand, South Africa
Dr Hamza Mohamed	iThemba Labs, South Africa

Mr Kave Moloudi	University of Johannesburg, South Africa
Dr Chane Moodley	QLab, Raphta, South Africa
Prof Mathew Moodley	University of KwaZulu-Natal, South Africa
Dr Razieh Morad	ithemba Lab, South Africa
Dr Kelvin Mpofu	CSIR, South Africa
Dr Patience Mthunzi-Kufa	CSIR, South Africa
Ms Precious Earldom Mulaudzi	University of Johannesburg, South Africa
Ms Nancy Mwenze	ithemba Lab, South Africa
Dr Oliver Jermaine Myers	Clemson University, USA
Dr Darryl Naidoo	CSIR, South Africa
Dr Pieter Neetling	Stellenbosch University, South Africa
Ms Lufuno Nemakhavhani	University of Johannesburg, South Africa
Dr Lindokuhle Nene	University of Johannesburg, South Africa
Prof Francesco Petruccione	Stellenbosch University, South Africa
Ms Shivani Pillay	University of KwaZulu-Natal, South Africa
Ms Ursula Pillay	University of KwaZulu-Natal, South Africa
Ms Leila Raquel Pincay Abadiano	Escuela Politécnica Nacional, Ecuador
Prof Luis Plaja	Universidad de Salamanca, Spain
Dr Sheeja Sheela Rajan	University of Johannesburg, South Africa
Prof Roberta Ramponi	Politecnico di Milano, Italy
Mr Brendon Roets	University of Johannesburg, South Africa
Ms Bala Saraswathi	University of KwaZulu-Natal, South Africa
Dr Paromita Sarbadhikary	University of Johannesburg, South Africa
Prof Zouheir Sekkat	University of Rabat, Morocco
Mr Ameeth Sharma	CSIR, South Africa
Prof Ilya Sinayskiy	University of KwaZulu-Natal, South Africa
Mr Sachleen Singh	University of the Witwatersrand, South Africa
Dr Christine Steenkamp	Stellenbosch University, South Africa
Prof Xiaodi Tan	Fujian Normal University, China
Dr Lungile Thwala	CSIR, South Africa
Mr Nkgaphe Tsebesebe	CSIR, South Africa
Ms Marie Louise Umuhire	University of KwaZulu-Natal, South Africa

Prof Sivakumar Venkataraman	University of KwaZulu-Natal, South Africa
Prof Ahmadou Wague	Université Cheikh Abta Diop,Senegal
Ms Hui Wang	Changchun Institute of Optics, Fine Mechanics and Physics, China
Prof Zhexuan Wang	Tsinghua University, China
Prof Nathalie Westbrook	Institut d'Optique, France
Prof Hong Yang	Peking University, China
Prof Site Zhang	Changchun Institute of Optics, Fine Mechanics and Physics, China
Prof Wei Zhang	Tsinghua University, China

Abstracts of Oral and Poster Presentations

Accurate and fast calculation of wavefront modulation caused by multilayered surfaces

Site Zhang[1*], Ying Zhang[1,2] and Yanghao Zhen[1,2]

[1]*Ley Laboratory of Advanced Manufacturing for Optical Systems,*
Changchun Institute of Optics, Fine Mechanics and Physics, Chinese Academy of Sciences,
Dongnanhu Street No. 3888, Changchun, China
[2]*University of Chinese Academy of Sciences, Yanqihu East Road No. 1, Beijing, China*

*e-mail: `zhangsite@ciomp.ac.cn`

1. Introduction

Multilayer coatings are widely used in optics as the key components to increase the reflectance, particularly for short-wavelength applications. The HR-coatings, although designated to only alter the amplitude, will affect the polarization and phase. Additionally, when reflected by a multilayered surface, the reflected field sees a lateral shift with respect to the incidence[1], as shown in Fig. **1**(a). For mirrors coated with Si/Mo multilayer coatings[2], when the angle of incidence reaches 7.5°, the lateral shift is nearly one wavelength for both polarization modes, as shown in Fig. **1**(b).
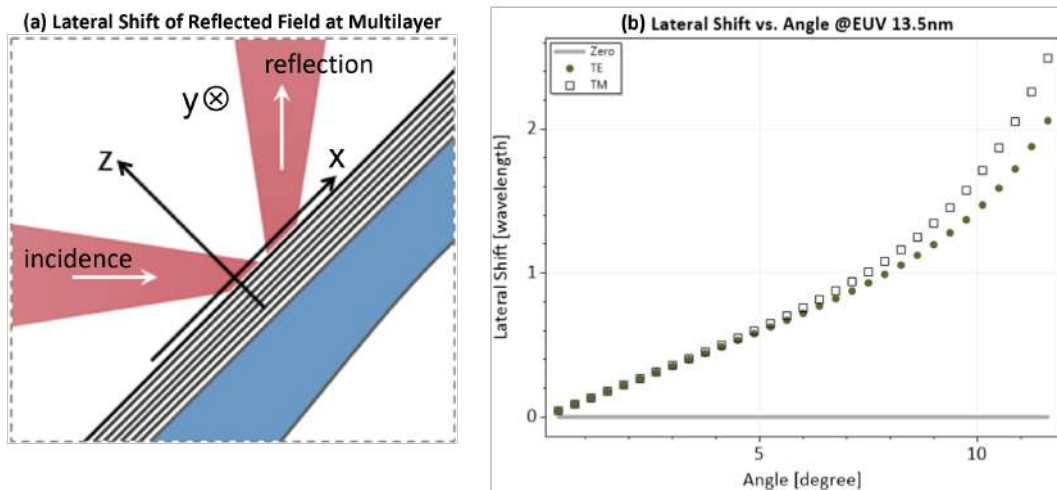
Figure 1: Reflection and lateral shift: (a) schematic of the lateral shift when reflected at multi-layered surface; (b) angle-dependent lateral shift for a 80-layer HR coating designed for 13.5 nm

In comparison to the visible and infrared cases, the short-wavelength applications often require thick coatings to obtain sufficiently high reflectance. Thus, the angle-dependent lateral shift and the corresponding wavefront modulation becomes non-negligible and must be analyzed with care.

2. Theory and Algorithm

Considering an infinitely large planar surface coated with laterally uniform multilayer, the reflected field can be calculated, by decomposing the incident field into plane waves with Fourier transform[4], as

$$E^{\mathrm{r}}(x) = \mathcal{F}^{-1}\left[r(k_x)\mathcal{F}\left[E^{\mathbf{in}}(x)\right](k_x)\right] , \tag{1}$$

where $\mathcal{F}$ and $\mathcal{F}^{-1}$ represents the forward and inverse Fourier transform respectively, $r(k_x)$ is the complex reflection coefficients calculated with respect to spatial frequency k_x. Eq. (1), despite of its rigorousness, requires numerical evaluation of two Fourier transform integrals.

In this work, we adopt the concept of homeomorphic Fourier transform[5] and show that the reflected field can be computed in a point-wise manner, as

$$E^{\mathrm{r}}(x - \Delta x) = \alpha(x) r(k_x(x)) E^{\mathbf{in}}(x) \exp(-i k_x(x) \Delta x), \qquad (2)$$

where $\alpha(x)$ is a real-valued scaling factor, $\Delta x = \mathrm{d}\phi(k_x)/\mathrm{d}k_x$ indicates the position/angle-dependent lateral shift, and $\phi(k_x) = \mathbf{Arg}\{r(k_x)\}$ is the phase part of the complex reflection coefficient $r(k_x)$. In comparison to a purely geometric-optics approach, where $E^{\mathrm{r}}(x) = r(k_x(x)) E^{\mathbf{in}}(x)$, the propose method in Eq. (2) takes the additional lateral shift and the phase change into account, and it still keeps the simplicity of point-wise operation.
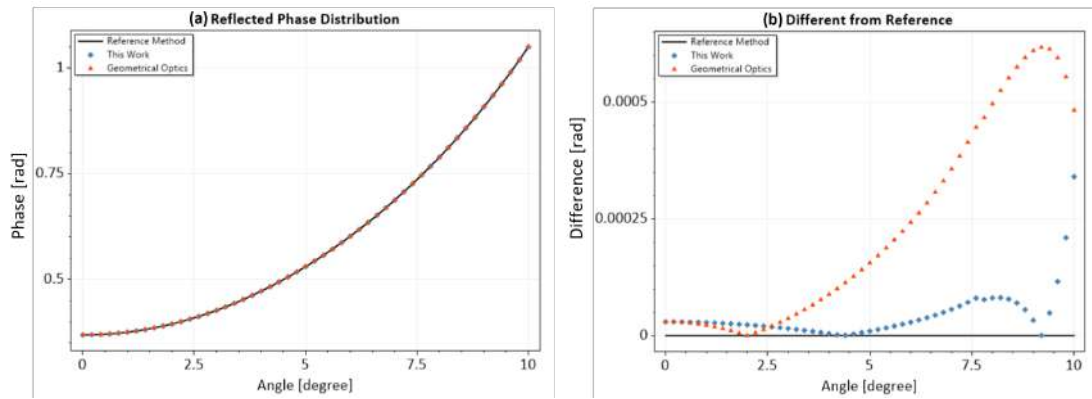
Figure 2: Reflection of a spherical wave from multilayered surface: (a) phase distribution calculated using different methods; (b) difference of the two methods from the reference [Eq. (1)]

The example and results in Fig. (**2**) validate the proposed method. It can be seen that the proposed method shows much better accuracy in comparison to the purely geometric-optics approach over the working angular range of the coating, as in Fig. **2**(b).

References

[1] M. Bal, F. Bociort, and J. J. Braat, "Influence of multilayers on the optical performance of extreme-ultraviolet projection systems", in *International Optical Design Conference* (SPIE 2002), vol. 4832, pp. 149-157.

[2] C. Montcalm, S. Bajt, P. B. Mirkarimi, E. A. Spiller, F. J. Weber, and J. A. Folta, "Multilayer reflective coatings for extreme-ultraviolet lithography", in *Emerging Lithographic Technologies II* (SPIE 1998), vol. 3331, pp. 42-51.

[3] J. Wang, C. Jin, L. Wang, and Y. Xie, "A model for multilayer analysis in a coated extreme ultra-violet lithography projection system", *Opt. Commun.* **332**, pp. 339-342 (2014).

[4] S. Zhang, C. Hellmann, and F. Wyrowski, "Algorithm for the propagation of electromagnetic fields through etalons and crystals", *Appl. Opt.* **56**, pp. 4566–4576 (2017)

[5] Z. Wang, O. Baladron-Zorita, C. Hellmann, and F. Wyrowski, "Theory and algorithm of the homeomorphic Fourier transform for optical simulations", *Opt. Express* **28**, pp. 10552-10571 (2020).

Artificial intelligence in photonics

Bo Gu

BOS Photonics, 100 Crossbow Lane, No.Andover, MA 01845, U.S.A.

*E-mail: b.gu@comcast.net

Abstract

Artificial intelligence (AI) is the most important new methodology in scientific research since adoption of quantum mechanics and it is providing exciting results in multiple fields of science and technology. Recently artificial intelligence has been used in photonics fields. We will review the current status and recent progress in this fast growing research area with an emphasis on the laser processing and micro machining fields.

References

[1] S. Russell and P. Norving, Artificial Intelligence: a Modern Approach. Pearson; 3rd Ed., 2010.

[2] S. Dutta, "An overview on the evolution and adoption of deep learning applications used in the industry," Wiley Interdisciplinary Reviews-Data Mining and Knowledge Discovery, e1257, vol. 8, 4, 2018

Attosecond Physics with Sculptured Circular Light Fields

Yunquan Liu[1*], Hong Yang[1] and Qihuang Gong[1]

1State Key Laboratory for Mesoscopic Physics and Frontiers Science Center for Nano-optoelectronics, School of Physics, Peking University, Beijing 100871, China

[*]E-mail: Yunquan.liu@pku.edu.cn

Laser-induced electron tunneling, triggering a broad range of ultrafast phenomena such as the generation of attosecond light pulses, photoelectron diffraction and holography, has laid the foundation of strong-field physics and attosecond science. Using the attoclock constructed by single-color elliptically polarized laser fields, previous experiments have measured the tunneling rates, exit positions, exit velocities and delay times for some specific electron trajectories, which are mostly born at the field peak instant where the laser electric field and the formed potential barrier are stationary in terms of the derivative versus time. From the view of the wave-particle dualism, the electron phase under a classically forbidden, tunneling barrier has not been measured, which is at the heart of quantum tunneling physics. Here we present a robust measurement of tunneling dynamics including the electron sub-barrier phase and amplitude. We combine attoclock technique with sculptured circular fields to accurately calibrate the angular streaking relation and to probe the non-stationary tunneling dynamics by manipulating a rapidly changing potential barrier. The sculptured attoclocks provides a general time-resolved approach to access the underlying quantum dynamics in intense-light-matter interactions.

References

1. M. Han et al., "Attoclock Photoelectron Interferometry with Two-Color Corotating Circular Fields, to Probe the Phase and the Amplitude of Emitting Wave Packets," " Phys. Rev. Lett. 120, 073202 (2018).
2. M. Han et al., "Unifying Tunneling Pictures of Strong-Field Ionization with an Improved Attoclock," Phys. Rev. Lett. 123, 073201 (2019).
3. P. Ge et al., "Universal Description of the Attoclock with Two-Color Corotating Circular Fields," Phys. Rev. Lett. 122, 013201 (2019).
4. Y. Fang et al. "Photoelectronic mapping of the spin–orbit interaction of intense light fields." Nat. Photonics (2020). https://doi.org/10.1038/s41566-020-00709-3
5. M. Han et al., "Complete characterization of sub-Coulomb-barrier tunneling with phase-of-phase attoclock," Nat Photonics 15, 765-771(2021).

Beam quality optimization to improve single-molecule spectroscopy signals

Michael A.C. Lovemore[1*], Towan Nöthling[1] and Schalk W. Bruwer[1], Tjaart P.J. Krüger[1]

[1]Department of Physics, University of Pretoria, Lynnwood Rd, Pretoria, South Africa

[*]E-mail: michael.lovemore98@gmail.com
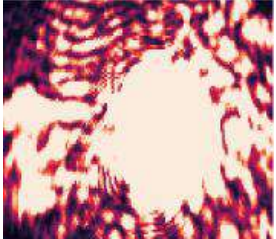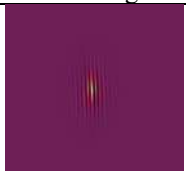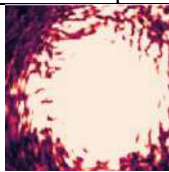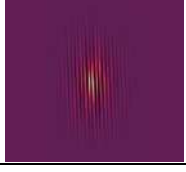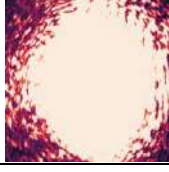
1. Introduction

Single-molecule spectroscopy (SMS) is a very sensitive and selective technique that can reveal fundamental information about single molecules within biological systems that cannot be resolved on the ensemble scale. Due to the low photon flux emitted by single molecules, it is important to optimize the signal-to-noise ratio. The background noise is typically minimized by using a high numerical aperture objective to focus the excitation light to the diffraction limit, and by focusing the emitted light through a confocal pinhole [1].

Gaussian and flat-top beams are known to have the smallest diffraction limits, directly implying that one could achieve a higher resolution in SMS [2,3] if such high-quality beams can be attained. Picosecond lasers are often used in SMS to get fluorescence lifetime information; however, these types of lasers are not aberration free. One way to get around this is to tailor the spatial profile of the beam by means of an encoded grayscale hologram on a spatial light modulator (SLM). The well-known orthogonal Zernike polynomials [4] can be utilized as a basis set to correct for any aberrations since an aberrated wavefront can be accurately described by a superposition of Zernike modes whose coefficient size is not affected by the number of terms used [5,6].
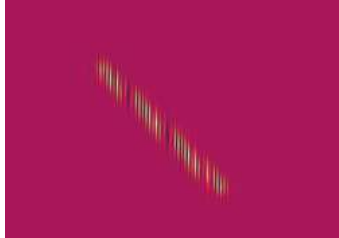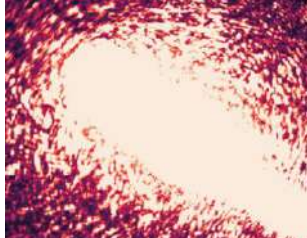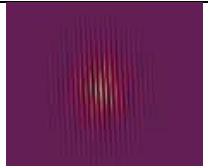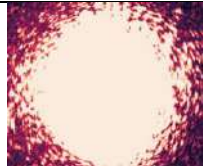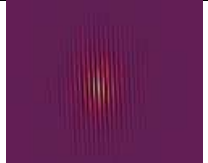
In this study, we aim to create an automated optimization procedure to generate a near-perfect Gaussian beam profile through the use of an SLM to attain the smallest achievable diffraction limit, such that our SMS signals can be improved. The method optimizes the Zernike coefficients used for the hologram generation in order to improve Gaussian beam quality to within a certain error margin.

2. Preliminary Results

Poor laser beam profile simulating hologram		Poor laser beam profile generated	
Iterations	Error value	Final Hologram	Final beam profile
2	0.01		
8	0.001		

Table 1 A few iterations to improve an initially poor Gaussian beam profile

Poor laser beam profile simulating hologram		Poor laser beam profile generated	
Iterations	Error value	Final Hologram	Final beam profile
4	0.01		
7	0.001		

Table 2 A few iterations to generate a Gaussian beam profile from an initial diagonal beam profile

We tested the effectiveness of our beam-correcting procedure by intentionally encoding a hologram related to a poor Gaussian profile (Table 1) and a diagonal beam (Table 2), respectively. After eight and seven iterations, respectively, the procedure was able to improve the beam quality to a near-Gaussian profile within an error margin of 0.001.

3. Conclusions

Our provisional results demonstrate the proof-of-concept of achieving a Gaussian beam profile by using Zernike polynomials as a basis set. We are currently improving our method to attain better quality in a significantly shorter time through a particle swarm optimization procedure.

Acknowledgments

References

[1] Krüger, Tjaart PJ, et al. "Fluorescence spectral dynamics of single LHCII trimers." *Biophys. J.* 98.12 (2010): 3093-3101.

[2] Paschotta, Rüdiger. *Field guide to laser pulse generation*. Vol. 14. Bellingham. SPIE (2008).

[3] Pawley, James, ed. *Handbook of biological confocal microscopy*. Vol. 236. Springer Science & Business Media (2006).

[4] Rosales-Guzmán, Carmelo, and Andrew Forbes. "How to shape light with spatial light modulators." SPIE (2017).

[5] Mafusire, Cosmas, and Tjaart PJ Krüger. "Strehl ratio and amplitude-weighted generalized orthonormal Zernike-based polynomials." *Appl. Opt.* 56.8 (2017): 2336-2345.

[6] Mafusire, Cosmas, and Tjaart PJ Krüger. "Zernike coefficients of a circular Gaussian pupil." *J. Mod Opt.* 67.7 (2020): 577-591.

Coherent diffraction imaging with structured x-ray photons

Edwin Fohtung[1]

[1]*Department of Materials Science and Engineering, Rensselaer Polytechnic Institute, 110 8th St, Troy, NY 12180, USA*

*e-mail: `fohtue@rpi.edu`

1. Introduction

Chiral crystals are materials with a lattice structure that has a well-defined handedness due to the lack of inversion, mirror, or other roto-inversion symmetries. Chirality is ubiquitous, drives many fundamental phenomena in condensed matter physics, and has significant scientific and technological implications. An important manifestation of chirality is the interaction between materials and light with handedness, such as molecular optical activity – the rotation of the polarization plane of light, chiral photonic waveguides, valley-selective light emission, and absorption, as well as magnetochiral effect and chiro-spintronics (including both spin detection and injection). These properties are the foundation of emerging photonic and spintronic devices. Understanding the crystal structure and electronic structure of chiral materials at high spatial resolution has been pursued for a long time. The conventional technique of using circular dichroism spectroscopy and focused-laser-based techniques suffer from low spatial resolution and low signal-noise ratio. The low signal-noise ratio is partially due to the small asymmetry ratio of circular dichroism (usually ~1% or below).

In this presentation, I will discuss our recent advancements in developing the X-ray coherent diffractive imaging (CDI) approach [1, 2, 3, 4, 5, 6] that utilizes OAM beams with opposite wavefront or phase helicity. CDI is a lensless nm high resolution 3D imaging technique that's primarily used for characterizing the structure of matter at the nanoscale. Over the years, it has become a powerful method for imaging with X-rays, electrons, and other wave-like probes. We demonstrate the BCDI technique in Fig. **1**, using a $BaTiO_3$ nanocrystal example from a recent publication on topological vortex dynamics [1]. The basic idea behind CDI is to recover an object's image from its coherent diffraction pattern without using a lens by using iterative phase retrieval algorithms on the measurements. I will address a specific issue related to chirality in structural and electronic order. We exploit the CDI method, which relies on OAM x-ray beams with opposing wavefronts or phase helicities, to probe individual structural dislocation pairs, chiral twin domains, and topological vortices and skyrmions in functional materials.

2. Conclusions

High-brilliance synchrotron radiation has advanced dichroic coherent diffractive imaging (CDI) beyond traditional optical polarimetry. My group has pioneered helical dichroic and birefringent CDI using twisted x-ray beams with orbital angular momentum (OAM). This method demands a fresh theoretical approach to the interaction of twisted x-rays with chiral matter. By leveraging the helical phasefront and beam polarization of twisted coherent beams, we've proposed innovative characterization techniques, such as x-ray helical dichroic CDI and in-line holography. These OAM-based interactions provide a refined method for examining chiral structures, making twisted x-ray an optimal tool for understanding chiral systems' fundamental structures and attributes at high resolutions.
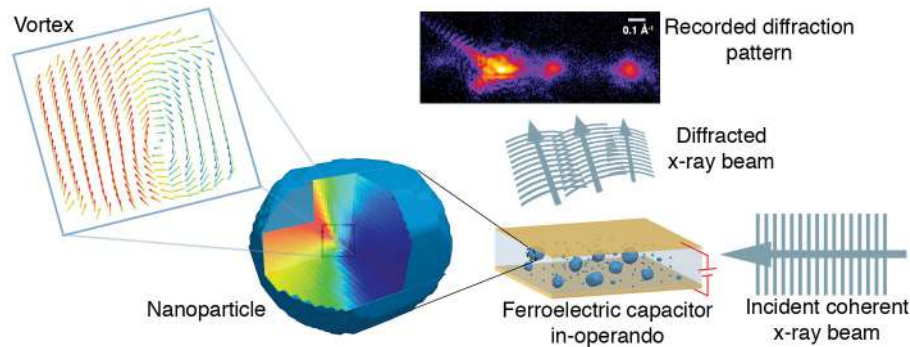
Figure 1: The experimental setup for BCDI and the inoperando functional capacitor. The figure illustrates the incident coherent X-ray beam scattered by a nanoparticle embedded in a conducting, non-polarizing polymer with attached electrodes. The resulting constructive interference patterns, recorded during the application of an external electric field to the particle, carry information on electron density and atomic displacement variations. This permits the reconstruction of the complex process of defect evolution and vortex monitoring [1]. This is an open access article distributed under the terms of the Creative Commons CC BY license, which permits unrestricted use, distribution, and reproduction in any medium, provided the original work is properly cited.

Acknowledgments

References

[1] D. Karpov, Z. Liu, T.D.S. Rolo, R. Harder, P.V. Balachandran, D. Xue, T. Lookman, and E. Fohtung, "Three-dimensional imaging of vortex structure in a ferroelectric nanoparticle driven by an electric field", *Nature Communications* **8**(1) (2017).

[2] X. Shi, J. Shi, and E. Fohtung, "Applicability of coherent x-ray diffractive imaging to ferroelectric, ferromagnetic, and phase change materials", *J. Appl. Phys* **131**, 40901 (2022). [Online]. Available: https://doi.org/10.1063/5.0072399.

[3] H. M. Quiney,G J Williams, and E. Fohtung,"Editorial for special issue on coherent diffractive imaging", *J. Opt.* **20**, 010201 (2018).

[4] A. Ulvestad, H. M. Cho, R. Harder, J. W. Kim, S. H. Dietze, E. Fohtung, Y. S. Meng, and O. G. Shpyrko, "Nanoscale strain mapping in battery nanostructures", *Applied Physics Letters* **104**(7), 073108 (2014).

[5] Z. Barringer, J. Jiang, X. Shi, E. Schold, A. Pateras, S. Cipiccia, C. Rau, J. Shi, and E. Fohtung, "Imaging defects in vanadium(III) oxide nanocrystals using Bragg coherent diffractive imaging", *CrystEngComm* **23**(36), 6239-6244 (2021).

[6] A. Pateras, R. Harder, S. Manna, B. Kiefer, R. L. Sandberg, S. Trugman, J. W. Kim, J. de la Venta, E. E. Fullerton, O. G. Shpyrko, and E. Fohtung, "Room temperature giant magnetostriction in single-crystal nickel nanowires", *NPG Asia Materials* **11**(1) (2019).

Deutsch-Josza Algorithm on Optical Vector Matrix Multipliers

Mwezi Koni [1*], Andrew Forbes [1] and Isaac Nape[1]

[1]*School Of Physics, University of the Witwatersrand, 1 Jan Smuts Avenue Johannesburg*

*e-mail: `mwezikoni5@gmail.com`

1. Abstract

Optical Vector Matrix Multipliers (OVMMs) hold potential for accelerating computational tasks requiring large matrix multiplication due their parallelism- the ability to send multiple light beams in space [1]. A particularly intriguing connection arises when considering quantum algorithms. By their intrinsic mathematical nature, quantum algorithms can often be distilled into vector-matrix multiplication problems. Here, quantum states, which encapsulate the essence of quantum systems, are portrayed as vectors in a complex Hilbert space, while the dynamics and transformations of these states, mediated by quantum gates, are characterised as matrices. The act of a quantum gate operating on a state directly parallels matrix-vector multiplication [2]. This structural and operational congruence suggests that OVMMs, with their capability for simultaneous processing of multiple light beams, might offer a fertile ground for the implementation of quantum algorithms. The inherent parallelism of OVMMs finds resonance with quantum mechanics' superposition principle, further strengthening the proposition. Building on this premise, our study introduces a novel approach to OVMM encoding through lattices of Gaussian modes instead of pixels, as depicted in Figure **1**a [3]. The experimental framework, employing two spatial light modulators (SLMs) facilitates this encoding. The first SLM encodes vector elements by imparting spatial information on the Gaussian states of light representing vector elements as a matrix. By propagating the resulting light to the next SLM, containing gate operation matrix, element-wise multiplication is carried out. The cylindrical lens and slit which perform one dimensional Fourier transform and select the zeroth momentum component act as the summing operator. Beyond its innovation, this method postulates reduced system noise due to the Gaussian modes' well-separated nature, potentially refining computational accuracy. Following this, as illustrated in Figure **1**b, the application of the Deutsch algorithm yielded promising outcomes.In our scheme, a measurement on the $|00...0\rangle$ is equivalent to extracting intesity on the first vector elements to establish whether $f(x)$ is constant or balanced. Preliminary trials computed matrices up to 16x16 dimensions, registering a fidelity marginally above 85%, showcased in Figure **2**. These findings hint at the broader applicability of OVMM in quantum computational simulations, marking a potential confluence of classical optical tools with quantum paradigms.

2. Conclusions

In this study, we have investigated the feasibility of employing Optical Vector Matrix Multipliers for quantum algorithm simulations, with an emphasis on the Gaussian mode encoding technique. Our preliminary findings offer some insights into the capability of OVMMs in this domain. While the results present a foundation, further studies are essential to delineate the full scope and limitations of such an approach within optical computing and quantum algorithm simulations.
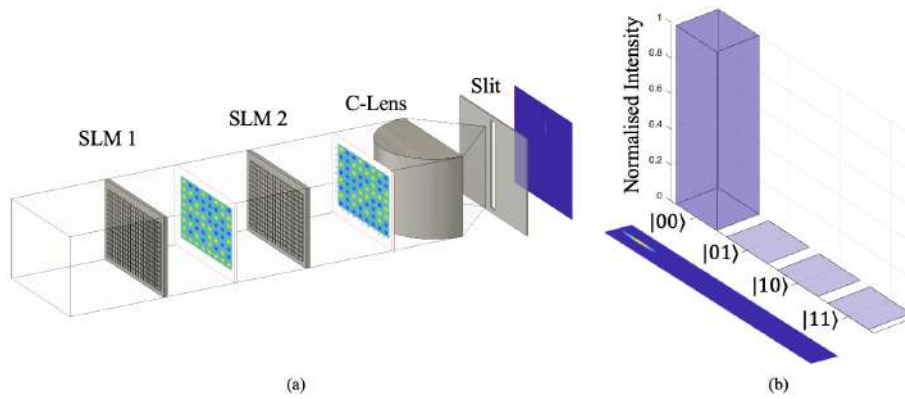
Figure 1: (a)A conceptual depiction of the OVMM setup highlighting the encoding technique using lattices of Gaussian modes instead of traditional pixels. (b)Illustration detailing the application of the Deutsch algorithm within the OVMM framework. It visually represents the correlation between the measurement on the $|00...0\rangle$ state and the extraction of intensity on the initial vector elements.
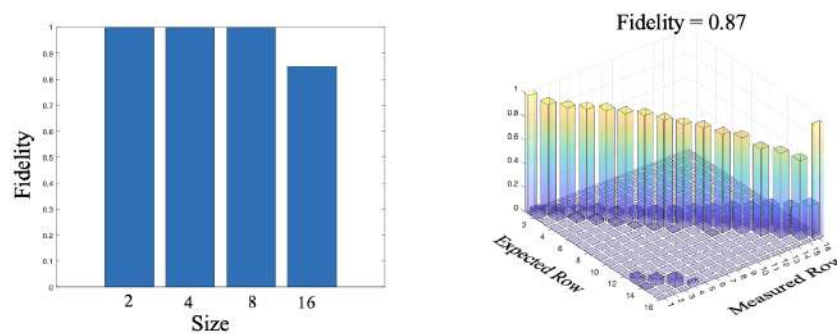
Figure 2: A fidelity plot showcasing the performance of our OVMM approach in computing matrices. The graph plots matrix dimensions against achieved fidelity, with particular attention to the peak performance of 16x16 dimensions registering a fidelity slightly above 85%

References

[1] Caulfield, H John and Dolev, Shlomi, "Why future supercomputing requires optics", *Nature Photonics* **4**, pp. 261–263 (2010).

[2] Nielsen, Michael A and Chuang, Isaac L, *Quantum computation and quantum information* (Cambridge university press, 2010).

[3] Spall, James and Guo, Xianxin and Barrett, Thomas D and Lvovsky, AI, "Fully reconfigurable coherent optical vector–matrix multiplication", *Optics Letters* **45**, pp. 5752–5755 (2020).

Development of a Cost Effective Fibre-based FSO System

Fortune Iga[1*] and Mitchell Cox[1]

[1]*Department of Electrical and Information Engineering, University of the Witwatersrand, 1 Jan Smuts Braamfontein, Johannesburg*

*e-mail: `igakayala@gmail.com`

1. Introduction

Fibre optic technology has revolutionized communication, enabling rapid data transmission over long distances. However, in South Africa, uneven distribution of fibre infrastructure has resulted in unequal internet access. Free space optical communication (FSO) offers a potential solution, by connecting users to nearby fibre infrastructure [1]. This talk presents a cost-effective bidirectional FSO prototype designed to couple light signals between two fibre cables separated by free space (see Fig. **1**). The system employs standard telecom fibre cables, which are cost-effective, readily available, and compatible with existing telecom hardware. Selecting the appropriate telecom fibre cable (SMF, OM1, OM2, OM3, OM4, and OM5) for the prototype requires evaluating their light transmission and reception capabilities, particularly in the presence of atmospheric turbulence.

Figure 1: Bidirectional FSO system which couples light between two fibre optic cables

2. Fibre Coupling in Atmospheric Turbulence

Atmospheric turbulence remains a significant challenge for fiber-based FSO systems. One of the pronounced effects of turbulence is beam wander, which leads to focal point misalignment in terms of lateral, longitudinal, and angular displacement at the receiving plane[2]. Consequently, this phenomenon results in power loss and deep fades, underlining the critical importance of precise alignment for efficient fiber coupling. To assess the resilience of standard fibre cables to focal point misalignment, a series of experiments were conducted. Misalignment was systematically induced on the fibre cables using a spatial light modulator. The aim was to understand how different fibre cables respond to controlled misalignment conditions and identify which cable exhibits the highest tolerance to misalignments. As seen from Fig. **2**, the OM1 fibre cable coupled the highest amount of optical power when faced with lateral, longitudinal and angular misalignments.

The FSO prototype uses a 75 mm plano-convex lens with a focal length of 200 mm, resulting in a numerical aperture of 0.18 and focal spot size of 5.26 μm at a wavelength of 1550 nm. The system underwent testing at the University of the Witwatersrand, covering a distance of 400 m.
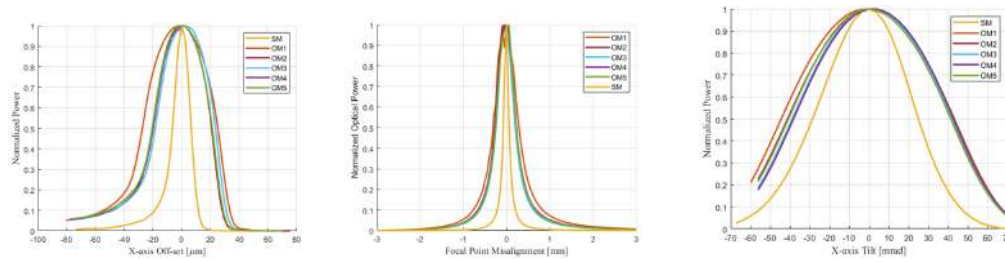
Figure 2: **Coupled Optical Power when faced with Focal point Misalignment. Left:** Coupled Power vs. Lateral Displacement **Middle:** Coupled Power vs. Longitudinal Misalignment **Right:** Coupled Power vs. Angular Misalignment

Performances of the OM1, OM4, and OM5 multi-mode fibre cables were tested. The average power coupled and scintillation indices experienced by each fibre cable were measured (see Fig. **3**). The light source used was a bidirectional small form factor pluggable transceiver module operating at wavelengths of 1510/1590 nm. The power coupled into each fibre cable was recorded using an infrared optical power meter. As seen from Fig. **3**, the OM1 fibre demonstrated the best performance among the tested cables. It exhibited the highest optical power coupling while experiencing the least amount of scintillation. This superior performance of the OM1 fibre suggests its robustness in handling the effects of atmospheric turbulence, making it a promising candidate for a reliable FSO system.
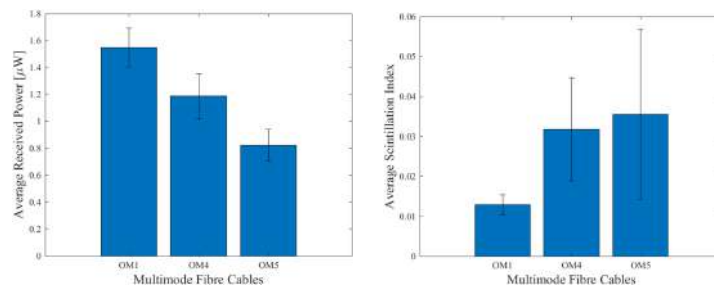
Figure 3: **Left**: Average Optical Power Coupled into Fibre Cables. **Right**: Scintillation Index experienced by Fibre Cables.

3. Conclusion

This research aims to provide an easily accessible FSO system which can be used to complement existing fibre infrastructure and help bridge the digital divide in South Africa. The findings from the misalignment tolerance experiments offer valuable insights in selecting a robust fibre cable for reliable FSO communication in challenging atmospheric conditions.

References

[1] M. A. Cox, L. Maqondo, R. Kara, G. Milione, L. Cheng and A. Forbes, "The Resilience of Hermite-and Laguerre-Gaussian Modes in Turbulence", *Journal of Lightwave Technology* **16**, pp. 3911–3917 (2019).

[2] M. A. Cox, L. Gailele, L. Cheng and A. Forbes, "Modelling the Memory of Turbulence-Induced Beam Wander", *arXiv: Signal Processing* (2019).

Development and In-Orbit Calibration of the New-Generation Solar Irradiance Spectrometer

Changchun Institute of Optics, Fine Mechanics and Physics, Chinese Academy of Sciences, China

Authors: Yue Li, Hui Wang

Email: liyue@ciomp.ac.cn

wangh@ciomp.ac.cn

Abstract:

High-precision observation of solar spectral irradiance plays a crucial role in gaining insights into the physical characteristics and activities of the Sun, space weather forecasting, as well as studying Earth's climate and ecology. Within the Earth's atmosphere, solar radiation is absorbed and scattered, particularly in the ultraviolet wavelength range, making it challenging to obtain accurate solar spectral irradiance data. Space-based observations can overcome these atmospheric interferences, providing more precise and comprehensive solar radiation data. Therefore, spaceborne instruments hold a special position in the field of solar spectral irradiance observations. However, the design of space instruments faces numerous constraints, including weight, size, power consumption, and the consideration of thermal regulation. On-orbit calibration of the instrument also presents several challenges.

This paper introduces the Solar Irradiance Spectrometer onboard the Fengyun-3 (05) satellite. The paper describes the principles, structure, and electronic design of the spectrometer. Additionally, the on-orbit calibration approach and a long-term degradation correction method for the instrument are presented. The observation results of the Solar Irradiance Spectrometer demonstrate its excellent spectral resolution in the visible wavelength range, effectively reflecting the detailed structure of solar radiation spectra. Currently, the development of the Fengyun-3(10) Solar Irradiance Spectrometer is underway. After the launch of this satellite, the instrument will enable network observations and further enhance irradiance observation accuracy.

Short Bios:

Yue Li earned his Ph.D. degree from Jilin University in 2012. He is currently a deputy researcher at the Changchun Institute of Optics, Fine Mechanics and Physics, Chinese Academy of Sciences. Dr. Li has over a decade of experience in optical engineering and his team has developed numerous optical instruments for various space missions.

Hui Wang is the deputy director of the International Cooperation Department and also serves as an editor for the journal "Light Science and Application." She has led multiple international cooperation projects, demonstrating her extensive experience in international collaboration.

Electron emission from graphene-hBN-graphene heterostructure

Zhexuan Wang, Fang Liu*, Yidong Huang*, Kaiyu Cui, Xue Feng and Wei Zhang

Department of Electronic Engineering, Tsinghua University, Beijing 100084, China

*E-mail: liu_fang@tsinghua.edu.cn, yidonghuang@tsinghua.edu.cn

1. Background

The low energy electron sources with accelerating voltage less than 1kV shows desirable properties for electron microscopy [1]. The short penetration depth of electron leads to high spatial resolution and high image contrast. And semiconductor and insulator materials can be detected directly due to the reduction of radiation damage and charging effects [2-4]. In this work, we propose and realize the low-voltage electron source based on planar graphene-hBN-graphene heterostructure (GBGH). By applying the external electric field strength of only $4 \times 10^4 \ V/m$, the maximum emission current density reaches $7mA/cm^2$. Tunable emission behaviors are observed and the emission I-V curve from GBGH is well explained according to the Fowler-Nordheim tunneling equation.

2. Results

Fig. 1(a) presents the schematic diagram of van der Waals heterostructure electron sources, where two graphene layers are insulated by hBN. Each of the graphene layer is contacted by an electrode. The schematic band structure of GBGH is shown in Fig. 1(b). The tunneled electrons emit from top graphene layer when their energy surpass the surface vacuum level. Otherwise, electrons flow as in-plane gate current.
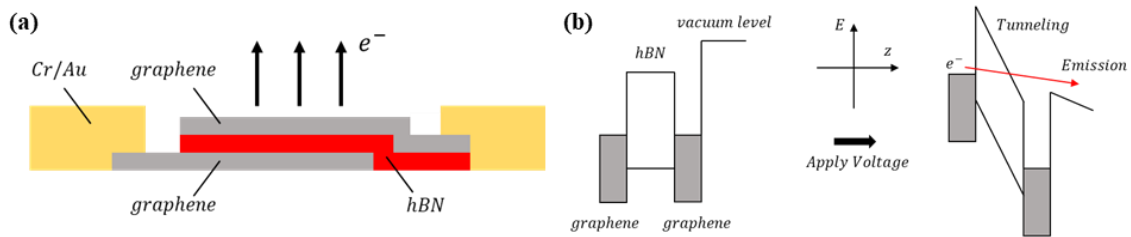
Figure 1 Electron source based on graphene-hBN-graphene heterostructure. (a) Schematic structure, (b) Schematic energy band.

We calculate the electrical properties of GBGH under different electric field strength by first-principle calculation. The heterostructure is modeled by three layers of Carbon, Boron and Nitride atoms as shown in Fig. 2(a). The supercell shape is consistent with pristine graphene and hBN hexagon unit cell as the lattice constant is optimized to 2.479Å in order to minimize the mismatch. Calculation results shown in Fig. 2(b) indicate that, under static electric fields, the projected band structure clearly changes. The energy difference between conduct band bottom of hBN and Dirac point is 3.317eV, which is considered as the potential barrier height in tunneling junction. As the applied electric field is normal to the interfaces, two graphene energy bands shift in opposite direction. The energy difference between two Dirac points reaches almost $10eV$, indicating that the Fermi level of bottom graphene layer is higher than the vacuum level of top graphene layer.
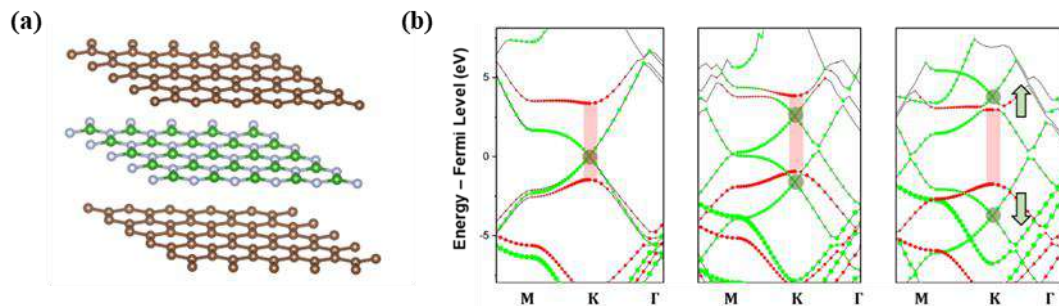
Figure 2 (a) Atomic structure. (b) Calculated projected bandstructure.

In experiment, we prepare the GBGH electron sources by mechanical exfoliation and stacking method. Few-layer graphene and hBN flakes is processed. Fig. 3(a) shows the transmission optical lens images, where the stacking area is measured as $59.29 \mu m^2$. Atomic Force Microscopy (AFM) is used to characterize the thickness and surface feature of heterostructure, as shown in Fig. 3(b). The thickness of few-layer hBN is $19.923 nm$ and the top graphene is $24 nm$.

The electrodes connecting to graphene layers are applied with negative voltages. Gate voltage of $-20V$ is set constantly while cathode voltage gradually changes. Anode collector is set at $500 \mu m$ above the substrate to collect emission electrons and ground. Therefore, the external electric field strength applied to the electron source is only 4×10^4 V/m. Measured results in Fig. 3(c) reveal that the stability of the emission current from GBGH is well performing at level of $0.1 nA$ and $1 nA$. Steady electron emission of over $1 nA$ and operating duration of $100s$ is observed from area of $59.29 \mu m^2$ stacking part. The maximum detected current density is over 7mA/cm^2.
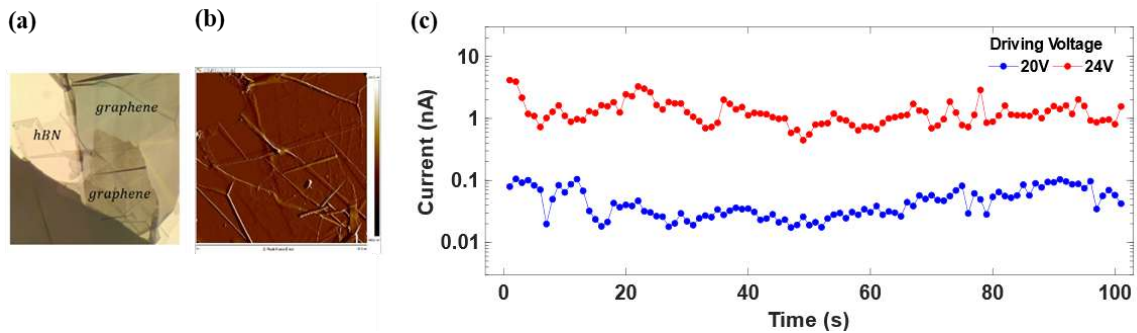
Figure 3 (a) Transmission optical lens images. (b) AFM measurements. (c) Electrons emission current behaviors.

3. Conclusion

We realize the low-voltage planar electron sources based on GBGH. The electric properties of GBGH is studied by first-principle calculation and the existence of tunneling junction in the static band structure of GBGH is verified. The electron sources is drived with an extremely low extracting voltage of $20V$ and driving voltage of about $24V$ experimentally, corresponding to the external electric field strength of only 4×10^4 V/m. Steady electron emission of over $1 nA$ and operating duration of $100s$ is observed from $59.29 \mu m^2$ stacking area in our experiments, and thus the maximum detected current density is $7 mA/cm^2$. The easy-fabrication and miniature on-chip electron sources with extremely low driving voltage will establish the promising prospect of the development of next-generation free electron devices.

References

[1] Brodusch, N., H. Demers, and R. Gauvin, Field Emission Scanning Electron Microscopy: New Perspectives for Materials Characterization. 2018.

[2] Ul-Hamid, A., A Beginners' Guide to Scanning Electron Microscopy. 2018.

[3] Bell, D. and N. Erdman, Low Voltage Electron Microscopy: Principles and Applications. 2013.

[4] Zewail, A.H., Four-Dimensional Electron Microscopy. Science, 2010. 328(5975): p. 187-193.

Fixing light with light

Sachleen Singh [1*], Bereneice Sephton[2], Wagner Tavares Buono[1], Vincenzo D' Ambrosio[2] and Andrew Forbes[1]

[1]*School of Physics, University of the Witwatersrand, Johannesburg 2050, South Africa*

[2]*University of Naples Federico II, Naples, Italy*

*e-mail: 2661774@students.wits.ac.za

1. Introduction

Typically aberrations are thought of as errors in the wavefront of light. These aberrations occur as light travels through optical systems, acquiring phase distortions along the way due to various factors like misalignment, imperfect optics, or even obstacles. These distortions, lead to a decrease in the quality of the light beam, which can result in various undesirable effects. For instance, if the eye's optical system has imperfections, aberrated incoming light will cause blurred eye vision [1]. Similarly, unwanted aberrations can degrade the quality of the optical trap affecting the rotational velocities of particles [2]. Even atmosphere or medium perturbations can induce distortions resulting in degraded signal quality through modal crosstalk [3].

However, these systems can be corrected using intricate adaptive optics systems. But before these aberrations are corrected these systems has to measure distorted wavefronts. This is often done with wavefront sensing techniques which can't keep pace with rapidly varying turbulence conditions and are less effective against higher-order aberrations[4].

We introduce an aberration correction technique based on the intrinsic properties of light itself [5]. By leveraging the natural phenomenon of optical phase conjugation based on a second-order nonlinear process called Difference Frequency Generation (DFG), we corrected the severe phase distortions within a light beam (signal). To elaborate more we designed a nonlinear interaction between a signal beam composed of Laguerre-Gaussian (LG) modes and an auxiliary Gaussian pump, such that both affected by same distortions effectively nullifying each other. The resulting DFG process not only facilitates the aberration correction but also enables obtaining the signal in a new frequency expanding the overall utility of the method. The reason it's called Difference Frequency Generation is that the new frequency is actually the difference between the frequencies of the input beams (pump and signal).

To achieve this nonlinear interaction we imaged both pump and signal beams onto a quasi-phase matched nonlinear crystal such that the output DFG mode is the product of pump and conjugate of signal mode

$$\mathrm{E}_{\mathrm{dfg}} = \mathrm{E}_{\mathrm{pump}} \times \mathrm{E}^*_{\mathrm{signal}} \tag{1}$$

The complex amplitudes for input beams will be altered due to system aberrations resulting in an additional aberration phase ϕ_p and ϕ_s on both pump and signal beams respectively.

$$\mathrm{E}'_{\mathrm{dfg}} = \mathrm{E}'_{\mathrm{pump}} \times \mathrm{E}'^*_{\mathrm{signal}} \tag{2}$$

$$\text{where} \qquad \mathrm{E}'_{\mathrm{pump}} = \mathrm{E}_{\mathrm{pump}} \exp(\mathrm{i}\phi_{\mathrm{p}}), \qquad \text{and} \qquad \mathrm{E}'_{\mathrm{signal}} = \mathrm{E}_{\mathrm{signal}} \exp(\mathrm{i}\phi_{\mathrm{s}})$$

But if both beams experience the same aberration then $\phi_p = \phi_s$ and it turns out that

$$\mathrm{E}'_{\mathrm{dfg}} = \mathrm{E}_{\mathrm{dfg}} \tag{3}$$

such that even after experiencing aberrations the output DFG mode is same as that of the unaberrated DFG mode. To ensure this we encoded same aberration phase employing spatial light modulator for each of the input beams [5].
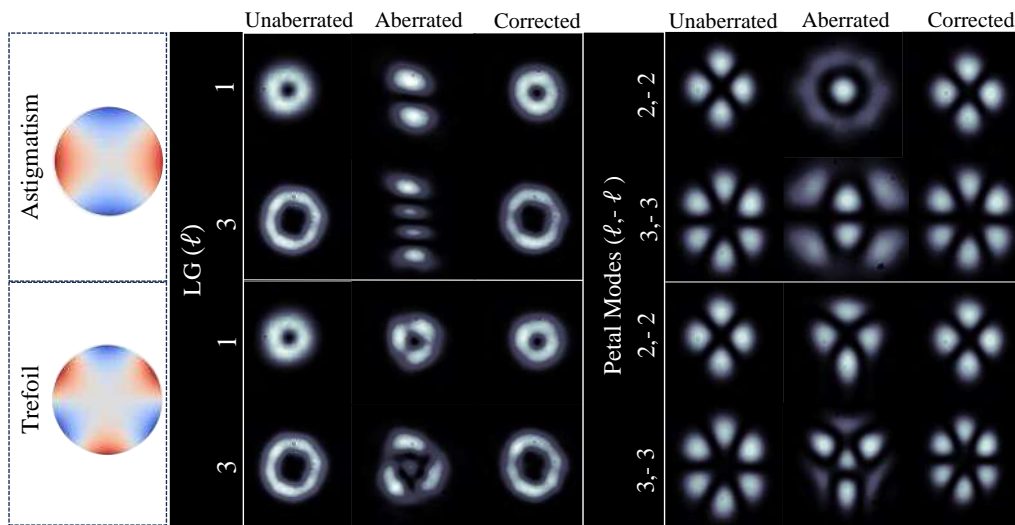
Figure 1: Above we present the correction for LG modes (left) and petal modes (right). The middle column is the aberrated beam profiles. The ℓ is the corresponding charge of the LG mode where petal modes are the superposition of two $\ell \,\&\, -\ell$ LG modes. The unaberrated beam and corrected beams on either side of the aberrated mode look very similar in their amplitude profiles showing the potential of the correction technique.

2. Results and discussion

In Fig. **1** the astigmatic aberration dissociates the LG mode of charge l to N = l + 1 bright lobes. Using the same astigmatism and trefoil on a Gaussian pump and allowing their image planes to coincide at the crystal plane, the splitting of bright lobes corrects itself into radially symmetric LG modes. Similarly, correction for superposition of LG modes or petal modes is shown on the right side of Fig. **1**. For instance, astigmatism turns superposition of LG modes with charge 2 and -2, into a bright spot with a ring around it. However, upon applying correction, it attains its petal structure similar to the unaberrated case. Likewise, for other petal modes be its trefoil or astigmatism, the unaberrated and corrected petal modes become completely identical to each other. Since this technique does not require any previous knowledge of the aberration, the correction procedure becomes independent of measurements provided both beams experience the same distortions. Thus, this presents a powerful tool for real-time aberration corrections making it highly useful for communication or trapping applications.

References

[1] M. Mujat, R. D. Ferguson, A. H. Patel, N. Iftimia, N. Lue, and D. X. Hammer, "High resolution multimodal clinical ophthalmic imaging system," *Optics express* **18**, 11607–11621 (2010).

[2] Y. Yang, Y.-X. Ren, M. Chen, Y. Arita, and C. Rosales-Guzmán, "Optical trapping with structured light: a review," *Advanced Photonics* **3**, 034001–034001 (2021).

[3] J. A. Anguita, M. A. Neifeld, and B. V. Vasic, "Turbulence-induced channel crosstalk in an orbital angular momentum-multiplexed free-space optical link," *Applied optics* **47**, 2414–2429 (2008).

[4] K. M. Hampson, R. Turcotte, D. T. Miller, K. Kurokawa, J. R. Males, N. Ji, and M. J. Booth, "Adaptive optics for high-resolution imaging," *Nature Reviews Methods Primers* **1**, 68 (2021).

[5] S. Singh, B. Sephton, W. T. Buono, V. Ambrosio and A. Forbes,"Light correcting light with non-linear optics," *Submitted* .

Future Perception Technology based on Nano-optoelectronics

Yidong Huang[1,2,*], Kaiyu Cui[1,2,*], Jian Xiong[1], Jiawei Yang[1], Fei Pan[1], Ning Wu[1],

Xue Feng[1,2], Fang Liu[1,2], and Wei Zhang[1,2]

[1] *Department of Electronic Engineering, Tsinghua University, Beijing 100084, China*

[2] *Beijing National Research Center for Information Science and Technology, Beijing 100084, China*

[*]E-mail: yidonghuang@tsinghua.edu.cn

1. Introduction

With the trend of the intelligent society, more dimensions and ultra-high precision of integrated sensors are required for the next generation of perceptual technology. In this work, spectral imaging as a new information dimension, and phonons as a new information carrier are explored based on manipulating light (photons) and mechanical motion (phonons) in periodic micro/nano structures. Accordingly, ultraspectral imaging chip, phonon lasing sensors and on-chip mechanical exceptional points are achieved, which pave the way for a new information dimension and a new information carrier of intelligent on-chip sensors.

2. Ultraspectral imaging chip

Traditional spectral analysis principles such as prism dispersion, grating diffraction or Fourier transform, are impossible to get dynamic spectral imaging of a target in real time. We demonstrated a one-shot miniaturized ultraspectral camera [1-3] fitting thousands of micro-spectrometers on a CMOS image sensor chip to realize real-time on-chip spectral imaging, as shown in Fig.1(a). Micro-spectrometers with high center-wavelength accuracy of 0.1nm and spectral resolution of 0.5 nm are realized.
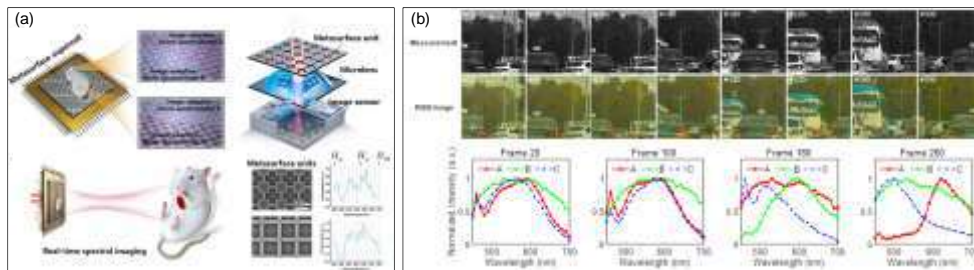
Figure 1 (a) Real-time ultraspectral imaging chip with reconfigurable metasurfaces [3]. (b) Rapid reconstruction of real hyperspectral data of an outdoor driving scene [4].

Moreover, we realize the fast reconstruction of spectral images and eliminate the mosaic effect by using the reconstruction algorithm ADMM-net [4]. The performance of image detail reconstruction using ADMM-net is significantly better than that using traditional point-by-point CVX spectral reconstruction algorithm, effectively eliminating the mosaic phenomenon in the spectral image. Here, the single reconstruction using ADMM-net takes only 18 milliseconds, which achieves about 5 orders of magnitude improvement compared with point-by-point spectral reconstruction. Furthermore, real-time spectral imaging of the outdoor driving scene was realized by using ADMM-net, as shown in Fig. 1(b). It can be seen that the concolorous sky and white cars can be distinguished via their reconstructed spectra. Thus, this result is promising to solve the problem of metamerism recognition in the automatic driving scene and avoid collision accidents.

3. On-chip phonon manipulation

As a system beyond photonics, the mechanical oscillators are easily coupled with various physical quantities. Detecting the changes in phonon frequency through light can realize the sensing of various physical quantities. We focus on the realization of phonon lasing because the linewidth of mechanical modes is a key parameter for achieving high sensing sensitivity [5-7], and in order to explore the way of higher precision perception, on-chip mechanical EPs is also studied [8-10].

By depositing masses with different weights on the optomechanical cavity, the measured mechanical frequency shift indicates a predicted minimum detected mass of 65 zeptograms (10^{-20} g), as shown in Fig. 2(a) [7]. The phonon lasing sensors show the potential of the ultra-sensitive sensing in various fields, such

as biological research, gas sensing, and environmental monitoring.

To further breaks through the limitation of linear response of phonon sensing, on-chip mechanical exceptional points (EPs) based on a silicon optomechanical zipper cavity was demonstrated [9]. EPs are special degenerate points of spectra that exist in the non-Hermitian system with unique physical effects and applications such as the Nth-order mode splitting near the EPs for high-sensitivity sensing capability. By tailoring the interaction between two mechanical modes through the optical field, we demonstrated anti-parity-time-symmetry mechanical EPs in an integrated optomechanical zipper cavity, as given in Fig. 2(b). This study provides an integrated on-chip platform for investigating the related physics of mechanical EPs, such as non-Hermitian phenomena, nonlinear effects, and phononic topology, and also suggests possible solutions to technical obstacles in applications such as ultrasensitive sensing and precision measurement of physical quantities.
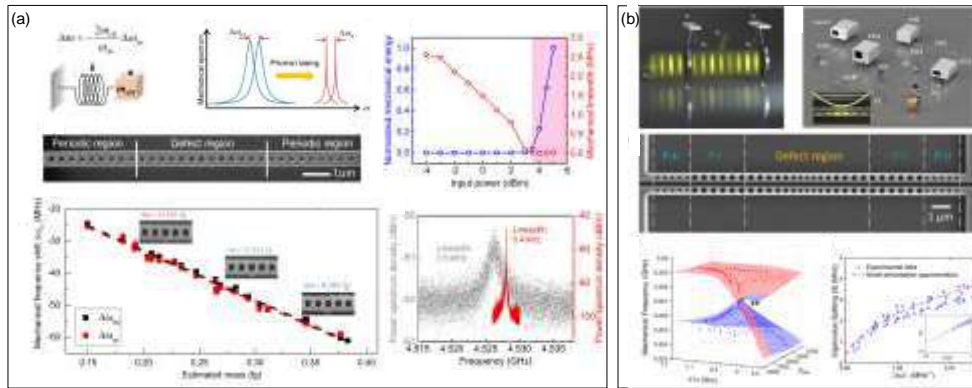
Figure 2 (a) On-chip optomechanical crystal (OMC) cavity-based mass sensing method [7]. (b) On-chip mechanical exceptional points based on an optomechanical zipper cavity [9].

Acknowledgments

References

[1] J. Xiong, X. Cai, K. Cui, Y. Huang, J. Yang, H. Zhu, W. Li, B. Hong, S. Rao, Z. Zheng, S. Xu, Y. He, F. Liu, X. Feng and W. Zhang, "Dynamic brain spectrum acquired by a real-time ultraspectral imaging chip with reconfigurable metasurfaces", Optica **9**, p. 461 (2022).

[2] J. Yang, K. Cui, X. Cai, J. Xiong, H. Zhu, S. Rao, S. Xu, Y. Huang, F. Liu, X. Feng and W. Zhang, "Ultraspectral Imaging Based on Metasurfaces with Freeform Shaped Meta-Atoms", Laser & Photonics Reviews **16**, p. 2100663 (2022).

[3] S. Rao, Y. Huang, K. Cui and Y. Li, "Anti-spoofing face recognition using a metasurface-based snapshot hyperspectral image sensor", Optica **9**, p. 1253 (2022).

[4] J. Yang, K. Cui, Y. Huang, W. Zhang, X. Feng and F. Liu, "Deep-learning based on-chip rapid spectral imaging with high spatial resolution", Chip **2**, p. 100045 (2023).

[5] J. Xiong, Z. Huang, K. Cui, X. Feng, F. Liu, W. Zhang and Y. Huang, "Phonon and photon lasing dynamics in optomechanical cavities", Fundamental Research **3**, p. 37 (2023).

[6] K. Cui, Z. Huang, N. Wu, Q. Xu, F. Pan, J. Xiong, X. Feng, F. Liu, W. Zhang and Y. Huang, "Phonon lasing in a hetero optomechanical crystal cavity", Photonics Research **9**, p. 937 (2021).

[7] F. Pan, K. Cui, Y. Huang, Z. Chen, N. Wu, G. Bai, Z. Huang, X. Feng, F. Liu and W. Zhang, "Phonon lasing enhanced mass sensor with zeptogram resolution under ambient conditions", Chip, p. 100050 (2023).

[8] Q. Xu, K. Cui, N. Wu, X. Feng, F. Liu, W. Zhang and Y. Huang, "Tunable mechanical-mode coupling based on nanobeam-double optomechanical cavities", Photonics Research **10**, p. 1819 (2022).

[9] N. Wu, K. Cui, Q. Xu, X. Feng, F. Liu, W. Zhang and Y. Huang, "On-chip mechanical exceptional points based on an optomechanical zipper cavity", Science Advances **9**, p. eabp8892 (2023).

[10] N. Wu, K. Cui, X. Feng, F. Liu, W. Zhang and Y. Huang, "Hetero-Optomechanical Crystal Zipper Cavity for Multimode Optomechanics", Photonics **9**, p. 78 (2022).

High Density Holographic Data Storage using Polarization Multiplexing

Xiaodi Tan[1,2,3], Jingyu Wang[1], Xianmiao Xu[1], Peiliang Qi[1], Shenghui Ke[1], Shujun Zheng[1], Tian Ye[1], Xinyi Yuan[1], Yi Yang[1,2], Xiao Lin[1,3], Zhiyun Huang[2,3] and Yuhong Ren[1]*

[1]Information Photonics Research Center, College of Photonic & Electronic Engineering, Fujian Normal University, Fuzhou, Fujian 350117, China

[2]Key Laboratory of Opto-Electronic Science and Technology for Medicine of Ministry of Education, Fujian Normal University, Fuzhou, Fujian 350117, Chinas

[3]Fujian Provincial Key Laboratory of Photonics Technology, Fujian Normal University, Fuzhou, Fujian 350117, Chinas

*E-mail: yhren@fjnu.edu.cn

In traditional holography, because the intensity distribution of two interference waves in which include amplitude and phase is recorded, only the same components of polarization state of two interference waves are considered. The actual polarization states of two interference waves are ignored. In polarization holography, not only amplitude and phase of two waves but also the polarization states of two waves, are recorded. As the reason, polarization holography is expected to have more abundant characteristics of reconstruction and a wide range of applications, such as holographic storage technology, multichannel polarization multiplexing, vector beams, and optical functional devices.

The old theory of polarization holography is based on Jones matrix formalism, where the angle between two lights to be interfered each other should be small, and the results are limited under the paraxial approximation[1]. However, since the tensor theory of polarization holography, in which the response of recording material to the polarized wave is treated as a tensor, is proposed K. Kuroda[2], the research of polarized holography has become hot, and has made a lot of new progress. The conditions of the null reconstruction, there is not reconstruction even Bragg condition is satisfied, in circular[3,4], linear[5] and elliptic[6] polarization holography were discovered. Another important research target is the condition of faithful reconstruction, in which the polarization state of the reconstructed wave is kept the same as that of the recording wave. In the tensor theory, the condition of faithful reconstruction is that some balance has to be satisfied in the case of linear[7], circular[3] and elliptical[8,9] polarization holography during 2015 and 2020. In this paper, the reconstruction characteristics of polarization holography which recorded by two linearly polarized state waves are discussed.

Linear polarization is the essential state, and any complex polarized state can be combined by linearly polarized state. There are also many researching works of reconstruction characteristics have been reported. for example: J Zang multi-channel recording at 90° [5,7,10]. C Wu not at 90° [11]. And it is also applied to data storage [12,13]. polarization holography for high density storage. The representative works are the dual- and four-channel polarization multiplexing scheme proposed by J Zang can separate and reconstruct the data pages loaded into the channel by adjusting the polarization state, which deeply taps the value of polarization information of light. In this review, the characteristic and behave of linear polarization holography have been introduced in detail, from principle to applications.

Acknowledgments

References

[1]   T. Todorov, L. Nikolova, and N. Tomova, "Polarization holography. 2: polarization holographic gratings in photoanisotropic materials with and without intrinsic birefringence," Appl. Opt. 23(24), 4588–4591 (1984).

[2]   Kazuo Kuroda, Yusugei Matsuhashi, Ryoshi Fujimura, and Tsutomu Shimura, "Theory of polarization holography," Opt. Rev. 18(5), 374–382 (2011).

[3] An'an Wu, Guoguo Kang*, Jinliang Zang, Ying Liu, Xiaodi Tan, Tsutomu Shimura and Kazuo Kuroda, "Null reconstruction of orthogonal circular polarization hologram with large recording angle," Optics Express, Vol. 23, No.7, 8880-8887 (2015).

[4] Jue Wang, Guoguo Kang*, An'an Wu, Ying Liu, Jinliang Zang, Peng Li, Xiaodi Tan, Tsutomu Shimura and Kazuo Kuroda, "Investigacion of the extraordinary null reconstruction phenomenon in polarization volume hologram," Optics Express, Vol.24, No.2, 1641-1647 (2016).

[5] Jinliang Zang, Guoguo Kang, Peng Li, Ying Liu, Fenglan Fan, Yifan Hong, Yong Huang, Xiaodi Tan, An'an Wu, Tsutomu Shimura and Kazuo Kuroda, "Dual-channel recording based on null reconstruction effect of orthogonal linear polarization holography," Optics Letters, Vol.42, No.7, 1377-1380 (2017).

[6] Long Shao, Jinliang Zang, Fenglan Fan, Ying Liu, and Xiaodi Tan*, "Investigation of the null reconstruction effect of an orthogonal elliptical polarization hologram at a large recording angle," Applied Optics, Vol.58, No.36, 9983-9989 (2019).

[7] Jinliang Zang, An'an Wu, Ying Liu, Jue Wang, Xiao Lin, Xiaodi Tan, Tsutomu Shimura, and Kazuo Kuroda, "Characteristics of Volume Polarization Holography with Linear Polarization Light," Optical Review, Vol.22, No.5, 829-831 (2015).

[8] Yiying Zhang, Guoguo Kang*, Jinliang Zang, Jue Wang, Ying Liu, Xiaodi Tan, Tsutomu Shimura, Kazuo Kuroda, "Inverse polarizing effect of elliptical-polarization recorded hologram at large cross angle," Optics Letters, Vol.41, No.17, 4126-4129 (2016).

[9] Zhiyun Huang, Youwu He, Tiangui Dai, Lili Zhu, Ying Liu, Xiaodi Tan*, "Prerequisite for faithful reconstruction of orthogonal elliptical polarization holography," Optical Engineering, Vol.59, No.10, 102409(7p) (2020).

[10] Jinliang Zang, Fenglan Fan, Ying Liu, Ran Wei, Xiaodi Tan*, "Four-channel volume holographic recording with linear polarization holography," Optics Letters, Vol.44, No.17, 4107-4110 (2019).

[11] Wu Chenhao, Chen Yuxin, Huang Zhiyun*, Song Haiyang, Tan Xiaodi*, "Orthogonal Reconstruction in Linear Polarization Holography," Laser & Optoelectronics Progress, Vol.58, No.4, 0409001(5p) (2021).

[12] Xiao Lin, Jinpeng Liu, Jianying Hao, Kun Wang, Yuanying Zhang, Hui Li, Hideyoshi Horimai, Xiaodi Tan*, "Collinear holographic data storage technologies," Opto-Electronic Advances, Vol.3, No.3, 190004(10p) (2020).

[13] Jianying Hao, Xiao Lin*, Yongkun Lin, Mingyong Chen, Ruixian Chen, Guohai Situ, Hideyoshi Horimai and Xiaodi Tan*, "Lensless complex amplitude demodulation based on deep learning in holographic data storage," Opto-Electronic Advances, Vol.6, No.3, 220157(15p) (2023).

Influence of 2 MeV Proton irradiation on Vanadium dioxide(VO$_2$)'s optical and electrical characteristics.

B.M. Mabakachaba[a,c,*], I.G. Madiba[b,c], N. Numan[b,c], Z.M. Khumalo[c], C.B. Mtshali[c], M. Nkosi[c], S. Halindintwali[a], M. Maaza[b,c]

[a]University of the Western Cape, Department of Physics, Robert Sobukwe Rd, Bellville, Cape Town 7535, South Africa
[b]UNESCO-UNISA Africa Chair in Nanosciences/Nanotechnology, College of Graduate Studies, University of South Africa (UNISA), Muckleneuk Ridge, P O Box 392, Pretoria, South Africa
[c]iThemba LABS-National Research Foundation, 1 Old Faure Road, Somerset West 7129, PO Box 722, Somerset West, Western Cape Province, South Africa
*Corresponding author e-mails: mabakachaba@gmail.com

Abstract

Vanadium dioxide thin films were successfully subjected to proton irradiation. X-ray diffraction (XRD), Atomic force microscopy(AFM), UV-Vis spectroscopy and two point probe techniques were utilized to evaluate the structural, morphology, optical and electrical characteristics of VO$_2$ before and after irradiation, while SRIM code was also used to simulate the radiation damage caused by the target ions. It was established that fluence variation altered the microstructure and morphology of thermochromic thin films. Pristine and proton-irradiated films were observed to be well-crystallized and well-oriented in the (01 1) plane at $2\theta \sim 28.05°$, confirming the existence of the VO2(M) phase. Since the majority of the ions were deposited in the substrate layer, the films retained their ideal structure configurations even after being subjected to irradiation. The study indicates that with the ion's projected penetration depth of 21.69 μm, most of the ions are distributed in the substrate, inflicting more damage there with the ion's lossing their energy in the film of interest through electronic energy loss.

Keywords— Phase transition, Vanadium dioxide, proton, exposure time/Fluence, Irradiation

Laser and Ion Beam Writing for Quantum Photonic Devices in Diamond

Roberta Ramponi[1,2*], Giulio Coccia[1,2], Yanzhao Guo[3,4], Akhil Kuriakose[5,6], Sahnawaz Alam[7], Sajedeh Shahbazi[8,9], Anthony J. Bennett[3,4], Vibhav Bharadwaj[8,9], J. P. Hadden[3,4], Ottavia Jedrkiewicz[5], Paweł Machnikowski[7], Alexander Kubanek[8,9], and Shane M. Eaton[1]

[1]*IFN-CNR Milano, p. Leonardo da Vinci 32, 20133 Milano, Italy*
[2]*Politecnico di Milano-Department of Physics, p. Leonardo da Vinci 32, 20133 Milano, Italy*
[3]*School of Engineering, Cardiff University, Queen's Buildings, The Parade, Cardiff CF24 3AA, United Kingdom*
[4]*Translational Research Hub, Maindy Road, Cardiff CF24 4HQ, United Kingdom*
[5]*IFN-CNR Como, via Valleggio 11, 22100 Como, Italy*
[6]*University of Insubria-DiSAT, via Valleggio 11, 22100 Como, Italy*
[7]*Institute of Theoretical Physics, Wrocław University of Science and Technology, 50-370 Wrocław, Poland*
[8]*Institute for Quantum Optics, Ulm University, Albert-Einstein-Allee 11, 89081 Ulm, Germany*
[9]*Center for Integrated Quantum Science and Technology (IQst), Ulm University, Albert-Einstein-Allee 11, 89081 Ulm, Germany*

*E-mail: roberta.ramponi@polimi.it

1. Introduction

The nitrogen-vacancy (NV) center is a defect in which two adjacent sites in diamond's tetrahedral lattice of carbon atoms are replaced. One site contains a nitrogen atom instead of carbon while the other is vacant. In its negatively charged state, the NV center gains an extra electron from the lattice, forming a ground state spin system which can be polarized with 532-nm light, even at room temperature. One of the spin states fluoresces much more brightly than the others so that fluorescence can be used for spin-state readout. At the same time, the NV's electron spin states are sensitive to magnetic and electric fields through the Zeeman and Stark effects, respectively. These properties make NVs in diamond very attractive both as an integrated and scalable platform for quantum information systems and for high sensitivity electromagnetic field quantum sensors.

An integrated optics platform in diamond is essential for both quantum information systems and quantum enabled electric and magnetic field sensing, where the NV is used as an optically detecting atomic probe. This is because of the ultimate stability and integration provided by monolithic waveguides, in addition to the potential for enhanced optical interaction with NVs.

Another promising quantum emitter in diamond is the Silicon vacancy (SiV), which has a narrow zero phonon line and a large Debye-Waller factor, making it suitable as a single photon source for quantum optics.

2. Results and Discussion

For the first time, 3D laser microprocessing is combined with ion implantation nanofabrication to exploit the advantages of both techniques to achieve integrated high quality quantum emitters and buried optical waveguides in diamond.

On one side, femtosecond laser micromachining has proved to be very efficient in the fabrication of a full portfolio of components in diamond chips, in particular waveguides, microchannels and NV quantum emitters in an intrinsically 3D geometry [1], thus allowing the realization of integrated quantum circuits and microfluidic components very promising for both quantum sensing and quantum information. A further advantage of this fabrication technique is that it provides large mode-field diameters, well matching fiber optic technology.

On the other side, ion implantation can be used to form NV quantum emitters at nanometric depths at the end facets of laser written 3D optical waveguides. This hybrid fabrication scheme enables development of two-dimensional quantum sensing arrays, facilitating spatially and temporally correlated magnetometry. This innovative method is also applied to implant SiV in laser written photonic circuits, to engineer light at the single photon level, which could enable next generation quantum computation systems in diamond [2].

Acknowledgments

References

[1] A. N. Giakoumaki, G. Coccia, V. Bharadwa, J. P. Hadden, A. J. Bennett, B. Sotillo, R. Yoshizaki, P. Olivero, O. Jedrkiewicz, R. Ramponi, S. M. Pietralunga, M. Bollani, A. Bifone, P. E. Barclay, A. Kubanek and S. M. Eaton, "Quantum technologies in diamond enabled by laser processing", Appl. Phys. Lett. **120**, 020502 (2022).

[2] M. K. Koch, M. Hoese, V. Bharadwaj, J. Lang, J. P. Hadden, R. Ramponi, F. Jelezko, S. M. Eaton, and A. Kubanek, "Super-Poissonian Light Statistics from Individual Silicon Vacancy Centers Coupled to a Laser-Written Diamond Waveguide", ACS Photonics **9**(10), pp. 3366–3373 (2022).

Magnetically-dressed CrSBr exciton-polaritons in ultrastrong coupling regime

Tingting Wang[1,2,*], Dingyang Zhang[1,*], Shiqi Yang[1,3,*], Zhongchong Lin[1], Quan Chen[4], Jinbo Yang[1], Qihuang Gong[1,5,6], Zuxin Chen[4,†], Yu Ye[1,2,5,†] and Wenjing Liu[1,5,6,†]

[1]*State Key Laboratory for Mesoscopic Physics and Frontiers Science Center for Nano-optoelectronics, School of Physics, Peking University, Beijing 100871, China*
[2]*Collaborative Innovation Center of Quantum Matter, Beijing 100871, China*
[3]*Academy for Advanced Interdisciplinary Studies, Peking University, Beijing 100871, China*
[4]*School of Semiconductor Science and Technology, South China Normal University, Foshan, 528225, China*
[5]*Yangtze Delta Institute of Optoelectronics, Peking University, Nantong 226010, China*
[6]*Collaborative Innovation Center of Extreme Optics, Shanxi University, Taiyuan, 030006, China*
⋆These authors contributed equally
†Corresponding author: chenzuxin@m.scnu.edu.cn, ye yu@pku.edu.cn, wenjingl@pku.edu.cn

The profound interplay between photons and matter excitations, such as excitons, phonons, and magnons, is crucial in studying light-matter interactions, bridging quantum states for coherent quantum information transmission, storage, and processing. This is essential for constructing photonic quantum networks. Over time, exciton-polaritons, with their dual light-matter nature, have garnered significant attention. Coupling them with magnetic orders has been limited by material availability with simultaneous exciton resonances and magnetic ordering. Here, we present findings on magnetically-dressed microcavity exciton-polaritons in van der Waals antiferromagnetic (AFM) semiconductor CrSBr coupled to a Tamm plasmon microcavity. Angle-resolved spectroscopy shows an exceptionally high exciton-polariton coupling (169 meV), persisting up to room temperature, revealing ultrastrong coupling. Temperature-dependent spectroscopy confirms the magnetic nature, transitioning from AFM to paramagnetism in CrSBr. An out-of-plane magnetic field effectively tunes polariton energy, maintaining ultrastrong exciton-photon coupling, attributed to spin canting modulating interlayer exciton interaction. Our work proposes a robust hybrid quantum platform, promising for quantum interconnects and transducers, with applications in emerging quantum technologies.
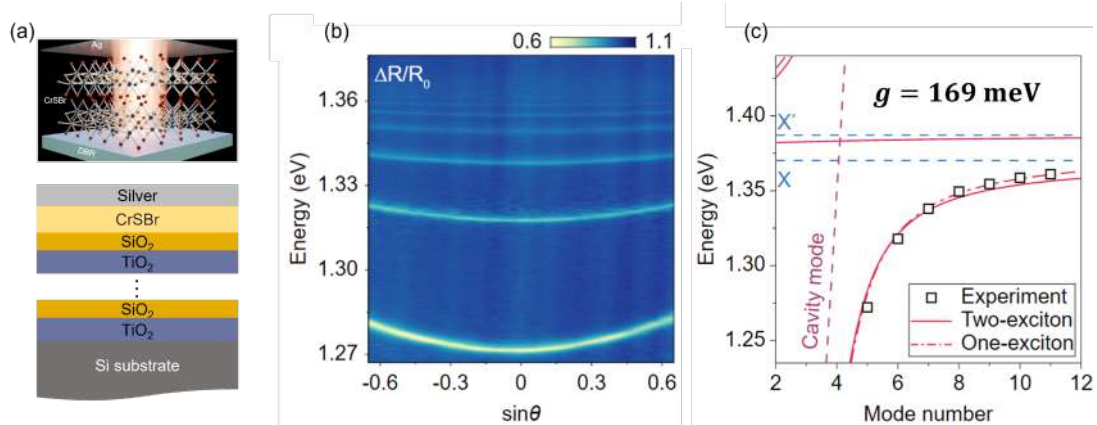
Figure 1. Ultrastrong coupling between CrSBr thin film and Tamm microcavities. (a) Schematic of the coupled structure. (b) Angle-resolved dispersion of the CrSBr-Tamm cavity coupled structure. (c) Coupling strength extracted from the fitting

1. Conclusions

In conclusion, we present a demonstration of ultrastrongly coupled exciton-polaritons within CrSBr, amenable to effective manipulation through interlayer magnetic order. These discoveries unlock avenues for intricate many-body physics within hybrid quantum systems, orchestrating coherent interactions among diverse quasiparticles across a broad energy spectrum. The integration of exciton-mediated coupling within photonic structures and magnetic orders holds the potential to rejuvenate constrained magnetic responses in passive photonic systems operating in the optical wavelength realm. This breakthrough could usher in photonic devices endowed with novel functionalities, including non-reciprocal transmissions, unconventional topologies, and magnetically adjustable Bose-Einstein condensates. Furthermore, the integration of vdW CrSBr with other 2D materials into heterostructures paves the way for highly integrated on-chip opto-electronic-magnetic devices.

References

[1] Tingting Wang, Dingyang Zhang, Shiqi Yang, Zhongchong Lin, Quan Chen, Jinbo Yang, Qihuang Gong, Zuxin Chen, Yu Ye, Wenjing Liu, Magnetically-dressed CrSBr exciton-polaritons in ultrastrong coupling regime, arXiv preprint arXiv:2302.07616

Modelling OAM crosstalk due to tilt and displacement with neural networks

Steven Makoni [*1], Ling Cheng[1] and Mitchell Cox[1*]

[1]*School of Electrical and Information Engineering, University of the Witwatersrand, Johannesburg, South Africa*

[*]e-mail: `mitchell.cox@wits.ac.za` and `1935885@students.wits.ac.za`

1. Introduction

Free-Space Optical (FSO) communication utilizes Orbital Angular Momentum (OAM) modes in Mode Division Multiplexing (MDM) [1], but turbulence-induced OAM crosstalk impairs performance, especially for higher OAM modes. Analytical models for OAM crosstalk exist for Gaussian modes but lack expressions for higher OAM modes [2]. Previous papers offered numerical expressions for misaligned OAM beam profiles that calculate the OAM spectrum due by using a decomposition method [3]. However, experimental verification of these calculated OAM spectrums was lacking. A novel method, based on optical geometric transformation, was introduced in reference [4] to experimentally determine the OAM spectrum and compare it with modal decomposition and simulation results. Nevertheless, an analytical expression of OAM crosstalk for an arbitrary ℓ input mode is yet to be established. In this work, we leverage machine learning to predict the OAM spectrum due to tilt and displacement. Our approach presents a simple multilayer neural network capable of predicting OAM crosstalk for an arbitrary ℓ input mode $\in$ [-5,5].

2. Methodology

The OAM spectrum due to tilt and displacement was measured using a custom-built experimental setup with a laser source (632.8 nm) emitting Laguerre-Gaussian beams. A spatial light modulator (SLM) controlled the tilt and displacement of the OAM beams and modal decomposition was optically performed for the OAM spectrum. A simulation model closely matched the experimental conditions, calculating the OAM spectrum for the same tilt and displacement combinations. The simulation used the same OAM modes as the experiment. From the simulated data, a dataset was generated to train and evaluate the neural network (NN), covering various ℓ input modes and tilt-displacement values.

3. Results and discussion

In Fig. **1**, the correlation and accuracy of OAM spectra of different input modes, ℓ (indicated with green color) are presented. The simulation results closely align with the experimental findings, thereby confirming the accuracy of the simulation model. The plots showcase diverse OAM spectra originating from different input modes, ℓ, each influenced by distinct random combinations of tilt and displacement settings. For visual clarity, the specific values of these combinations are omitted, with the emphasis placed on highlighting the agreement between the measured and simulated OAM spectra, as well as showcasing the predictive capabilities of the MLP model in replicating the observed OAM spectrum. The trained neural network effectively predicts the OAM spectrum for different tilt and displacement values, closely matching the experimental and simulated results.
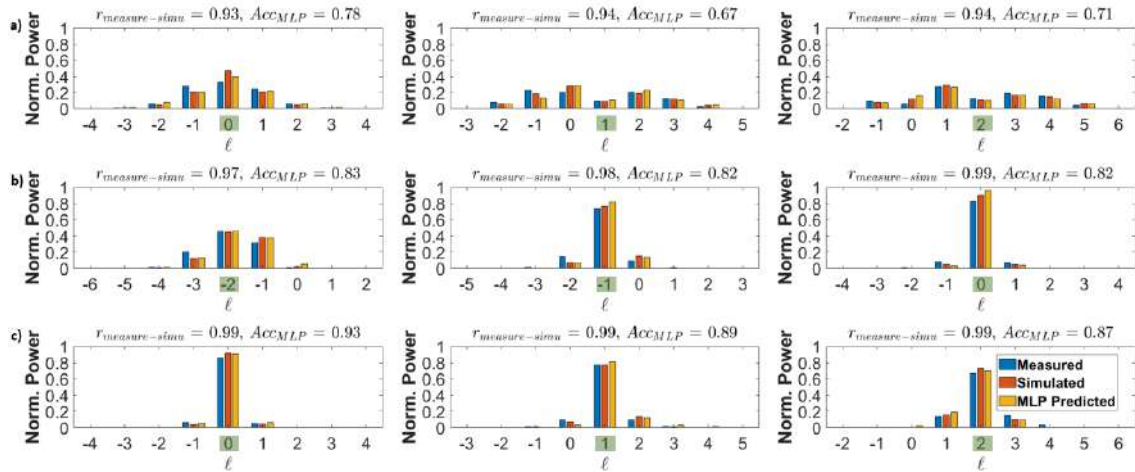
Figure 1: The correlation ($r_{measure-simu}$), and accuracy (Acc_{MLP}) of OAM spectrum across various cases imposed: (a) focusing on lateral displacement only, (b) considering tilt only, and (c) a combination of both tilt and lateral displacement. In the graph, blue bars represent the ground truth modal decomposition, red bars depict the simulated decomposition utilized for NN training, and orange bars represent the NN's predictions. The green ℓ value indicate the input mode

The comparison between experimental, simulated, and predicted OAM spectra shows a strong correlation, highlighting the reliability of the neural network approach in capturing the complex relationship between tilt, displacement, and OAM crosstalk for arbitrary ℓ input modes.

4. Conclusions

The neural network's accuracy indicates its efficiency in predicting OAM crosstalk in MDM systems, including higher OAM modes where analytical expressions were absent. Our proposed neural network-based approach presents a promising solution for practical FSO communication systems, filling a gap in the existing literature by providing an analytical expression for arbitrary ℓ input modes. This research holds potential for enhancing MDM system design and performance in turbulent atmospheric conditions. Nonetheless, it is crucial to address potential limitations in the training dataset and improve the model's performance under varying turbulence conditions.

References

[1] J. Wang and et al, "Orbital angular momentum and beyond in free-space optical communications", *Nanophotonics* **4**, pp. 645–680 (2022).

[2] J. Lin, X. C. Yuan, M. Chen, and J. C. Dainty, "Application of orbital angular momentum to simultaneous determination of tilt and lateral displacement of a misaligned laser beam", *J. Opt. Soc. Am. A* **27**, pp. 2337–2343 (2010).

[3] M. V. Vasnetsov and V. A. Pas'ko and M. S. Soskin, "Analysis of orbital angular momentum of a misaligned optical beam", *New Journal of Physics* **7**, pp. 46 (2005).

[4] M. P. J. Lavery and G. C. G. Berkhout and J. Courtial and M. J. Padgett, "Measurement of the light orbital angular momentum spectrum using an optical geometric transformation", *Journal of Optics* **6**, pp. 46 (2011).

Multiple single-photon chiral edge states generated in the fractal photonic anomalous Floquet topological insulator

Yan Li[1,2,3*], Meng Li[1,2*], Chu Li[1,2], and Qihuang Gong[1,2,3]

[1] *State Key Laboratory for Artificial Microstructure and Mesoscopic Physics, School of Physics, Peking University, Beijing 100871, China.*

[2]*Frontiers Science Center for Nano-Optoelectronics, Peking University, Beijing 100871, China.*

[3]*Hefei National Laboratory, Hefei 230088, China.*

*E-mail: li@pku.edu.cn; mengli2016@pku.edu.cn

1. Introduction

Anomalous Floquet topological insulator (AFTI) has nonzero winding numbers to support topological edge modes, though its standard topological invariants like Chern numbers are zero [1]. Although photonic AFTIs have been widely investigated, most of them usually support only one kind of chiral edge mode even at a large lattice size and just propagate along the outer boundaries of lattices [2,3], which are unscalable and unapplicable for multi-state topological quantum systems. Recently, the emerging fractal TIs generated by selectively removing lattice sites from the normal topological insulators have attracted much attention for their self-similarity and non-integer dimension [4]. One advantage is to support more topological nontrivial modes with fewer bulk sites using a single lattice and becomes more significant with the growth of fractal generations. Though the fractal photonic AFTI was touched upon in the theoretical simulation [4], it has not been experimentally realized, yet. So far, all experimental works on quantum state transport in laser direct-written photonic topological insulators have been limited to the zero-dimensional topological bound states, exhibiting no topological edge transport properties [5,6].

Here, we demonstrate the first experimental realization of fractal photonic AFTIs based on dual Sierpinski carpet lattice using the femtosecond laser direct writing and observe high-visibility Hong-Ou-Mandel interferences of multiple single-photon chiral edge states that dynamically transport along various boundaries of the fractal lattice.

2. Lattice design

We select the dual Sierpinski carpet (DSC) to construct fractal photonic AFTIs. Its basic iterative process is shown in Fig. 1a, where G(1) and G(2) are the first and second generation, respectively. The one-period waveguide structure of G(1) is constructed by a series of discrete horizontal and vertical directional couplers (DCs), arranged at the 4-step perfect hopping driving protocol (Fig. 1b) to obtain the highest transfer efficiency and preserve chiral edge modes. In each step, only one kind of coupling is switched on and the other three are off, and the theoretical transmittivity of each DC is set as 100%. As shown in the quasi-energy spectrum (Fig. 1c). the fractal AFTI with 64 sites supports four kinds of modes: 17 outer edge modes, 7 inner edge modes IEA, 24 inner edge modes IEB and 16 bulk modes.
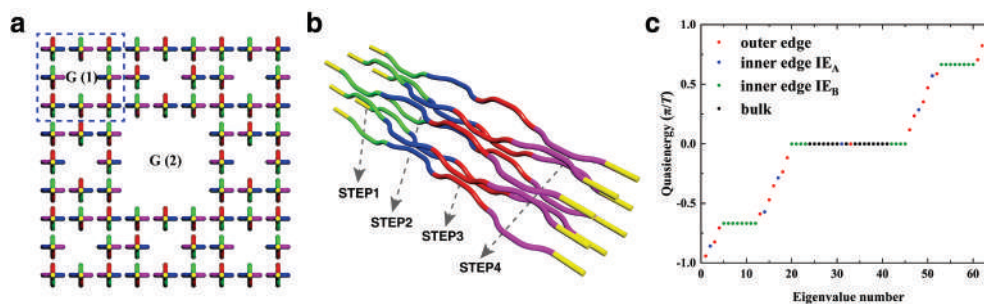
Figure 1 The structure and quasi energy spectrum of the fractal photonic AFTI. **a,** Sketch of the fractal lattice based on the dual Sierpinski carpet. The part in the blue dashed square represents G(1), and the whole is the G(2). **b,** Four-step coupling protocol in one period embodied by G(1). **c,** Quasi energy spectrum of the fractal AFTI.

3. Experimental results

We fabricate the fractal AFTIs in the 70-mm-long borosilicate glass (Eagle2000, Corning) using the femtosecond laser direct writing (FLDW). As shown in Fig. 2a, by the single-site excitation, the observed topological edge transport behavior of outer edge modes and inner edge modes exhibits scattering-free propagating along lattice boundaries and turning all corners. Furthermore, we launch 808 nm single-photon pairs via the Type-I spontaneous parametric down conversion into the fractal lattice to generate a pair of single-photon chiral edge states with topologically protected quantum correlation at separate lattice boundaries. Figure 2b indicates the outer edge state and the inner edge state IE_A after propagating one period for quantum interference, and the measured Hong-Ou-Mandel (HOM) interference visibility V is $91.0\pm2.1\%$ on a DC with a reflectivity R of 0.48, which is higher than 90%, implying that generated single-photon chiral edge state are highly indistinguishable.
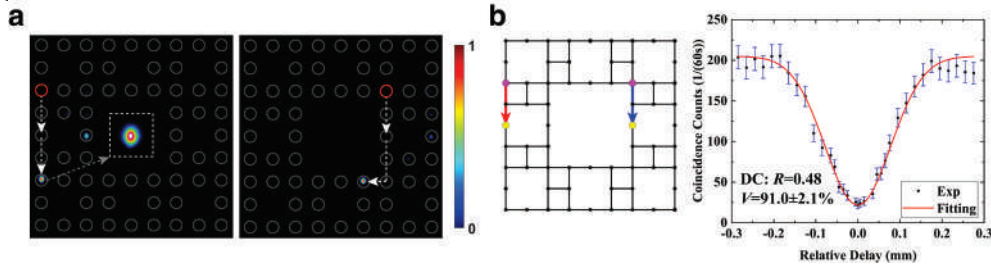
Figure 2 Transport of chiral edge modes and quantum interference of single-photon chiral edge states. **a,** Experimentally observed output intensity distribution of the outer edge mode and the inner edge mode IE_A when light is injected into the waveguide marked by red circle and propagates in the lattice with two periods. **b,** Quantum interference of single-photon outer edge state and inner edge state IE_A.

4. Conclusions

We have experimentally realized the fractal photonic AFTI based on DSC structure using FLDW and performed on-chip high-visibility quantum interferences of multiple propagating single-photon chiral edge states for the first time. The successful generation and control of indistinguishable single-photon chiral edge states shows potentials in generating topologically protected entangled states or performing quantum logical operations. This work lays the foundation for the scalable topological photonic quantum computation, quantum simulation of multiparticle systems and high-capacity quantum information transmission.

References

[1] M. S. Rudner, N. H. Lindner, E. Berg, et al. "Anomalous Edge States and the Bulk-Edge Correspondence for Periodically Driven Two-Dimensional Systems", Phys. Rev. X **3**, p. 031005 (2013).

[2] L. J. Maczewsky, J. M. Zeuner, S. Nolte, et al. "Observation of photonic anomalous Floquet topological insulators", Nat. Commun. **8**, p. 13756 (2017).

[3] S. Mukherjee, A. Spracklen, M. Valiente, et al. "Experimental observation of anomalous topological edge modes in a slowly driven photonic lattice", Nat. Commun. **8**, p. 13918 (2017).

[4] T. Biesenthal, L. J. Maczewsky, Z. Yang, et al. "Fractal photonic topological insulators", Science **376**, p. 1114-1119 (2022).

[5] J. L. Tambasco, G. Corrielli, R. J. Chapman, et al. "Quantum interference of topological states of light", Sci. Adv. **4**, p. eaat3187

[6] Y. Wang, B. Y. Xie, Y.H. Lu, et al. "Quantum superposition demonstrated higher-order topological bound states in the continuum", Light Sci. Appl. **10**, p. 173 (2021).

Open Quantum Walks and Open Quantum Brownian Motions

Ilya Sinayskiy [1,2*]

[1] *School of Chemistry and Physics, University of KwaZulu-Natal, Durban 4001, South Africa*

[2] *National Institute for Theoretical and Computational Sciences (NITheCS), Stellenbosch, South Africa*

*e-mail: `sinayskiy@ukzn.ac.za`

Open Quantum Walks (OQWs) were introduced as quantum analogues to classical Markov chains [1, 2]. Unlike unitary quantum walks [3], OQWs are driven by dissipative interaction with the environment and are formulated using the language of open quantum systems [4]. Open Quantum Brownian Motion (OQBM) is derived from Open Quantum Walks through a scaling limit [5]. OQBM describes a Brownian particle equipped with an additional quantum degree of freedom [6]. Both OQWs and OQBMs exhibit rich dynamical behaviour [7]. While OQWs have a well-defined classical limit and satisfy the central limit theorem [8], the asymptotic behaviour of OQBMs is markedly non-Gaussian. In this presentation, I will introduce OQWs and OQBMs, and discuss their properties and recent developments. Furthermore, I will review the scheme for the quantum optical implementation of these walks and explore other possible realizations [9].

References

[1] S. Attal, F. Petruccione, C. Sabot and I. Sinayskiy, "Open Quantum Random Walks", *J Stat Phys* **147**, pp. 832 (2012).

[2] S. Attal, F. Petruccione and I. Sinayskiy, "Open quantum walks on graphs", *Phys Lett A* **376** 18, pp. 1545-1548 (2012).

[3] S.E. Venegas-Andraca, "Quantum walks: a comprehensive review", *Quantum Inf Process* **11**, pp. 1015 (2012).

[4] H.-P. Breuer and F. Petruccione, *The Theory of Open Quantum Systems* (OUP, 2002).

[5] M. Bauer, D. Bernard, and A. Tilloy, "Open quantum random walks: Bistability on pure states and ballistically induced diffusion", *Phys. Rev. A* **88**, pp. 062340 (2013).

[6] M. Bauer, D. Bernard, and A. Tilloy, "The open quantum Brownian motions", *J Stat Mech* pp. P09001 (2014).

[7] I. Sinayskiy and F. Petruccione "Open quantum walks", *Eur Phys J Spec Top*, **227**, pp. 1869 - 1883 (2019).

[8] S. Attal, N. Guillotin-Plantard and C. Sabot "Central Limit Theorems for Open Quantum Random Walks and Quantum Measurement Records", *Ann Henri Poincare*, **16**, pp. 15 - 43 (2015).

[9] I. Sinayskiy and F. Petruccione "Quantum optical implementation of open quantum walks", *Int J of Quant Inf*, **12**, pp. 1461010 (2014).

Twisting the uncertainty principle

Neelan Gounden[1*], Jenna Epstein[1], Pedro Ornelas[1], Geoff Beck[1], Isaac Nape[1] and Andrew Forbes[1]

[1]*School of Physics, University of the Witwatersrand, Private Bag 3, Wits 2050, South Africa*

*E-mail: *2097061@students.wits.ac.za*

1. Theoretical Background

Uncertainty relations are core to both classical and quantum physics, and lend themselves to tests across many degrees of freedom. An example of these relations is: Heisenberg's uncertainty principle which provides a limit to which the accuracy of **linear** position (Δx) and **linear** momentum (Δp) of a quantum particle can be measured simultaneously.

$$\Delta x \Delta p \geq \frac{\hbar}{2} \tag{1}$$

A similar relationship forms when one looks at **angular** position ($\Delta \phi$) and **orbital angular** momentum ($\Delta \ell$) [1]. In the extreme case where the paticle is localised to a infinitesimally small region ($\Delta \phi \rightarrow 0$), the uncertainty in the **angular** momentum of the particle would approach an unbounded value ($\Delta \ell \rightarrow \infty$).
Using light this relationship can be tested and verified.

Karl Popper wanted to investigate the uncertainty principle within systems consisting of quantum entangled particles. He believed that these systems would yield different results to that when the uncertainty principle is tested with single photons [2]. Looking at a source which produces two entangled photons as seen in Fig. 1 if photon A were to be localised ($\Delta \phi_A \rightarrow 0$) if the **angular** momentum of photon A were to be measured one would obtain ($\Delta \ell_A \rightarrow \infty$), however the question being investigated by Popper is that of whether the spread of the **angular** momentum for photon B would mimic the spread of the **angular** momentum for photon A in this case?
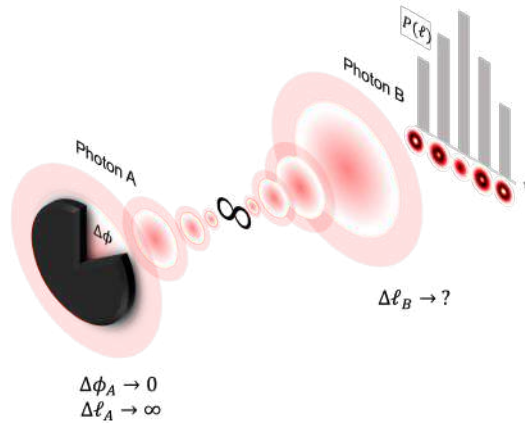
Figure 1: The red rings represents two entangled photons (photon A and B) being generated from a source and propagating (to the left and right respectively), whereby one photon is incident on the angular slit while the orbital angular momentum of the other photon is measured.

2. Experimental considerations

Popper's conjecture has already been tested using **linear** position and **linear** momentum [3] , however we conducted an experiment using a **new** pair of non-commutative variables (**angular position and OAM**) to test Popper's conjecture. The experimental setup consisted of a 355nm laser which produces a pump photon which is incident on a non-linear crystal whereby Spontaneous Parametric Down-Conversion (SPDC) occurs leading to the generation of two entangled photons which are correlated in terms of orbital angular momentum (OAM). This quantum entangled state can be represented as [4,5]:

$$|\psi\rangle = \Sigma_\ell c_\ell |\ell\rangle_A |-\ell\rangle_B \tag{3}$$

Using digital holgraphy and spatial light modulators [5], one of these entangled photons (photon A) will be

incident on an angular slit which allows us to control the angular position of the photon. Simultaneously an OAM measurement will be performed on the entangled photon which is not passing through the slit (photon B). By detecting the two entangled photons in coincidence, OAM spectra can be obtained as seen in the barplots in Fig. 2. Using these OAM spectra a plot for the uncertainty in OAM of the photon B which is not passing through the slit can be plotted against the angular width of the angular slit which photon A passes through.

3. Results
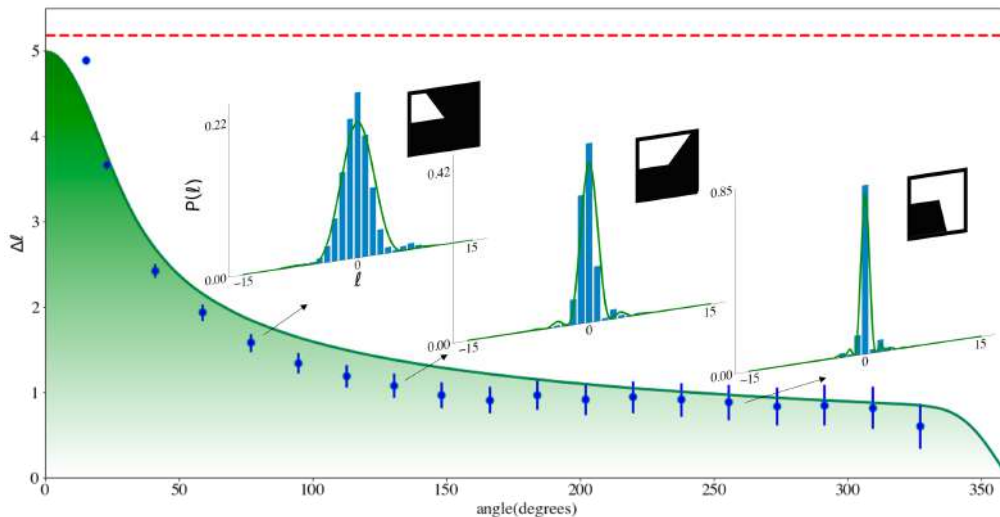
Figure 2: Normalised OAM spectra are generated from coincidence counts (blue bar plot) while being compared to the theoretical model (green plot). Using the normalised OAM spectra which are being generated the widths of these spectra are calculated and plotted against the width of the angular slit (blue scatter plot points), while being compared to the widths of the theoretical spectra (green curve). The red dashed line represents the width of the initial quantum entangled state (SPDC spectrum which is produced at the non-linear crystal)

The results shown in Fig. 2 represents the uncertainty in OAM for photon B ($\Delta\ell_B$) given that the position of photon A has been localised ($\Delta\phi_A$).

4. Discussion and Conclusions

From the results it can be seen that the uncertainty in OAM of photon B does not approach infinity however it approaches some finite value, this finite value happens to be the uncertainty in OAM of the initial quantum entangled state. This value is indicated by the red dashed line in Fig. 2. From the results it can be seen:

$$\Delta\ell_B = \Delta\ell_{SPDC} \text{ provided that } \Delta\phi_A \to 0 \qquad (3)$$

In a system with entangled photons if a **'non-local'** OAM measeurement is performed on a photon which is being localised in terms of its angular position by measuring the OAM of its entangled twin. The OAM spread of the entangled twin is limited by the OAM spread of the initial quantum entangled state and cannot exceed that value [6].

References

[1] B. Jack, P. Aursand, S. Franke-Arnold, D. G. Ireland, J. Leach, S. M. Barnett, and M. J. Padgett, Journal of Optics 13, 064017 (2011)
[2] T. Qureshi, American journal of physics 73, 541 (2005).
[3] E. Bolduc, E. Karimi, K. Pich´e , J. Leach, and R. W. Boyd, Journal of Optics 19, 104002 (2017).
[4] Yudong Lian, Xuan Qi, Yuhe Wang, Zhenxu Bai, Yulei Wang, Zhiwei Lu, Optics and Lasers in Engineering 151, 106923,(2022)
[5] Isaac Nape, Bereneice Sephton, Pedro Ornelas, Chane Moodley and Andrew Forbes, APL Photonics 8, 051101 (2023)
[6] C. D. RICHARDSON and J. P. DOWLING, International Journal of Quantum Information 10, 1250033 (2012).

Unveiling the Potential: Targeting Cancer Stem Cells with Nano-Photodynamic Therapy

Anine Crous[*]

[1]*Laser Research Centre, University of Johannesburg, P.O. Box 17011, Doornfontein, Johannesburg, South Africa, 2028*

[*]E-mail: acrous@uj.ac.za

1. Introduction

Photodynamic therapy (PDT) is a promising approach for the treatment of various malignancies, leveraging light-dependent and reactive oxygen species (ROS)-related cell death mechanisms with non-toxic photosensitizers (PS) (1). While PDT has shown considerable efficacy against bulk tumor cells, a challenging subset of tumor cells known as cancer stem cells (CSCs), responsible for tumor initiation and recurrence, often display resistance to treatment (2). This study investigates the potential of utilizing $AlPcS_4Cl$-nanoPDT in conjunction with gold nanoparticles (AuNPs) as a strategy to target and eliminate CSCs. Intracellular localization of $AlPcS_4Cl$ was examined, and a comprehensive battery of biochemical assays was conducted, including assessments of viability, proliferation, cytotoxicity, and Annexin V/PI cell death. Morphological examinations were also performed to gain insights into cellular alterations induced by this novel therapeutic approach. Our findings reveal enhanced absorption and intracellular localization of the therapeutic $AlPcS_4Cl$ in CSCs when delivered via AuNPs.

2. Figures and tables

A nanobioconjugate (NBC) was assembled by combining a photosensitizer (PS) known as $AlPcS_4Cl$, AuNPs, and antibodies, as seen in Fig 1. The NBC underwent rigorous characterization through various spectroscopic techniques. Subsequently, the photodynamic effects of NBC on lung CSCs were assessed using biochemical assays conducted 24 hours after irradiation, with the aim of establishing its effectiveness as an anticancer treatment.
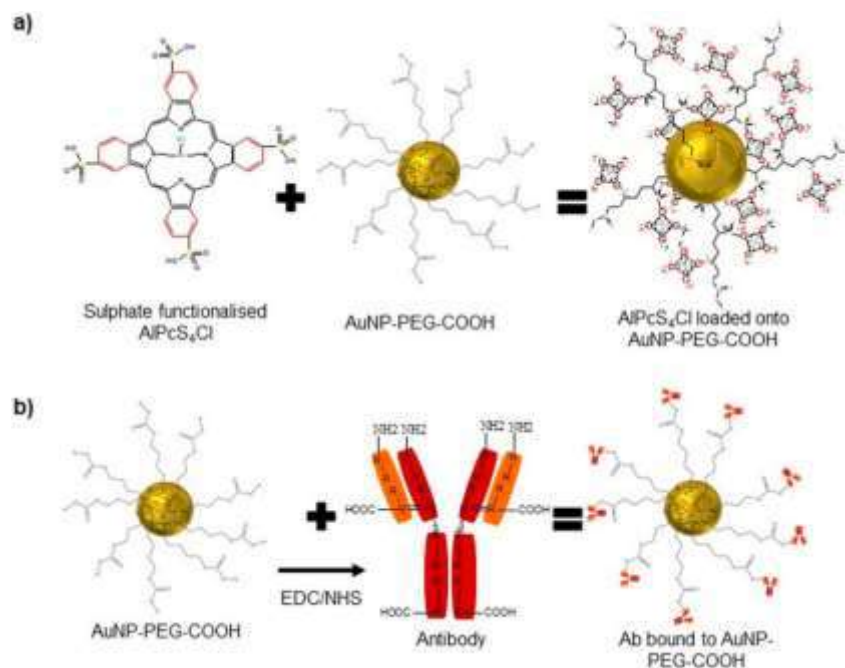
Figure 1 The nanobioconjugate (NBC) was created by combining a photosensitizer (PS) called AlPcS4C, gold nanoparticles (AuNPs) with carboxylic acid-functionalized polyethylene glycol (AuNP-PEG-COOH), and an antibody (Ab) known as Anti-CD133. This involved two main steps:(a) The sulfate-functionalized PS was loaded onto the AuNPs through a process of ligand exchange and adsorption. (b) The Ab was conjugated to the AuNPs using EDC-NHS chemistry (3).

3. Conclusions

In conclusion, the outcomes of this study have demonstrated a remarkable reduction in CSC survival and proliferation rates, an enhanced cytotoxic effect, and a heightened occurrence of apoptotic cell death. These findings collectively highlight the remarkable efficacy of our innovative treatment approach. Importantly, the incorporation of AuNPs as drug carriers has significantly amplified the impact of photodynamic therapy, ultimately resulting in the complete eradication of CSCs. This research underscores the potential of nano-Photodynamic Therapy as a targeted strategy for overcoming the treatment resistance posed by cancer stem cells, thereby opening promising avenues for more effective cancer therapies in the future.

Acknowledgments

References

1.	Zhang ZJ, Wang KP, Mo JG, Xiong L, Wen Y. Photodynamic therapy regulates fate of cancer stem cells through reactive oxygen species. World J Stem Cells. 2020;12(7):562-84.
2.	Shen S, Xia J-X, Wang J. Nanomedicine-mediated cancer stem cell therapy. Biomaterials. 2016;74:1-18.
3.	Crous A, Abrahamse H. Effective Gold Nanoparticle-Antibody-Mediated Drug Delivery for Photodynamic Therapy of Lung Cancer Stem Cells. International Journal of Molecular Sciences. 2020;21(11):3742.

Optical properties of rare earth metal, Tb, dopped in cubic ceria nanoparticles

M. Akbari[1,2], F. Abedi[1,2], N. Numan, M. Maaza[1,2]

[1] UNESCO-UNISA Africa Chair in Nanoscience and Nanotechnology (U2ACN2), College of Graduate Studies, University of South Africa (UNISA), Pretoria, South Africa

[2] Material Research Division, Nanoscience African Network (NANOAFNET), iThemba LABS-National Research Foundation, Somerset Africa West 7129, South Africa

Abstract: The purpose of this study is to investigate the effect of rare earth metal (Tb) doping on ceria nanoparticles (CNPs) synthesized using the hydrothermal method. An aqueous solution of cerium salts and a hydrothermal reactor is used in this method to create controlled high-pressure and high-temperature conditions that promote the formation of nanoparticles. Fourier Transform Infrared Spectroscopy (FT-IR), Powder X-ray Crystallography (PXRD), Scanning Electron Microscopy (SEM), Energy-Dispersive X-ray Spectroscopy (EDS), Transmission Electron Microscopy (TEM), and Raman Spectroscopy are used in this study to synthesize and characterize both un-doped and doped CNPs. The synthesized compounds have a nanostructured cubic phase. The morphology of all doped and un-doped CNPs was cubic, and their approximate size was determined using XRD and TEM in the 5-20 nm range. The calculated bandgap energy (Eg) from UV-vis diffuse reflectance spectroscopy (DRS) is also obtained, and the optical results show variations with values ranging from 2.5 to 3.2 eV. Furthermore, the optical band gap energy was calculated using DFT, confirming the optical properties of the doped nanoceria samples obtained through the experimental approach.

Polarization-Sensitive Fourier Ptychographic Microscopy for Large Area, High-Resolution Birefringence Imaging

Eugene Egbert Fouche[1*], Gurthwin Wendell Bosman[1] and Pieter Herman Neethling[1]

[1]Physics Department, Stellenbosch University, Private Bag XI, Matieland 7602, South Africa

[*]E-mail: 21598835@sun.ac.za

1. Abstract

Polarized light microscopy can reveal sample features that are not visible in ordinary light microscopy [1]. By placing polarizers before and after the sample in various configurations, it is possible to measure the anisotropy properties of a sample and improve contrast. Fourier Ptychographic Microscopy (FPM) is a powerful technique to increase the resolution of a microscope, by using illumination from multiple angles and ideas from Ptychography and Synthetic Aperture imaging. FPM uses a low numerical aperture objective for a large field of view and achieves a resolution that is comparable with that of a high NA objective. This results in a very large space-bandwidth product for the imaging setup.

Recently, these two techniques have been combined for polarization-sensitive Fourier Ptychographic Microscopy (pFPM) to image anisotropic samples over a large area with a high-resolution and measure their birefringent properties [1-3].

When polarized light passes through a birefringent material, the polarization state of the light is altered due to a phase delay acquired between the components of the incident light that are polarized along the fast and slow axis of the birefringent material. When using polarization-sensitive imaging to view these samples, we can create a map of the phase delay δ and the optical axis orientation θ at each point in the sample.

As in FPM, an LED array is used as illumination source to illuminate the sample from multiple angles. The incoming light passes through a circular polarizer before interacting with the sample, after which the now elliptically polarized light is analysed with a linear polarizer and camera. By performing a traditional FPM experiment 4 times, with the analyser oriented at 0°, 45°, 90° and 135° for each different run, it is possible to extract the phase delay δ and the optical axis orientation θ from the different measurements [2]. Jones calculus is used to describe the interaction of the polarized light with the sample and linear polarizer. The resulting intensities for each orientation of the analyser differ due to the interaction of the light with the sample, and can be used to calculate δ and θ.

Recent work in this area has looked at samples such as plant cell walls, monosodium urate crystals and cardiac tissue [1-3]. In this work, thin sections (30 µm) of rock samples (mafic granulite, granite) were considered (Fig. 1) in order to identify different crystal domains and to identify different minerals in the sample (FOV 4 mm^2, resolution 1.6 µm). It beautifully illustrates the advantage of polarization-sensitive imaging, and the different domains of the sample (where crystal growth is oriented in a certain direction) can be clearly seen. Knowledge about the size and orientation of the domains, as well as the mineral content, is important in mineral extraction. pFPM can be used to distinguish between different domains and identify different minerals through quantitative access to the birefringent properties (δ and θ) of these rock samples.
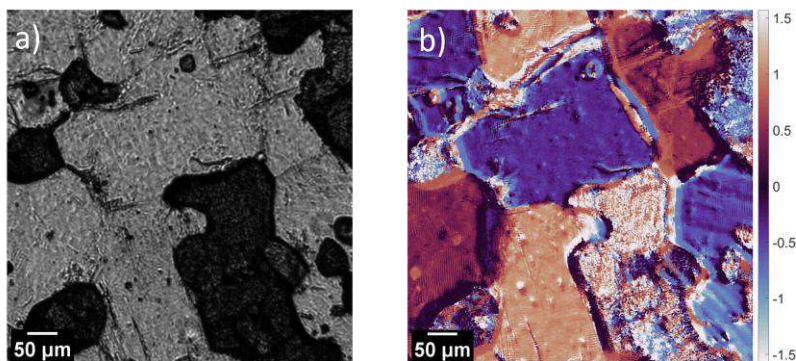
Figure 1 Mafic granulite thin section. a) Image of the sample with no polarizer present. The darker features are visible, but the different domains are not. b) Reconstruction of the optical axis orientation θ, using the FPM reconstructed images with the various polarizer configurations. The different coloured regions show areas of different crystal orientation, which are not visible in the image without a polarizer.

2. Conclusions

Polarization-sensitive Fourier Ptychographic Microscopy can be used to view birefringent rock samples with greater contrast, and to identify different minerals and crystal domains, through quantitative access to their birefringent properties.

Please consider this abstract for an **oral presentation**, I have prepared another abstract for a poster presentation.

References

[1]   S. Song, J. Kim, S. Hur, J. Song, and C. Joo, "Large-Area, High-Resolution Birefringence Imaging with Polarization-Sensitive Fourier Ptychographic Microscopy," *ACS Photonics*, vol. 8, no. 1, pp. 158–165, Jan. 2021, doi: 10.1021/ACSPHOTONICS.0C01695.

[2]   M. Gholami Mayani, K. R. Tekseth, D. W. Breiby, J. Klein, and M. N. Akram, "High-resolution polarization-sensitive Fourier ptychography microscopy using a high numerical aperture dome illuminator," *Opt. Express*, vol. 30, no. 22, p. 39891, 2022, doi: 10.1364/oe.469115.

[3]   X. Dai *et al.*, "Quantitative Jones matrix imaging using vectorial Fourier ptychography," *Biomed. Opt. Express*, vol. 13, no. 3, p. 1457, 2022, doi: 10.1364/boe.448804.

Optical biosensors for the detection of human immunodeficiency virus

Masixole Yvonne Lugongolo[1], Saturnin Ombinda-Lemboumba[1], Patience Mthunzi-Kufa[1,2,3]

[1]Council for Scientific and Industrial Research, National Laser Centre, P.O. Box 395, Pretoria, 0001, South Africa.

[2]Division of Medical Virology, Faculty of Health Sciences, University of Cape Town, South Africa.

[3]University of KwaZulu-Natal, School of Chemistry and Physics, Westville Campus, University Road, Durban, South Africa.

Abstract

Optical biosensors are compact analytical tools that have a biorecognition element combined with a transducer system, which emits an optical signal that is directly proportional to the analyte concentration. Biorecognition elements are generally biological materials such as tissues, cells, nucleic acids, antigens, antibodies, and enzymes. Optical biosensors utilize the interaction of optical fields with the analyte for optical detections. They offer some advantages over conventional analytical methods due to their fast detection abilities, high sensitivity, real time analysis, specificity, portability, and cost effectiveness. These properties capacitate optical biosensors to perform efficiently in fields like clinical diagnostics and healthcare, environmental analysis and monitoring as well as biotechnological industry. In the current study, home-built optical biosensor systems; localized surface plasmon resonance and transmission spectroscopy were used to detect HIV. The results showed that the virus was detected after binding to the antibody on the surface of a gold coated slide and photonic crystal as demonstrated by the change in transmittance intensity and wavelength shift thus differentiating between the sample with the virus and the one without the virus. These outcomes will contribute towards the development of a multiplex optical biosensing device for the detection of viral infection and viral load as point of care diagnostic platforms for use in resource limited settings.

Photodynamic therapy of melanoma induced by biogenic metallic silver nanoparticles chromophore

Glory Kah[1*], Rahul Chandran[1] and Heidi Abrahmse[1]

[1]*Laser Research Centre, University of Johannesburg, Doornfontein Campus,*

Johannesburg, South Africa.

*E-mail: glorykah26@yahoo.com

1. Abstract

Melanoma is a very aggressive cancer that often begins in melanocytes. Its development and progression are problematic to predict. Melanoma treatment is linked with difficulties and setbacks, leading to an elevation in its incidence globally [1]. Typically, melanoma often affects the skin tissues and accounts for about 80% of deaths in cases of dermatological cancer. Therapeutic guidelines for melanoma cases include radiotherapy, surgery, chemotherapy, targeted therapy, and immunotherapy. Treatment for patients with melanoma at an early stage is more efficient, although the efficacy of treatment for cases with advanced melanoma is much lower. The survival rate within 5 years for treated cases of advanced melanoma is just 16%. This is associated with the poor sensitivity of traditional treatment procedures, leading to an increase in mortality and morbidity [2]. This shows that more effective alternative treatment procedures are needed for patients with melanoma. Photodynamic therapy (PDT) is proposed as an encouraging non-invasive therapeutic procedure for neoplastic and premalignant lesions. The PDT procedure requires three key factors, namely a photosensitizer (PS), an appropriate visible light source, and the presence of oxygen [3]. The stimulation of the PS by light with a suitable wavelength would generate singlet oxygen and reactive oxygen species (ROS), which can subsequently provoke the death of tumour cells [4]. This study, hence, explores the effectiveness of bio-mediated silver nanoparticles (AgNPs) in melanoma PDT. Biosynthesised AgNPs were characterized using UV-vis spectroscopy, high-resolution transmission electron microscopy (HRTEM), and zeta potential analysis. The HRTEM was also used to evaluate the intercellular uptake of AgNPs by the A375 cells (melanoma cells). The dark toxicity effect of AgNPs was studied, and the minimal concentration of AgNPs to stimulate a toxic effect on A375 cells was considered for the PDT procedure (Figure 1). The A375 cells were then treated with AgNPs only, PDT only, and AgNPs plus PDT. The cytotoxic impact of the various treatments on the A375 cells was elevated using biochemical assays including MTT (3-(4,5-dimethylthazolk-2-yl)-2,5-diphenyl tetrazolium bromide), lactate dehydrogenase (LDH), and Trypan blue exclusion (TBE) assays. Morphological studies were done microscopically, while the mechanism for cell death was assayed using the flow cytometric Annexin V and propidium assay. The characterized AgNPs were confirmed to be stable, spherical-shaped, and of average sizes less than 50 nm. The HRTEM image showed that the AgNPs were internalized in the treated cells. Morphological studies of treated cells show damaged and dead cells. Also, the combined AgNPs and PDT treatment led to a decrease in cell growth and viability and apoptotic-induced cell death. This shows that the biogenic AgNPs-mediated PDT caused increased cytotoxicity and finally programmed cell death and these are key components for cancer therapy. Therefore, metallic chromophores like AgNPs may be considered PS for the melanoma PDT procedure.

The laser parameter used during the study were measured and calculations were made according to the formula below (Eq. 1).

$$\text{Irradiation time} = \frac{Fluency\ (J/\ cm^2)}{Power\ output\ (W/\ cm^2)} \tag{1}$$

2. Figure 1
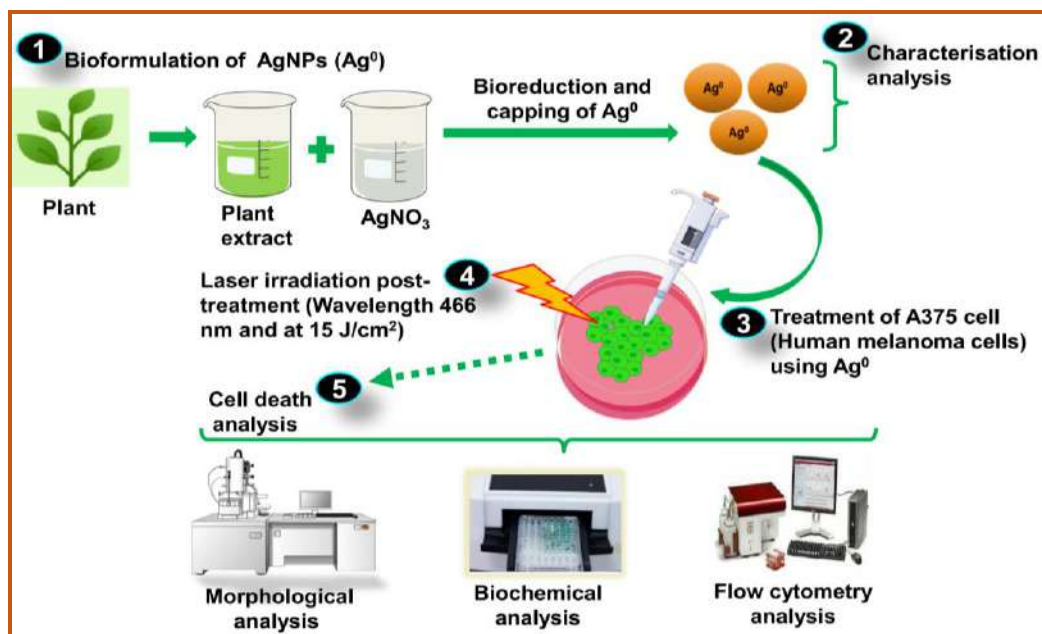
Figure 1 Schematic illustration of experimental procedure as indicated in the abstract.

3. Conclusions

This study reveals that AgNPs are excellent chromophores for mediating melanoma PDT. Increased cytotoxicity associated with a decrease in A373 cell proliferation and viability shows that these cells were sensitive to the AgNPs plus irradiation treatment. Nonetheless, further studies are needed to outline the mechanisms involved in AgNP-mediated PDT of melanoma. This could pave the way for the possible utilisation of AgNP-mediated PDT for cancer in clinical settings.

References

[1] M. K. Tripp, M. Watson, S. J. Balk, S. M. Swetter, and J. E. Gershenwald, "State of the Science on Prevention and Screening to Reduce Melanoma Incidence and Mortality: The Time is Now," *CA Cancer J Clin*, vol. 66, no. 6, pp. 460–480 (2016).

[2] X.-Y. Li *et al.*, "Susceptibility and Resistance Mechanisms During Photodynamic Therapy of Melanoma," Frontiers in Oncology, vol. 10 (2023).

[3] N. W. Nkune, C. A. Kruger, and H. Abrahamse, "Synthesis of a novel nanobioconjugate for targeted photodynamic therapy of colon cancer enhanced with cannabidiol," Oncotarget, vol. 13, no. 1, pp. 156–172 (2022).

[4] G. Kah, R. Chandran, and H. Abrahamse, "Biogenic Silver Nanoparticles for Targeted Cancer Therapy and Enhancing Photodynamic Therapy," Cells, vol. 12, no. 15, Art. no. 1 (2023).

Quantum enhancement in the limit of detection measurement of a phase-based plasmonic biosensor with loss

Kelvin Mpofu [1*], Saturnin Ombinda-Lemboumba[1] and Patience Mthunzi-Kufa[1] [2] [3]

[1] *Council for Scientific and Industrial Research (CSIR) , National Laser Centre , Pretoria , South Africa*

[2] *School of Chemistry and Physics , University of KwaZulu-Natal , Durban 4041, South Africa*

[3] *Orthopaedic Biomechanics Lab , Division of Biomedical Engineering ,*
Department of Human Biology , Faculty of Health Sciences ,
University of Cape Town ,Anzio Road , Observatory , South Africa

[*]e-mail: `kmpofu@csir.co.za`

Abstract

The authors simulate how quantum states of light, such as the NOON state, can enhance the limit of detection of a plasmonic phase-sensing biosensor beyond the shot-noise limit set by the coherent state.

1. Introduction

As the world continues to recover from the COVID-19 pandemic, the need for rapid detection, high sensitivity, and high precision in our biosensors has become very apparent. The rapid evolution of viral strains over the years has been a major concern, as it has led to the spread of epidemics and pandemics [1]. In phase-based biosensors, a phase shift is used to infer the presence of specific molecules in the sample. In the phased-based surface plasmon resonance (SPR) biosensor, a Krestchmann configuration-based plasmonic biosensor is integrated into one of the Mach-Zender interferometer arms. Although classical phase-based SPR biosensors are highly sensitive, their limit of detection (LOD) is bound by the shot-noise limit (SNL) imposed on the coherent state of light. When quantum states of light are used as probe input states in the SPR biosensor, the biosensor is generally referred to as a quantum plasmonic biosensor. Quantum states of light have been shown to enhance detection to below the SNL in an intensity-based SPR sensing setup [2, 3]. In this work, the effect of the NOON state on enhancing the detection precision below the SNL is considered. This work shows how the use of quantum states of light in SPR biosensing gives an enhancement over using classical states and some limitations which may need to be overcome. Quantum SPR biosensors represent the future of optical biosensing.

2. Methodology

Here the authors theoretically model the phase-based biosensing experiment shown in Fig. 1, and show that by using the NOON quantum state as the probe state, the performance of a plasmonic biosensor can be enhanced. In Fig. 1 the ISS step refers to a preprocessing step where there might be mode mixing or entanglement generation in the case of the NOON state. In the figure, we see a Krestchmann configuration setup integrated into an interferometric system. The signal mode (mode **a**) goes to the prism and probes the system, whereas the reference mode (mode **b**) bounces off a mirror and goes directly to the second beam splitter. The input states can be any quantum
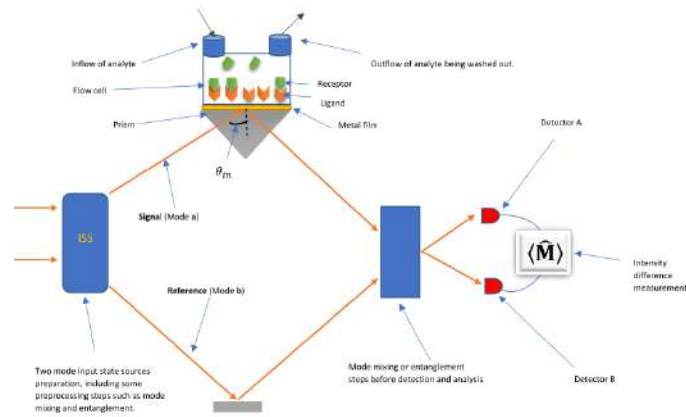
Figure 1: This figure shows the phase-based plasmonic biosensing setup modelled in this work. In the described experiment the BSA will bind electrostatically to the metal film.

or classical state. An intensity difference measurement is important in order to extract the phase and phase shift and also has the added advantage of removing any background noise from the signal we are interested in. The authors compared the NOON quantum state's limit of detection to that of the two-mode coherent (TMC) classical state, whose measurement noise is limited by the shot-noise limit, when both are used in a simple bovine serum albumin (BSA) dilution biosensing experiment (see Fig. **2**). In Fig. **2** results are shown for when an application of the phase-based setup is considered, where the setup is applied to a simple reaction on the surface of the biosensor in which BSA is being mixed with water, thus changing its concentration and the refractive index of the solution of interest. Fig. **2** (a) shows that when the angle of incidence of the light source to the setup is changed there is a shift to the right of the phase-based resonance curve (the blue line is for an incidence angle of $73°$ and the orange line is $75°$). Fig. **2** (b) shows the simulated LOD when the two states of light are introduced as input. The black curve is the LOD in the refractive index when laser light or the coherent state is used, and the red curve is the LOD for the NOON state. In Fig. **2** (b) it is assumed that there are no losses in the system, and here the NOON state clearly outperforms the coherent state. Fig. **2** (c) shows the same phenomenon as (b), but with the inclusion of a 10% loss to the environment in the simulation and immediately we see that the NOON state does not perform as well as the coherent state because it is not robust against losses to the environment. This is a big limitation which forces us to consider other quantum states that are robust against losses to the environment. To calculate the limit of detection (LOD) of the measurement of the refractive index from the phase, see Eq. 1 derived using the error-propagation formula is used;

$$\Delta \mathrm{n} = \Delta \phi |\frac{\partial \phi}{\partial \mathrm{n}}|^{-1}, \tag{1}$$

where n is the refractive index on the biosensor surface and ϕ is the phase due to the SPR biosensor. The minimum detectable phase shifts, $\Delta \phi$, for the coherent and NOON states have been calculated for this work.

3. Conclusion

In this work, it is shown that by using the NOON state of light as a probe in the phase-based plasmonic biosensor we can enhance the LOD of the measurement of the refractive index. The NOON state is unfortunately not robust against losses in the system, and when minor losses are introduced, it quickly fails to surpass the SNL. The knowledge that it is possible in theory to break the SNL is a great positive, though. The answer may lie in considering other quantum states of
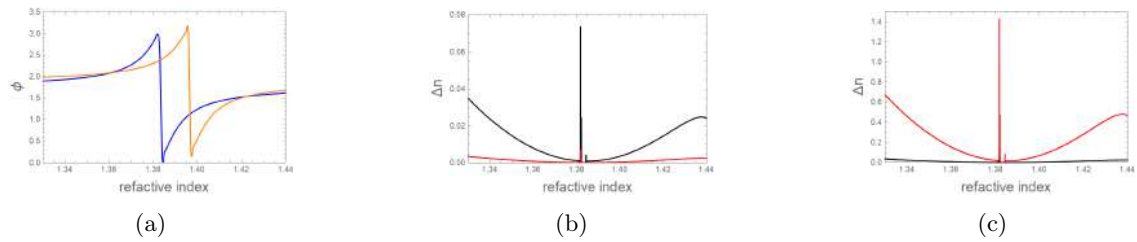
Figure 2: Results from simulation of the phase based setup. (a) shows a phase shift when BSA concetraion in water changes which changes the refractive index of the solution on the binding surface. (b) shows the LOD when using both NOON (red) and TMC (back) states without any loss in the setup. (c) Shows the same result as (b) but assuming a 10% loss in the setup.

light such as the squeezed states of light or Fock states known to be robust against losses. This is a possible direction for future research, both theoretical and experimental.

References

[1] P. Singh, Surface Plasmon Resonance: A Boon for Viral Diagnostics, Life sciences Journal, 8, 12245-12249 (2017).

[2] K. Mpofu, G. Maguire, H. Kruger and M. Tame, Measuring kinetic parameters using quantum plasmonic sensing, Physical Review A, 105, 3 (2022).

[3] K. Mpofu, G. Maguire, H. Kruger and M. Tame, Experimental measurement of kinetic parameters using quantum plasmonic sensing, Journal of Applied Physics, 131, 8, (2022).

Quantum ghost imaging: Back to basics

Dr Chané Moodley[1*] and Prof Andrew Forbes[2]
[1]QLAB, Raphta (PTY) LTD, Waterfall, Johannesburg, 2090
[2]Structured Light Lab, School of Physics, University of the Witwatersrand, Johannesburg, 2000

Although quantum ghost imaging is an established field of study, it's crucial to grasp the fundamental elements before progressing in the development of technology and applications related to it. In quantum ghost imaging, pairs of entangled photons are employed to reconstruct an image. The correlation between these photon pairs is what enables image reconstruction, in contrast to the use of single photon detection. These entangled photons are separated into two paths: one photon illuminates the object, while the other photon is collected by a spatially resolving detector. Initially, in quantum ghost imaging experiments, spatially resolving detectors were achieved by physically moving a single-pixel detector across a transverse scanning area. Later, advancements introduced the use of highly sensitive single-photon cameras to eliminate the need for a physically moving detector. However, these advanced cameras are costly and have limited spectral sensitivity. In this talk, we provide a tutorial-style presentation of the essential components necessary for demonstrating quantum ghost imaging. In the past, imaging speeds were limited by the slow and inefficient scanning capability of spatially resolved detectors, along with the low levels of light inherent in quantum experiments. Furthermore, we touch on the application of deep learning algorithms to enhance both image reconstruction speed and resolution. Additionally, we showcase a straightforward approach to reconstruct phase and complex amplitude images using both degenerate and non-degenerate quantum ghost imaging optical configurations.

The Dose–Response Relationship of Photobiomodulation Therapy on Adipose-derived Stem Cells into Osteoblast-like Cells.

Daniella Da Silva[1], Anine Crous[1*] and Heidi Abrahamse[1]

[1]*Laser Research Centre, Faculty of Health Sciences, University of Johannesburg, P.O. Box 17011, Doornfontein, Johannesburg, South Africa, 2028*

*E-mail: acrous@uj.ac.za

1. Introduction

Osteoporosis is a metabolic bone disease that affects millions of individuals worldwide [1]. Osteoporosis has been shown to be treatable using stem cells (SCs), especially when adipose-derived stem cells are used (ADSCs) [2]. Photobiomodulation (PBM) has sparked interest on an international scale because of its' ability to proliferate stem cells and improve their differentiation capacity [3]. The combined use of osteogenic differentiation inducers and PBM has demonstrated enhanced proliferation and differentiation of ADSCs into osteoblast-like cells [4].

2. Methodology

This *in vitro* study (Figure 1) combined the use of osteogenic differentiation inducers and PBM at a near-infrared (NIR) wavelength of 825 nm, a green wavelength of 525 nm, and their combination wavelengths using multiple fluences of 1, 3, 5, 7 and 10 J/cm^2 were investigated to determine the proliferation and differentiation effectiveness of immortalised ADSCs into osteoblasts. The laser parameters have been specified in Table 1 where the calculation for irradiation time was determined with the formula seen in Equation 1. Flow cytometry identified osteoblast antigens by having utilised early and late osteoblast protein surface markers. Alizarin red Stain recognized calcium deposits in cells within culture. Spectrophotometry evaluated the activity of alkaline phosphatase. Inverted light microscopy was used to identify cell morphology. Mitochondrial Membrane Potential was identified using immunofluorescence and spectrophotometry. The genetic expression of transcription factors was determined using Real Time-PCR.
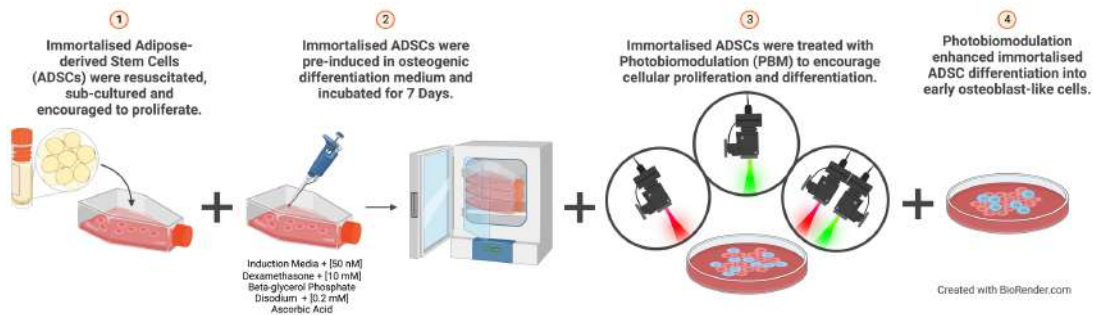
Figure 1 The combined use of osteogenic differentiation inducers and photobiomodulation improved both the proliferation and differentiation potential of immortalised ADSCs into early osteoblast-like cells.

Laser	Light Source	Wavelength (nm)	Power Output (mW)	Power Density (mW/cm^2)	Area (cm^2)	Emission	Fluence (J/cm^2)	Time of Irradiation (s)
Near infra-red (NIR)	Diode Laser	825	515	53.53	9.62	Continuous Wave	1, 3, 5, 7 and 10	19, 56, 93, 131 and 187
Green (G)	Diode Laser	525	553	57.48	9.62	Continuous Wave	1, 3, 5, 7 and 10	17, 52, 87, 122 and 174

Table 1 Laser Parameters

$$mW/cm^2 = \frac{mW}{\pi \times (r^2)}$$

$$W/cm^2 = \frac{mW/cm^2}{1000}$$

$$Time\ (s) = \frac{J/cm^2}{W/cm^2}$$

Equation 1 Laser irradiation time. Where mW/cm^2 is the power density, W/cm^2 is the intensity, and s is the exposure time.

3. Conclusion

Photobiomodulation and osteogenic differentiation inducers increased ADSC proliferation and osteoblast-like cell differentiation. On immortalised ADSCs, NIR and green PBM wavelengths and fluences were examined. Osteoblast antigens, calcium deposits, alkaline phosphatase activity, cell morphology, mitochondrial membrane potential, genetic expression of transcription factors, flow cytometry, Alizarin red staining, spectrophotometry, inverted light microscopy, immunofluorescence, and Real Time-PCR were positive. Scientific discoveries and a standardised PBM-based osteogenic differentiation *in vitro* approach improve osteoporosis treatment. This could treat metabolic bone disease osteoporosis, which affects millions globally. This study was *in vitro*, thus more research and clinical trials are needed to confirm this therapy's efficacy and safety in people. This study improves our understanding of stem cell-based therapies and PBM for osteoporosis and other bone diseases, offering hope for better treatments and outcomes.

Acknowledgments

References

[1] O. Johnell and J. A. Kanis, "An estimate of the worldwide prevalence and disability associated with osteoporotic fractures," *Osteoporosis International*, vol. 17, no. 12, pp. 1726–1733, Dec. 2006, doi: 10.1007/s00198-006-0172-4.

[2] P. C. Baer and H. Geiger, "Adipose-derived mesenchymal stromal/stem cells: Tissue localization, characterization, and heterogeneity," *Stem Cells International*. 2012. doi: 10.1155/2012/812693.

[3] J. J. Anders, P. R. Arany, G. D. Baxter, and R. J. Lanzafame, "Light-emitting diode therapy and low-level light therapy are photobiomodulation therapy," *Photobiomodulation, Photomedicine, and Laser Surgery*, vol. 37, no. 2. Mary Ann Liebert Inc., pp. 63–65, Feb. 01, 2019. doi: 10.1089/photob.2018.4600.

[4] S. Y. Lee, J. H. Lee, J. Y. Kim, Y. C. Bae, K. T. Suh, and J. S. Jung, "BMP2 increases adipogenic differentiation in the presence of dexamethasone, which is inhibited by the treatment of TNF-α in human adipose tissue-derived stromal cells," *Cellular Physiology and Biochemistry*, vol. 34, no. 4, pp. 1339–1350, Nov. 2014, doi: 10.1159/000366341.

Topological high-harmonic spectroscopy: observing matter response from the topology of the harmonic field.

Luis Plaja[*], Ana García-Cabrera, Roberto Boyero-García, Óscar Zurrón-Cifuentes, Javier Serrano, Julio San Román and Carlos Hernández García

Grupo de Investigación en Aplicaciones del Láser y Fotónica, Departamento de Física Aplicada, Universidad de Salamanca, E-37008, Salamanca, Spain

[*]E-mail: lplaja@usal.es

High-order harmonic generation is possibly one of the most striking consequences of the interaction of intense laser fields with matter. Well beyond the academic interest, high harmonic generation has been proven as an extraordinary and useful tool for the generation of coherent short-wavelength radiation, in the form of bursts of attosecond duration.

Until recently, HHG has been mainly studied in atomic, molecular gases and plasmas. However, this scenario is changing rapidly. During the last decade two independent breakthroughs have boost a renewed interest in new forms of harmonic production. On the one side, the experimental demonstration of HHG in solids [1] sparkled the interest in the study of the non-perturbative optical phenomena in crystalline structures. Due to their higher electron density, the obvious advantage of solids is the increased efficiency of the harmonic production. However, soon there were revealed more advanced and complex possibilities by using high-harmonic spectroscopy to reveal structural information of solid targets, as the energy dispersion or details of the intraband electron motion [2].

On the other hand, there has been also a considerable interest in exploiting HHG driven by structured light. Structured light has a non-trivial, and sometimes interleaved, distribution of spin and angular momentum. In this sense, HHG offers an extraordinary playground, as is capable to map some of the structural parameters of the driving field to the harmonic field. Indeed, it has been demonstrated the generation of short-wavelength light vortices from drivers carrying orbital angular momentum [3,4]. Also, driving vector beams are known to produce XUV vector beams [5].
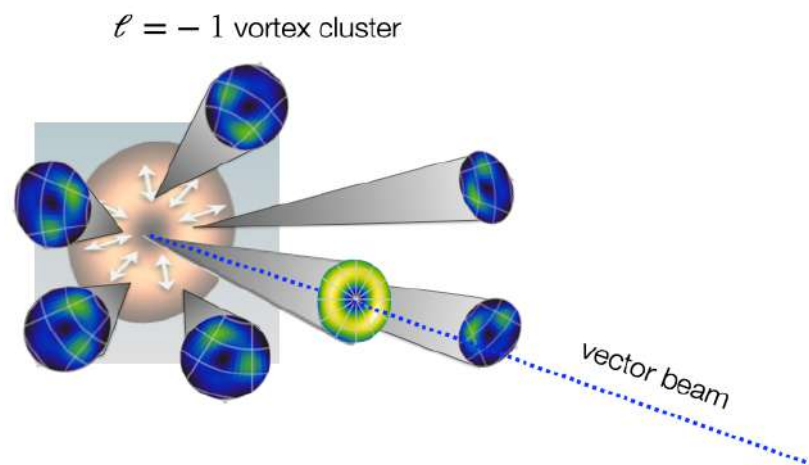
Figure 1 Scheme of the topological multibeam harmonic field from graphene driven by a radial vector beam.

Merging these two advancements in the field, a interesting aspect is the possibility to study the interplay of the crystalline target symmetries with the topology of the structured driving light. Infact, some types of structured fields have well-defined topological characteristics. For instance, light vortices can be characterized by their topological charge, and vector beams by their Poincaré's index. It raises therefore as a very fundamental question how these topological characteristics are translated to the XUV

field. As mentioned above, for the case of isotropic targets (atomics gases) the conservation rules of the topological charge and Poincare's index are simple. For solids, where the energy dispersion geometry is far from isotropic, one should expect these conservation rules to be convoluted with the structural parameters of the crystal. In this unexplored scenario a main concern is to associate the differences between the topological characteristics of the harmonic field and the driver field to fundamental properties of the target's response. *Topological high-harmonic spectroscopy*, therefore, would provide such information about the target by looking to the topological properties of the harmonic emission.

Low dimensional crystals offer an extraordinary scenario for proof of principle of topological spectroscopy, as their narrow widths (typically of atomic size) exclude propagation phenomena that may obscure relevant phenomena. In this talk we shall analyse the characteristics of HHG from graphene irradiated by radial vector beams. We shall demonstrate that graphene's non-linear anisotropy [6,7], arising from its crystalline structure, couples with the azimuthally variant polarization of the driver beam to generate a complex structured harmonic field. We interpret this structure as the superposition of a central vector beam with a topological background structured as a cluster of vortices (see figure). We shall also demonstrate that there is a close connection between the disposition of the vortex cluster and graphene's non-linear response allowing for the recovery of information about the target response.

References

[1] S. Ghimire, D. A. Reis, "High-harmonic generation from solids." Nature Phys **15**, 10–16 (2019)

[2] T. Luu , M. Garg , S. Kruchinin, *et al.* "Extreme ultraviolet high-harmonic spectroscopy of solids." Nature **521**, 498–502 (2015). https://doi.org/10.1038/nature14456

[3] M. Zürch, C. Kern, P. Hansinger, *et al* "Strong-field physics with singular light beams. " Nature Phys **8**, 743–746 (2012). https://doi.org/10.1038/nphys2397

[4] C. Hernández-García, A. Picón, Julio San Román, and L. Plaja, Attosecond Extreme Ultraviolet Vortices from High-Order Harmonic Generation", Physical Review Letters **111**, 083602 (2013)

[5] C. Hernández-García, A. Turpin, J. San Román, *et al.* "Extreme ultraviolet vector beams driven by infrared lasers," Optica **4**, 520 (2017).

[6] O. Zurrón-Cifuentes, R. Boyero-García, C. Hernández-García, *et al.*, "Optical anisotropy of non-perturbative high-order harmonic generation in gapless graphene," Opt. Exp. **27**, 7776–7786 (2019).

[7] N. Yoshikawa, T. Tamaya, and K. Tanaka, "High-harmonic generation in graphene enhanced by elliptically polarized light excitation," Science **356**, 736–738 (2017).

.

Trapping ytterbium isotopes for unsharp quantum measurements

Christine Steenkamp[1*], Nancy Payne[1], Siann Bester[1], Deon Janse van Rensburg[2],
Naleli Matjelo[3], Ncamiso Khanyile[4]

[1]*Department of Physics, Stellenbosch University, [2]Eindhoven University of Technology, [3]Department of
Physics & Electronics, National University of Lesotho, [4]Eighty20*

[*]E-mail: cmsteen@sun.ac,za

1. Introduction

Quantum technology enabling applications such as quantum communication, quantum key distribution and quantum computing is a fast-growing field of increasing industrial importance. Trapped ions have been successfully used to reach important milestones in the field of quantum computing as trapped ions can fulfill the criteria of scalability, easy initialization, useful coherence times, control mechanisms suitable to realize quantum gates, qubit-specific measurements, and the potential to be miniaturized and integrated with opto-electronics [1].

An inherent property of quantum systems is that measurements affect the state of the system. This precludes experimental real-time monitoring of quantum systems. However, unsharp measurements yield information on the state of a target system with minimal disturbance of its state by making measurements on an auxiliary system that is weakly entangled with the target [2]. In theoretical studies, unsharp measurements have been applied to state monitoring [3] and feedback control [4]. Unsharp measurements allow the realization of quantum simulators that makes it possible to study complex systems that cannot be simulated by classical computers, such as many-body systems in solid state materials, chemistry, and quantum biology [5]. However, experimental work in this field is limited.

We report on an ongoing project to trap, selectively manipulate, and entangle two isotopes of ytterbium (^{171}Yb and ^{174}Yb) in a Paul trap, with the long-term goal to demonstrate entanglement and unsharp measurements in this experiment. Using two isotopes of the same element, ^{171}Yb and ^{174}Yb, reduces the equipment cost of the system whilst allowing species-specific single ion addressing. Unsharp measurement using ytterbium ions has to our knowledge not been demonstrated yet.

2. Experimental methods

The ^{171}Yb and ^{174}Yb ions are trapped in a linear Paul trap and cooled and manipulated using five tunable external cavity diode lasers. Frequency-shifted sidebands are added by means of electro-optic modulators and fast switching of laser beams is achieved by FPGA control of acousto-optic devices. Microwave radiation, channeled with a microwave horn, is used to excite the qubit transitions. A CMOS camera and photodiodes are set up to image and measure fluorescence.

For the ^{171}Yb ions, two levels of the $4f^{14}$ $6s$ $^2S_{1/2}$ state are used as hyperfine qubit levels, and suitable transitions to the $^2P_{1/2}$ state exist for state preparation and detection. For ^{174}Yb ions the Zeeman-shifted fine structure levels of the $^2S_{1/2}$ state are used as qubit levels. As no closed state detection cycle exists for ^{174}Yb, state shelving to the metastable $^2D_{5/2}$ state must be used to enable state detection.

The protocol of unsharp measurement requires the ions to be cooled to the vibrational ground state of the trap. A sequence of laser pulses entangles the internal states of the target and auxiliary ions with the vibrational mode of the ions in the trap. A fluorescence measurement on the auxiliary ion yields information on the state of the target ion. The strength of the noninvasive measurement is controlled by the characteristics of the pulse sequence. [2]

3. Results and discussion

During 2017 the first ion trapping in Africa was achieved, trapping ^{171}Yb ions (see Figure 1). Rabi oscillations between the qubit states of ^{171}Yb ions were measured as proof of principle quantum behaviour [6].
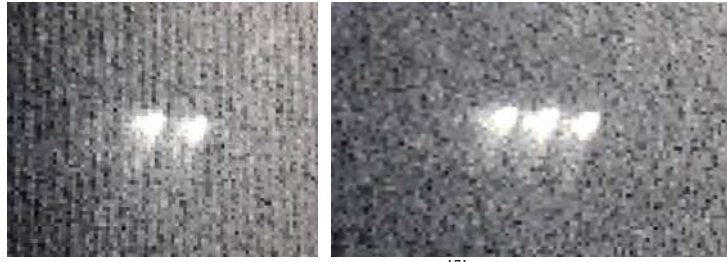
Figure 1 Fluorescence images of two and three[171]Yb ions in the Paul trap.

Significant improvements have been made to the experimental setup since the first trapping. New trap electrodes were designed and installed. The trap fields were simulated to determine parameters for stable trapping and determine motional frequencies of the trapped ions. The lasers were stabilised by frequency locking to custom optical cavities in temperature-controlled vacuum [7].

Rate equation simulations were done to determine the feasibility of the state shelving technique and using the same laser for sideband cooling of the ions to bring the ions to the ground vibrational state.

As the [171]Yb ion is not a pure qubit, but a four-state system, density matrix theory was used to study the dynamics of the [171]Yb ion pumped by radio frequency radiation. As practical application comparison of simulation to experimental Rabi frequency results quantified the effect of trap losses and collisions. The study also showed that variation of the external magnetic field and detuning of the radio frequency can yield saturation resonance conditions, extrema in steady state populations and electromagnetically induced transparency [8].

4. Conclusions

The project is developing a cost-effective experimental setup for the investigation of ion trapping, entanglement and unsharp measurements, using [171]Yb and [174]Yb ions. The first experimental trapping has been achieved. New results regarding the manipulation of [171]Yb qubits have been produced by simulation. The hands-on training of postgraduate students contributes to human capital development in the field of quantum technology in Southern Africa.

Acknowledgments

References

[1] H. Häffner, C.F. Roos and R. Blatt, "Quantum computing with trapped ions", Physics Reports 469, 155-203 (2008).

[2] S.K. Choudhary, T. Konrad, H. Uys, "Implementation schemes for unsharp measurements with trapped ions", Physical Review A 87, 012131 (2013).

[3] T. Konrad and H. Uys, "Maintaining quantum coherence in the presence of noise through state monitoring", Phys. Rev. A. 85, 012102 (2012).

[4] P.J.W du Toit, S.C. Burd, T. Konrad, H. Uys, Real-time state estimation and feedback control of an oscillating qubit via self-fulfilling prophecy (SFP), METROLOGIA 56(1), 104003 (2019).

[5] R. Blatt and C.F. Roos, "Quantum simulations with trapped ions", Nature Physics, 8(4), 277-284 (2012).

[6] N.J. Matjelo, "Implementation of an ytterbium 171 trapped ion qubit", PhD dissertation, Stellenbosch University, 2020.

[7] D.A. Janse van Rensburg, "Laser frequency stabilization for trapped Yb+ experiments", MSc thesis, Stellenbosch University, 2020.

[8] S. Bester, C.M. Steenkamp, "Optical Bloch modeling of magnetic dipole transitions in a four-state system and its application in ion trapping: tutorial", J. Opt. Soc. Am. B 40, 830-848 (2023).

Vortex Crystals in Self-Trapped Optical Beams

Jose Guerra, Angel Paredes and Humberto Michinel

[1]*IFCAE. Instituto de Física e Ciencias Aeroespaciais. Universidade de Vigo.*
Edificio Manuel Martínez-Risco. Campus Universitario de As Lagoas s/n. 32004 Ourense, Spain.

e-mail: `hmichinel@uvigo.es`

1. Introduction

In the present work, we introduce self-trapped vortex soliton crystals that are formed in two-dimensional coherent beams propagating in optical media with competing nonlinearities, where focusing effects are dominant at intermediate powers and self-defocusing increase at higher intensities yielding a cubic-quintic (CQ) dependence of the refractive index with the amplitude of the wavefunction. This type of optical nonlinearity can be achieved, for instance, by appropriately preparing a quantum state within a cold gas of Rb atoms, [1, 2] and it can be described by the following dimensionless equation in a 1+2D geometry:

$$i\frac{\partial \psi}{\partial \tau} + \nabla_\perp^2 \psi + \left(|\psi|^2 - |\psi|^4\right)\psi = 0, \tag{1}$$

2. Self-Trapped Vortex Crystals

In Fig. (**1**, left-top) we plot contours of $|\psi|^2$ (upper row) and their corresponding phase maps (lower row) displaying vortex crystals that have been found by numerically solving Eq. (1) for three different stationary configurations: triangle (a, d), pentagon (b, e) and heptagon (c, f). The vortex arrays shown are stationary with single charged vortices in the vertices of the polygons and opposed vortices in the centres with charge 1, 2 and 3 respectively for the triangle, pentagon and heptagon.

To explain this surprising behavior, we use the fact that the velocity drift velocity v_i induced by a vortex of topological charge m_i placed at a distance l_i from another phase singularity, is perpendicular to the line joining the two vortices, directly proportional to the product of their charges and inversely proportional to the distance between them[3]. Applying basic symmetry to a regular N-polygon with odd number of sides and single positively charged vortices placed in their vertices, the total drag velocity induced in one vortex by the rest of them will be (see Fig. **1**, left-bottom):

$$v = \sum_i^{(N-1)/2} v_i = \sum_i^{(N-1)/2} \frac{2\cos(\alpha_i)}{l_i} \tag{2}$$

For a regular polygon inscribed in a circle of radius r and N sides of length l_i like those of Fig. (**1**, left-bottom), we have that $r\cos(\alpha_i) = l_i/2$ and the previous formula yields a velocity drift induced on each vortex by the others located in the remaining vertices $v = (N-1)/2$, where N is odd natural number.

Therefore, the cases of a triangle, pentagon and heptagon with central vortex of charges m = -1, -2 and -3 respectively, will yield vortex patterns that will evolve without any change on its shape. The case of the triangle is the only one stable, as is demonstrated by simulating a collision between two identical beams with opposite phases (see Fig. **1**, right).
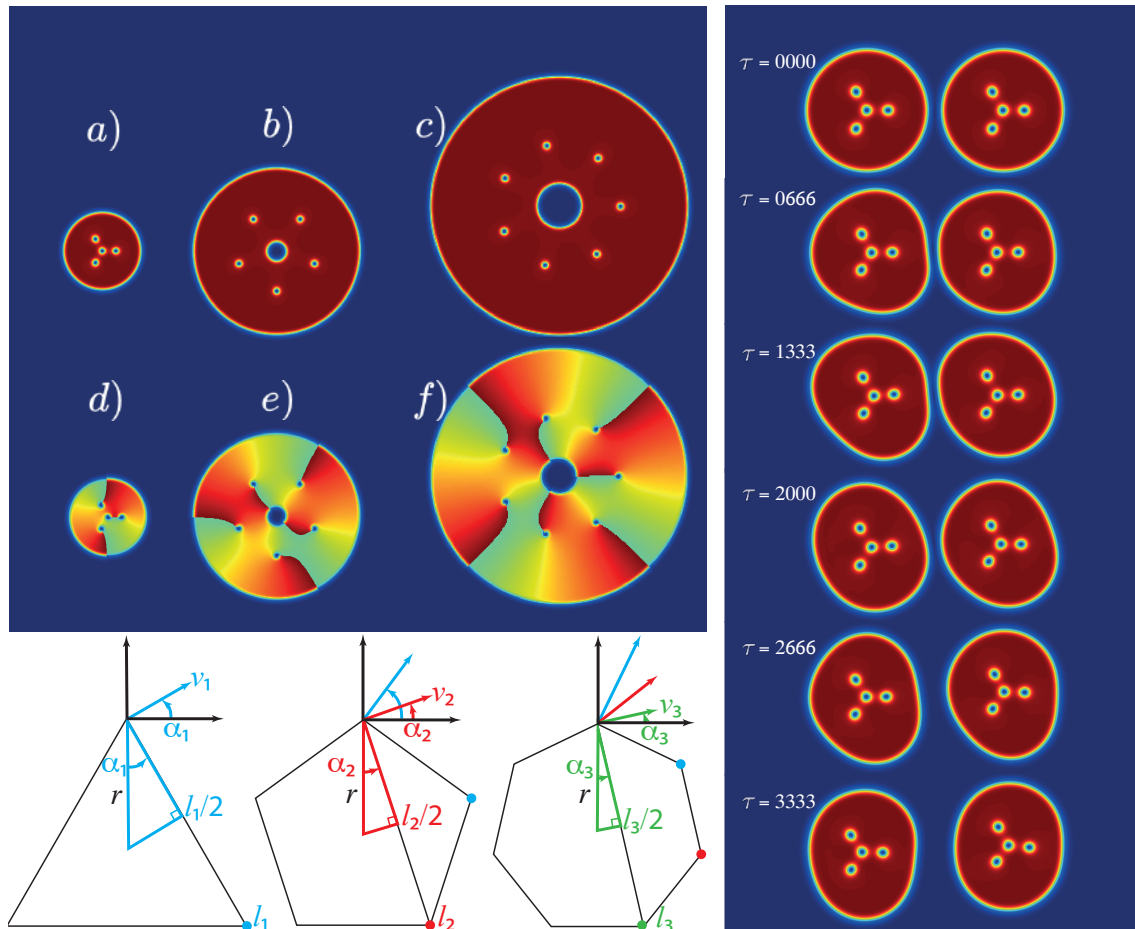
Figure 1: Left-top: contour plots of $|\psi|^2$ (upper row) and their corresponding phase maps (lower row) of various self-trapped vortex crystals that have been found by numerically solving Eq. (1) for three different stationary configurations: triangle (a,d), pentagon (b,e) and heptagon (c,f). Left-bottom: vector sketch of dragging velocities for each case. Right: collision of two beams hosting vortex crystals.

3. Conclusions

We have introduced a new type of stable nonlinear waves that take the form of regular vortex patterns hosted in self-focused coherent light beams that propagate without distortion in cubic-quintic nonlinear optical materials.

Acknowledgments

References

[1] H. Michinel, M. J. Paz-Alonso and V. M. Pérez-García, *Phys. Rev. Lett.* **96**, 023903 (2006).

[2] Zhenkun Wu, et. al, *Phys. Rev. A.* **88**, 063828 (2013).

[3] P. Coullet, L. Gil, L., and F. Rocca, *Opt. Comm.*, (**73**), 403–408 (1989).

List of Posters

P01: Entanglement-based technique robust against the effects of atmospheric turbulence by exploiting spatial coherence properties.

Marie Louise Umuhire, *University of KwaZulu-Natal*

P02: Optical Emission Spectroscopy Measurements of Electron Density in a Laser Induced CNiCo Plasma

Ursula Monica Pillay, *University of KwaZulu-Natal*

P03: Optical emission spectroscopy study on laser induced CNiY plasmas at room temperature

Bala Saraswathi Amirthapandian, *University of KwaZulu-Natal*

P04: Stark Spectroscopy of Plant Photosystem I's Red Pigments

Michael Lovemore, *University of Pretoria*

P05: Synthesis and characterisation of high-temperature Boron nanostructures and computational modelling

Sadiq Nafiu Aliyu , *University of KwaZulu-Natal*

P06: Physics-Informed Neural Networks for Quantum Optics

Shivani Mahashakti Pillay, *University of KwaZulu-Natal*

P07: Quantum Simulation of Fokker-Plank Equations for Q Functions of Quantum Optical Systems

Ian Joel David, *University of KwaZulu-Natal*

P08: Fourier Ptychographic Microscopy for Large Area, High-Resolution Imaging

Eugene Egbert Fouche, *Stellenbosch University*

P09: High-resolution phase-sensitive coherent anti-Stokes Raman scattering spectroscopy by time-domain ptychographye

Jan Anthonie de Beer, *Stellenbosch University, South Africa*

P10: Exploring metallic nanoparticles for enhanced multiplexed SERS for diagnostics

Lungile Thwala, *CSIR, South Africa*

P11: Determination of cadmium in cocoa beans using laser-induced breakdown spectroscopy

Leila Raquel Pincay Abadiano, *Escuela Politécnica Nacional, Ecuador*

P12: Optical properties of biosynthesized nanoscaled Eu2O3 for red luminescence and potential antidiabetic applications

Hamza Mohamed, *University of South Africa, South Africa*

P13: Stokes reconstruction of Chiral fields

Light Mkhumbuza, *University of Witwatersrand, South Africa*

P14: Monitoring the metabolics of single yeast cells through fluorescence microscopy using integrated optical tweezers and microfluidic setup

Le Roi Alexander Du Plessis, *Stellenbosch University, South Africa*

P15: Photobiomodulation promotes wound healing in a diabetic cellular model

Dimakatso B. Gumede, *University of Johannesburg, South Africa*

P16: Photobiomodulation at 830 nm Promotes Cellular Viability and Reduces Cell Death in Fibroblast Diabetic Hypoxic Wounded Cells

Patricia Kasowanjete, *University of Johannesburg, South Africa*

P17: Preparation and in vitro evaluation of the anticancer photodynamic therapy efficacies of ionic phthalocyanine derivatives and their nanoparticle conjugates

Lindokuhle Cindy Nene, *University of Johannesburg, South Africa*

P18: Photobiomodulation at 830 nm modulates NF-B and apoptosis in wounded and diabetic wounded fibroblast cells

Tintswalo Nomsa Mgwenya, *University of Johannesburg, South Africa*

P19: Enhancement of Raman Spectroscopy on SARS-CoV-2 detection using machine learning

Nkgaphe Tsebesebe, *CSIR, South Africa*

P20: Determining the physical properties of a perturbed optically trapped particle using Mie scattering

Anneke Erasmus, *Stellenbosch University, South Africa*

P21: Photo-thermal effects of Citrate Gold Nanoparticle on Lung Cancer

Kave Moloudi, *University of Johannesburg, South Africa*

P22: Dose response cytotoxicity studies with naturally derived photosensitizers against cancer cells

Nosipho Fakudze, *University of Johannesburg, South Africa*

P23: Curcumin-based Nanoconjugates and their promising approaches to cancer treatment

Lufuno Gracious Nemakhavhani, *University of Johannesburg, South Africa*

P24: Optimisation of ADSC Seeding Density for use in 3D Culture with Photobiomodulation: A Pilot Study

Brendon Roets, *University of Johannesburg, South Africa*

P25: Synthesis of Graphene Oxide-Gold Nanorods Nanocomposite-Porphyrin Conjugate for Improved Dual Cancer Phototherapy Performance

Thabang Calvin Lebepe, *University of Johannesburg, South Africa*

P26: Comparative study of tetrapyrrolic photosensitizer mediated phototherapy against breast cancer cell subtypes

Paromita Sarbadhikary, *University of Johannesburg, South Africa*

P27: Curcumin-loaded solid lipid nanoparticles mediated photodynamic therapy-induced apoptosis in human lung cancer cells

Jose Merlin Jayaraj, *University of Johannesburg, South Africa*

P28: WiFoO: Democratizing Long-Range Free Space Optics Using 802.11 Over Optical

Mikaeel Dindar, *University of Witwatersrand, South Africa*

P29: Synergistic anticancer effects of gold nanoparticle-herceptinhypocrellin B conjugates in human breast cancer cells

Sheeja Sheela Rajan, *University of Johannesburg, South Africa*

P30: Photobiomodulation for enhanced neural embryoid body formation of Stem cells

Precious Earldom Mulaudzi, *University of Johannesburg, South Africa*

P31: Ag-H2O Nanofluids Synthesized via Pulsed Laser Liquid-Solid Interaction for Enhanced Photonics Integrated Circuit Cooling

Snenkosi Welcome Dlamini, *University of South Africa, South Africa*

P32: The UV-VIS spectrum of conjugated metal nanoparticles with some purposed COVID-19 drugs: a DFT study

Razieh Morad, *University of South Africa, South Africa*

P33: Nanofluid by pulsed laser ablation in liquid: Parameter influence

Meisam Aligholami, *University of South Africa, South Africa*

P34: Surface Enhanced Raman Spectroscopy and SERS/Drop-Coating Deposition Raman as Feasible Mechanisms for Detecting Dopants in Complex Matrices

Moses Juma, *University of South Africa, South Africa*

P35: Silver-Based Nanostructured Surface-Enhanced Raman Spectroscopy Technique for Enhancing Dexamethasone Detection

Nancy Mwikali Mwenze, *University of South Africa, South Africa*

P36: Biomimicry Highly reflecting material for radiative cooling

Nandipha L. Botha, *University of South Africa, South Africa*

P37: Development and In-Orbit Calibration of the New-Generation Solar Irradiance Spectrometer

Hui Wang, *Changchun Institute of Optics, Fine Mechanics and Physics, China*

Entanglement-based technique robust against the effects of atmospheric turbulence by exploiting spatial coherence properties

Marie Louise Umuhire [1*], Yaseera Ismail[1], Stutti Joshi[2] and Francesco Petruccione[3]

[1]*School of Chemistry and Physics, University of KwaZulu-Natal, address*

[2]*Department of Physics, Indian Institute of Technology Delhi, Hauz Khas, New Delhi 110016, India*

[3]*School of Data Science and Computational Thinking, Stellenbosch University, Merriman Ave, Stellenbosch, 7600*

*e-mail: `ulouizia@gmail.com`

1. Introduction

Quantum communication is a promising data transfer technique capable of securely transmitting information among authorised distant parties. The most prominent technique of quantum communication involves using entanglement for generating, encoding and distributing single photons through optical fibre channels or free space channels [1, 2]. However, atmospheric turbulence presents a challenge for free-space quantum communication techniques that use entanglement since the break up of entanglement, hence the coincidence count detections and the visibility are affected [3]. However, there is an alternative technique capable of negating the influence of atmospheric turbulence. This is done by generating entangled photons using partially spatially coherent properties.

This work involves implementing free space entangled photons using a fully and a partially spatially coherent pump beams. The effects of atmospheric turbulence are assessed by exploiting spatial coherent pump properties and varying the atmospheric turbulence strength for different propagation distances.

2. Implementation of entangled photons passing through atmospheric turbulence

The interaction of a pump beam with a nonlinear crystal (NLC) generates two entangled photons known as the signal and the idler photons through a spontaneous parametric down-conversion (SPDC) process at the crystal plane. Fig. **1** describes the experimental setup which is initiated by a fully spatial coherent pump beam passing through a rotating ground glass diffuser (RGGD) and a two-lens system to turn into a partially spatially coherent pump beam, then focused on an NLC responsible for producing entangled photons through the SPDC process. Thereafter, the two entangled photons are focused on the spatial light modulator (SLM) responsible for moderating the effects of atmospheric turbulence. By using single photons detectors $D1$ and $D2$ connected to a personal computer (PC), the coincidence counts of the signal and the idler photons are recorded.
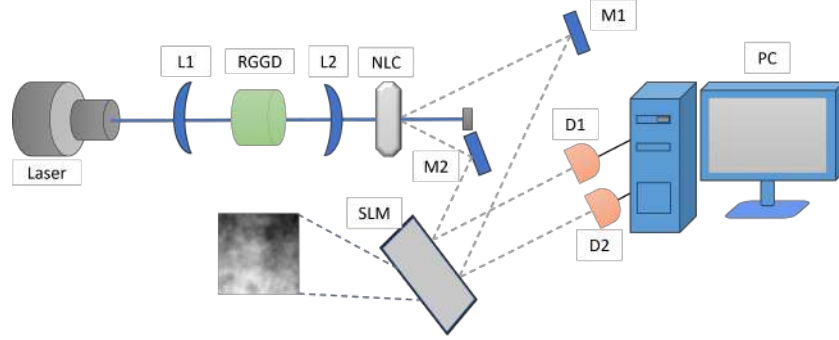
Figure 1: Generation of partially spatially coherent down-converted photons. RGGD denotes a rotating ground glass diffuser, and $L1$ and $L2$ are lenses. NLC represents a nonlinear crystal, $M1$ and $M2$ are two mirrors, SLM denotes a spatial light modulator, $D1$ and $D2$ single-photon detectors, and PC is a personal computer.

3. Results and Analysis

The coincidence count rate depends on the beam waist and spatial coherence length of the pump beam, σ and δ respectively, and the strength of the atmospheric turbulence C_n^2 at different propagation distances. In this work, the effects of atmospheric turbulence are studied using the Kolmogorov Model of turbulence for $C_n^2 = 10^{-14} m^{-2/3}$ and $C_n^2 = 5 \times 10^{-14} m^{-2/3}$ representing weak and strong turbulence respectively at different propagation distance of z = 1 km, 5 km, 7 km and 20 km. The coincidence counts recorded for the implementation entangled photons using a fully spatially coherent pump beam ($\delta = \infty$) and using a partially spatially coherent pump beam for $\delta = 0.0876$mm, 0.0417mm, and 0.0253mm are given as follows:
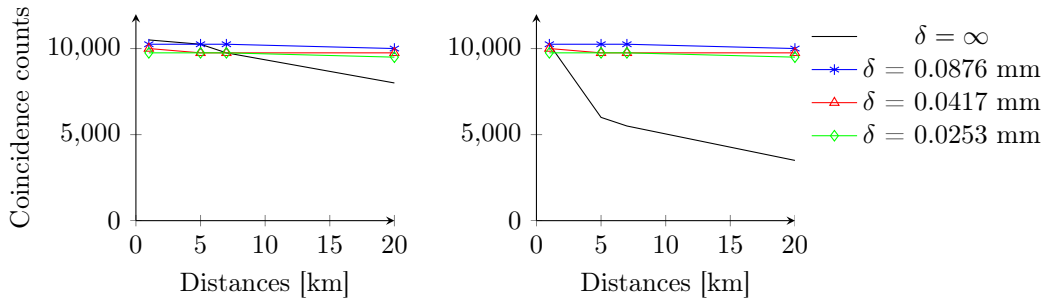
Figure 2: Coincidence counts of entangled photons created using a fully spatially coherent pump beam ($\delta = \infty$), and using a partially spatially pump beam ($\delta = 0.0876$mm, 0.0417mm, and 0.0253mm) for weak (left) and strong (right) turbulence at different propagation distances of z = 1 km, 5 km, 7 km and 20 km.

With the results displayed in Fig. **2**, an exponential decrease in coincidence counts is observed as the the turbulence varies from weak to strong for different distances for entangled photons generated using a fully spatially coherent pump beam. Another observation is that the coincidence counts for entangled photons generated using a partially spatially coherent pump beam are almost constant as the turbulence varies from weak to strong for different propagation distances.

4. Conclusion

With the results obtained in this work, we can strongly confirm that partially spatially entangled photons are resilient to the effects of atmospheric turbulence especially for long propagation distances. These results can be useful for the implementations of free space quantum communication techniques.

Acknowledgements

References

[1] S.K. Liao, W.Q. Cai, W.Y Liu *et al.*, "Satellite-to-ground quantum key distribution", *Nature* **549**, pp. 43–47 (2017).

[2] J. Yin, Y. Cao, Y. H. Li, S. K. Liao, L. Zhang, J. G. Ren et al., "tellite-based entanglement distribution over 1200 kilometers", *Science* **356**, pp. 1140 (2017).

[3] Y. Ismail, S. Joshi, A. Forbes, F. Petruccione, "Instrumentation limitation on a polarization-based entangled photon source", *JOSA B* **34**, pp. 1084-1089 (2017).

Optical Emission Spectroscopy Measurements of Electron Density in a Laser Induced CNiCo Plasma

Ursula Monica Pillay[1*] and Mathew Kisten Moodley[1]

[1]*School of Chemistry & Physics, University of KwaZulu-Natal, Private Bag X5400, Durban, South Africa*

[*]E-mail: pillayu1@ukzn.ac.za

1. Introduction

While there are many diagnostic techniques that are suitable for the determination of electron density, spectroscopy is the simplest method with regards to the instrumentation [1]. The electron density is essential for plasma temperature measurements using the Saha-Boltzmann plot method and for using the McWhirter criterion to confirm that the plasma is in Local Thermodynamic Equilibrium (LTE). In this paper we report on the electron density and its dependence on time elapsed after the laser pulse and spatial separation from the target surface.

A graphite composite target comprising 98% graphite, 1% nickel and 1% cobalt was ablated in a heated furnace at 1073 K. Light emissions from the ablation events were captured by an Andor ME5000 echelle spectrograph. The delay time was varied from 0 ns to 3000 ns in increments of 100 ns. These measurements were repeated at different distances from the target surface ranging from 0 mm to 6 mm. In this way, the spatial and temporal evolution of the plasma plume was tracked.

The local electric field created by plasmas causes spectral broadening. This phenomenon, the Stark effect, results in a broadening of the spectral line. Stark broadening occurs when emitters and charged particles, such as electrons or ions, collide [2]. The quadratic Stark widths of several spectral peaks were measured and used to calculate the electron density of the plasma.

The full width half maximum (FWHM) of the Stark broadened lines and the electron density n_e are related by Eq. (1) [3]

$$\Delta\lambda_{\frac{1}{2}} = 2W\left(\frac{n_e}{10^{16}}\right) + 3.5A\left(\frac{n_e}{10^{16}}\right)^{\frac{1}{4}} \times \left(1 - \frac{3}{4}N_D^{-1/3}\right)W\left(\frac{n_e}{10^{16}}\right)A^0 \tag{1}$$

where W is the electron impact parameter, A is the ion broadening parameter and N_D is the number of particles in the Debye sphere. Since the Stark broadening is greatly influenced by electron impact, the ion correction factor may be disregarded and Eq. (1) then reduces to

$$\Delta\lambda_{\frac{1}{2}} \approx 2W\left(\frac{n_e}{10^{16}}\right) \tag{2}$$

2. Results and Discussion

We have measured the Stark broadened profiles of several spectral peaks for each of the elements present in the composite target. The wavelengths of the spectral peaks are given in Table 1. A plot of electron density for individual carbon and nickel lines is given in Fig. 1 and Fig. 2 respectively. A plot of electron density versus distance from the target surface for carbon and nickel is given in Fig 3.
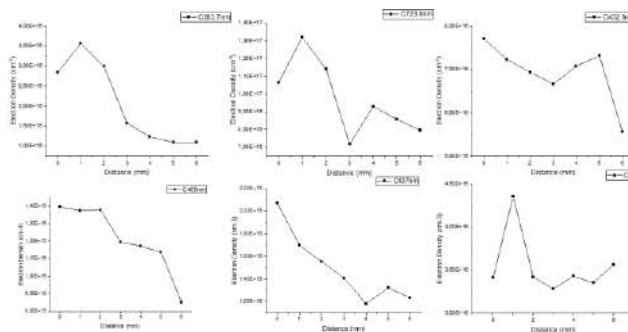
Figure 1 Electron densities for individual carbon emission lines.
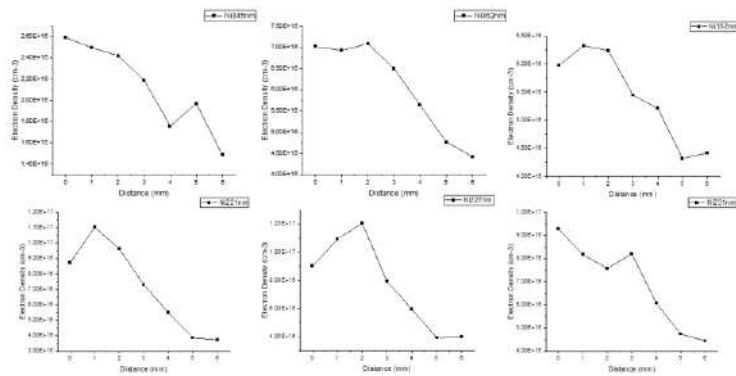
Figure 2 Electron densities for individual nickel emission lines.
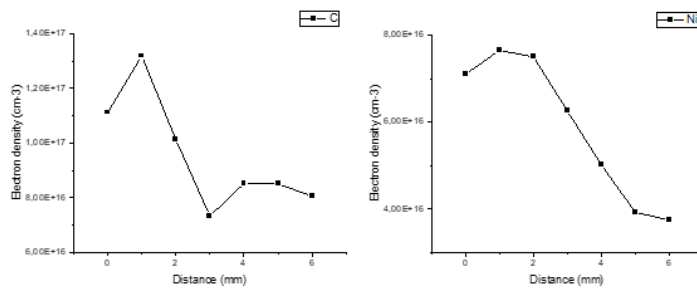
Figure 3 Electron density as a function of distance from the target surface**.**

Carbon (nm)	Nickel (nm)
437.3	345.9
481.9	362.0
283.7	352.6
723.8	221.7
432.6	227.1
465.2	231.7

Table 1 List of carbon and nickel emission lines used to determine the electron densities.

3. Conclusions

We have observed that the electron density decreases with increasing distance from the target surface. For carbon, from 1mm to 3mm and for nickel, from 2mm to 5mm the electron density decreases linearly with distance from the target surface. This is in partial agreement with the literature. Our results also show an initial increase in electron density.

Acknowledgments

References

[1] S.S. Harilal, C.V. Bindhu, R.C. Isaac, V.P.N. Nampoori and C.P.G. Vallabhan, "Electron density and temperature measurements in a laser produced carbon plasma", J. Appl. Physics. 82(5) p. 2140–2146 (1997).

[2] J.A.A. C. Aragón, "Characterization of laser induced plasmas by optical emission spectroscopy: A review of experiments and methods," *Spectrochimica Acta Part B: Atomic Spectroscopy,* vol.63, pp. 893–916, 2008.

[3] H. R. Griem, "Plasma Spectroscopy", (McGraw-Hill, New York, 1964).

Optical emission spectroscopy study on laser induced CNiY plasmas at room temperature

Bala Saraswathi Amirthapandian

School of Chemistry and Physics,
Westville campus,
University of Kwa-Zulu Natal, South Africa
E-mail: saraswathiamir@gmail.com

1. Introduction

The optical emission spectroscopy (OES) of laser-induced plasmas is called laser-induced breakdown spectroscopy (LIBS), a potent tool for the studies of laser-matter interaction and enables fast contactless analysis of any material. The development in laser-induced plasma characterization allows the measurement of two or three-dimensional distribution of plasma parameters, further used to study the atomistic process and the evolution of plasmas. This work is focused on the optical emission spectroscopy of the laser induced plasma (LIP) produced from the ablation process of CNiY target inside the furnace at room temperature and the temporal investigation of the evolution of carbon plasmas along with the catalysts influence on it is presented here with the corresponding plots of the evolution maps of electron density and electron temperature. In this way, we hope to study the nucleation dynamics and use this information to improve the synthesis process of any nanostructures.

The OES data were collected with the help of Andor- Mechelle 5000 spectrograph and the temporal evolution of the plasmas were obtained by changing the pulse delay. The electron density of the LIP was determined by the "stark broadening profile" with the help of the following expression,

$$\lambda_{\text{FWHM}} = 2\times10^{-16}\ \mathbf{w}\mathbf{N}_e \qquad \text{-------------------(1)}$$

where,

$\lambda_{\textbf{FWHM}}$ and $\mathbf{w}$ are the full width half maximum and electron impact parameters of the stark broadened lines.

And the electron temperature was calculated by the Saha- Boltzmann method since it utilizes the parameters of the emission lines of different ionization species the accuracy of this method is greater relative to the Boltzmann method.

$$\ln\left(\frac{I_{21}^z \lambda_{21}}{g_2^z A_{21}^z}\right)^* = -\frac{1}{TK_B}E_2^{z*} + \ln\left(\frac{hcN^0}{U^0(T)}\right) \qquad \text{------------------(2)}$$

The above expression includes the ionization parameters of different ionization levels. The local thermodynamic equilibrium condition was examined with the help of McWhirter criterion, and the temperature was found by slope from the Saha-Boltzmann linear fitting plots with greater accuracy.

2. Plots of electron density and temperature
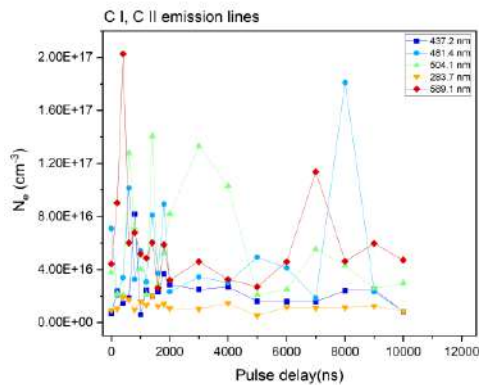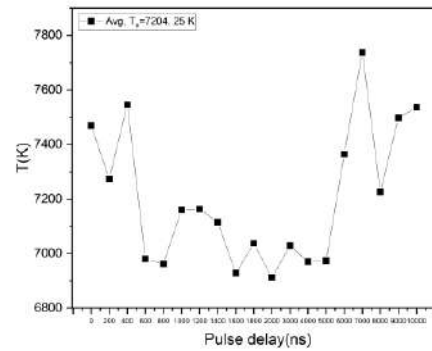
| Fig: 1 | Fig: 2 |

Figures 1 and 2 are the examples of plasma density and temperature evolution of carbon with respect to varying pulse delays.

3. Conclusions

The OES study was conducted on the CNiY target at room temperature. The electron densities and temperatures by Saha- Boltzmann method of the laser induced plasmas were determined along with the catalysts and their temporal evolution was analyzed. Sudden rise of electron densities and temperatures were observed at higher pulse delays for carbon and the catalysts as well. The corresponding phenomenon for this pattern and the influence of active line transitions of the catalysts on carbon is now being undergone.

References

[1] Brandon Seesahai, Plasma Temperature Measurements in the Context of Spectral Interference, 2016 (Stars)

[2] Hongbing et al., J Laser Opt Photonics 2018, Comprehensive Study on the Electron Temperature and Electron Density of Laser-Induced Mg Plasma, Journal of Lasers, Optics & Photonics

[3] C. Aragón *, J.A. Aguilera, Characterization of laser induced plasmas by optical emission spectroscopy: A review of experiments and methods, Spectrochimica Acta Part B 63 (2008) 893–916

[4] David Edmond Motaung, Mathew Kisten Moodley, E. Manikandan, and Neil J. Coville, In situ optical emission study on the role of C 2 in the synthesis of single-walled carbon nanotubes, Journal of Applied Physics 107, 044308 (2010); doi: 10.1063/1.3311563

[5] Hans R. Griem, Plasma Spectroscopy

Stark Spectroscopy of Plant Photosystem I's Red Pigments

Michael A.C. Lovemore[1*], Towan Nöthling[1] and Cory van Galen[3], Md Wahadozsamen[2], Robert Stanley[3] and Tjaart P. J. Krüger[1]

[1]Department of Physics, University of Pretoria, Lynnwood Rd, Pretoria, South Africa

[2]Department of Physics, University of Dhaka, Nilkhet Rd, Dhaka, Bangladesh

[3]Department of Chemistry, Temple University, Broad St, Philadelphia, United States

[*]E-mail: Michael.lovemore98@gmail.com

1. Introduction

Photosynthesis is the ever-important biological process in various organisms that converts absorbed light energy into chemical energy with near-100% quantum efficiency The initial energy transport and conversion occur within photosystems, which comprise dense clusters of pigment molecules, arranged in precise positions by proteins. Photosystem I (PSI) contains a subset of chlorophylls (Chls) that absorb at wavelengths longer than the reaction centre Chls at around 700 nm. These so-called 'red Chls' assist in increasing the cross-sectional area for absorption, allowing light to be absorbed in shady conditions, and they may assist in photoprotection. The large red-shift arises from the mixing of strong excitonically coupled states with charge-transfer (CT) states [1]. Most of these red Chls are found in the peripheral light-harvesting complex (LHCI) of PSI. It has been suggested that some red Chls lie on the interface between LHCI and the PSI core. Although the red Chls contribute a small fraction to the absorption cross-section, they play a significant role in the excitation energy transfer dynamics. CT states are sensitive to an external electric field, making Stark spectroscopy a powerful method to investigate the electronic nature of these red Chls.

In this study, we performed Stark fluorescence (SF) spectroscopy on plant PSI-LHCI supercomplexes to quantify the Stark effect of the red Chls in this system by resolving the different spectral contributions and extracting the corresponding electro-optical properties. The data analysis was done using the Liptay formalism [2], which involves the simultaneous fit of the fluorescence (F) and SF spectra using a superposition of zeroth-, first-, and second-order derivatives of Gaussian functions according to

$$\Delta I_F(v) = (fF_{ext})^2 \left[A I_F(v) + B v^3 \frac{d\left[\frac{I_F(v)}{v^3}\right]}{dv} + C v^3 \frac{d^2\left[\frac{I_F(v)}{v^3}\right]}{dv^2} \right]. \qquad (1)$$

At the magic angle (54.7°), the electro-optical parameters of the samples, i.e., the difference dipole moment and molecular polarizability between the ground and excited states connected by the optical transition, can be extracted from the coefficients in Eq. 1 as follows:

$$\Delta\alpha = 2hcB_{54.7°}, \qquad (2)$$

$$\Delta\mu = hc\sqrt{6C_{54.7°}}. \qquad (3)$$

2. Results

The F and SF spectra of PSI-LHCI could be fitted well with two Gaussians (Fig. 1). The corresponding electro-optical parameters are summarized in Table 1. Band 1 describes the properties of the lowest excitonic state, which contributes most to the emission. It is associated with a small, negative $\Delta\alpha$, indicative of a small, light-induced CT state, as confirmed by the small magnitude of $\Delta\mu$. Band 2 describes the properties of the red Chls. Both $\Delta\mu$ and $\Delta\alpha$ are larger than those of band 1, which is expected, but the magnitudes are smaller than predicted. On the other hand, the sign of $\Delta\alpha$ for band 2 indicates an intrinsic CT character, as expected. Both bands have a small, negative ZDC, indicating a low field-induced change in emission intensity.
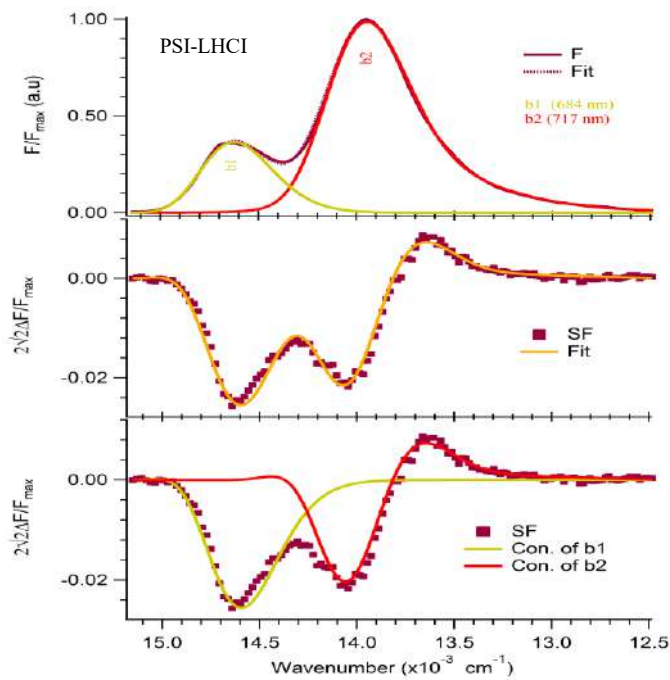
Figure 1 Stark fluorescence spectra of plant PSI-LHCI super-complex

Band	ZDC	$\Delta\alpha$ [Å^3/f^2]	$\Delta\mu$ [D/f]
b1 (684nm)	-0.067	-89.48	1.22
b2 (717nm)	-0.005	143.17	3.09

Table 1 Electro-optical properties corresponding to the spectra in Fig 1.

3. Conclusions

Stark fluorescence of the plant PSI-LHCI supercomplex was successfully performed and analysed. Two bands were resolved, one corresponding to the lowest exciton state and one corresponding to an exciton-CT hybrid state (red Chls). A comparative Stark absorption and fluorescence study on the PSI core complex and PSI-LHCI supercomplex is expected to reveal the characteristics and functions of the different red Chl pigment pools.

Acknowledgments

References

[1] Croce, Roberta, et al. "The low-energy forms of photosystem I light-harvesting complexes: spectroscopic properties and pigment-pigment interaction characteristics." *Biophys. J.* 93.7 (2007): 2418-2428.

[2] Bublitz, Gerold U., and Steven G. Boxer. "Stark spectroscopy: applications in chemistry, biology, and materials science." *Annu. Rev. Phys. Chem*. 48.1 (1997): 213-242.

SYNTHESIS AND CHARACTERISATION OF HIGH-TEMPERATURE BORON NANOSTRUCTURE AND COMPUTATIONAL MODELLING.

N.S. Aliyu[1]*, M.A. Adebisi[1], M.N. Pillay[1], B.S. Amirthapandian[1], U.M. Pillay[1], M.K. Moodley[1]

School of Chemistry and Physics, University of KwaZulu Natal, South Africa.

*E-mail: sadaliyu@gmail.com

Abstract

The synthesis of boron nanostructures (BNSs) at different high- temperatures using the double-pulsed laser ablation (DPLA) technique from bulk boron and their computational modelling using the molecular dynamics (MD) method DFT in Gaussian Simulator embedded with Ovito in the Gaussian view are reported. In this regard, the structural evolution of the boron crystalline and the bulk boron has been investigated employing DFT calculation combined with a GausSum considering the effect of temperature (1200-1400°C), particle size (50 to 200nm) and shape (sheets and nanotubes) on radial distribution functions, intra-atomic distances, coordination numbers, core-to-surface concentration profiles, surface energies Gibb's energy and the enthalpy analysis. The experiment used a q-switched Nd: YAG laser with 532 and 1064 nm combined beam wavelengths to ablate a solid boron target. A vapor–solid process at a furnace temperature and pressure supported boron nanostructures' growth with metal catalysts (1% Ni and 1% Co) in a tube furnace in flowing argon gas. Phase purity and crystallinity of the synthesised BNNs at 1200, 1300, and 1400°C were determined by X-ray diffraction (XRD), and the results from XRD confirm that each BNS is preferentially grown in the c-axis (100) direction of alpha boron. Electron microscopy revealed that each BNS had a length of 2 to 6 μm and a width of 50 to 200 nm, while the chemical nature of the BNSs is identified from energy – dispersive X–ray spectroscopy (EDX). Each BNS's UV–Vis absorption spectra exhibited a sharp absorption peak at 295, 300 and 315 nm, from the computational and experimental, respectively, which is consistent with DFT calculation. Photoluminescence measurements of each BNF showed a strong emission peak at 445, 450 and 520 nm, respectively. Image analysis shows the average diameter of each BNF synthesised to be 25.10, 20.13, and 19.09 nm. The lattice distance of each BNS is found to be 0.35, 0.32, and 0.30 nm, respectively. Raman spectroscopy revealed the fundamental vibrational modes of BNSs at E_g and A_{1g} in both computational and experimental.

Keywords: BNSs, DFT, XRD, Gaussian Simulator, molecular dynamics, HRTEM, Raman spectroscopy.

INTRODUCTION

There is a fascinating interest in the simulation, modelling, and synthesis of boron nanomaterials because boron has unique chemical and physical properties [1]. Bulk boron can be tuned, and completely new structural materials can be created by varying the type and composition of constituent elements, the atomic ordering, size, and shape of the nanomaterials [2]. The boron nanomaterial has various applications, including the nuclear industry for neutron absorption, aerospace, biomedical applications, and computer hardware [3]. This study aims to analyse the structural properties at high temperatures and pressure, determine the nucleation reaction transformation energy involved, and establish a bridge between the theory and the experiment. Therefore, to build a bridge between the theoretical calculation and experiment and to be able to predict many experimental results. This work focuses on icosahedral boron-rich solids whose complex structure is nearly based on B_{12} icosahedral, as the inter-icosahedral bonds are more potent than the intra-icosahedral ones [4]. In the computational part, the structural evolutions of boron nanomaterial have been studied using the molecular dynamics (MD) method DFT in Gaussian Simulator embedded with Ovito in the Gaussian view [5]. From the thermodynamics simulations, it has been observed that the structural evolution, the crystallisation of the material and atomic arrangements of the nanomaterials exhibited thermal stability as the temperature increased [6]. As the simulated nanostructure crystallite size's particle size decreased, the particles became more heat-resistant. However, they mostly preserved their stable crystalline structure, shape, and mixing pattern at high temperatures. Also, it has been observed that the 6 nm nanoparticles owned the FCC lattice structure at room temperature are consistent with the first-order type structure of the synthesised via dual pulsed laser chemical vapour deposition (LCVD) [7].

Materials and method

Sample Preparation and Characterisation of BNMs

In the experiment, the boron nanomaterial was synthesised via LVCD. The material was prepared as a hot-pressed boron mixed with a transitional metal (Cobalt and Nickel) 1% each employing piston and sleeves with a dimension of 17mm diameter and 23mm thick as a target. This target was placed inside an oven at 222 degrees Celsius to consolidate the target and burn out the ethanol and other impurities for 24 hours. Therefore, the sample was placed inside the centre of a large ceramic tube in the furnace where a temperature of 1200, 1300 and 1400 degrees were used to synthesise as prepared nanostructures with the help of argon gas. A laser-assisted Nd: YAG (Physics spectra GCR-4), operating at a dual pulsed wavelength (1064nm and 532nm) temporarily separated by the paths difference of 20ns, was also employed. As prepared nanomaterials were collected from the back of the ceramic tube for sonication with a point sonicator and centrifuge for 40000rpm for 4hrs at room temperature. The nanomaterial was characterised using XRD, SEM, EDS, Raman, UV-vis Photoluminescence and 4- point probe techniques. The Raman experiment's result and the Raman spectroscopy's theoretical calculation were agreed upon in the first-order Raman spectroscopy result.

Raman spectrum/peaks	β-Boron at G_1 Position cm^{-1}	β-Boron at G_2 Position cm^{-1}	α-Boron at G_3 Position cm^{-1}	α-Boron at G_3 Position cm^{-1}	α-Boron at G_3 Position cm^{-1}
Calculated 1200°C	626	943	1153	1280	1365
Experiment At1473K	Very weak	779.44	1139.01	1279.80	weak

Conclusions

BNSs were synthesised at three different high-temperatures, 1200, 1300 and 1400 °C by the laser ablation of a solid boron target composed of boron and mixed metal catalysts (Ni/Co) in an argon atmosphere at a flow rate and gas pressure of 200 sccm and 400 Torr, respectively which were confirmed with the DFT calculations in Gaussian. An analysis of the isolated materials by FESEM and HR-TEM substantiated the growth model from boron nanoparticles for each BNS. According to microscopic analysis, each BNS's diameters were between 50 and 200 nm, and their lengths ranged from 2 to 6µm. Image analysis revealed the average diameter of each BNF as 25.10, 20.13, and 19.09 nm, respectively. The lattice distance of each BNS is found to be 0.35, 0.32, and 0.30 nm, respectively, through SAED. Each BNS's crystallinity and phase were confirmed using PXRD. Each BNS's vibrational modes (G_1, G_2 and G_3) were determined using Raman spectroscopy of first order, and it was consistent with the molecular dynamics (MD) method DFT in Gaussian Simulator embedded with Ovito in the Gaussian view. Each BNS's UV–Vis absorption spectra exhibited a sharp absorption peak at 295, 300 and 315 nm, from the computational and experimental, respectively, which is also consistent with DFT calculation. The XRD results show that each BNS is preferentially grown in the c-axis (100) direction of alpha boron, confirmed by Raman spectroscopy results. Thus, each BNS synthesised via the DPLA technique showed good crystallinity and phase properties for applications in electronic devices. Bringing boron-based low-dimensional systems closer to real-life applications will enable further fundamental research on nanostructures' structural, magnetic, optical, electrical, mechanical, and thermal properties for both theoretical and experimental.

Acknowledgements

References

[1] Alaei Sholeh. Structural, Electronic and Magnetic Properties of Various Nanosystems: Molecular Dynamics Simulations and Density Functional Theory Calculations. PhD thesis, Middle East Technical University, 2014.

[2] Vast N, Baroni S, Zerah G, Besson J M, Polian A, Grimsditch M and Chervin J C 1997 Phys. Rev. Lett. 78 693

[3] D. A Young, phase diagram of the elements (University of California Press Berkelay. CA. 1991).p.88

SYNTHESIS AND CHARACTERISATION OF HIGH-TEMPERATURE BORON NANOSTRUCTURE AND COMPUTATIONAL MODELLING.

N.S. Aliyu[1]*, M.A. Adebisi[1], M.N. Pillay[1], B.S. Amirthapandian[1], U.M. Pillay[1], M.K. Moodley[1]
School of Chemistry and Physics, University of KwaZulu Natal, South Africa.
*E-mail: sadaliyu@gmail.com

Abstract

The synthesis of boron nanostructures (BNSs) at different high- temperatures using the double-pulsed laser ablation (DPLA) technique from bulk boron and their computational modelling using the molecular dynamics (MD) method DFT in Gaussian Simulator embedded with Ovito in the Gaussian view are reported. In this regard, the structural evolution of the boron crystalline and the bulk boron has been investigated employing DFT calculation combined with a GausSum considering the effect of temperature (1200-1400°C), particle size (50 to 200nm) and shape (sheets and nanotubes) on radial distribution functions, intra-atomic distances, coordination numbers, core-to-surface concentration profiles, surface energies Gibb's energy and the enthalpy analysis. The experiment used a q-switched Nd: YAG laser with 532 and 1064 nm combined beam wavelengths to ablate a solid boron target. A vapor–solid process at a furnace temperature and pressure supported boron nanostructures' growth with metal catalysts (1% Ni and 1% Co) in a tube furnace in flowing argon gas. Phase purity and crystallinity of the synthesised BNNs at 1200, 1300, and 1400°C were determined by X-ray diffraction (XRD), and the results from XRD confirm that each BNS is preferentially grown in the c-axis (100) direction of alpha boron. Electron microscopy revealed that each BNS had a length of 2 to 6 µm and a width of 50 to 200 nm, while the chemical nature of the BNSs is identified from energy – dispersive X–ray spectroscopy (EDX). Each BNS's UV–Vis absorption spectra exhibited a sharp absorption peak at 295, 300 and 315 nm, from the computational and experimental, respectively, which is consistent with DFT calculation. Photoluminescence measurements of each BNF showed a strong emission peak at 445, 450 and 520 nm, respectively. Image analysis shows the average diameter of each BNF synthesised to be 25.10, 20.13, and 19.09 nm. The lattice distance of each BNS is found to be 0.35, 0.32, and 0.30 nm, respectively. Raman spectroscopy revealed the fundamental vibrational modes of BNSs at E_g and A_{1g} in both computational and experimental.

Keywords: BNSs, DFT, XRD, Gaussian Simulator, molecular dynamics, HRTEM, Raman spectroscopy.

INTRODUCTION

There is a fascinating interest in the simulation, modelling, and synthesis of boron nanomaterials because boron has unique chemical and physical properties [1]. Bulk boron can be tuned, and completely new structural materials can be created by varying the type and composition of constituent elements, the atomic ordering, size, and shape of the nanomaterials [2]. The boron nanomaterial has various applications, including the nuclear industry for neutron absorption, aerospace, biomedical applications, and computer hardware [3]. This study aims to analyse the structural properties at high temperatures and pressure, determine the nucleation reaction transformation energy involved, and establish a bridge between the theory and the experiment. Therefore, to build a bridge between the theoretical calculation and experiment and to be able to predict many experimental results. This work focuses on icosahedral boron-rich solids whose complex structure is nearly based on B_{12} icosahedral, as the inter-icosahedral bonds are more potent than the intra-icosahedral ones [4]. In the computational part, the structural evolutions of boron nanomaterial have been studied using the molecular dynamics (MD) method DFT in Gaussian Simulator embedded with Ovito in the Gaussian view [5]. From the thermodynamics simulations, it has been observed that the structural evolution, the crystallisation of the material and atomic arrangements of the nanomaterials exhibited thermal stability as the temperature increased [6]. As the simulated nanostructure crystallite size's particle size decreased, the particles became more heat-resistant. However, they mostly preserved their stable crystalline structure, shape, and mixing pattern at high temperatures. Also, it has been observed that the 6 nm nanoparticles owned the FCC lattice structure at room temperature are consistent with the first-order type structure of the synthesised via dual pulsed laser chemical vapour deposition (LCVD) [7].

Materials and method
Sample Preparation and Characterisation of BNFs
In the experiment, the boron nanomaterial was synthesised via LVCD. The material was prepared as a hot-pressed boron mixed with a transitional metal (Cobalt and Nickel) 1% each employing piston and sleeves with a dimension of 17mm diameter and 23mm thick as a target. This target was placed inside an oven at 222 degrees Celsius to consolidate the target and burn out the ethanol and other impurities for 24 hours. Therefore, the sample was placed inside the centre of a large ceramic tube in the furnace where a temperature of 1200, 1300 and 1400 degrees were used to synthesise as prepared nanostructures with the help of argon gas. A laser-assisted Nd: YAG (Physics spectra GCR-4), operating at a dual pulsed wavelength (1064nm and 532nm) temporarily separated by the paths difference of 20ns, was also employed. As prepared nanomaterials were collected from the back of the ceramic tube for sonication with a point sonicator and centrifuge for 40000rpm for 4hrs at room temperature. The nanomaterial was characterised using XRD, SEM, EDS, Raman, UV-vis Photoluminescence and 4- point probe techniques. The Raman experiment's result and the Raman spectroscopy's theoretical calculation were agreed upon in the first-order Raman spectroscopy result.

Type of spectrum/ peaks	β-boron at G_1 position cm^{-1}	β-boron at G_2 position cm^{-1}	α-boron at G_3 cm^{-1}	α-boron at G_3 cm^{-1}	α-boron at G_3 cm^{-1}
Calculated	626cm	943	1153	1280	1365
Excperimental		779.44	1139.01	1279.80	

Conclusions

BNSs were synthesised at three different high-temperatures, 1200, 1300 and 1400 °C by the laser ablation of a solid boron target composed of boron and mixed metal catalysts (Ni/Co) in an argon atmosphere at a flow rate and gas pressure of 200 sccm and 400 Torr, respectively which were confirmed with the DFT calculations in Gaussian. An analysis of the isolated materials by FESEM and HR-TEM substantiated the growth model from boron nanoparticles for each BNS. According to microscopic analysis, each BNS's diameters were between 50 and 200 nm, and their lengths ranged from 2 to 6μm. Image analysis revealed the average diameter of each BNF as 25.10, 20.13, and 19.09 nm, respectively. The lattice distance of each BNS is found to be 0.35, 0.32, and 0.30 nm, respectively, through SAED. Each BNS's crystallinity and phase were confirmed using PXRD. Each BNS's vibrational modes (G_2 and G_3) were determined using Raman spectroscopy, and it was consistent with the molecular dynamics (MD) method DFT in Gaussian Simulator embedded with Ovito (this capable of interpret the molecular orbital energies) in the Gaussian view. Each BNS's UV–Vis absorption spectra exhibited a sharp absorption peak at 295, 300 and 315 nm, from the computational and experimental, respectively, which is also consistent with DFT calculation. The XRD results show that each BNS is preferentially grown in the c-axis (100) direction of alpha boron, confirmed by Raman spectroscopy results. Thus, each BNS synthesised via the DPLA technique showed good crystallinity and phase properties for applications in electronic devices. Bringing boron-based low-dimensional systems closer to real-life applications will enable further fundamental research on nanostructures' structural, magnetic, optical, electrical, mechanical, and thermal properties for both theoretical and experimental.

References

[1] A. Onestone and P. W. Giggs, "Optical properties of the Giggs photon", Phys. Rev. P **6**, p. 430–439 (1905).

[2] P. W. Giggs and A. Onestone, *Teaching Giggs photon optics* (Academic Stress, New York, 2033).

[3] M. C. Intosh and S. Windows, "New trends on photonics of the Giggs photon", in XXL Conference on optical properties of the Giggs photon (2036), vol. 1264, pp. 454–465.

[4] D. A Young, phase diagram of the elements (University of California Press Berkelay. CA. 1991).p.88

[6]
[7]

Physics-Informed Neural Networks for Quantum Optics

Shivani Mahashakti Pillay [1*], Ilya Sinayskiy[2,3], Edgar Jembere [1] and Francesco Petruccione[3,4]

[1] *School of Mathematics, Statistics and Computer Science, University of KwaZulu-Natal, Durban 4001, South Africa*

[2] *School of Chemistry and Physics, University of KwaZulu-Natal, Durban 4001, South Africa*

[3] *National Institute for Theoretical and Computational Sciences (NITheCS), Stellenbosch, South Africa*

[4] *School of Data Science and Computational Thinking, Stellenbosch University, Stellenbosch 7604, South Africa*

*e-mail: `217039130@stu.ukzn.ac.za`

Abstract

Finding adequate solutions to differential equations is a fundamental problem in mathematics. Physics-Informed Neural Networks (PINNs) present a novel methodology for solving differential equations with neural networks [1, 2]. PINNs are trained to minimise a loss function incorporating the residual of the differential equation and terms reflecting the initial and boundary conditions. PINNs have gained significant traction in recent years and have been used to solve a number of fundamental equations in physics. These include the Allen-Cahn equation, the Korteweg-de Vries equation, the 1D non-linear Schrodinger equation [2] and the incompressible Navier-Stokes equations [3]. Despite their popularity, PINNs have not yet been used to solve equations in quantum optics. There are many differential equations in quantum optics that could be solved with PINNs. The Focker-Planck Equation, for example, could be solved to find the Q-Function [4]. In this work, PINNs will be applied to a few equations in quantum optics. An architecture for the PINN that suits the chosen equations will have to be found. The approximated solution of these equations will be verified by comparison to analytical solutions, where possible.

Keywords— Physics-Informed Neural Networks, Differential Equations, Quantum Optics, Q-Function

References

[1] I. E. Lagaris, A. Likas and D. I. Fotiadis, "Artificial neural networks for solving ordinary and partial differential equations", *IEEE transactions on neural networks* **9**, pp. 987–1000 (1998).

[2] M. Raissi, P. Perdikaris and G. E. Karniadakis, "Physics-informed neural networks: A deep learning framework for solving forward and inverse problems involving nonlinear partial differential equations", *Journal of Computational physics* **378**, pp. 686–707 (2019).

[3] X. Jin, S. Cai, H. Li and G. E. Karniadakis, "Nsfnets (navier-stokes flow nets): Physics-informed neural networks for the incompressible navier-stokes equations", *Journal of Computational Physics* **426**, p. 109951 (2021).

[4] H. Carmichael, *Statistical methods in quantum optics 1: master equations and Fokker-Planck equations*, vol. 1 (Springer Science & Business Media, 1999).

Quantum Simulation of Fokker-Plank Equations for Q Functions of Quantum Optical Systems

I. J. David [1,2*], I. Sinayskiy[1,2] and F. Petruccione[1,2,3]

[1]*School of Chemistry and Physics, University of KwaZulu-Natal, Durban 4001, South Africa*

[2]*National Institute for Theoretical and Computational Sciences (NITheCS), Stellenbosch, South Africa.*

[3]*School of Data Science and Computational Thinking, Stellenbosch University, Stellenbosch 7604, South Africa.*

*e-mail: `ian.david@nithecs.ac.za`

One of the earliest proposals for quantum computers is the need to simulate quantum systems [1, 2]. The simulation of closed quantum systems, or Hamiltonian simulation, has been explored in recent years. Novel methods have been developed, improving the widely used and well-known Suzuki Lie Trotter product formulas [3, 4, 5]. Various quantum systems have been simulated using these methods [6, 7, 8]. However, little work has been done to apply these methods to quantum optical systems. Simulating quantum optical systems with quantum computers is important as it allows one to better understand the system's dynamics without performing experimental implementations of these quantum optical systems. A key issue with using quantum computers to simulate quantum optical systems is that the truncation error incurred from mapping bosons to qubits sometimes negates the advantage that could be achieved by these quantum algorithms [9]. There is a way to overcome this; instead of using Hamiltonian simulation to simulate the Hamiltonian evolution of a quantum optical system directly, one could use an alternate representation of the state of the system, such as the Q representation and derive a Fokker Plank Equation (FPE) for this representation that can be efficiently solved using quantum algorithms for solving Partial Differential Equations (PDEs). Solving this equation can lead us to a complete understanding of the dynamics of the quantum optical system. In this work, we propose using quantum algorithms for solving PDEs to solve the FPE for the Q representation in quantum optics. We will consider the FPE for various quantum optical systems and develop discretization strategies for these equations to use Hamiltonian simulation or the quantum linear systems solver (HHL) to solve the FPE. This work shall also compare these methods' error and gate complexities and show which is better suited for simulating these quantum optical systems. This work will also compare the complexities and errors between our proposed methods and the error and complexities associated with directly simulating the Hamiltonian evolution.

References

[1] R. P. Feynman, "Simulating physics with computers", *Int. J. Theor. Phys* **21** (1982).

[2] Y. Manin, "Computable and uncomputable", *Sovetskoye Radio, Moscow* **128** (1980).

[3] A. M. Childs and N. Wiebe, "Hamiltonian simulation using linear combinations of unitary operations", *arXiv preprint arXiv:1202.5822* (2012).

[4] A. M. Childs, A. Ostrander and Y. Su, "Faster quantum simulation by randomization", *Quantum* **3**, p. 182 (2019).

[5] G. H. Low and I. L. Chuang, "Hamiltonian simulation by qubitization", *Quantum* **3**, p. 163 (2019).

[6] J. Liu and Y. Xin, "Quantum simulation of quantum field theories as quantum chemistry", *Journal of High Energy Physics* **2020**, pp. 1–48 (2020).

[7] T. Farrelly and J. Streich, "Discretizing quantum field theories for quantum simulation", *arXiv preprint arXiv:2002.02643* (2020).

[8] J. Zhang, M.-H. Yung, R. Laflamme, A. Aspuru-Guzik and J. Baugh, "Digital quantum simulation of the statistical mechanics of a frustrated magnet", *Nature Communications* **3**, p. 880 (2012).

[9] M. Hanada, J. Liu, E. Rinaldi and M. Tezuka, "Estimating truncation effects of quantum bosonic systems using sampling algorithms", *arXiv preprint arXiv:2212.08546* (2022).

Fourier Ptychographic Microscopy for Large Area, High-Resolution Imaging

Eugene Egbert Fouche[1*], Gurthwin Wendell Bosman[1] and Pieter Herman Neethling[1]

[1]*Physics Department, Stellenbosch University, Private Bag XI, Matieland 7602, South Africa*

*E-mail: 21598835@sun.ac.za

1. Abstract

In conventional brightfield microscopy there is a trade-off between resolution and field of view [1]. A sample can be imaged at a high resolution, at the cost of imaging only a small area. Similarly, a larger area can be imaged, but with a lower spatial resolution. Fourier Ptychographic Microscopy (FPM) overcomes this tradeoff by enabling imaging with a large field of view at high resolution. This is done by using an array of LEDs to illuminate the sample from various angles. For each illumination angle an image is captured and the resulting sequence of images is used to reconstruct the sample at a higher resolution [2]. Consequently, low numerical aperture (NA) optics can be used to obtain a large field of view, while the improved resolution is comparable with that of high NA optics. In this way a high-resolution, large field of view image of a sample can be reconstructed from a sequence of low-resolution, large field of view images. This is useful in e.g. digital pathology, where it is desirable to see a large area of the tissue, but also have a high-resolution [3].

The Abbe diffraction limit gives a lower bound to the resolution of an imaging system. It depends on the wavelength of the illumination source and the NA of the objective, as seen in Eq. (1). By using FPM, the effective NA of the system is increased, which means that smaller features can be resolved by the imaging system. Fig. 1 shows experimental results that demonstrate the resolution improvement offered by FPM.

$$R = \frac{\lambda}{2\text{NA}} \tag{1}$$
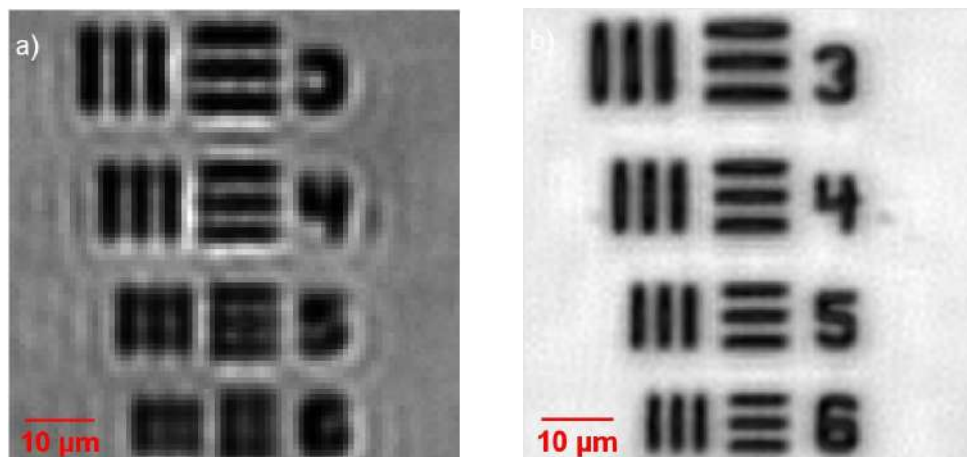
Figure 1 USAF resolution test target, group 7, elements 3-6. a) Raw image of the target taken through a microscope. b) Reconstructed image using the same microscope objective and the sequence of images acquired in the FPM process. In the raw image, the lines of element 5 and 6 cannot be resolved, but in the reconstructed FPM image the different lines are resolved. This shows the resolution improvement offered by FPM.

This contribution will explain the principles behind FPM and show results from experiments and simulations. It will also demonstrate other advantages of FPM, such as phase imaging, defocus correction and aberration correction. Fig. 2 shows a schematic illustrating the FPM setup and working principle.
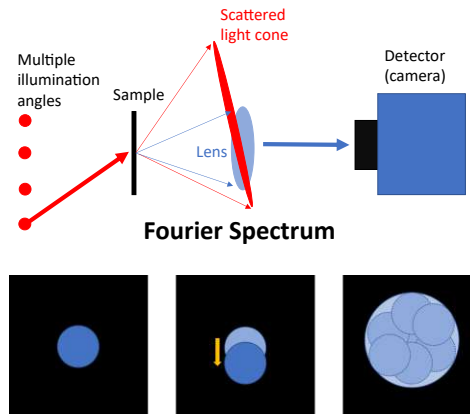
Figure 2 Diagram of the FPM setup and the working principle. When the sample is illuminated from greater angles, information from different sections of the Fourier spectrum are captured. Since a larger portion of the Fourier spectrum can be reconstructed from the sequence of images, a higher resolution reconstruction of the sample is possible.

2. Conclusions

Fourier Ptychographic Microscopy offers a simple way to significantly improve the resolution of an imaging system, while keeping a large field of view. The principles behind how FPM works will be explained, and experimental results as well as simulations will be shown to illustrate the technique.

Please consider this abstract for a **poster presentation**, I have prepared another abstract for an oral presentation.

Acknowledgments

References

[1]   P. C. Konda, L. Loetgering, K. C. Zhou, S. Xu, A. R. Harvey, and R. Horstmeyer, "Fourier ptychography: current applications and future promises," *Opt. Express*, vol. 28, no. 7, p. 9603, 2020, doi: 10.1364/oe.386168.

[2]   G. Zheng, R. Horstmeyer, and C. Yang, "Wide-field, high-resolution Fourier ptychographic microscopy," *Nat Photonics*. 2013 September 1; 7(9): 739–745. doi:10.1038/nphoton.2013.187.

[3]   G. Zheng, C. Shen, S. Jiang, P. Song, and C. Yang, "Concept, implementations and applications of Fourier ptychography," *Nat. Rev. Phys.*, vol. 3, no. 3, pp. 207–223, 2021, doi: 10.1038/s42254-021-00280-y.

High-resolution phase-sensitive coherent anti-Stokes Raman scattering spectroscopy by time-domain ptychography

J.Anthonie de Beer*

Gurthwin W. Bosman

Pieter H. Neethling

Physics Department, Stellenbosch University, Stellenbosch

*e-mail: 18978762@sun.ac.za

Femtosecond time-resolved coherent anti-Stokes Raman scattering (tr-CARS) is a highly sensitive method of vibrational spectroscopy, ideal for label-free chemical sensing. The time-resolved vibrational spectra reveal information on intra- and intermolecular phase dynamics [1, 2].

In broadband multiplex tr-CARS, a femtosecond laser pulse supplies both pump and Stokes fields, to access many vibrational states, while a second narrow band laser then probes the system. The pump pulse bandwidth determines the accessible vibrations. Temporal resolution is achieved by delaying the probe pulse relative to the pump (Fig. **1**). Dephasing information can then be seen in the decay in the delayed probe CARS spectrogram.

We propose a femtosecond tr-CARS method with an ultra-broadband pump/Stokes pulse and a femtosecond probe pulse. Needing only a single laser pulse source, this design is both low-cost and simpler compared to multi-laser configurations, inherently synchronized and phase stable. Using short pulses for all fields in the CARS process allows the use of higher probe intensities and thus higher signal strengths.
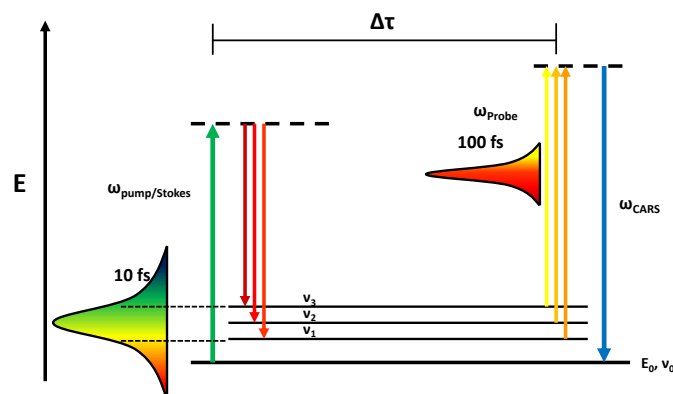
Figure 1: Femtosecond CARS with delayed femtosecond probe energy level diagram

In our design an All-Normal Dispersion Photonic Crystal Fibre (ANDi-PCF) is pumped by a near-infrared 100 fs pulse. The ANDi-PCF produces a stable ultra-broadband spectrum with a fixed spectral phase relationship [3]. The pulse is compressed down to 10 fs using a spatial light modulator in a 4f-shaper configuration. Compression is done by in-house developed time-domain ptychographic compression algorithm, i^2PIE [4]. The 10 fs pump pulse and collinear 100 fs probe

pulse is tightly focused onto the sample. A linear delay stage in the probe beam path allows for arbitrary probe delays.

Normally, a femtosecond probe pulse would yield insufficient spectral resolution due to its large spectral bandwidth. To overcome this, we set our probe time-delays such that consecutive probes partially overlap (Fig. **1**). This overlap creates a redundancy in the measured spectrogram which is then analysed using an adapted iterative ptychographic algorithm to recover the lost resolution. The ptychographic engine also reconstructs the object phase, producing a high-resolution amplitude and phase object for the vibrational coherence.
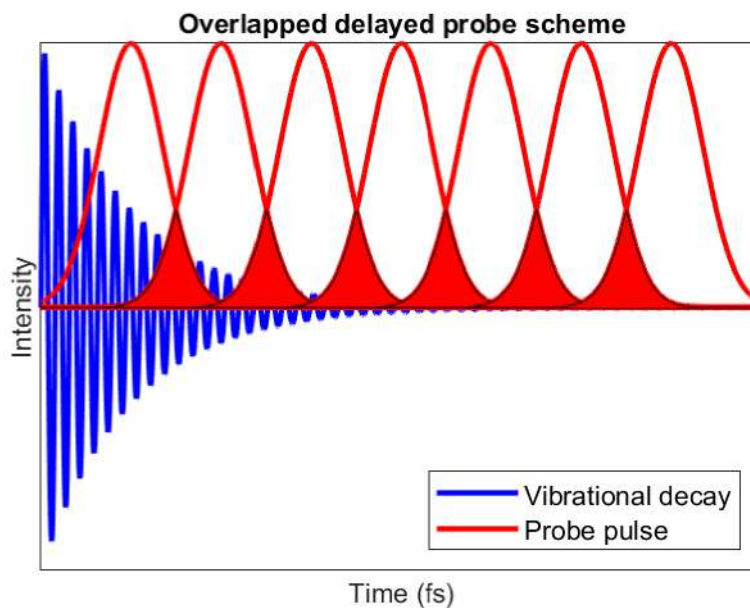
Figure 2: Temporally overlapping probes create redundancy that enables resolution to be ptychographically reconstructed

This single-source time-domain CARS scheme using ptychographic reconstruction of the spectrogram, opens up CARS spectroscopy to any laboratory equipped with a femtosecond oscillator. It can be easily expanded to non-linear label-free scanning microscopy, with the addition of a sample scanning stage. The ability to retrieve the temporal evolution of both the amplitude and phase of excited vibrational levels allows us to investigate inter- and intramolecular vibrational energy transfer.

References

[1] Carlos R. Baiz, et al. "Vibrational Spectroscopic Map, Vibrational Spectroscopy, and Intermolecular Interaction", *Chem. Rev.* **120**, pp. 7152-7218 (2020).

[2] Y. R. Shen, "Phase-Sensitive Sum-Frequency Spectroscopy", *Annual Review of Physical Chemistry* **64**, pp. 129–150 (2013).

[3] A. M. Heidt, "Pulse preserving flat-top supercontinuum generation in all-normal dispersion photonic crystal fibers", *J. Opt. Soc. Am. B* **27**, pp. 550–559 (2010).

[4] Ruan Viljoen, et al. "Implementation of temporal ptychography algorithm, i2PIE, for improved single-beam coherent anti-Stokes Raman scattering measurements", *J. Opt. Soc. Am. B* **37**, pp. A259-A265 (2020).

Exploring metallic nanoparticles for enhanced multiplexed SERS for diagnostics.

Lungile Thwala[1], Lebogang Thobakgale[1], Zenande Mcotshana[1, 2], Moratoa Tlomatsane[1, 3], Saturnin Ombinda-Lemboumba[1], Masixole Lugongolo[1], Patience Mthunzi-Kufa[1, 4]

[1]*Department of Biophotonics, Council for Scientific and Industrial Research, Meiring Naudé Rd, Brummeria, Pretoria, 0184, South Africa*

[2]*Department of Chemical Engineering, University of Cape Town, Cape Town 7925, South Africa*

[3]*Medical Virology, University of Cape Town, Cape Town, South Africa*

[4]*School of Chemistry and Physics, University of KwaZulu-Natal, Durban 4001, South Africa.*

[*]E-mail: LThwala@csir.co.za

1. Introduction

Evidence suggests that several underlying diseases including diabetes, kidney diseases, and cardiovascular disorders increase the severity and mortality in SARS-CoV-2 and HIV infections. SARS-CoV-2 can exert direct effects on pancreatic β-cells, subsequently resulting in glucose and metabolic instabilities whilst HIV infections are associated with insulin resistance, hyperlipidaemia, and lipodystrophy. When it comes to diagnostics and disease management, while physicians focus on the prognosis and mortality caused by viral diseases, it is necessary to be thorough about metabolic chronic illnesses that could cause complications.

Owing to its remarkable sensitivity and capability for multiplexing, Surface-Enhanced Raman Spectroscopy (SERS) emerges as a potent analytical approach with substantial promise in the realms of bioanalysis and diagnostics. When integrated with an immunoassay approach, this technique attains a remarkable level of specificity. Nevertheless, it's worth noting that Raman signal intensity is exceedingly faint, approximately $10-6$ times the intensity of the original laser light. As a result, signal enhancement becomes necessary, a task effectively accomplished through the plasmonic phenomena exhibited by metallic nanoparticles.

2. Methods

This current work focuses on exploring different nanoparticles that can be used for SERS-based pathogen and metabolic disorder-biomarkers detection for rapid viral infection and chronic disease diagnosis using SARS-CoV-2 and a diabetes biomarker, glucose.

Herein, functionalized metallic nanoparticles (NPs) that can selectively capture the S-protein expressed coronavirus and glucose molecules were synthesized and immobilized on a glass slide using methods adapted from José-Yacamán and colleagues [1-3]. We assessed which NP system offers high sensitivity and specificity for both disease-biomarkers using simulated saliva containing SARS-CoV-2 virions and glucose. It was observed that metallic NPs such as gold (Au), copper (Cu) and a combination

of these (AU-Cu nanostructures) gave higher signals compared to silver. It was also observed that SERS amplification requires that the plasmonic nanoparticles be in contact with the analyte, since studies carried out without the NPs gave very low signals.

3. Conclusions

We have successfully demonstrated that utilizing surface-enhanced Raman spectroscopy (SERS) through gold, copper, and gold-copper nanostructures enables the simultaneous acquisition of distinct signatures for both SARS-CoV-2 virion particles and glucose molecules. Furthermore, the primary proteins S and N yield clearly defined spectra. This implies that Raman-SERS spectroscopy has the potential not only for virus identification but also for investigating protein structures.

It is important to note that our study is in preliminary stages. To evaluate the sensitivity and specificity of SERS, further clinical testing and direct comparisons with other testing methods are essential. Should this technique be refined, a SERS test conducted on saliva could yield rapid results, requiring only the application of cost-effective mass-produced nanoparticles.

This proposed detection method would empower medical professionals to extract more comprehensive insights from a single test, aiding in the diagnosis of disease conditions and identifying potential underlying factors or ailments that could have life-threatening consequences.

References

[1] J. Jesús Velázquez-Salazar, et al "Controlled Overgrowth of Five-Fold Concave Nanoparticles into Plasmonic Nanostars and Their Single-Particle Scattering Properties", ACS Nano. 13, 9, 10113–10128 (2019)

[2] X. Sun, "Glucose detection through surface-enhanced Raman spectroscopy: A Review" Analytica Chimica Acta 1206, 339226, (2022).

[3] J. E. Sanchez et al, "Detection of SARS-CoV-2 and its S and N proteins using surface enhanced Raman spectroscopy", RSC Adv., 11, 25788 (2011).

Optical properties of biosynthesized nanoscaled Eu$_2$O$_3$ for red luminescence and potential antidiabetic applications

Hamza Elsayed Ahmad Mohamed[1,2]*, Khaoula Hkiri[1,2], , Malik Maaza[1,2]

[1] *UNESCO UNISA Africa Chair in Nanoscience and Nanotechnology, College of Graduate Studies, University of South Africa, Pretoria, South Africa*

[2] *Nanoscience African Network (NANOAFNET), Materials Research Department, iThemba LABS, Cape Town, South Africa*

*E-mail: hamza@aims.ac.za

This contribution reports on the optical properties of biosynthesised Eu$_2$O$_3$ nanoparticles bioengineered for the first time by a green and cost effective method using aqueous fruit extracts of Hyphaene thebaica as an effective chelating and capping agent. The morphological, structural, and optical properties of the samples annealed at 500∘C were confirmed by using a high-resolution transmission electron microscope (HR-TEM), x-ray diffrac tion analysis (XRD), UV–Vis spectrocopy, and photoluminescence spectrometer. The XRD results confirmed the characteristic body-centered cubic (bcc) structure of Eu$_2$O$_3$ nanoparticles with an average size of 20 nm. HRTEM revealed square type morphology with an average size of ~6 nm. Electron dispersion energy dispersive x-ray spectroscopy spectrum confirmed the elemental single phase nature of pure Eu$_2$O$_3$. Furthuremore, the Fourier transformed infrared spectroscopy revealed the intrinsic characteristic peaks of Eu−O bond stretching vibrations. UV–Vis reflectance proved that Eu$_2$O$_3$ absorbs in a wide range of the solar spectrum from the VUV–UV region with a bandgap of 5.1 eV. The luminescence properties of such cubic structures were characterized by an intense red emission centered at 614 nm. It was observed that the biosynthesized Eu$_2$O$_3$ nanoparticles exhibit an efficient red-luminescence and hence a potential material as red phosphor. In vivo experiments revealed antidiabetic potential which was complemented by in vitro and in vivo assays. The α-glucocidase and α-amylase enzyme inhibition revealed an IC50 value of 12 μg mL-1 and 540 μg mL-1 for Eu$_2$O$_3$ NPs respectively. The DPPH antioxidant assay revealed an IC50 of 250 μg mL-1. In vivo assays revealed that that the application of the Eu$_2$O$_3$ NPs has lowered the blood level glucose from 561.89±2.16*** mg dL-1 to 193.00±0.88*** mg dL-1 from the start of the treatment. No major alteration of the blood biochemistry parameters were observed after treatment.

Stokes reconstruction of Chiral fields.

Light Mkhumbuza [1], Angela Dudley[1], Kayn A. Forbes[2] and Isaac Nape[1]

[1]*School of Physics, University of the Witwatersrand, Private Bag 3, Wits 2050, South Africa*

[2]*School of Chemistry, University of East Anglia, Norwich Research Park, Norwich NR4 7TJ, United Kingdom*

*e-mail: 2106520@students.wits.ac.za

1. Abstract and theoretical background

   Chirality is a fundamental concept in the field of optics as it provides a means to study and manipulate the interactions between light and matter. Chirality refers to a property of certain objects that cannot be superimposed on their mirror images. Circularly polarized light has been investigated to carry optical chirality, this is due to being proportional in helicity to the photon $\sigma = \pm 1$ whereby the positive and negative correspond to left and right handed circularly polarized light respectively [1]. Recently a new class of structured light [2] called vector vortex beams (VVB) which also is associated with chirality have gained a lot of interest in both classical and quantum optics. VVBs are modes which posses and inherit inhomogeneous polarization structure and show an azimuthal phase dependence in the transverse plane of $e^{i\ell\phi}$, here $\ell \in \mathbb{Z}$. VVBs can also be understood as the superposition of two orthogonally polarized beams both carrying optical OAM through the azimuthal phase factor $e^{i\ell\phi}$ [3]. In this work we measure the highly optical chirality densities of these higher-order chiral structured beams and how the Pancharatnam topological charge ℓ_p influence these beams . To validate our theory, we provide experimental results in the near field using vectorial modes consisting of Laguerre Gaussian (LG) spatial profiles. All of this is achieved through the utilisation of digital holography and geometrical phase control of light.

   Theoretically we start with a horizontally polarised LG with $\ell = 0$ (Gaussian mode):

$$\mathrm{LG}_{\ell_p}(r,\phi) = R_\ell(r)e^{i\ell_p\phi} \tag{1}$$

$$= \mathcal{C}_{\ell_p}\left(\frac{\sqrt{2}r}{w}\right)^{\ell_p} e^{-r^2/w^2}e^{i\ell_p\phi}, \tag{2}$$

in polar coordinates, $\mathbf{r} = (r,\phi)$, where w is the waist size of the Gaussian mode (e^{-r^2/w^2}), radial orders set to $p = 0$. The resulting field is modulated with a q-plate, at the $z = 0$ plane, yielding the mapping

$$\mathrm{LG}_{\ell_p}\hat{\mathbf{x}} \xrightarrow{\text{q-plate}} \mathbf{U} = R_{\ell_p}(r)e^{i\ell_A\phi}\hat{\sigma}_+ + R_{\ell_p}(r)e^{i\ell_B\phi}\hat{\sigma}_-, \tag{3}$$

where $\ell_A = \ell_p + 2q$ and $\ell_B = 2\ell_p - 2q$ and $2q$ is the topological charge of the plate. Here ℓ_p serves as the Pancharatman topological index of the resulting field $\mathbf{U}$ because $2\ell_p = \ell_A + \ell_B$. The resulting field is then propagated in Rayleigh range whilst performing Stokes polarimetry at each plane to analyse how the polarization structures of the field changes in propagation.

2. Experiment and results
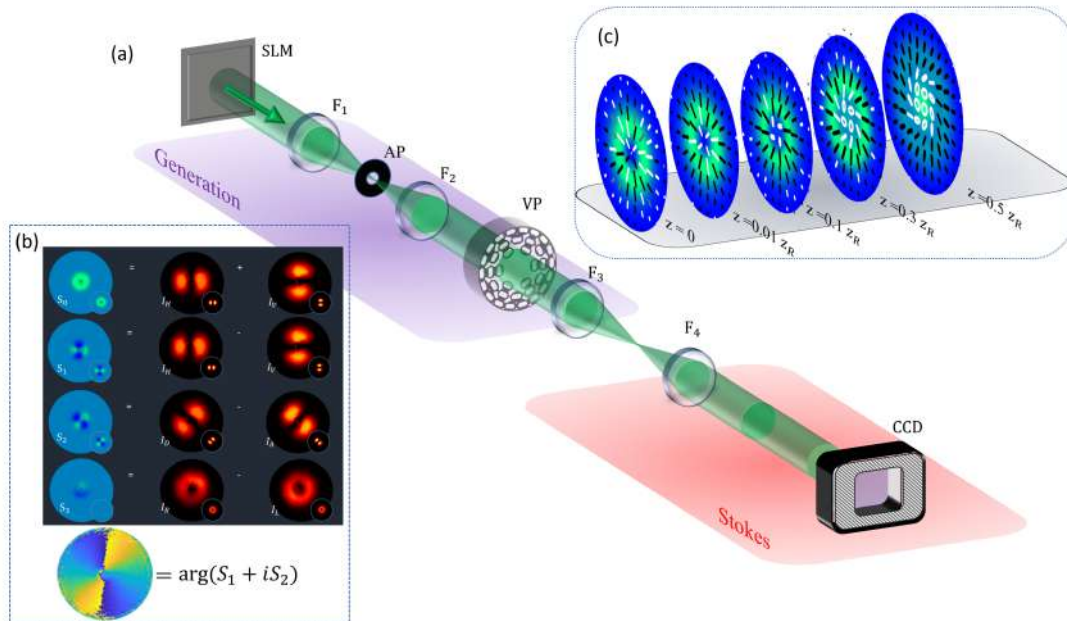
Figure 1: Fig.1(a)Experimental setup, marking the mode generation and Stokes polarimetry: We generate the VVB by shining a gaussian laser beam from a 633nm HeNe laser source onto a spatial light modulator (SLM) encoded with a hologram to generate an LG beam of $\ell = 1$. We then image the plane of the SLM using an imaging system onto a Q-plate (VP) which serves as a spin-orbit coupling device. The plane of the Q-plate is then imaged onto the near field whilst we perform Stokes measurements. Fig.1(b) Reconstructed polarisation components: Represents all polarisation components and how we use them to compute the four Stokes measurements, which become useful in determining the polarisation order of this field,this is done from the Stokes phase $\Phi_{12} = \arg\left(S_1 + iS_2\right)$. Fig.1(c) Accompanying S3 profiles as a funcgtion of propagation distance: Here we represent S_3 of the Stokes measurements in propagation, we can clearly see how the polarisation structure evolves as it propagates becoming more radially polarised in the central region of the beam. This simply shows us that in the near field we do not see the full amplitude we need to let the beam propagate so the full amplitude can evolve in propagation.

3. Conclusion

In this work, we have demonstrated how to generate cylindrical vector vortex and shown that the Pancharatnam topological charge influences the optical field's chirality density. In illustrating such we have outlined the execution of the Stokes measurements digitally and as a function of propagation.

References

References

[1] Dale Green and Kayn A Forbes. Optical chirality of vortex beams at the nanoscale. *Nanoscale*, 15(2):540–552, 2023.

[2] Andrew Forbes, Michael de Oliveira, and Mark R Dennis. Structured light. *Nature Photonics*, 15(4):253–262, 2021.

[3] Carmelo Rosales-Guzmán, Karen Volke-Sepulveda, and Juan P Torres. Light with enhanced optical chirality. *Optics letters*, 37(17):3486–3488, 2012.

Monitoring the metabolics of single yeast cells through fluorescence microscopy using integrated optical tweezers and microfluidic setup

Leroi Du Plessis, Gurthwin Bosman, Pieter Neethling

[1]*Physics Department, Stellenbosch University, Western Cape, South Africa, 7600*

*e-mail: pietern@sun.ac.za

Optical Tweezers has become a unique and versatile tool for measuring mechanical force in the orders of femto newtons, making it the standardized method in biophysics for measuring the forces of molecular motors and the mechanical properties of DNA [1]. The easy maneuverability and stability of single beam optical traps make them ideal for single cell studies, making it possible to monitor the live response a single cell to different external environmental conditions such as pH, temperature and ion concentration, as appose to ensemble average measurements. To do this to use a microfluidic chip to accurately control the external environment of the cells under study. This chip no only allows for the precise control of different chemical concentrations, but can also allow rapid changes in the environment which allows for the monitoring of short term responses and reversible processes of trapped cells [2]. The integration of microfluidic chambers with optical tweezers has become popular in the past decade due to the fact that they can easily be manufactured using soft lithography methods and the use of PDMS(Polydimethylsiloxane) making them inexpensive and desirable for cell studies [3]. By combining the manipulation capabilities of optical tweezers with the control of microfluidic chips, we can create a stable platform for measuring cellular uptake of therapeutic drugs under varying environmental conditions, and the cell's response to these thereputics, which could lead to a better understanding of the bioavailability of these drugs and thus to better dosing protocols. Measuring the cellular uptake is important for determining treatment regimes as underestimation of the bioavailibility can lead to the abuse of prescribed drugs [4].

The principle of single beam optical trapping of single eukaryotes can be described adequately by geometrical ray optics. Due to the difference in the refractive index between the surrounding fluid and index of the cell, the optical rays gets diverted away from their original trajectory. The full interaction of a ray is illustrated in figure 1. By considering the momentum that a single ray carries and the conservation of the total momentum of the system after the interaction, one can derive the force that is applied to the single cell by expanding the single ray setting to that of a focused Gaussian decomposed into a set of n rays. The total force is described by Eq. 1, where P described the power of each ray, n the refractive index in each medium and $\boldsymbol{r}$ the directional unit vector of each ray where the subscripts i, r and t denote the incident, reflected and transmitted rays respectively. The total force vector is often written in terms of the sum of the scattering force, which directs the cell in the direction of beam propagation, and the gradient force, which holds the cell at the center of the beam. Due to the focusing of the beam there exist a position along the propagation axis at which the net force on the cell is zero, therefore creating a stable single beam trap.

$$\boldsymbol{F}_{obj} = \sum_{n} \left[\frac{n_i P_i^{(n)}}{c} \boldsymbol{r}_i^n - \sum_{m} \frac{n_t P_{t,m}^{(n)}}{c} \boldsymbol{r}_{t,m}^n - \frac{n_r P_{r,0}^{(n)}}{c} \boldsymbol{r}_i^n \right] \qquad (1)$$

In order to create an efficient platform for monitoring the cellular uptake, the conditions under which stable trapping for a designated cell is achieved must be determined as well as the parameters
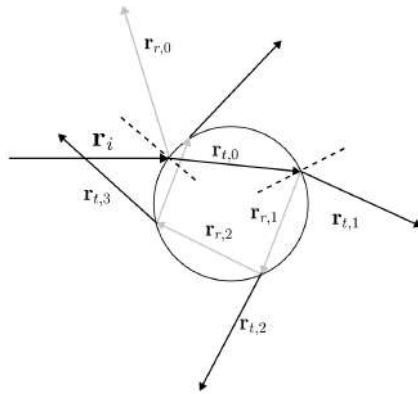
Figure 1: Illustration of a single ray interacting with a spherical particle. The change in the momentum of the initial ray results in a net force being applied to the particle. The resulting force of a set of rays representing a beam with a certain distribution is given by Eq. 1.

at which influence to cell function and environmental temperature change is at a minimum. We start by looking at single yeast cells (Saccharomyces cerevisiae) which serve as a basis for many metabolic studies due to their easy availability and cultivation. They also are known for their strong response to external stimuli [5]. These initial studies will lead to the development of protocols for larger and more medically relevant cells such as cardiomyoblasts.

In our setup, we combine an optical tweezers with a fluorescence module in order to make spectroscopic measurements of trapped cells. Using the autofluoresence of NADH(nicotinamide adenine dinucleotide (NAD) + hydrogen (H)) which is a product in many metabolic processes and is found throughout eukaryotes [6], one can monitor the metabolic response of a cell through the fluorescence intensity, as a function of environmental parameter such as pH, temperature and nutrient or toxin levels. We will extensively describe the experimental setup and show initial results of fluorescence spectroscopy measurements.

References

[1] C. J. Bustamante *et al.*, "Optical tweezers in single- molecule biophysics", *Nat Rev Methods Primers* **1**, 25 (2018).

[2] E. Eriksson *et al.*, "A microfluidic system in combination with optical tweezers for analyzing rapid and reversible cytological alterations in single cells upon environmental changes", *Lab Chip* **7**(1), pp. 71–76 (2007).

[3] M. Tehranirokh *et al.*, "Microfluidic devices for cell cultivation and proliferation", *Biomicrofluidics* **7**(5), 051502 (2013).

[4] A. Cragg *et al.*, "Risk Factors for Misuse of Prescribed Opioids: A Systematic Review and Meta-Analysis", *Annals of Emergency Medicine* 74(5), pp. 634–646 (2019).

[5] E. V. Grosveld *et al.*, "A Systematic Survey of Characteristic Features of Yeast Cell Death Triggered by External Factors", *Journal of Fungi* **7**, 886 (2021).

[6] L. Zhou *et al.*, "Regulation of lactate production at the onset of ischaemia is independent of mitochondrial NADH/NAD+: insights from in silico studies.", *The Journal of Physiology* **569**, pp. 925–937 (2005).

Photobiomodulation promotes wound healing in a diabetic cellular model

Dimakatso B. Gumede[1*] and Nicolette N. Houreld[1]

[1]*Laser Research Centre, Faculty of Health Sciences, University of Johannesburg, P.O. Box 17011, Doornfontein, South Africa, 2028*

*E-mail: dgumede@uj.ac.za

1. Introduction

Wound healing is a tightly regulated process that promotes tissue repair following injury. However, this process is deregulated in disease conditions, leading to poor wound healing and the development of chronic wounds. Diabetes mellitus is a metabolic disorder that is caused by high blood glucose due to insulin insufficiency or insulin resistance. The hyperglycemic state leads to poor wound healing and contributes towards the development of chronic diabetic ulcers, which increases the risk of lower limb amputations in diabetic patients [1]. Current wound treatments include glycemic control, wound dressing, debridement, and pain management. However, these treatments are moderately effective leading to reoccurrence of diabetic ulcers, therefore improved treatment strategies are required for diabetic ulcers.

Photobiomodulation (PBM) has been shown to improve the healing of diabetic wounds at wavelengths between 520 nm and 830 nm [2], but the mechanism(s) of action have not been fully investigated. Studies have indicated that PBM activates the TGF-β signaling pathways [3], but it has not been determined if PBM also activates Wnt/β-catenin to promote and accelerate wound healing. The aim of this study was to investigate whether PBM induces healing in diabetic wounded cells at a wavelength of 660 nm and fluence of 5 J/cm^2 via activation of the Wnt/β-catenin signaling pathway.

2. Methodology

Human dermal fibroblasts (WS1) were continuously cultured in high glucose medium (22.6 mM D-glucose) to create an *in vitro* diabetic cellular model. Diabetic cells (D) were seeded at a density of 6 x 10^5 in 35 mm diameter culture plates 24 h prior to irradiation. To create a "wound', a central scratch was created in the middle of the cell culture plate using a 1 mL pipette tip. The cells were subjected to laser irradiation at a wavelength of 660 nm and a fluence of 5 J/cm^2 (100 mW/cm2; 445.05 s) using the formula (1) shown below.

$$mW/cm^2 = \frac{mW/cm^2}{\pi (r^2)}$$

$$W/cm^2 = \frac{mW}{1000}$$

$$Time \ (s) = \frac{5 \ J.cm^2}{W/cm^2}$$

(1)

The sample groups were analyzed 24 and 48 h post-irradiation. Cell migration was assessed through inverted microscopy in diabetic wounded (DW) cells. Cell viability was measured using the Trypan blue exclusion assay, where the number of colorless (viable) and blue (non-viable) stained cells are counted, and the percentage viability calculated.

3. Results

Cell migration was analyzed (Fig. 1) at 0 h, 24 h and 48 h post-irradiation (0 J/cm^2; 5 J/cm^2) and showed an increase in cell migration in irradiated cells compared to the non-irradiated cells. The cell viability data indicates that PBM does not cause cytotoxicity in irradiated cells (Fig. 2) at 24 and 48 h post-irradiation, which showed similar viability of 70%±7 in irradiated sample groups when compared with the non-irradiated group.
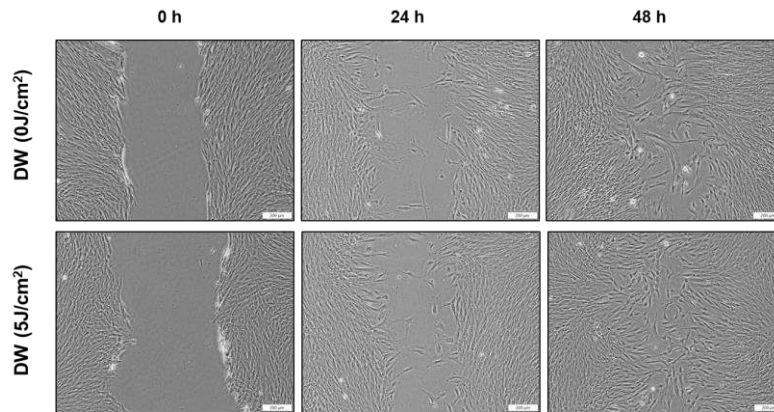
Figure 1 Inverted light microscopy was used to assess cell migration in diabetic wounded cells (DW) at 0, 24 and 48 h after irradiation at a wavelength of 660 nm and a fluence of 0 J/cm^2 or 5 J/cm^2. Two biological repeats were performed.
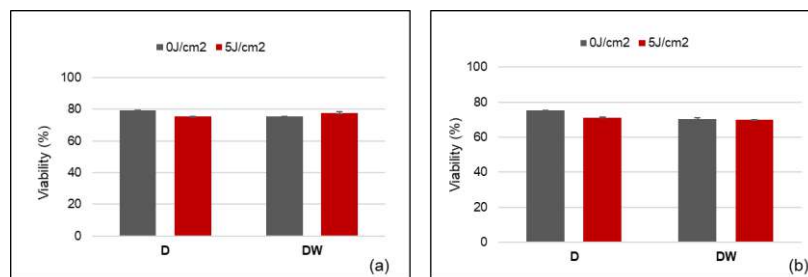
Figure 2 Cell viability (%) in irradiated diabetic (D) and wounded diabetic (DW) cells was determined by the trypan blue exclusion assay 24 h (a) and 48 h (b) post-irradiation. Data is presented as means ± SD (n = 2).

4. Conclusions

The preliminary data shows that PBM induces increased "wound" closure in irradiated DW cells compared to non-irradiated cells. The cell viability data further showed that irradiation at 660 nm and a fluence of 5 J/cm^2 does not induce cell death.

References

[1] W.D. Aumiller, H.A. Dollahite, "Pathogenesis and management of diabetic foot ulcers", JAAPA. 28 (2015).
      https://journals.lww.com/jaapa/Fulltext/2015/05000/Pathogenesis_and_management_of_diabetic_foot.6.aspx.

[2] E. Mester, A. Korényi-Both, T. Spiry, A. Scher, S. Tisza, "Stimulation of wound healing by means of laser rays. (Clinical and electron microscopical study)", Acta Chir Acad Sci Hung. 14 (1973) p. 347–356.

[3] P.R. Arany, A. Cho, T.D. Hunt, G. Sidhu, K. Shin, E. Hahm, G.X. Huang, J. Weaver, A.C.-H. Chen, B.L. Padwa, M.R. Hamblin, M. Barcellos-Hoff, A.B. Kulkarni, D. J Mooney, "Photoactivation of endogenous latent transforming growth factor-β1 directs dental stem cell differentiation for regeneration", Sci Transl Med. 6 (2014) 238ra69. https://doi.org/10.1126/scitranslmed.3008234.

Photobiomodulation at 830 nm Promotes Cellular Viability and Reduces Cell Death in Fibroblast Diabetic Hypoxic Wounded Cells

Patricia Kasowanjete[1], Sathish Sundar Dhilip Kumar[1] and Nicolette N. Houreld[1*]

[1]Laser Research Centre, University of Johannesburg, P.O. Box 17011, Doornfontein, Johannesburg, 2028, South Africa

[*]E-mail: nhoureld@uj.ac.za

1. Introduction

Diabetes mellitus (DM) is a metabolic disease characterised by hyperglycemia. Patients with DM are more likely to develop chronic ulcers on their lower limb. These wounds are primarily brought on by neuropathy which results in the development of persistent, unnoticed wounds that are challenging to manage, treat and heal. There are several factors that are linked to delayed wound healing in DM, and these include abnormal fibroblast migration, proliferation, and differentiation, and increased apoptosis. Hypoxia reduces cellular responses and is an important cause of delayed wound healing. Several treatment modalities have been explored for diabetic wound healing however, the effects of the available treatments are temporary with a high incidence of relapse. Hence, new effective treatment strategies for diabetic wounds are required. Photobiomodulation (PBM), an application that utilises low-powered light in the visible red and near-infrared (NIR) spectrum, has been shown to stimulate biological systems. The absorbed light accelerates and activates an array of cellular processes that leads to downstream physiological effects which renders improved wound healing. The effects of PBM at the cellular and molecular level are not fully investigated, despite the strong evidence of its effectiveness. Therefore, the present study investigated the effects of PBM at 830 nm on cellular viability in fibroblast diabetic wounded and diabetic hypoxic wounded cell models.

2. Methodology

This study used commercially available human skin fibroblast (WS1) cells. The cells were grouped into two models, namely diabetic wounded (DW) and diabetic hypoxic wounded (DHW). In *vitro* diabetic cell models were created by continuously growing cells under high glucose concentration (22.6 mM) [1]. Wounded models were created via the central scratch assay on a confluent monolayer of cells using a 1 mL sterile pipette. A hypoxic cell model was made by incubating the cells in an anaerobic environment (anaerobic chamber with anaerobic gas pack and indicator) for 4 h before PBM. Migration rate was determined and calculated from captured images at 0, 24 and 48 h. The distance between the wound margins was measured and used in Eq. (1).

$$At_{0h} - At_{time} / At_{0h} \times 100 \tag{1}$$

Where At_{0h} is the scratch area at 0 h and At_{time} is the correspondent scratch area at different time points [2,3]. Cells were irradiated at a wavelength of 830 nm with a fluence of 5 J/cm², power density 11 mW/cm² and irradiation time of 7 min 16 s, and non-irradiated cells (0 J/cm²) were used as controls. Cells were incubated for 24 and 48 h post-irradiation and the effect of PBM on viability was determined by the Trypan blue exclusion assay. B-cell lymphoma 2 (Bcl-2), a regulator of apoptosis, was assessed using the enzyme-linked immunosorbent assay (ELISA) [4].

3. Results

There was a significant increase in viability in both irradiated DW and DHW cell models at 24 h (*P<0.05*) and at 48 h (*P<0.05* and *P<0.01*, respectively) (Fig. 1). At 24 h and 48 h, there was a significant increase in Bcl-2 in DHW cells (*P=0.035* and *P=0.002*, respectively), while a significant decrease was seen in DW cells (*P=0.007* and *P=0.002*, respectively) (Fig. 2). There was a significant increase in migration rate in irradiated DHW cells (*P=0.05*) at 24 h, while at 48 h there was a significant increase in both irradiated DW and DHW cells (*P=0.04*) (Fig. 3).
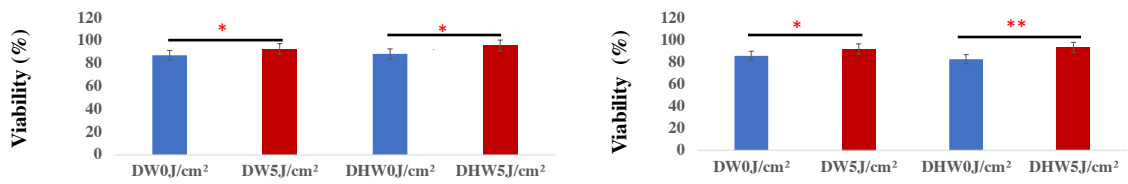
Figure 1 Cellular viability (percentage, %) was assessed using the Trypan blue exclusion assay in irradiated (5 J/cm²) and non-irradiated (0 J/cm²) diabetic wounded (DW) and diabetic hypoxic wounded (DHW) cells at 24 and 48 h post-irradiation at a wavelength of 830 nm (n=3). Significant probability is shown as *P<0.05* and *P<0.01** (SEM).
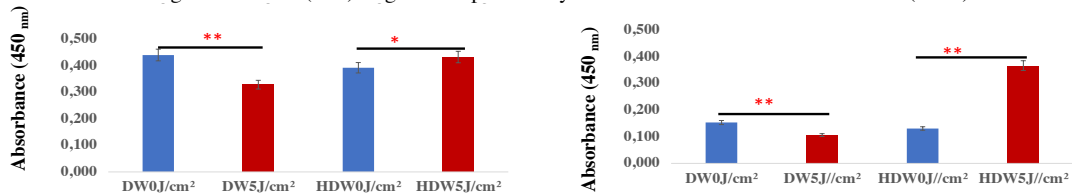
Figure 2 Bcl-2 was determined in non-irradiated (0 J/cm²) and irradiated (5 J/cm²) diabetic wounded (DW) and diabetic hypoxic wounded (DHW) cells at 24 and 48 h post-irradiation at a wavelength of 830 nm (n=3). Significant probability is shown as *P<0.05* and *P<0.01** (SEM).
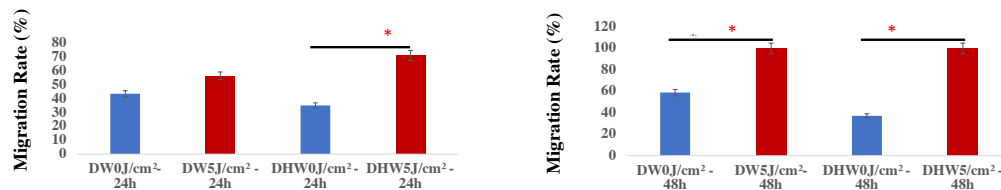
Figure 3 Migration rate was determined in non-irradiated (0 J/cm²) and irradiated (5 J/cm²) diabetic wounded (DW) and diabetic hypoxic wounded (DHW) cells at 24 and 48 h post-irradiation at a wavelength of 830 nm (n=3). Significant probability is shown as *P<0.05* (SEM).

4. Conclusion

There are several factors that contribute to delayed wound healing such as a lack of oxygen supply. The present study investigated the effect of PBM in diabetic wounded (DW) and diabetic hypoxic wounded (DHW) cell models. These results suggest that PBM at 830 nm enhanced in vitro diabetic wound healing by promoting cellular viability and migration and reducing cell death in experimental models. DHW models appeared to respond more favorably to PBM, with significant increases in Bcl-2, this may be since these cells are more 'stressed'. It is well-known that stressed cells respond more favourably to PBM, as is evident from the results shown.

References

[1] N. Houreld, H. Abrahamse, "Low-Intensity Laser Irradiation Stimulates Wound Healing in Diabetic Wounded Fibroblast Cells (WS1)", Diabetes Technology &Therapeutics. 12, (2010), 971–8.doi.org/10.1089/dia.2010.0039.

[2] F. Felice, *et al*., "Effect of different chitosan derivatives on in vitro scratch wound assay: a comparative study". Int J Biol Macromol. 76 (2015) 236–241.doi.org/10.1016/j, ijbiomac.2015.02.041.

[3] M. Fronza *et al*., "Hyaluronidase Modulates Inflammatory Response, and Accelerates the Cutaneous Wound Healing". PLoS One. 9 (2014) e112297. doi: 10.1371/journal.pone.0112297.

[4] D.R. Abbott, R.T, Abbott, S.D Jenson, *et al.,* "Apoptosis of positive lymphoma cells by a Bcl-2 interacting small molecule. J Hematopathology **2**, 113–119. doi.org/10.1007/s12308-009-0028-x

Preparation and *In Vitro* Evaluation of the Anticancer Photodynamic Therapy Efficacies of Carboxyphenoxy Zinc Phthalocyanine and their Triphenylphosphinated-Nanoparticle Conjugates

Lindokuhle Cindy Nene and Heidi Abrahamse*

Laser Research Centre, Faculty of Health Sciences, University of Johannesburg, P.O. Box 17011, Doornfontein 2028, South Africa
*E-mail: habrahamse@uj.ac.za

1. Background

Photodynamic therapy (PDT) is dependent on the efficient reactive oxygen species (ROS) generation by a sensitizing probe and cancer specificity [1]. Phthalocyanines (Pcs) are macrocyclic organic dyes which have demonstrated impressive ROS yields during PDT and therefore, promising therapeutic efficacies in cancer therapy [2]. This work reports on the development of a nanoconjugate composed of carboxyphenoxy Zn(II) Pc and cationic triphenylphosphine-labelled gold nanoparticles (AuNPs). This nano-conjugate is designed to enhance the specificity of the treatments and therefore maintain its non-invasive nature. The triphenylphosphine moiety has been widely used in the development of anticancer therapeutics and has shown selective accumulation within the mitochondria [3]. A summary of the preparation of the nano-conjugate and the photo-induced ROS yields are shown in the Fig. 1 below.
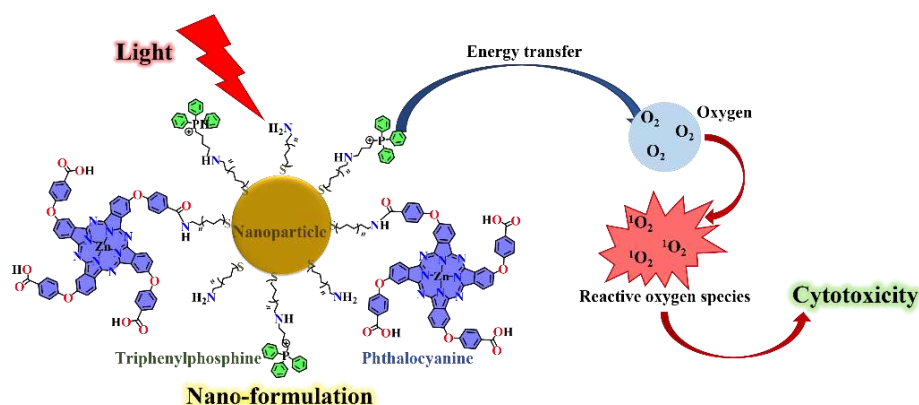
Figure 1 Preparation of cationic phthalocyanine-bovine serum and gold nanoparticle conjugates and their mechanism of reactive oxygen species generation to induce cytotoxicity in photodynamic therapy.

Pc-NPs conjugates are known to harvest photon energy from the light to which they are exposed, and thereafter transfer the energy to molecular oxygen (O_2) to yield cytotoxic ROS such as singlet oxygen ($^1O_2$), Fig. 1. This work focuses on the ROS yields and *in vitro* PDT activities of cationic Pc-AuNPs conjugates, Pc and Au alone.

2. Methodology

The efficiency of the ROS yields of the complexes were determined by calculating singlet oxygen quantum yields (Φ_Δ) during PDT and were determine using a compartive method defined in the literature [4], using Eq. 1 below.

$$\Phi_\Delta = \Phi_{\Delta(std)} \cdot \frac{R \cdot I_{(std)}}{R_{(std)} \cdot I} \tag{1}$$

The Φ_Δ of the complexes are determine by multiplying the Φ_Δ of the standard ($\Phi_{\Delta(std)}$) with the quotient of the rate of $^1O_2$ yields of the test samples (R) by light absorption efficiency of the standard ($I_{(std)}$), to rate of $^1O_2$ yields of the standard ($R_{(std)}$) by the light absorption efficienc of the test simple (I), Eq. 1. The *in vitro* PDT of Pcs and conjugates were performed on Human Malignant melanoma A375 cancer cell line. The cells were exposed to the complexes and irradiated with 680 nm laser light at 10 J.cm^{-2}. The cell viabilities post-treatments were determined using the MTT assays. The cellular percentages were calculated Eq. 2 below. Where the test samples are cells treated with complexes and light, and the control samples are untreated cells.

$$\text{Cell survival} = \frac{Abs(test)_{570nm}}{Abs(control)_{570nm}} \ x \ 100(\%) \tag{2}$$

1. Results

The Pcs alone showed higher $^1O_2$ yields compared to the Pc-BSA. However, the $^1O_2$ yields were increased for the Pcs-BSA-AuNPs compared to the Pcs alone and the Pc-BSA adduct, Table 1. This observation may be explained by a phenomenon known as the heavy atom effect, where heavy metallic NPs such as the AuNPs have been reported to enhance the $^1O_2$ yields of Pcs.
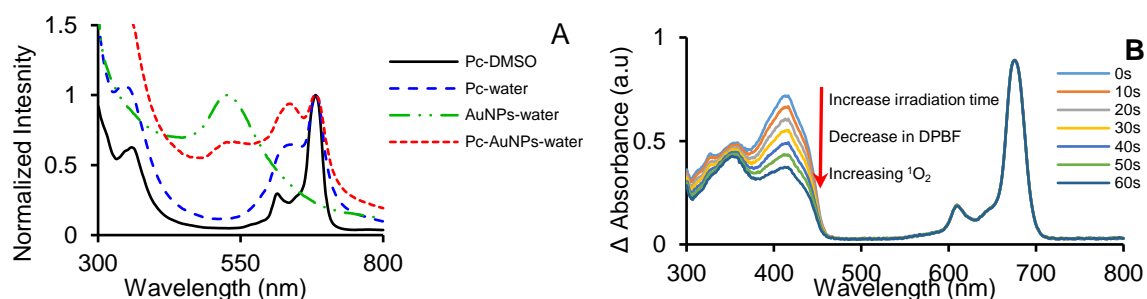
Figure 2 A) UV-vis spectra of Pc, AuNP and Pc-AuNPs and B) photo-induced singlet oxygen generation monitored by degradation of DPBF by Pc in DMSO over 1 min at 10 s intervals.

From the rate of DPBF degradation, the Φ_Δ of the complezes were calculated. This measures the photon energy transfered to O_2 to form $^1O_2$ from the total absorbed during photoactivation. Table 1 summarises photoactivity.

Table 1. Summary of the photo-activities of the complexes and cell survival percentages post PDT treatments.

Complexes	Pc	AuNPs	Pc-AuNPs
Φ_Δ	0.56	-	0.67
Cell survival (%)	48.7 (97)	-	36.0 (85)

Values in brackets are for dark toxicity studies.

The UV-vis spectra show strong absorption of Pcs in the near infrared región. The spectra for nanoconjugate show presance of the peaks from both the Pcs and AuNPs, Fig. 2. The complexes also showed evidence of $^1O_2$ generation under light exposure, Table 1. Therfore are a promising candidate for PDT of cancers. The cell survival percentages were hiher for cells exposed to Pcs, Au and AuPcs alone without light. In combination with light, the percentages decreased. This suggests photo-dependance of the therapy and therefor controllability. The cytotoxicity was further increase in the presence of the AuNPs for the Pc-AuNPs, Table 1.

2. Conclusions

Cationic therapeutics are beneficial in improving solubility and overall photo-activity for cancer treatments. The use of metallic NPs are beneficial in further enhancing the therapeutic efficacies of Pcs in PDT through the enhancement of their ROS generation. Therefore, Pc-NPs conjugates are promising photosensitizers for anticancer therapies.

Acknowledgments

References

[1] G.Gunaydin, M. E. Gedik and Seylan Ayan, "Photodynamic Therapy—Current Limitations and Novel Approaches", Front. Chem. **9**, 691697 (2021).

[2] H. Lu and N. Kpbayashi, "Optically Active Porphyrin and Phthalocyanine Systems", Chem. Rev. **110**, 6184-6261 (2016).

[3] H. Chen, Z. Fang, M. Song and K. Liu, "Mitochondrial targeted hierarchical drug delivery system based on HA-modified liposomes for cancer therapy", Eur. J. Med. Chem. **241**, 114648 (2022).

[4] D. O. Oluwole, N. Nwaji, L. C. Nene, L. Mokone, E. Dube and T. Nyokong, "Novel nano-dyad of homoleptic sandwich-type phthalocyanines with nitrogen doped graphene quantum dots for nonlinear optics", New J. Chem. **42**, 10124-10133 (2018).

[5] D. Kalyane, N. Raval, R. Maheshwari, V. Tambe, K. Kalia and R. K. Tekade, "Employment of enhanced permeability and retention effect (EPR): Nanoparticle-based precision tools for targeting of therapeutic and diagnostic agent in cancer", Mater. Sci. Eng. C, **98**, 1252-1276 (2019).

Photobiomodulation at 830 nm modulates NF-κB and apoptosis in wounded and diabetic wounded fibroblast cells

Tintswalo N Mgwenya[1], Heidi Abrahamse[1] and Nicolette N Houreld[1*]

[1]*Laser Research Center, Faculty of Health Sciences, University of Johannesburg, Doornfontein, Johannesburg, 2026, South Africa*

*E-mail: nhoureld@uj.ac.za

1. Introduction

Wound healing is a multifaceted and evolving process that focuses on repairing and regaining the function of damaged tissues. Various researchers have put forth differing perspectives on the effectiveness of photobiomodulation (PBM) at various wavelengths, specifically red and near-infrared (NIR), in promoting the healing of diabetic wounds [1-2]. The transcription factor nuclear factor kappa B (NF-κB) plays a crucial role in modulating inflammatory responses through its regulation of the viability, activation, and differentiation of cells, as well as control over apoptosis. The dysregulation of NF-κB is implicated in the pathogenesis of several inflammatory disorders, including diabetes [3]. Increased levels of pro-inflammatory cytokines in chronic wounds impede the wound healing process by prolonging the inflammatory phase. The aim of this study was to examine the impact of PBM at a wavelength of 830 nm on the levels of NF-κB and apoptosis in wounded and diabetic wounded WS1 fibroblast cells.

2. Methodology

WS1 human skin fibroblast cells were divided into two groups (n=3), namely wounded (W) and diabetic wounded (DW). A wound was simulated via the central scratch assay, and a diabetic cell model was created by continuously growing the cells for several passages in high glucose media (22.6 mM glucose) [4]. Cells (6 x 10^5 in 3.4 cm diameter culture plates) were exposed to PBM at a wavelength of 830 nm with a fluence of 5 J/cm^2 (Table 1). Control cells did not undergo any PBM (0 J/cm^2). Twenty-four hours post-PBM, NF-κB was determined by the enzyme linked immunosorbent assay (ELISA). Additionally, apoptosis, necrosis, and viability were determined via flow cytometry and Annexin V/PI staining.

Variables	Diode Laser
Wavelength (nm)	830
Wave emission	Continuous wave
Power output (mW)	106
Fluence / Irradiance (J/cm^2)	5
Energy (J)	45.37
Output power density (mW/cm^2)	11.68
Spot size (cm^2)	9.1
Irradiation time (s)	428

Table 1 Laser parameters.

3. Results

Research has demonstrated the efficacy of PBM in enhancing the rate of diabetic wound healing by promoting cellular processes, while exhibiting few adverse effects. The utilization of devices in the red and NIR wavelength in PBM has shown considerable potential as a method for enhancing the rate of wound healing, reducing pain, and enhancing skin functionality. This is attributed to the ability of light to directly penetrate wounds and modulate biochemical pathways involved in these processes [2]. The findings from this study indicated that there was a significant increase in NF-κB levels in both W and DW groups (Fig. 1). The Annexin V/PI staining results (Table 2) showed a decrease in percentage viability in the irradiated DW group when compared to the irradiated W group, although not significant. The proportion of cells displaying early apoptosis was higher in the non-irradiated and irradiated DW group compared to the non-irradiated and irradiated W group, respectively (P=0.055 and P=0.032, respectively). Although not significant, the DW group showed an increase in the proportion of cells in

early and late apoptosis post-PBM. There was a significant increase in necrosis in DW groups (P=0.044).
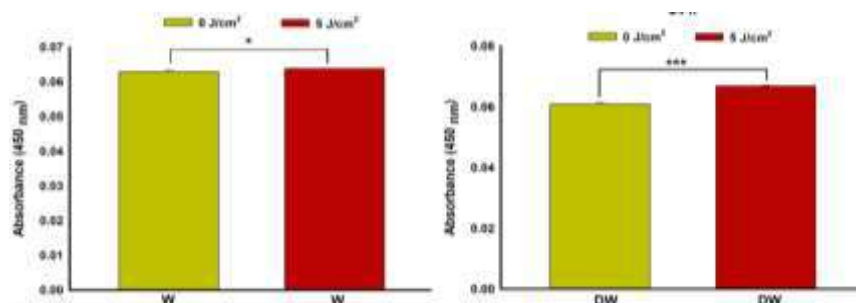
Figure 1 Nuclear factor-kappa B (NF-κB) in WS1 fibroblast wounded (W) and diabetic wounded (DW) groups 24 h post-PBM at 830 nm with 5 J/cm^2. Statistical significance in comparison to the control group (0 J/cm^2) is denoted as *P<0.05 and ***P<0.001 (SEM, n=3).

24 h	Viability (%)		Early Apoptosis (%)		Late Apoptosis (%)		Necrosis (%)	
	0 J/cm^2	5 J/cm^2	0 J/cm^2	5 J/cm^2	0 J/cm^2	5 J/cm^2	0 J/cm^2	5 J/cm^2
W	96.43 ± 0.45	97.13 ± 0.33	0.73 ± 0.25	0.77 ± 0.26	0.6 ± 0.16	0.37 ± 0.05	2.23 ± 0.29	1.7 ± 0.36
DW	94.3 ± 1.08	95.77 ± 0.74	2.13 ± 0.69	2.27 ± 0.60	0. 7 ± 0.08	1.07 ± 0.21	1.4 ± 0.22	2.37 ± 0.42*

Table 2 Cellular responses in wounded (W) and diabetic wounded (DW) cells irradiated at 830 nm and 5 J/cm^2 as measured by Annexin V/PI staining. Irradiation-free cells were used as controls (0 J/cm^2). Statistical significance in comparison to the control group (0 J/cm^2) is denoted as *P < 0.05 (SEM, n=3).

4. Conclusion

At a wavelength of 830 nm and a fluence of 5 J/cm^2, PBM induced wound healing in fibroblasts after 24 h. This impact was characterized by a significant increase in NF-κB levels and the proportion of viable populations in both W and DW groups. Although there was an increase in the proportion of necrotic cells post-PBM in DW groups, the percentage was relatively low (2.37%), with most cells within the viable population (95.77%).

Acknowledgments

References

[1]   O. A. Oyebode and N. N. Houreld, "Photobiomodulation at 830 nm Stimulates Migration, Survival and Proliferation of Fibroblast Cells," Diabetes, Metab. Syndr. Obes. p. 2885–2900 (2022).

[2]   N. N. Houreld, P. R. Sekhejane, and H. Abrahamse, "Irradiation at 830 nm stimulates nitric oxide production and inhibits pro-inflammatory cytokines in diabetic wounded fibroblast cells," Lasers Surg. Med. p. 494–502 (2010).

[3]   K. I. Ko *et al.*, "Diabetes-induced NF-kB dysregulation in skeletal stem cells prevents resolution of inflammation," Diabetes. p. 2095–2106 (2019).

[4]   S. Martinotti and E. Ranzato, *Scratch Wound Healing Assays*, Ed. New York,NY, USA: Methods in Molecular Biology, 2019. doi: 10.1385/1592598307.

Enhancement of Raman Spectroscopy on SARS-CoV-2 detection using machine learning

Nkgaphe Tsebesebe[1,2*], Kelvin Mpofu[1], Sphumelele Ndlovu[1], Sudesh Severasu[2] and Patience Mthunzi Kufa[1,2,3]

[1]*Council for Scientific and Industrial Research, National Laser Centre, P.O Box 395, Building 46A, Pretoria 0001, South Africa*

[2]*Department of Human Biology, Division of Biomedical Engineering, University of Cape Town, Cape Town 7925, South Africa*

[3]*School of Chemistry and Physics, University of KwaZulu-Natal, Durban 4001, South Africa*

*e-mail: `ntsebesebe@csir.co.za`

1. Abstract

Raman spectroscopy is an optical spectroscopic technique that provides detailed information about molecular composition and molecular structure. This work integrates Raman spectra and machine learning algorithms to detect SARS-CoV-2. Machine learning algorithms (support vector machine, decision tree, and gradient boosting algorithms) are trained to analyze and classify Raman spectra as healthy and SARS-CoV-2 infected. The hyperparameter tuning improved the performance of the Support vector machine from 90.32% to 95.16%, decision tree from 83.87% to 90.32%, and gradient boost from 91.94% to 95.16% on 62 Raman spectra. The algorithms produced evidence of high recall and specificity. Hence, integrating Raman spectroscopy with machine learning has the potential to serve as an alternative diagnostic tool.

2. Introduction

Raman spectroscopy is an optical spectroscopic technique mainly used to investigate the vibrational modes associated with chemical bonds in a sample [1]. The technique obtains sample-specific spectral fingerprints (Raman spectrum) of different samples [2]. These Raman spectra are inelastic scattering spectra based on the Raman effect obtained using scattered light with a different frequency from the incident light [3]. Hence, they contain numerous bands at various frequencies, which are characteristic of the structural features and functional groups of a particular molecule [2]. This makes Raman spectroscopy a sensitive and accurate technique to reflect changes in material composition and structure [2]. As such, the technique has received increasing interest in medical diagnosis [2]. On the other hand machine learning techniques have shown considerable success in feature learning, Raman signal extraction, and modeling complex relationships to overcome challenges in Raman-based chemical analysis. Therefore, the integration of machine learning with Raman spectroscopy has been shown to reduce the false positive rate and reduces the detection cycle [3]. In this work, the machine learning algorithms (support vector machine, decision tree, and gradient boosting algorithms) are trained to analyze Raman spectra and classify them as healthy and infected with SARS-CoV-2.

3. Methodology

The current work follows supervised learning where algorithms (support vector machine, decision tree, and gradient boosting) were provided with labelled Raman spectra to analyze and predict the

output. The study use Python code to facilitate the machine learning implementation on Google Colab to perform the process shown in Fig. **1**.
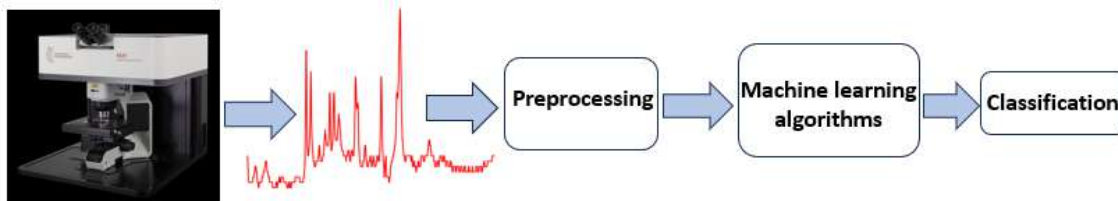
Figure 1: A schematic representation of the research approach

4. Results

Table **1** shows a performance of the algorithms in terms of accurate predictions of the Raman spectra in healthy and SARS-CoV-2 infected. Before hyperparameter optimization, the support vector machine achieves 90.32% in classifying 62 Raman spectra as healthy and SARS-CoV-2 infected. The decision tree achieves an accuracy of 83.87%. Lastly, the gradient boost achieves accuracy of 91.94%. The optimized models (support vector machine, decision tree, and gradient boosting) achieve 95.16%, 90.32% and 95.16% respectively. The f1 scores of all models are above 90%, implying good recall and precision. As such, hyperparameter tuning has shown to be a crucial step for machine learning models to interpret Raman spectra. Therefore, the optimized models of this study can be used in addition to disease diagnosis in the medical field.

Algorithms	Before Hyperparameter optimization (Accuracy %)	After Hyperparameter optimization (Accuracy %)	F1 Score of optimized models
Support Vector Machine	90.32	95.16	95.89
Decision tree	83.87	90.32	91.43
Gradient boost	91.94	95.16	95.89

Table 1: Performance of machine learning algorithms on Raman spectra

5. Conclusions

The current research focused on improving the accuracy of the machine learning algorithm in classifying Raman spectra as healthy and SARS-CoV-2 infected. Hyperparameter tuning has demonstrated to control the learning process, and hence the parameters impact the performance of machine learning algorithms. The optimized parameters improved performance of the Support vector machine from 90.32% to 95.16%, the decision tree from 83.87% to 90.32%, and gradient boost from 95.16% to 95.16%. The algorithms produced evidence of high recall and specificity. As a result, hyperparameter optimization plays an important role in integrating Raman spectroscopy with machine learning. Optimized machine learning models of the current work have the potential to serve as an alternative diagnostic tool from Raman spectra.

Acknowledgments

References

[1] H. Katie and K. Emma and S. Abeer and M. David and A., Rasha and S. Valerie, "Raman spectroscopy: Current applications in breast cancer diagnosis, challenges and future prospects", *British journal of cancer* **126**, pp. 1125–1139 (2022).

[2] Z. Yuwei and R. Liang and W. Qi and W., Zhining and L., Chengcheng and D. Yi, "Raman spectroscopy: A potential diagnostic tool for oral diseases", *Frontiers in Cellular and Infection Microbiology* **12**, pp. 61–65 (2022).

[3] Z. Wandan and W. Qi and X. Zhiping and L. Zhiping and Q. Han, "Application of XGBoost algorithm in the detection of SARS-CoV-2 using Raman spectroscopy", *Journal of Physics: Conference Series* **1775**, pp. 012007–012010 (2021).

Determining the physical properties of a perturbed optically trapped particle using Mie scattering

Anneke Erasmus[1], Gurthwin W Bosman[1], Erich G Rohwer[1], Pieter H Neethling[1*]

[1]*Physics department, Stellenbosch University, Stellenbosch, Western Cape, South Africa, 7600*

*e-mail: `pietern@sun.ac.za`

Spectral information in the Mie scattering of white light from a spherical particle is analysed to determine the diameter and refractive index of a particle [1]. When broadband white light is incident on a spherical, microscopic particle, due to total internal reflection, specific wavelengths resonate within the particle. These resonances are also referred to as whispering gallery modes or morphologically dependent resonances. By measuring the spectrum of the back scattered light from the particle using an objective lens, the resonances can be identified as peaks on the spectrum. The particle's physical properties (diameter and refractive index) are determined by fitting a simulated spectrum calculated using Mie theory to the measured data. From the simulation [2], in figure **1**, a diameter increase of 3 nm results in an observable red shift of the peaks.
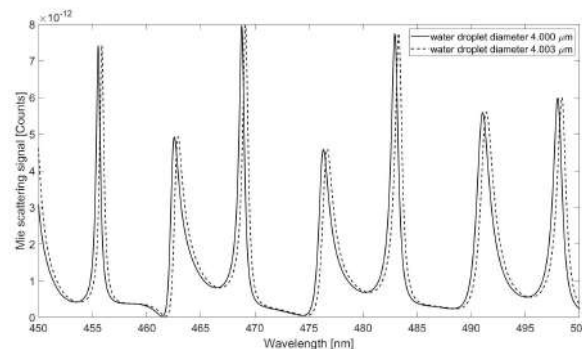
Figure 1: The figure shows a MiePlot simulation of white light scattering from a water droplet suspended in air. A spectral shift of 0.4 nm is seen when the diameter of the droplet increases by 3 nm.

In this work, we measure the diameter and refractive index of aerosol droplets ($2 - 8 \ \mu$m) suspended in air. To isolate an individual droplet, a counter propagating optical trap is used [3]. To trap a transparent, dielectric particle, a laser is focused into the sample. The light applies a scattering force and a gradient force that is proportional to the gradient of the intensity of the light. The resultant force on the particle creates a stable trap. Figure **2** shows two NIR-infrared (975 nm) trap lasers focused and overlapped in a sample chamber with two long working distance air objectives (numerical apertures of 0.7). The trap is located near the foci. A white light LED (WL LED (Mie)) illuminates the trapped particle and the back scattering from the particle is collected by the objective (OBJECTIVE 1) and measured with a spectrometer.

Droplets of NaCl-water solution were optically trapped in air using this system and the diameter and refractive index of the trapped droplets are determined from the spectrum of the back scattered light. An example of the spectrum of the scattered light from such a droplet is shown in figure **3**. Mie theory was used to fit a simulated spectrum [4] to the measured spectrum. The diameter and refractive index of the droplet were determined to be 4.80(6) μm and 1.374(1) respectively.
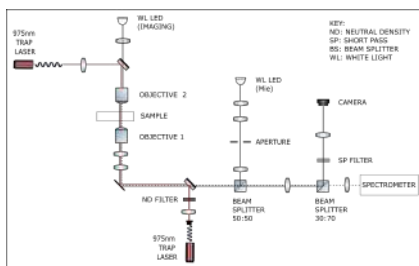
Figure 2: Two counter propagating beams (975 nm) are focused and the foci are over lapped in space to create an optical trap. The back scattering of white light from the trapped particle is detected on a spectrometer.
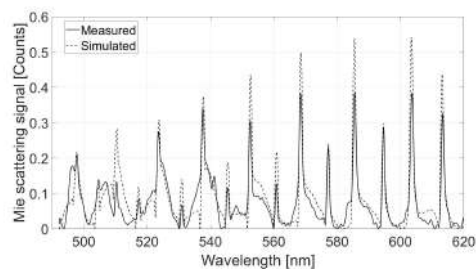
Figure 3: The measured spectrum of the scattered light (solid line) from an optically trapped NaCl-water droplet suspended in air is compared to a simulated spectrum (dotted line) for a droplet with diameter 4.80(6) μm.

By integrating the Mie scattering technique with the optical trap, the system is used to study an individual particle, negating ensemble averaging. We aim to expand this work by perturbing the trapped particle and studying changes in the scattered light. The study of aerosol particles is relevant in climate research and applications [5], [6].

References

[1] S. H. Jones, M. D. King, and A. D. Ward, "Determining the unique refractive index properties of solid polystyrene aerosol using broadband Mie scattering from optically trapped beads", *Phys. Chem. Chem. Phys.*, **15**(47), pp. 20735–20741, (2013).

[2] P. Laven, "MiePlot." Philip Laven, 2021, [Online]. Available: http://www.philiplaven.com/mieplot.htm.

[3] A. Ashkin, "Acceleration and Trapping of Particles by Radiation Pressure", *Phys. Rev. Lett.*, **24**(4), pp. 156–159 (1970).

[4] Mie scattering demo program written by Martin Fierz (martin@fierz.ch), August 2005. The Dynamic Link Library was adapted by Dr AD Ward and is based on Bohren and Huffman Mie code.

[5] M. D. King, K. C. Thompson, and A. D. Ward, "Laser Tweezers Raman Study of Optically Trapped Aerosol Droplets of Seawater and Oleic Acid Reacting with Ozone: Implications for Cloud-Droplet Properties", *J. Am. Chem. Soc.*, **126**(51), pp. 16710–16711 (2004).

[6] B. R. Bzdek, R. M. Power, S. H. Simpson, J. P. Reid, and C. P. Royall, "Precise, contactless measurements of the surface tension of picolitre aerosol droplets", *Chem. Sci.*, **7**(1), pp. 274–285 (2016).

Photo-thermal Effects of Citrate Gold Nanoparticle on Lung Cancer Cells

Kave Moloudi, Heidi Abrahamse and Blassan P. George *

Laser Research Centre, Faculty of Health Sciences, Doornfontein Campus, University of Johannesburg,

Johannesburg 2028, South Africa; 223138872@student.uj.ac.za (K.M.);

* Correspondence: blassang@uj.ac.za; Tel.: +27-11-599-6926

Abstract:

Lung cancer shows the highest global incidence of malignancy, with significantly high morbidity and mortality and is often detected at a late stage. It is considered the second most common cancer with a prediction of two million new cases and 1.76 million deaths annually worldwide. Gold nanoparticles (GNPs) have shown promising potential as a photo-thermal agent in cancer therapy due to their unique optical and physical properties. But the stability of these nanoparticles is a critical factor that can affect their efficacy in cancer treatment. This study aims to use citrate to improve the stability of GNPs photo-thermal application and to evaluate the cytotoxicity of citrate-GNPs as a single and combination treatment with 525 nm laser light on A549 lung cancer cells. Data from this experiment showed that the citrate-GNPs at a concentration of 100 µg/mL(mxaimum safe concentarion) increased the temperature ($\Delta T=8 \pm 0.5°C$) and decreased A549 cells viability to 75%. under photo-thermal effects of 525 nm laser. To sum up, our study showed that citrate is a good stabilizer for GNPs due to its ability to form a strong electrostatic layer around the particles, preventing aggregation and maintaining their stability. Moreover, citrate-GNPs can be used as a photo-thermal agent in cancer therapy.

Keywords: Photo-thermal therapy, citrate, laser; lung cancer, reactive nitrogen species.

1. Introduction

Lung cancer shows the highest global incidence of malignancy, with significantly high morbidity and mortality (1.76 million deaths annually worldwide) and is often detected at a late stage [1, 2]. Common strategies for the treatment of lung cancer are surgery, hormone therapy and chemo-radiotherapy. However, these conventional treatments cause severe side effects in normal tissue and induce resistance. But some new therapeutic procedures, including hormone therapy, targeted therapy, as well as photodynamic therapy (PDT), can be helpful in combination with conventional treatments to overcome these limitations [3, 4].

GNPs have unique optical and electronic properties that make them useful in a variety of applications, including biomedical imaging, drug delivery, and sensing [5, 6]. Their size and shape can be precisely controlled, allowing for tailoring of their properties for specific applications. Additionally, their biocompatibility and low toxicity make them attractive for use in biomedical applications. However, various factors, such as pH, temperature, and ionic strength, can affect their stability and aggregation behaviour, which must be carefully considered when designing experiments or applications involving gold nanoparticles [7-10]. Consequently, modifying the surface of inorganic nanomaterials with proper coating is essential for their biomedical applications [11, 12]. In this study, we investigated the photo-thermal effects of citrate-stabilized GNPs on A549 lung cancer cells *in vitro*.

2. Materials and methods

2.1. Cell culture and treatment

A549 human lung cancer cells were seeded in T 25-flask, containing DMEM medium supplemented with 10% Fetal Bovine Serum (FBS) and 1% Penicillin-Streptomycin-Glutamine (100X). Then, the cells were harvested and counted. To evaluate the cytotoxicity of citrate-GNPs (0, 25, 50, 75 and 100 µg/mL) and 525 nm laser therapy (5 J/cm^2), the cells were plated at densities of 20,000 cells in 100 μL of growth media per well in a 96-well plate (Corning Cat. No. 4520). The cytotoxicity was analyzed after 24 h treatment using MTT assay.

2.2. Citrate gold nanoparticles and characterization

Commercial citrate-GNPs was purchased from Sigma (St. Louis, MO, USA), and then the concentration, diameter and dynamic light scattering (DLS) of the citrate-GNPs were investigated using UV-vis (7315 spectrophotometer-Jenway) and Malvern Zetasizer Nano ZS-90 instrument.

2.3. Thermal curve with and without citrate-GNPs

The thermal response of citrate-GNPs (100 µg/mL) under laser irradiation with the power of 370 mW/cm^2 and 5 J/cm^2 for 25 min was assessed via the thermal recording approach. Then, the thermal changes were recorded via a thermometer (Brannan) with a sensitivity of 0.5°C. The thermal changes of the medium were recorded as the control.

3. Statistical analysis

All the experiments were performed in triplicate and expressed as mean values $\pm$ SD (standard deviation). One-way ANOVA test was performed using the SPSS software (Version 18), followed by Tukey's test post-hoc analysis. The p-value <0.05 was considered to be statistically significant.

4. Results

Result from temperate cure and MTT assay showed that citrate-GNPs at the 22 nm size (Zeta) increased the temperature of cell culture media by about 8+-0.5°C after 15 min irradiation and decreased the cell viability to 75% under photo-thermal effects of 525 nm laser after 24 h treatment as shown in Fig 1.
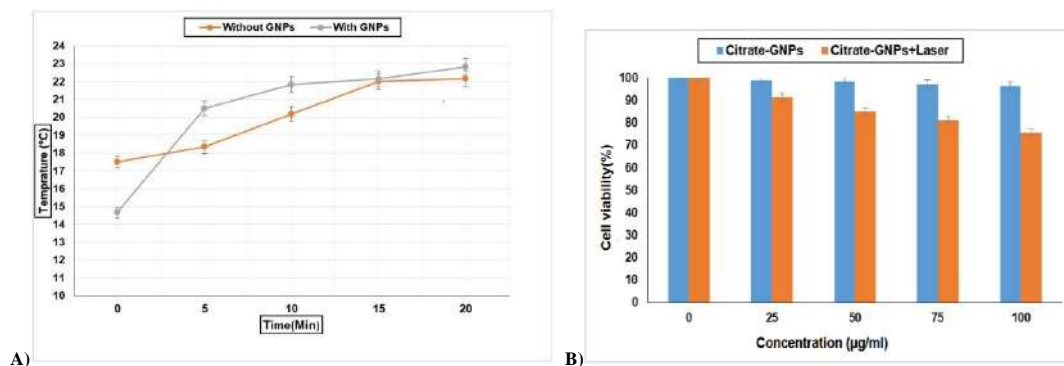
Figure 1. Citrate-GNPs (A) Temperature curve and (B) cytotoxicity against A549 lung cancer cells.

5. Conclusions

To sum up, our study showed that citrate is a good stabilizer for GNPs due to its ability to form a strong electrostatic layer around the particles, preventing aggregation and maintaining their stability. Moreover, citrate-GNPs can be used as a photo-thermal agent in cancer therapy.

Acknowledgements

References

1. Bade BC, Cruz CSD: **Lung cancer 2020: epidemiology, etiology, and prevention**. *Clinics in chest medicine* 2020, **41**(1):1-24.
2. Yessenbayev D, Khamidullina Z, Tarzhanova D, Orazova G, Zhakupova T, Kassenova D, Bilyalova Z, Igissinova G, Sayakov U, Dzhumabayeva F: **Epidemiology of Lung Cancer in Kazakhstan: Trends and Geographic Distribution**. *Asian Pacific Journal of Cancer Prevention* 2023, **24**(5):1521-1532.
3. Leiter A, Veluswamy RR, Wisnivesky JP: **The global burden of lung cancer: current status and future trends**. *Nature Reviews Clinical Oncology* 2023:1-16.
4. Hirsch FR, Scagliotti GV, Mulshine JL, Kwon R, Curran WJ, Wu Y-L, Paz-Ares L: **Lung cancer: current therapies and new targeted treatments**. *The Lancet* 2017, **389**(10066):299-311.
5. Moloudi K, Khani A, Najafi M, Azmoonfar R, Azizi M, Nekounam H, Sobhani M, Laurent S, Samadian H: **Critical parameters to translate gold nanoparticles as radiosensitizing agents into the clinic**. *Wiley Interdisciplinary Reviews: Nanomedicine and Nanobiotechnology* 2023:e1886.
6. Zhang S, Lin L, Huang X, Lu Y-G, Zheng D-L, Feng Y: **Antimicrobial properties of metal nanoparticles and their oxide materials and their applications in oral biology**. *Journal of Nanomaterials* 2022, **2022**.
7. Khan MY, Roy M: **Synthesis, limitation and application of gold nanoparticles in treatment of cancerous cell**. *Int J Sci Res in Multidisciplinary Studies Vol* 2019, **5**:9.
8. Balasubramanian SK, Yang L, Yung L-YL, Ong C-N, Ong W-Y, Liya EY: **Characterization, purification, and stability of gold nanoparticles**. *Biomaterials* 2010, **31**(34):9023-9030.
9. Wang Y, Quinsaat JEQ, Ono T, Maeki M, Tokeshi M, Isono T, Tajima K, Satoh T, Sato S-i, Miura Y: **Enhanced dispersion stability of gold nanoparticles by the physisorption of cyclic poly (ethylene glycol)**. *Nature communications* 2020, **11**(1):6089.
10. Kang H, Buchman JT, Rodriguez RS, Ring HL, He J, Bantz KC, Haynes CL: **Stabilization of silver and gold nanoparticles: preservation and improvement of plasmonic functionalities**. *Chemical reviews* 2018, **119**(1):664-699.
11. Keshavarz M, Moloudi K, Paydar R, Abed Z, Beik J, Ghaznavi H, Shakeri-Zadeh A: **Alginate hydrogel co-loaded with cisplatin and gold nanoparticles for computed tomography image-guided chemotherapy**. *Journal of biomaterials applications* 2018, **33**(2):161-169
12. Pissuwan D, Niidome T, Cortie MB: **The forthcoming applications of gold nanoparticles in drug and gene delivery systems**. *Journal of controlled release* 2011, **149**(1):65-71.

Dose response cytotoxicity studies with naturally derived photosensitizers against cancer cells

Nosipho T Fakudze, Paromita Sarbadhikary, Blassan P George*, and Heidi Abrahamse

Laser Research Centre, Faculty of Health Sciences, University of Johannesburg
*P.O. Box 1701, Doornfontein 2028, South Africa*
*E-mail: blassang@uj.ac.za,

1. Background

Cancer is the second leading cause of death worldwide and accounts for 9.3 million deaths as stated by World Health Organization in 2022[1]. Breast cancer has the leading incident rate exceeding lung cancer statistics with new cases at approximately 2.3 million [2]. Conventional breast cancer treatments such as radiation, chemotherapy, hormone receptor, and surgery cause multiple side effects, and this has caused a shift in cancer treatment research towards natural products [3]. Natural products have been used in traditional medicine throughout history for different ailments with success [4]. The diversity of plants, their beneficial primary and secondary phytocompounds make them advantageous as cost-effective cancer treatment strategy with minimal induced side effects [5]. Photodynamic therapy (PDT) is an alternative therapy that utilizes 3 components: molecular oxygen, photosensitizer, and light and has been used for the cancer treatment [6]. In this study, naturally derived photosensitizers (PS) pheophorbide-a and hypericin were used to treat breast cancer cells. Hypericin is derived from the medicinal plant *Hypericum perforatum* and pheophorbide-a is a chlorophyll derivative[7,8].

2. Results

MCF-7 breast cancer cells were treated with different concentrations of pheophorbide-a and hypericin for 3 h followed by light irradiation with parameters as shown in Table 1. 24 h post irradiation cytotoxicity results showed significant loss of cell viability as shown by MTT (3-[4,5-dimethylthiazol-2-yl]-2,5 diphenyl tetrazolium bromide) assay and morphological analysis (Figure 1 (a) and (b)). As seen in Figure 1 (a) 0.09 and 0.2 μM of hypericin induced ~50% and 95% loss in cell viability respectively. While pheophorbide-a induced ~50% and 90% cell death at a concentration of 0.5 and 1.2 μM. Morphological analysis (Figure 1 (b) also showed altered cellular morphological in both hypericin and pheophorbide-a induced PDT groups. The presence of rounded cells with loss of adherence property and decrease in cell number was seen in both the treatment groups. Thus, the results indicated strong phototoxic efficacy of both the naturally derived PSs against breast cancer cells. Whereby, hypericin showed strong PDT effect at lower concentrations compared to pheophorbide-a, irradiated at a light dose of 1 J/cm^2.

(a)
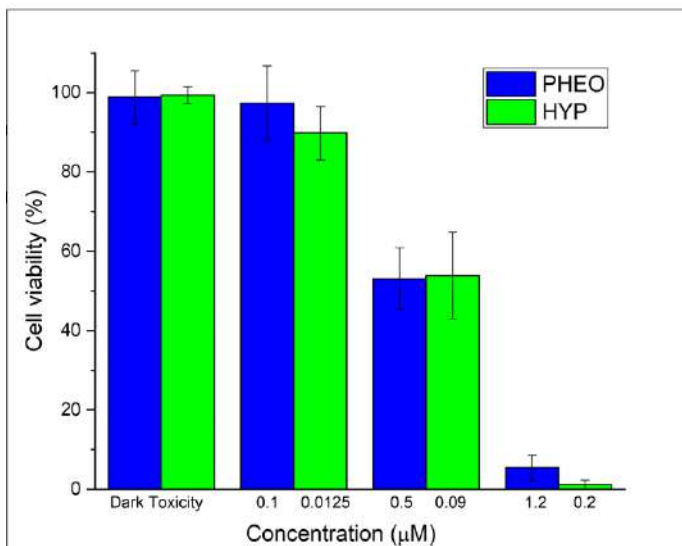
(b)
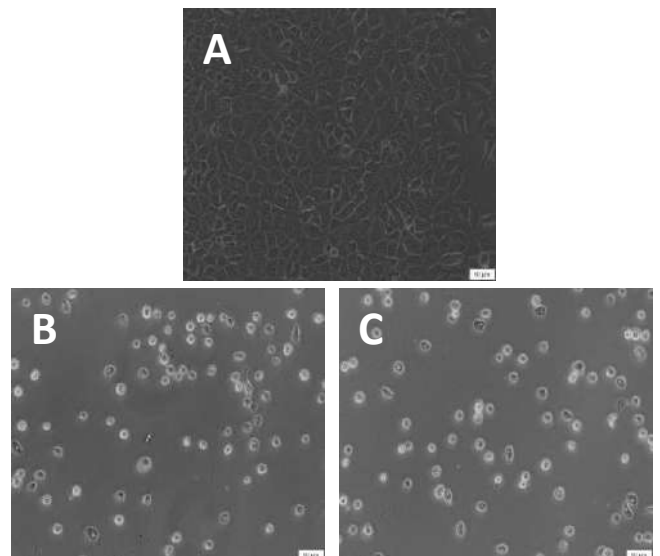
Figure 1 (a) Viability of MCF-7 cells after treatment with pheophorbide-a and hypericin with and without PDT. (b) Morphological changes of MCF-7 cells after treatment with PS. A control/untreated cells, B hypericin treated cell at 0.2 μM and C pheophorbide-a treated cells at 1.2 μM.

Name	Pheophorbide-a	Hypericin
Light source type	LED	Semiconductor (Diode)
Wavelength (nm)	660	594
Wave Emission	continuous	continuous
Spectrum	Red (visible light)	Red (visible light)
Power (mW/cm^2)	7.08	92
Fluency (J/ cm^2)	1	1
Irradiation duration	2 m 20 s	2 m 53 s

Table 1 Light source parameters

3. Conclusions

This study showed that the both hypericin and pheophorbide-a are promising PDT agent against breast cancer cells as indicated by significant cell death shown by morphological analysis and MTT cell viability assay. Thus, these naturally derived PSs are worth in-depth investigation as anticancer effect for treatment of cancers. Further investigation is currently underway on the efficacies of these photosensitizers in combination therapy with certain phytochemicals.

Acknowledgments

References

[1] World Health Organization, Non communicable diseases, (2022). https://www.who.int/news-room/fact-sheets/detail/noncommunicable-diseases (accessed August 7, 2023).
[2] H. Sung, J. Ferlay, R.L. Siegel, M. Laversanne, I. Soerjomataram, A. Jemal, F. Bray, Global Cancer Statistics 2020: GLOBOCAN Estimates of Incidence and Mortality Worldwide for 36 Cancers in 185 Countries, CA. Cancer J. Clin. 71 (2021) 209–249. https://doi.org/10.3322/caac.21660.
[3] A.G. Waks, E.P. Winer, Breast Cancer Treatment, JAMA. 321 (2019) 316. https://doi.org/10.1001/jama.2018.20751.
[4] G.M. Cragg, J.M. Pezzuto, Natural Products as a Vital Source for the Discovery of Cancer Chemotherapeutic and Chemopreventive Agents, Med. Princ. Pract. 25 (2015) 41–59. https://doi.org/10.1159/000443404.
[5] G. Zhang, C. Zhang, J. Sun, Y. Xiong, L. Wang, D. Chen, Phytochemical Regulation of RNA in Treating Inflammatory Bowel Disease and Colon Cancer: Inspirations from Cell and Animal Studies, J. Pharmacol. Exp. Ther. 376 (2021) 464–472. https://doi.org/10.1124/jpet.120.000354.
[6] M.H. Abdel-Kader, Photodynamic Therapy: From Theory to Application, Springer Science & Business Media, 2014.
[7] A. Saide, C. Lauritano, A. Ianora, Pheophorbide a: State of the Art, Mar. Drugs. 18 (2020) 257. https://doi.org/10.3390/md18050257.
[8] J. Zhang, L. Gao, J. Hu, C. Wang, P.-L. Hagedoorn, N. Li, X. Zhou, Hypericin: Source, Determination, Separation, and Properties, Sep. Purif. Rev. 51 (2022) 1–10. https://doi.org/10.1080/15422119.2020.1797792.

Dendrimer-based Nanoconjugates and their promising approaches to cancer treatment

Lufuno Gracious Nemakhavhani, Heidi Abrahamse, Sathish Sundar Dhilip Kumar*
Laser Research Centre
Faculty of Health Sciences
University of Johannesburg
South Africa
Email*:sathishd@uj.ac.za

1. Introduction

Melanoma is a type of melanocyte cancer characterized by the production of melanin in the epidermis basal layer of the skin. Metastatic melanoma is a cancer that has spread to other parts of the body, including the lymph nodes, brain, bones, or lungs, and is thus difficult to treat (Sherrell, 2022). There are several methods of treating melanoma, such as chemotherapy, surgery, radiotherapy, and biological therapy, but each is expensive and has side effects. The side effects of the therapies include alopecia, neuropathy, fatigue, nausea, vomiting, gastrointestinal toxicity, and myelosuppression (Luke, J.J. & Schwartz, G.K ,2013). Recently, it has been demonstrated that combining nanotechnology with photodynamic therapy (PDT) can effectively treat melanoma. Curcumin is a photosensitizer derived from the Curcuma longa plant, which exhibits antioxidant, anti-inflammatory, anti-carcinogenic, and anti-infectious properties, making it an effective drug for treating tumors (Nabavi et al., 2018). Due to Curcumin's hydrophobic characteristics, rapid metabolism, and low permeability to cells, a drug carrier is required for effective delivery. Gold nanoparticles (AuNPs) have advanced features such as a large surface-to-volume ratio and the ability to tune their charge, hydrophilicity, and functionality via surface chemistries, making them excellent non-toxic drug delivery carriers (Farooq et al., 2018). A dendrimer is a hyperbranched molecule comprised of three polymers layers exhibiting nanoscale dimensions. The dendrimers are water soluble, while the three-dimensional hollow inside may trap hydrophobic chemotherapeutic agents such as curcumin and can penetrate through cells to deliver the drugs. A dendrimer-based stabilizer is commonly used to prevent AuNPs from overgrowing and aggregating to achieve efficient drug delivery (Sakamoto et al., 2017). This project aims to develop curcumin-loaded dendrimer gold nanoconjugate (C-DGN) to treat melanoma effectively. The project will investigate the preparation, physicochemical characterization, and cellular responses of synthesized DGN. The advantage of such a system is that it will enhance skin cancer treatment modalities.

2. Materials and Methods

2.1 Preparation of Dendrimer Gold Nanoconjugates (DGN)

In this study, G4-PAMAM-NH2 dendrimer was used to prepare DGN and subsequent step-son experiments were conducted according to Kim et al (2004).

2.2 UV Visible spectrophotometry

The surface plasmon resonance (SPR) pattern of synthesized DGN was determined by ultraviolet-visible (UV–vis) spectrophotometry (Jenway, 7315 Spectrophotometer) at room temperature. Deionized water was used as a blank. The spectral analysis was performed at a resolution of 1 nm between 400 and 800 nm.

2.3 HR-TEM

The morphology (size and shape) of DGN was determined using high-resolution transmission electron microscopy (HRTEM, JEOL-JEM 2100F). The sample was prepared by drop-casting the DGN and C-DGNs solution onto a carbon-coated copper TEM grid. Before casting onto the grid, the sample solution was centrifuged at 10,000 rpm for 5 min. The isolated samples were dispersed in deionized water (100 μL) and sonicated in an ultrasonic bath for 15 min. Images were recorded on a HRTEM operating at an acceleration voltage of 200 keV.

3. Results

In this study, the SPR pattern of synthesized DGN was measured in a UV-Spectrophotometer (Figure 1a) the SPR peak band of DGNs appeared at 546 nm. The preliminary results of UV-vis analysis were further confirmed by HRTEM measurements. Typically HRTEM images of DGN are shown in Figure 1b. HRTEM results revealed that the synthesized DGN is in the range of 2-5 nm in size.

a)   b)
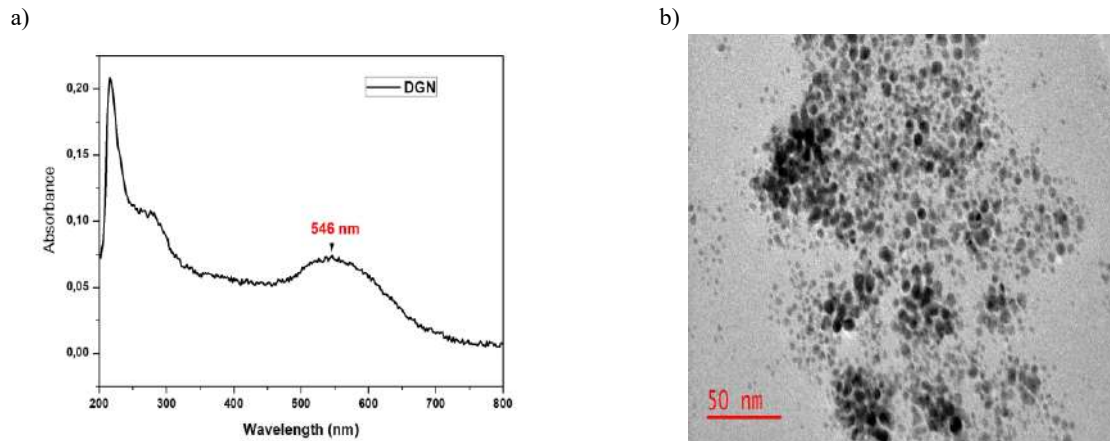
Figure 1[a] UV spectrophotometric analysis of DGN, and [b] High-Resolution Transmission Electron Microscopic image of DGN

Conclusion
In conclusion, we successfully synthesized DGN using rotary vaccum method following by magnetic stirring method. The sperical morphology and small size of DGN were confirmed by HRTEM images. Overall these findings suggested that the synthesized DGN have the potential to load curcumin and can be successfully used for the treatment of melanoma.

References
[1] Sherrell. Z. 2022. What to know about metastatic melanoma. MedicalNewsToday. Metastatic melanoma: Symptoms, treatment, and outlook (medicalnewstoday.com) Date of access: 03 Mar. 2023.

[2] Luke, J.J. & Schwartz, G.K. (2013). Chemotherapy in the management of advanced cutaneous malignant melanoma. Clinics in dermatology, 31(3):290-297.

[3] Nabavi, S.M., Russo, G.L., Tedesco, I., Daglia, M., Orhan, I.E., Nabavi, S.F., Bishayee, A., Nagulapalli Venkata, K.C., Abdollahi, M. & Hajheydari, Z. (2018). Curcumin and melanoma: From chemistry to medicine. Nutrition and cancer, 70(2):164-175.

[4] Sakamoto,K., Lochhead,R.Y., Maibach,H.I., et al. (2017). Cosmetic science and technology: theoretical principles and applications Elsevier.

[5] Farooq, M.U., Novosad, V., Rozhkova, E.A., Wali, H., Ali, A., Fateh, A.A., Neogi, P.B., Neogi, A. & Wang, Z. (2018). Retracted article: Gold nanoparticles-enabled efficient dual delivery of anticancer therapeutics to HeLa cells. Scientific reports, 8(1):2907.

[6] Kim, Y-G., Oh S-K., Crooks RM. (2004). Preparation and Characterization of 1-2 nm Dendrimer-Encapsulated Gold Nanoparticles Having Very Narrow Size Distribution. Chem. Mater 16, 167-172.

Optimisation of ADSC Seeding Density for use in 3D Culture with Photobiomodulation: A Pilot Study.

Brendon Roets[1], Heidi Abrahamse[1] and Anine Crous[1*]

[1]*Laser Research Centre, Faculty of Health Science, University of Johannesburg, P.O. Box 17011, Doornfontein, Johannesburg, South Africa, 2028.*

* E-mail: acrous@uj.ac.za

1. Introduction

Stem cell therapy requires a sufficient number of cells to be proliferated *in vitro* to ensure effective *in vivo* repair of damaged tissues (1). Three-dimensional cell culture and photobiomodulation (PBM) strategies improve gene expression patterns, proliferation and differentiation in culture (2, 3). However, the initial seeding density has a dramatic effect on stem cell proliferation and viability (4, 5). Therefore, optimisation is required to improve culture efficiency and reduce both culture time and cost. The aim of this pilot study was to identify the optimal seeding density of Immortalised Adipose-derived stem cells (ADSCs) in 96-well TrueGel3D-hydrogel plates, exposed to PBM. To compensate for the high proliferation rates expected with PBM in the red and near infrared wavelengths (6).

2. Methodology

Immortalised ADSCs (ASC52telo hTERT, ATCC® SCRC-4000™) were seeded at various densities (1 x 10^3 cells, 10 x 10^3 cells and 1 x 10^6 cells) in TrueGel3D-hydrogels in 96-well plates and exposed to PBM (525 nm, 660 nm, 825 nm, 525 nm and 660 nm combination and 525 nm and 825 nm combination; with two fluencies of 5 and 10 J/cm^2). The morphology was observed, and proliferation and viability were measured at 24 hours, 48 hours and 7 days post-exposure (Fig 1). To determine the optimal seeding density. The laser parameters have been specified in Table 1 where the calculation for irradiation time was determined with the formula seen in Eq. (1).
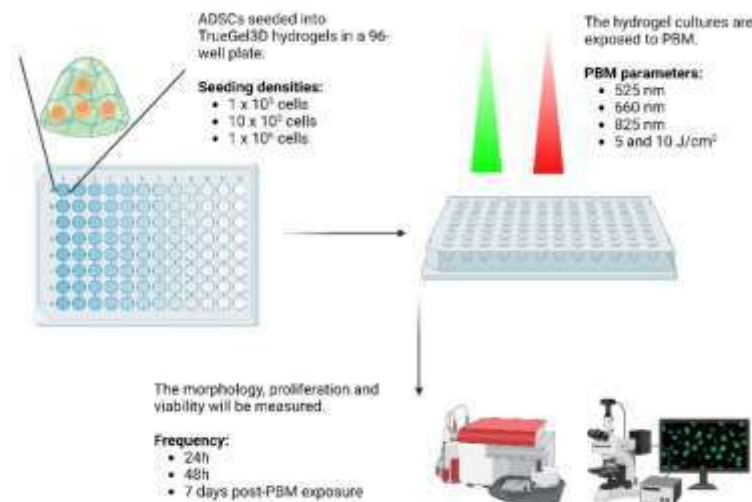
Figure 1: Determination of optimal seeding density of ADSCs cultured in TrueGel3D-hydrogels, with PBM stimulation.

Laser	Light Source	Wavelength (nm)	Power Output (mW)	Power Density (mW/cm^2)	Area (cm^2)	Emission	Fluence (J/cm^2)	Time of Irradiation (s)
Near infra-red (NIR)	Diode Laser	825	515	53.53	9.62	Continuous Wave	5 and 10	93 and 186
Red (R)	Diode Laser	660	92.8	10.22	9.1	Continuous Wave	5 and 10	518 and 1036
Green (G)	Diode Laser	525	553	57.48	9.62	Continuous Wave	5 and 10	86 and 172

Table 1: Laser parameters

$$mW/cm^2 = \frac{mW}{\pi \times r^2}$$

$$W/cm^2 = \frac{mW/cm^2}{1000}$$

(1)

$$Time\ (s) = \frac{J/cm^2}{W/cm^2}$$

Equation 1: Laser irradiation time. Where mW/cm2 is the power density, W/cm2 is the intensity, and s is the exposure time.

3. Conclusion

The optimal seeding density will be used to create the best possible culture conditions for future experiments using TrueGel3D-hydrogel plates. This translates to the collection of more reliable data, culture efficiency in future experiments, possible cost reduction and adds to the standardisation of PBM protocols.

References

1.   Mastrolia I, Foppiani EM, Murgia A, Candini O, Samarelli AV, Grisendi G, et al. Challenges in clinical development of mesenchymal stromal/stem cells: concise review. Stem cells translational medicine. 2019;8(11):1135-48.
2.   Yin Q, Xu N, Xu D, Dong M, Shi X, Wang Y, et al. Comparison of senescence-related changes between three-and two-dimensional cultured adipose-derived mesenchymal stem cells. Stem Cell Research & Therapy. 2020;11(1):1-12.
3.   Chang S-Y, Carpena NT, Kang BJ, Lee MY. Effects of photobiomodulation on stem cells important for regenerative medicine. Medical Lasers; Engineering, Basic Research, and Clinical Application. 2020;9(2):134-41.
4.   Lam D, Enright HA, Peters SK, Moya ML, Soscia DA, Cadena J, et al. Optimizing cell encapsulation condition in ECM-Collagen I hydrogels to support 3D neuronal cultures. Journal of neuroscience methods. 2020;329:108460.
5.   Lode A, Bernhardt A, Gelinsky M. Cultivation of human bone marrow stromal cells on three-dimensional scaffolds of mineralized collagen: influence of seeding density on colonization, proliferation and osteogenic differentiation. Journal of tissue engineering and regenerative medicine. 2008;2(7):400-7.
6.   Wang Y, Huang Y-Y, Wang Y, Lyu P, Hamblin MR. Red (660 nm) or near-infrared (810 nm) photobiomodulation stimulates, while blue (415 nm), green (540 nm) light inhibits proliferation in human adipose-derived stem cells. Scientific reports. 2017;7(1):7781.

Synthesis of Graphene Oxide-Gold Nanorods Nanocomposite-Porphyrin Conjugate for Improved Dual Cancer Phototherapy Performance

Thabang Calvin Lebepe[1, 2*] and Oluwatobi Samuel Oluwafemi[1, 2]

[1.] *Department of Chemical Science, University of Johannesburg, Johannesburg, 2028, South Africa.*

[2.] *Centre for Nanomaterials Sciences Research, University of Johannesburg, Johannesburg, 2028, South Africa*

*E-mail: calvyn.tl@gmail.com

1. Introduction

The mortality rate caused by cancer is increasing yearly [1], and the current conventional cancer treatments are known for many side effects, leading to patients' scarring and drug resistance [2, 3]. Therefore, finding a new therapeutic agent or modifying the existing therapeutic agents is imperative for better performance and efficiency. Phototherapeutic treatments such as photothermal and photodynamic have shown to be non-invasive, highly comprehensive, and precise with low side effects. Here in, we report the synthesis and characterisation of an improved synergetic phototherapeutic agent based on the combination of photothermal and photodynamic therapy. The phototherapeutic agent consists of cationic porphyrin (5,10,15,20-tetrakis(N-methyl pyridinium-3-yl)porphyrin, TMePyP) and gold nanorods (AuNRs) anchored on graphene oxide (GO) sheet.

2. Experimental

The TMePyP (water-soluble cationic porphyrin) was synthesised by the Adler-Longo method and followed by methylation. The structural and optical properties of TMePyP were confirmed using UV-Vis, zeta analyser, PL, FTIR, and NMR. While GO and AuNRs were synthesised using Hummer's and seed-mediated methods. The GO was modified with polyvidone to stabilise AuNRs during the incorporation. Lastly, TMePyP was anchored on GO@AuNRs to form GO@AuNRs-TMePyP nanocomposite. The as-synthesis were tested for stability in different pH solutions, stability in culture medium and cytotoxicity.

3. Results

The as-synthesised AuNRs absorbed at 850 nm, with a size average of 36.60 nm and a width of 5.96 nm. TEM image and Zeta potential charge confirmed the incorporation of AuNRs on the GO sheet. The GO-incorporated AuNRs (GO@AuNRs) showed improved photothermal profiling of AuNRs when irradiated with a laser. GO@AuNRs showed high photothermal efficacy than bare AuNRs and GO with excellent ON and OFF photothermal cycles. The TMePyP was then anchored on the surface of GO@AuNRs. The GO@AuNRs-TMePyP exhibits good stability in both culture media (RPMI and PBS) and at different pH solutions (4, 7 and 10). The singlet oxygen production of GO@AuNRs-TMePyP increased when compared to TMePyP, with a quicker release reaction rate of 0.056 min^{-1}. The cytotoxicity of GO, AuNRs, and TMePyP evaluated against Mouse bladder tumour line-2 (MBT-2) cancer cell lines using MTT assay showed that GO@AuNRs-TMePyP was more biocompatible and less light-sensitive than bare TMePyP even at a high concentration of 100 μg/mL. These results indicated that the as-synthesised nanocomposite is a promising dual photodynamic and photothermal agent for cancer therapy.

4. Conclusion

In summary, a synergistic phototherapeutic agent was prepared with enhanced thermal and colloidal stability and photothermal and photodynamic properties, and it will be of prodigious interest for many plasmonic and biomedical applications, especially in photothermal cancer treatment.

References

[1] World Health Organization, WHO report on cancer: setting priorities, investing wisely and providing care for all 2020. https://apps. who. int/iris/handle/10665/330745. License: CC BY-NC-SA. (Accessed May, 05 2021).

[2] H. Sung, et al., Global cancer statistics 2020: GLOBOCAN estimates of incidence and mortality worldwide for 36 cancers in 185 countries, CA Cancer J. Clin. 71(3) (2021).https://doi.org/10.3322/caac.21660

[3] T.C. Lebepe, et al., Graphene Oxide-Gold Nanorods Nanocomposite-Porphyrin Conjugate as Promising Tool for Cancer Phototherapy Performance, Pharmaceuticals 14(12) (2021) 1295

Comparative study of tetrapyrrolic photosensitizer mediated phototherapy against breast cancer cell subtypes

Paromita Sarbadhikary[1]*, Blassan P. George[1], Heidi Abrahamse[1]

[1] *Laser Research Centre, Faculty of Health Sciences, University of Johannesburg, P.O. Box 1701, Doornfontein 2028, South Africa*

*E-mail: paromitas@uj.ac.za

1. Background

Photodynamic therapy (PDT) presents a potential role as an alternative modality to treat breast cancer in comparison to conventional therapies. PDT works by exposing a photosensitizer (PS), a photoactivable drug, to red or near-infrared light. This causes multitude of reactive oxygen species (ROS) to be produced in the tumor mass, which causes tumor mass damage [1]. Naturally derived tetrapyrrolic structure-based PSs are found to be efficient *in vivo* PDT agent [2]. One such tetrapyrrole PS is pheophorbide-a, a plant-derived chlorophyll metabolite, which have excellent photophysical properties, preferential tumor accumulation, and relatively less biological harmfulness [3]. One of the most widely used treatment strategies against breast cancer is Doxorubicin, which is a Food and Drug Administration (FDA) approved chemotherapeutic agent. However, it has been reported that because of the consistent use of Doxorubicin, P-glycoprotein expression is stimulated in breast cancer cells, further mediating chemoresistance [4]. A number of studies have shown effectiveness of PDT against a number of chemoresistant cancer cells [5]. This study uses PDT at 660 nm light irradiation to investigate the *in vitro* anticancer efficacy of pheophorbide-a against wildtype breast cancer MCF-7 cells and Doxorubicin treated MCF-7 (MCF-7/DOX) cells.

2. Results

Both the breast cancer cell types were treated with different concentrations of pheophorbide-a for 3 h in dark, followed by irradiation at 1 J/cm^2 using BioTHOR 660 (±20 nm) LED Plate Illuminator at a power output of 7.08 mW/cm^2. Cell viability analysis 24 h post irradiation determined using MTT (3-[4,5-dimethylthiazol-2-yl]-2,5 diphenyl tetrazolium bromide) assay showed MCF-7/DOX were more resistant to pheophorbide-a mediated PDT. As shown in Figure 1(a) ~90% loss in cell viability was observed in wildtype MCF-7 at a concentration of 1.6 μM, while 2.4 μM concentration of pheophorbide-a was required to induce 90% cell death in MCF-7/DOX cells.
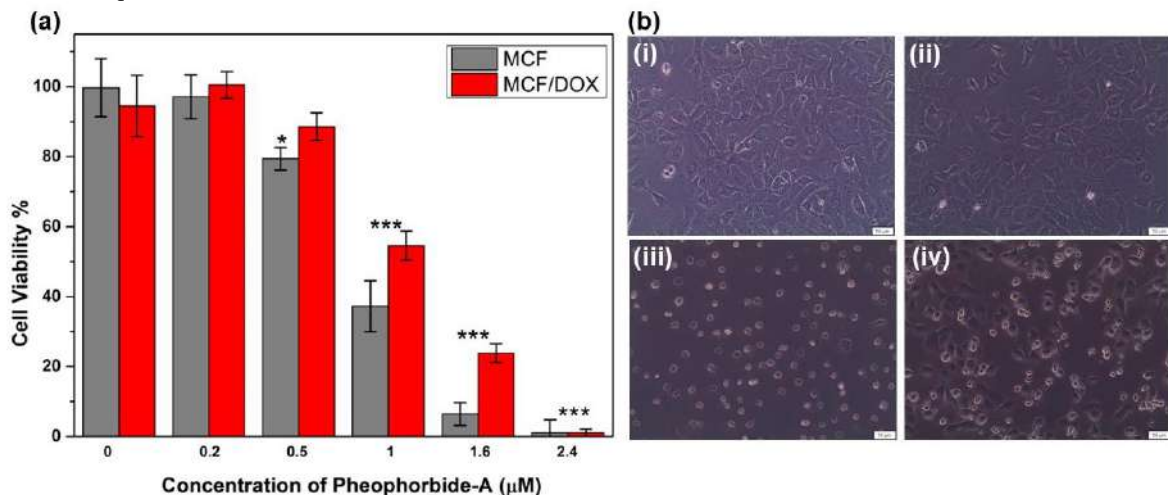
Figure 1 (a) Concentration dependent phototoxicity induced by pheophorbide-a in wild type MCF7 and MCF-7/DOX cells irradiated with 1 J/cm^2 at 660nm. ($p < 0.001$***). (b) Cellular Morphology of untreated (i) wild type MCF-7, (ii) MCF-7/DOX, and 24 h post PDT treatment in (iii) wild type MCF-7, (iv) MCF-7/DOX resistant cells with 1.6 μM of pheophorbide-a at light dose of 1 J/cm^2 at 660nm. (200x Magnification).

The morphological changes in wild type MCF-7 and MCF-7/DOX cells after PDT is shown in Figure 1(b). The cells in untreated group appear healthy with intact cell membrane. While the cells treated with

1.6 µM pheophorbide-a PDT showed drastic morphological changes with severe cellular and cell membrane damage. The damage was more significant in wild type MCF-7 with almost all cells showing cell death. However, in the case of MCF-7/DOX the effect seems to be moderately cytotoxic as almost 30-40% cells are showing viable morphology.

All these results suggested, pheophorbide-a induces effective photodynamic activity against MCF-7/DOX but at higher concentrations compared to the wild type MCF-7 cells. Thus, as per our preliminary results, pheophorbide-a is an effective PDT agent against chemotherapeutic drug treated or multidrug resistant breast cancer cell in comparison to other reported PSs [6–9].

3. Conclusions

In conclusion, plant derived chlorophyll derivatives can be a promising candidate for effective PDT, as an alternative treatment option for drug resistant carcinomas. However, more study is required to identify the precise cell death signaling pathway induced by pheophorbide-a mediated PDT and to provide mechanistic insights at protein, gene, and transcriptome levels.

References

1. Ostańska, E.; Aebisher, D.; Bartusik-Aebisher, D. The Potential of Photodynamic Therapy in Current Breast Cancer Treatment Methodologies. *Biomedicine & Pharmacotherapy* **2021**, *137*, 111302, doi:10.1016/j.biopha.2021.111302.
2. Roeder, B. Tetrapyrroles: A Chemical Class of Potent Photosensitizers for the Photodynamic Treatment of Tumours. *Laser Med Sci* **1990**, *5*, 99–106, doi:10.1007/BF02031370.
3. Saide, A.; Lauritano, C.; Ianora, A. Pheophorbide a: State of the Art. *Mar Drugs* **2020**, *18*, 257, doi:10.3390/md18050257.
4. Mirzaei, S.; Gholami, M.H.; Hashemi, F.; Zabolian, A.; Farahani, M.V.; Hushmandi, K.; Zarrabi, A.; Goldman, A.; Ashrafizadeh, M.; Orive, G. Advances in Understanding the Role of P-Gp in Doxorubicin Resistance: Molecular Pathways, Therapeutic Strategies, and Prospects. *Drug Discovery Today* **2022**, *27*, 436–455, doi:10.1016/j.drudis.2021.09.020.
5. Spring, B.Q.; Rizvi, I.; Xu, N.; Hasan, T. The Role of Photodynamic Therapy in Overcoming Cancer Drug Resistance. *Photochem Photobiol Sci* **2015**, *14*, 1476–1491, doi:10.1039/c4pp00495g.
6. Teiten, M.H.; Bezdetnaya, L.; Merlin, J.L.; Bour-Dill, C.; Pauly, M.E.; Dicato, M.; Guillemin, F. Effect of Meta-Tetra(Hydroxyphenyl)Chlorin (MTHPC)-Mediated Photodynamic Therapy on Sensitive and Multidrug-Resistant Human Breast Cancer Cells. *J Photochem Photobiol B* **2001**, *62*, 146–152, doi:10.1016/s1011-1344(01)00178-6.
7. Capella, M.A.M.; Capella, L.S. A Light in Multidrug Resistance: Photodynamic Treatment of Multidrug-Resistant Tumors. *J Biomed Sci* **2003**, *10*, 361–366, doi:10.1007/BF02256427.
8. Tsai, T.; Hong, R.-L.; Tsai, J.-C.; Lou, P.-J.; Ling, I.-F.; Chen, C.-T. Effect of 5-Aminolevulinic Acid-Mediated Photodynamic Therapy on MCF-7 and MCF-7/ADR Cells. *Lasers Surg Med* **2004**, *34*, 62–72, doi:10.1002/lsm.10246.
9. Chekwube, A.E.; George, B.; Abrahamse, H. Phototoxic Effectiveness of Zinc Phthalocyanine Tetrasulfonic Acid on MCF-7 Cells with Overexpressed P-Glycoprotein. *Journal of Photochemistry and Photobiology B: Biology* **2020**, *204*, 111811, doi:10.1016/j.jphotobiol.2020.111811.

Curcumin-loaded solid lipid nanoparticles mediated photodynamic therapy-induced apoptosis in human lung cancer cells

J.P. Jose Merlin[1]*, Anine Crous[1], Heidi Abrahmse[1]

[1]*Laser Research Centre, University of Johannesburg, Doornfontein Campus, Johannesburg, South Africa.*

*E-mail: jjayaraj@uj.ac.za

1. Abstract

Cancer is a major public health concern around the world, with significant fatality rates. Cancer research is now being progressed through determining the cause of cancer, chemoprevention, diagnosis and therapy, and patient survival [1]. The study's major goal is to create curcumin-loaded solid lipid nanoparticles that could operate as a photosensitizing agent to cause apoptosis in cancer cells. Ample literature evidence suggests that flavonoids, such as curcumin, can act as effective photosensitizers when integrated into solid lipid nanoparticles [2]. Photodynamic therapy (PDT) is a type of cancer treatment that has fewer adverse effects than chemo and radiotherapy [3]. Nanoparticle drug delivery systems are a novel approach to enhancing treatment outcomes while minimizing side effects and successfully killing treatment-resistant cancer cells [4]. The advancement of cancer therapies will result in a shift from conventional therapy to precision medicine [5]. Cancer is the main cause of death in South Africa, accounting for roughly 10% of all deaths. One in every fifty South Africans will develop cancer during their lifetime, and one in every hundred will die because of cancer. Controlling cancer using curcumin-loaded solid lipid nanoparticle-mediated PDT could aid in minimizing the growing strain on our healthcare system and ensuring South Africa's future economic prosperity.

2. Methodology

PDT-induced apoptosis caused by curcumin-loaded solid lipid nanoparticles in human lung cancer cell lines by achieving the following goals: Synthesis and characterisation of curcumin-loaded solid lipid nanoparticles, the effects of PDT- curcumin-loaded solid lipid nanoparticles on cell survival, cytotoxicity, cell proliferation, cellular morphological changes, DNA damage, apoptosis, biochemical investigations, and molecular alterations in cancer cells were used to investigate the dose-dependent impact and phototoxicity of curcumin-loaded solid lipid nanoparticles. This study will help to clarify how PDT in curcumin-loaded SLNs can operate as a photosensitizing agent to trigger programmed cell death in cancer cells.

3. Figures and tables

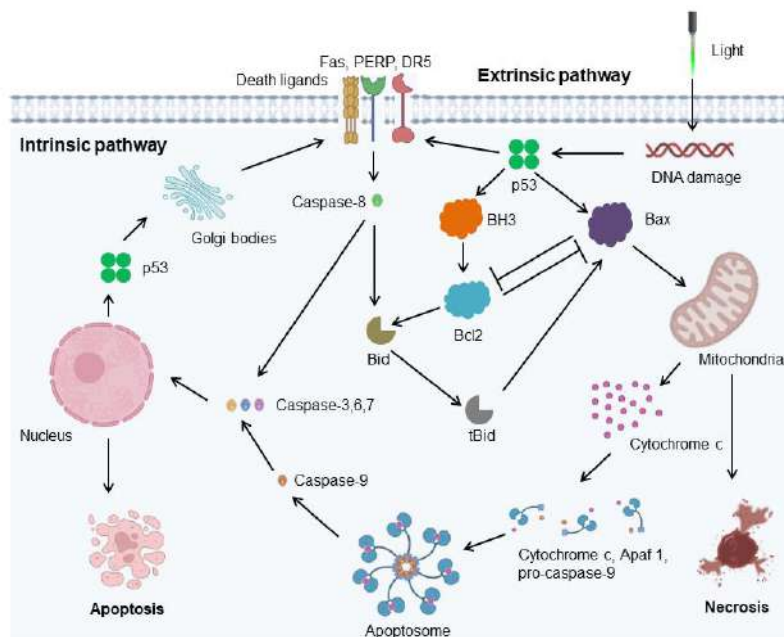| Light Source	Wavelength (nm)	Power Output (mW)	Power Density (mW/cm^2)	Area (cm^2)	Emission	Fluence (J/cm^2)	Time of irradiation (s)
Diode Laser	405, 470	515	53.53	9.62	Continuous Wave	5, 10, 15	93, 186, 279

Table 1 Laser parameters.

Figure 1 Cell death mechanism of PDT.

4. Conclusions

A switch from traditional therapy to precision medicine will be brought about by the development of cancer therapies. Therefore, curcumin-loaded solid lipid nanoparticle-mediated PDT for the treatment of cancer may help to lessen the increasing burden on our healthcare system and ensure the future economic success of South Africa.

References

[1] J.P.J. Merlin, S. Mathavarajah, G. Dellaire, K.P.J. Murphy, H.P.V. Rupasinghe, "A dietary antioxidant formulation ameliorates DNA damage caused by γ-Irradiation in normal human bronchial epithelial cells *in vitro*", Antioxidants. 11, 1407 (2022).

[2] S. Yeo, M.J. Kim, Y.K. Shim, I. Yoon, W.K. Lee, "Solid lipid nanoparticles of curcumin designed for enhanced bioavailability and anticancer efficiency", ACS Omega. 7, 35875-35884 (2022).

[3] K. Tryfonidis, D. Zardavas, B.S. Katzenellenbogen, M. Piccart M, "Endocrine treatment in breast cancer: Cure, resistance and beyond", Cancer Treat. Rev. 50, 68–81 (2016).

[4] Y.X. Wang, J.M. Idee, "A comprehensive literatures update of clinical researches of superparamagnetic resonance iron oxide nanoparticles for magnetic resonance imaging", Quant. Imaging. Med. Surg. 7, 88-122 (2017).

[5] P. Krzyszczyk, A. Acevedo, E.J. Davidoff, et al, "The growing role of precision and personalized medicine for cancer treatment", Technology (Singap. World Sci.). 6, 79-100 (2019).

WiFoO: Democratizing Long-Range Free Space Optics Using 802.11 Over Optical

Mikaeel Dindar [1*], Mitchell A. Cox[1]

[1]*School of Electrical and Information Engineering, University of the Witwatersrand, Johannesburg, South Africa*

*e-mail: `hello@mikaeel.io`

Free space optical (FSO) communication has tremendous potential to aid in the connection of low-income communities lacking last-mile infrastructure. FSO systems can provide this last-mile connectivity with much lower capital expenditure than traditional wired networks [1]. They also have advantages over regular RF-based wireless systems, which suffer from spectrum licensing concerns. Thus, a niche exists for low-cost, short-medium range FSO systems where performance can be sacrificed in favor of availability and reliability.

However, traditional FSO systems are expensive, and low-cost attempts make use of hardware that is not optimized for wireless operation such as SFP transceivers. WiFi (IEEE 802.11) is an RF-based consumer standard which has allowed for the proliferation of high-performance, wireless optimized networking at low-costs. WiFi systems make use of adaptive modulation, error correction and user transparent retransmission in order to maximize utilization of available channel capacity in noisy and congested RF environments. Adaptive modulation also prevents complete link failure by instead reducing throughput to suit channel conditions. Thus, an FSO system built using WiFi technology could benefit from all of these optimizations without a significant increase in cost.

We propose a system making use of RF over optical technology to transmit the RF signals generated by a WiFi system through an FSO channel. WiFi-modulated signals such as QAM have been demonstrated over FSO links [2], but this has not been done with a full WiFi system and as such, fails to benefit from the aforementioned optimizations of the full WiFi stack, such as adaptive modulation and error correction. We have developed a proof of concept for such a system using standard lab equipment and WiFi hardware provided by a partnering South African startup, this setup is shown in figure **1**. An RF mixer was used to shift the center frequency of the WiFi signal from 2.4GHz to 60MHz to remove the requirement for high frequency optical hardware and the frequency shifted signal was transmitted intensity modulation and direct detection.

Real-world testing was used to evaluate the demonstration system. The setup was powered by a battery and taken to an open field, with results shown in Fig. **2**. System performance is measured
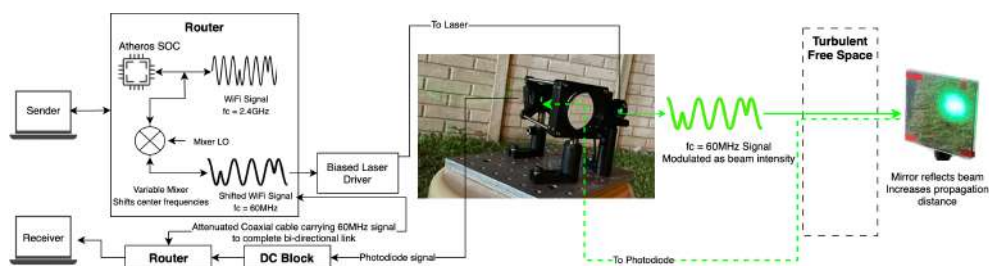
Figure 1: Block diagram of the demonstration system and its signal path. One direction of the link is completed optically while the other uses a cable. The size of the received beam at 580m is visible on the rear wall
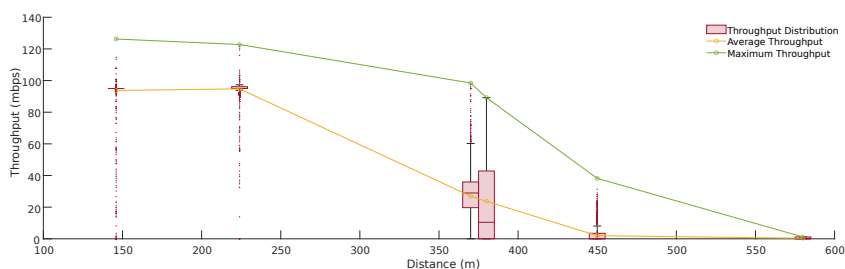
Figure 2: Average and maximum achieved throughput for various distances. The link only suffers a complete failure at distances above 600m

Figure 3: Components of new hardware version, extensive use of 3d-printed components, off-the-shelf electronics, and open-source hardware designs minimize costs.

using a modified version of the open-source utility iPerf which transmits a known UDP data stream across the link and records all packets, received and dropped, in order to determine the throughput and error rate.

Without extensive tuning, the link performed admirably, with a low-speed but functional link working at distances up to 580 m, averaging 1 Mbps, with more usable speed obtained at distances around 450 m, averaging 20 Mbps. At distances under 300 m, the system has little trouble providing performance at full speed.

In this way,we have demonstrated a novel WiFi-based FSO system that has the potential to be developed into an extremely low-cost FSO system shown in figure **3** that could bridge rural communities by providing an alternative for last-mile deployments. Our demonstrations of an extremely rudimentary, but fully functional system have shown strong link performance up to 300 m with a link maintained up to 600 m. We expect significantly better performance by simply increasing the transmit beam size slightly, and moving to a 75 mm receive aperture. Our approach offers significant advantages over conventional (and considerably more expensive) FSO systems that may otherwise exhibit total link failure on occasion.

References

[1] M. P. J. Lavery et al., "Tackling Africa's digital divide", *Nature Photon*, **12**, pp. 249–252 (2018).

[2] K. Kazaura et al., "Experimental evaluation of a radio-on-FSO communication system for multiple RF signal transmission", in *Free-Space Laser Communication Technologies XXI*, SPIE, Feb. 2009, pp. 46–57.

Synergistic anticancer effects of gold nanoparticle-herceptin-hypocrellin B conjugates in human breast cancer cells

Sheeja S. Rajan[1]*, Rahul Chandran[1], Heidi Abrahmse[1]

[1]*Laser Research Centre, University of Johannesburg, Doornfontein Campus,*

Johannesburg, South Africa.

*E-mail: srajan@uj.ac.za

Abstract

In recent years, the combination of nanotechnology and targeted photodynamic therapy has emerged as a promising approach to cancer treatment [1]. This study investigates the effect of gold nanoparticle-herceptin-hypocrellin B conjugates on breast cancer cells, with the aim to enhance therapeutic efficacy while minimizing adverse effects. Herceptin, a monoclonal antibody, specifically targets HER2 receptors overexpressed in certain breast cancer cells, making it an attractive candidate for targeted therapy. Hypocrellin B, a natural photosensitizer, has shown potential in photodynamic therapy (PDT) by generating cytotoxic reactive oxygen species upon light activation. Gold nanoparticles (AuNPs) serve as carriers for drug delivery, offering enhanced stability, biocompatibility, and the ability to encapsulate therapeutic agents [2]. NPs are used as carriers to load and precisely deliver these PSs and other auxiliary agents to the tumor locations, improving PSs accumulation in the tumor itself [3]. In this study, Herceptin and hypocrellin B were successfully conjugated to AuNPs, forming a multifunctional nanoconstruct. The effects of the conjugates were evaluated on HER2-positive breast cancer cells *in vitro*. Cellular uptake studies demonstrated efficient internalization of the nanoconjugates by cancer cells, confirming their potential as targeted drug delivery vehicles. Subsequent PDT studies showed increased cytotoxicity in cells treated with the nanoconjugates compared to free hypocrellin B, with minimal impact on non-cancerous cells. Furthermore, the induction of apoptosis was observed in breast cancer cells treated with nanoconjugates, as evidenced by morphological changes and DNA damage. The selectivity of Herceptin in guiding the nanoconjugates to HER2-positive cells played a vital role in achieving this outcome. This study highlights the promising potential of gold nanoparticle-herceptin-hypocrellin B conjugates as a targeted therapeutic approach for HER2-positive breast cancer. The combination of targeted therapy and photodynamic therapy in a single nanoconstruct offers a novel strategy to improve treatment efficacy while minimizing side effects in breast cancer management. Further, *in vivo* investigations and clinical studies are warranted to validate the translational potential of this nanoformulation for the breast cancer treatment.

The laser power output and exposure time for the irradiation experiments will be measured using the formula

$$\text{Irradiation time} = \frac{\text{Fluency (J/ cm}^2)}{\text{Power output (W/ cm}^2)}$$
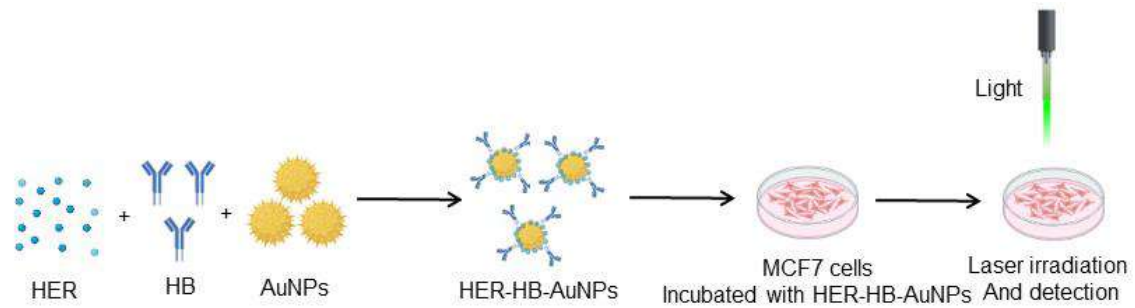
Figure 1 Synthesis of Her-HB-AuNPs and its anticancer effects: NPs are used as carriers to load and precisely deliver these PSs and other auxiliary agents to the tumor locations, improving PSs accumulation in the tumor itself.

Conclusions

The remarkable potential of gold nanoparticle-herceptin-hypocrellin B conjugates as a focused therapy strategy for HER2-positive breast cancer is highlighted by this study. The combination of nanotechnology and photodynamic therapy integrated into a unique nanoconstruct offers a revolutionary way to manage breast cancer while increasing treatment effectiveness and reducing adverse effects.

Acknowledgments

References

[1] G. Kah, R. Chandran, and H. Abrahamse, Curcumin a natural phenol and its therapeutic role in cancer and photodynamic therapy: A review", Pharmaceutics. 15(2), 639 (2023).

[2] A. Crous and H. Abrahamse, "Effective Gold nanoparticle-antibody-mediated drug delivery for photodynamic therapy of lung cancer stem cells", Int. J. Mol. Sci. 21, 3742 (2020).

[3] J. Li, S. Wang, F. Fontana, C. Tapeinos, M-A. Shahbazi, H. Han, and H.A. Santos, "Nanoparticles-based phototherapy systems for cancer treatment: current status and clinical potential", Bioact. Mater. 23, 471-507 (2023).

Photobiomodulation for enhanced neural embryoid body formation of Stem cells.

Precious Earldom Mulaudzi[1], Heidi Abrahamse[1] and Anine Crous[1*]

[1]Laser Research Centre, Faculty of Health Sciences, University of Johannesburg, P.O. Box 17011, Doornfontein, Johannesburg, South Africa, 2028

[*]E-mail: acrous@uj.ac.za

1. Introduction

Embryoid bodies are three dimensional aggregates that are derived from pluripotent stem cells [1]. Embryoid bodies formation is an important step in direct differentiation of undifferentiated stem cells into specific cell types [2]. Adipose-derived stem cells (ADSCs) have been identified as ideal candidates in embryoid generation. This is mainly because they can be manipulated to transdifferentiate into neural cells [3]. Photobiomodulation has attracted global interest as it can be used to increase ADSCs proliferation and differentiation [4]. Photobiomodulation has been found to increase intracellular activities, enhance cell proliferation, and support stem cell differentiation while using low intensity light [5].

2. Methodology

This *in vitro* study (Figure 1) aims to differentiate adipose-derived stem cells into neural embryoid bodies with the use of neuronal differentiation inducers to determine differentiation effectiveness and PBM at a near-infrared (NIR) wavelength of 825nm at fluences of 3 and 5 J/cm^2 were investigated to determine the rate of proliferation. Specific laser parameters applied are represented in Table 1 and calculation of irradiation time was determined using formula in Equation 1. Cells were characterized with flow cytometry using stem cell markers and early neuronal markers. Cell morphology was and biochemical assay was performed to observe proliferation, cytotoxicity and viability.
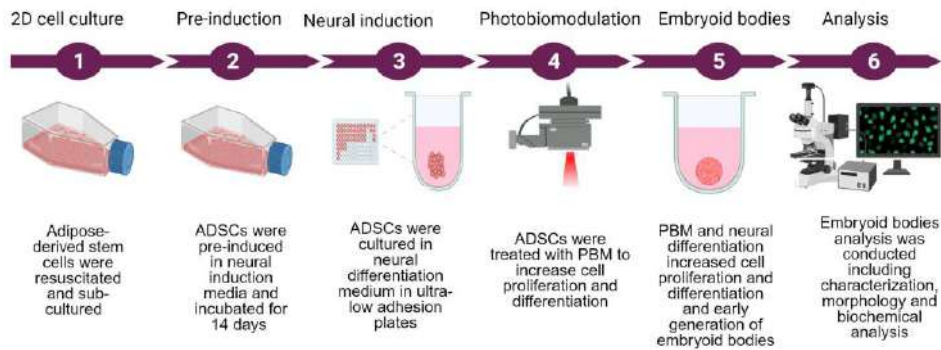
Figure 1 The combined use of neural induction differentiation inducers and photobiomodulation improved both the proliferation and differentiation potential of ADSCs into embryoid bodies.

	Near infra-red (NIR)
Light Source	Diode Laser
Wavelength (nm)	825
Power Output (mW)	515
Power Density (mW/cm2)	53.53
Area (cm2)	9.62
Emission	Continuous Wave
Fluence (J/cm2)	3 and 5
Time of Irradiation (s)	56 and 93

Table 1 Laser Parameters

$$mW/cm^2 = \frac{mW}{\pi \times (r^2)}$$

$$W/cm^2 = \frac{mW/cm^2}{1000}$$

$$Time\ (s) = \frac{J/cm^2}{W/cm^2}$$

Equation 1 Laser irradiation time.

mW/cm^2 is the power density, W/cm^2 is the intensity, and s is the exposure time.

3. Conclusion

Photobiomodulation and neural differentiation inducers increased ADSC proliferation and differentiation into neural embyoid bodiesat 5 J/cm^2. This study was *in vitro*, thus more research and clinical trials are needed to confirm this therapy's efficacy and safety in people. This study improves our understanding of stem cell-based therapies and PBM for neurogenesis.

Acknowledgments

References

[1]   G. Pettinato, X. Wen, and N. Zhang, "Formation of Well-defined Embryoid Bodies from Dissociated Human Induced Pluripotent Stem Cells using Microfabricated Cell-repellent Microwell Arrays," Scientific Reports , vol. 4, no. 1, pp. 1–11, Dec. 2014, doi: 10.1038/srep07402.

[2]   J. M. Brickman and P. Serup, "Properties of embryoid bodies," Wiley Interdiscip Rev Dev Biol, vol. 6, no. 2, p. e259, Mar. 2017, doi: 10.1002/WDEV.259.

[3]   L. Luo, D. H. Hu, J. Q. Yin, and R. X. Xu, "Molecular mechanisms of transdifferentiation of adipose-derived stem cells into neural cells: Current status and perspectives," Stem Cells International, vol. 2018, no. 1. Hindawi Limited, pp. 1–14, 2018. doi: 10.1155/2018/5630802.

[4]   P. Bikmulina et al., "Photobiomodulation in 3D tissue engineering," J Biomed Opt, vol. 27, no. 09, pp. 0909011-090901-1–24, Sep. 2022, doi: 10.1117/1.jbo.27.9.090901.

[5]   D. Da Silva, A. Crous, and H. Abrahamse, "Photobiomodulation: An effective approach to enhance proliferation and differentiation of adipose-derived stem cells into osteoblasts," Stem Cells Int, vol. 2021, no. 1, pp. 1–13, 2021, doi: 10.1155/2021/8843179.

Ag-H$_2$O Nanofluids Synthesized via Pulsed Laser Liquid-Solid Interaction for Enhanced Photonics Integrated Circuit Cooling.

Snenkosi Dlamini[1-2], M. Akbari[1-2], Adebisi[3], Balla[3], L.Gaza[-2], M. Moodley[3], M. Maaza[1-2],

[1]UNESCO-UNISA Africa Chair in Nanosciences-Nanotechnology, College of Graduate Studies, University of South Africa, Muckleneuk ridge, PO Box 392, Pretoria, South Africa

[2]Nanosciences African Network (NANOAFNET), Materials Research Dept., iThemba LABS-National Research Foundation of South Africa, 1 Old Faure Road, Somerset West, Western Cape 7129, PO Box 722, South Africa

[3]School of Physics & Chemistry, University of Kwazulu-Natal,Westville, Durban- South Africa

Corresponding Presenter: *Snenkosi Dlamini

*Email: swthegreat@gmail.com or 48443824@unisa.ac.za

Abstract:

The relentless advancement of our ICT-driven society has fueled an unprecedented demand for efficient cooling solutions in nanoelectronics, data storage centers, and solar energy technologies. In response to this pressing need, nanofluids have emerged as a promising technology, offering potential solutions for effectively dissipating the generated heat. Among these, Ag-H$_2$O nanofluids hold promise due to their tailored properties and potential for enhanced thermal performance. Photonics Integrated Circuits (PICs) are pivotal components in contemporary optical communications, presenting unique challenges in thermal control and packaging. Laser arrays, integral to PICs, operate within tight temperature limits and require sub-ambient temperatures to maintain performance while facing moderate heat loads and high device-level heat fluxes. Efficient cooling solutions are paramount to unlock the full potential of PICs in optical communication systems. This contribution focuses on the thermal enhancement achieved by nanoparticles dispersed in base fluids and investigates the impact of nanoparticle concentration on the contact angle and stability of Ag-H$_2$O nanofluids. Pulsed Laser Liquid-Solid Interaction is employed for the precise engineering of these nanofluids, tailoring their properties for optimal thermal conductivity. To gain comprehensive insights into the physical properties, we conducted several studies, encompassing optical, morphological, and contact angle investigations. Additionally, we examined the influence of different concentratios on the stability and thermal conductivity of the nanofluids.

Keywords: Nanoelectronics, Nanofluids, Thermal enhancement, Nanoparticles, Base fluids, Contact angle, Pulsed Laser Liquid-Solid Interaction, Thermal conductivity, Optical properties, Morphological investigations.

The UV-VIS spectrum of conjugated metal nanoparticles with some purposed COVID-19 drugs: a DFT study

Razieh Morad[*1,2], Mahmood Akbari[1,2] and Malik Maaza[1,2]

[1]*UNESCO-UNISA Africa Chair in Nanoscience and Nanotechnology (U2ACN2), College of Graduate Studies, University of South Africa (UNISA), Pretoria, South Africa*

[2]*Material Research Division, Nanoscience African Network (NANOAFNET), iThemba LABS-National Research Foundation, Somerset West 7129, South Africa.*

[*]E-mail: rmorad@tlabs.ac.za

Spectra calculations hold a crucial position within theoretical modeling, benefiting from remarkable advancements in high-level computational techniques. These calculated spectra not only find direct application but also aid in rectifying potential errors in experimental observations. Additionally, theoretical computations play a significant role in assisting with experimental assignments.

The absorption UV–Vis spectrum of metal nanoparticles, both in their bare form and when coated with different compounds, serves as vital evidence to compare with experimental results. This spectrum offers valuable insights into how adsorbent molecules influence the electronic structures of NPs. Similarly, noble metal nanoparticles are also recognized for their intense plasmonic absorption spectra in the UV–Vis range, which can be modulated by coating them with various drugs or compounds. By studying the variations in the absorption spectra of coated silver and gold nanoparticles, researchers can gain a deeper understanding of their optical properties and explore potential applications in drug delivery, sensing, and other areas of nanotechnology.

Here, we examined the interactions between some proposed drugs for COVID-19 such as HCQ (Hydroxychloroquine) and icosahedral silver and gold clusters. The investigations were carried out using the PBE-D3/TZP level of theory, considering the influence of relativistic effects (ZORA). To understand how drug molecules affect the electronic structures and plasmonic absorption spectra of noble metal particles, we employed the recently developed TD-DFT + TB method. This method combines a full DFT ground state with tight-binding approximations. Excited states calculations were performed at optimized geometries using the asymptotically corrected LB94 xc-functional, and the absorption spectra were obtained within the energy range of 0.0–6.0 eV. All these calculations were executed using the Amsterdam Density Functional (ADF2019.1) program.

As depicted in Figure 1, the plasmonic spectrum of the AgNP-HCQ complex showed minimal changes compared to bare AgNP, with only a slight dampening of the intensity of peaks around 5.5 eV. In contrast, for the AuNP-HCQ complex, the adsorption of HCQ resulted in a noticeable alteration in the plasmonic peak of gold within the 4.0–4.5 eV range. The high-intensity peak exhibited a blue shift, indicating a more pronounced perturbative effect of HCQ adsorption on the electronic structure and plasmonic spectrum of AuNP when compared to AgNP.
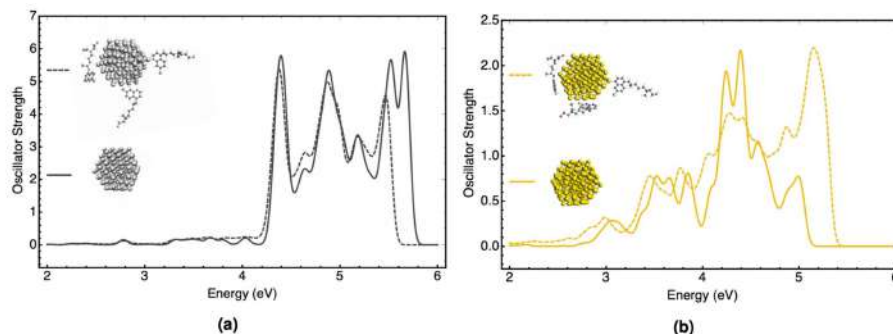
Figure 1 Comparison of the plasmonic absorption spectra of bare (solid line) and complexed (dash line) for **(a)** AgNP-HCQ and **(b)** AuNP-HCQ at the TD-DFT + TB level of theory. Spectra have been broadened with a σ = 0.1 eV Gaussian.

Nanofluid by pulsed laser ablation in liquid: Parameter influence

M. Aligholami [1,2*], M. Akbari[1,2], M. Maaza[1,2]

[1]*UNESCO−UNISA Africa Chair in Nanoscience & Nanotechnology Laboratories (U2AC2N), College of Graduate Studies, University of South Africa (UNISA), Muckleneuk Ridge, PO Box 392, Pretoria, 0003, South Africa*

[2]*Nanosciences African Network (NANOAFNET), iThemba LABS−National Research Foundation, PO Box 722, Somerset West 7129, Western Cape Province, South Africa*

*E-mail: agh.meisam@gmail.com;
18039545@mylife.unisa.ac.za

Abstract

Pulsed laser ablation in liquid, PLAL, with 1064 nm wavelength laser is used to ablate metal target in aqueous and non-aqueous host fluids to synthesize nanofluid, a homogenous colloidal suspension. In this regard an experimental investigation is carried out to discuss the influence of PLAL parameters, such as ablation time, in the synthesized nanofluids properties. Different intensity of the absorption extracted from UV-Vis spectroscopy confirmed the formation and suspension of metal nanoparticles in the host fluids. Energy dispersive spectroscopy (EDS) and transmission electron microscopy (TEM) were done. The morphological characterizations reflected that the nanoparticles seem to be homogeneous. The size distribution analysis was done accordingly.

1. Introduction

Energy transport is one of the main challenges in the engineering sector which can be addressed by the enhancement of working fluid and technological domain. Conventional working fluids such as water, oil, etc. has not enough potential to transfer heat due to their lower thermal conductivity. However, metals such as copper in particular has higher thermal conductivity. So, uniform suspension of metal nanoparticles in a host fluid would be a great solution for modification of properties of conventional working fluids. There are several techniques for creating metallic nanoparticle-based nanofluids. As an alternative technique for creating nanoparticle-based nanofluids, pulsed laser ablation of solid materials in liquids demonstrated great promise in this method. The benefit of this technique is due to the combination of two primary effects, namely, the conventional ablation and the acoustic processes. The interaction between the matter and the incident laser attribute to the ablation process while the explosion of the native gas bubbles which is take place as a result of local overheating at the interface of matter-liquid interface. As represented in Fig. 1, several phenomena occurred during irradiation of the matter inside the liquid. Acoustic transient proceeded by thermoelastic expansion, which induces a bubbles' cavitation phenomenon. The energy absorption at the target-liquid interface rises the temperature of the local water. Thermoelastic-stress waves is produced as a result of thermal expansion of the heated volume. The local overheat of the target and the dynamics of the vapor plume contributes to acoustic excitations which in turn underlay the explosion of gas bubbles contributing to the ablation at the surface of the melted target. It is worth to note that the size of synthesized nanoparticles affected by the bubbles nucleation rate and the implosion cycle. In this regard, Khamliche et al. produced copper nanoparticles-ethylene glycol (Cu-EG) based nanofluid by performing pulsed Nd:YAG laser ablation of copper target in ethylene glycol base fluid. The impact of the ablation time on the thermal conductivity performance of the Cu-EG nanofluid was investigated. It is reported that Cu-EG nanofluids formed after 5 min of ablation had a 15% improvement in the thermal conductivity at 318 K, whereas samples obtained after 30 min ablation had a 24% improvement in thermal conductivity [1]. Also, Several studies [2-4] focus on laser ablation in liquid approach, which is known as a green technique, to synthesize nanoparticles. It is noted that different parameters such as laser pulse wave length, laser time duration, pulse repetition rate, energy density, focusing condition, etc. influence size and shape of the nanoparticles which may affect its optical and thermophysical properties accordingly.

Thus, in this study PLAL approach is used for dispersion of metal nanoparticles inside distilled water and ethanol. The PLAL technology, as demonstrated, was applied in the current investigation and its

basic working principle involved a brief interaction (nanosecond regime) between a pulsed focused laser beam impinging on metal targets while they were submerged in DW and ethanol. The rotating target is subjected to pulses from the entering Nd-YAG laser beam which contributes to the creation of the clusters of the ablated materials. A glass beaker filled with 25 mL of host fluid and the metal target is placed inside the beaker, as shown in Fig 1. A pulsed Nd: YAG laser with an output energy of 80 mJ/pulse, a wavelength of 1064 nm, and a repetition rate of 10 HZ was utilized in the experiment. The ablation was done for different durations to ensure enough nanoparticle volume fraction.
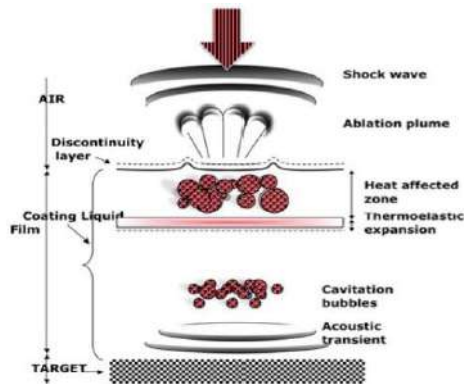

Fig. 1. Possible mechanisms causing the ablation in PLAL [5].

2. Conclusions

The present study aims to synthesize and characterize nanofluids via pulsed laser ablation in liquid method. To do so, metal target was ablated for different durations under the laser wave length of 1064 nm and laser energy of 80 mJ/pulse. Optical and morphological characterizations of the samples reflected the formation of uniform nanoparticles in distilled water and ethanol.

Acknowledgments

This section is not numbered.

References

[1] T. Khamliche, S. Khamlich, M.K. Moodley, B.M. Mothudi, M. Henini, M. Maaza, "Laser fabrication of Cu nanoparticles based nanofluid with enhanced thermal conductivity: Experimental and molecular dynamics studies", *Journal of Molecular Liquids*, Vol. 323, pp. 114975 (2021). *https://doi.org/10.1016/j.molliq.2020.114975*.

[2] Hameed Naser, M. A. Alghoul, Mohammad Kamal Hossain, Nilofar Asim, M. F. Abdullah, Mohammed Sabah Ali, Feras G. Alzubi, and N. Amin, "The role of laser ablation technique parameters in synthesis of nanoparticles from different target types", Journal of Nanoparticle Research, Vol. 21, pp. 249, 2019. *https://doi.org/10.1007/s11051-019-4690-3*.

[3] Amir Reza Sadrolhosseini, Suraya Abdul Rashid, Azmi Zakaria, and Kamyar Shameli, "Green fabrication of copper nanoparticles dispersed in walnut oil using laser ablation technique", Journal of Nanomaterials, Vol. 2016, 2016. *https://doi.org/10.1155/2016/8069685*.

[4] Amir Reza Sadrolhosseini and Ahmad Shukri bin Muhammad Noor, "Laser ablation synthesis and optical properties of copper nanoparticles", Journal of materials research, Vol. 8, pp. 2629-2636, 2013. *https://doi.org/10.1557/jmr.2013.244*.

[5] Mbambo, M.C., Khamlich, S., Khamliche, T. et al. "Remarkable thermal conductivity enhancement in Ag—decorated graphene nanocomposites based nanofluid by laser liquid solid interaction in ethylene glycol", Scientific Report, Vol. 10, pp. 10982, 2020. *https://doi.org/10.1038/s41598-020-67418-3*.

Surface Enhanced Raman Spectroscopy and SERS/Drop-Coating Deposition Raman as Feasible Mechanisms for Detecting Dopants in Complex Matrices

Moses Juma*[1,2,3], Zephania Birech[3], Nancy Mwenze[1,2,3], Simon Dhlamini[3] and Malik Maaza,[1,2]

[1]*UNESCO-UNISA-iTLABS/NRF Africa Chair in Nano-Sciences & Nanotechnology, CGS, University of South Africa, Muckleneuk ridge, Pretoria 0001, South Africa*

[2]*NANOAFNET, iThemba LABS-National Research Foundation of South Africa, 1 Old Faure Road, Cape Town 7129, Western Cape, South Africa*

[3]*Department of Physics, University of Nairobi, P.O Box 30197-00100, Nairobi, Kenya.*

Email: jmwabwire@gmail.com

Conventional Raman spectroscopy has, despite being used extensively in forensic analysis, limited capabilities when better sensitivities are required. This work leveraged on SERS and SERS/DCDR as feasible approaches that solve the limitations of conventional Raman spectroscopy. The two mechanisms have been used in the detection of Trenbolone acetate; a dopant prohibited by the World Anti-doping Agency (WADA) for its androgenic properties.

For SERS, silver nanoparticles were used to enhance the Raman spectra with an enhancement factor of X 16 even for sub-ppb dopant concentration. SERS benefited immensely from the electrical and chemical enhancement properties of silver nanoparticles achieving a remarkable enhancement factor. After SERS, a drop coating deposition was done by varying aliquot volumes that were drop coated on Aluminum foil to benefits from its hydrophilic nature. The work showed that a small aliquot volume (2μl) provided better signals after obtaining 30 average spectra from the edge of the formed coffee ring.

To elucidate the behavior of molecules during SERS and DCDR, a principal component analysis, (PCA) was done on the data collected using SERS and DCDR. The PCA showed that although DCDR provided a better signal enhancement, it suffers from hot

spots that require more spectra to be taken for each sample. For each sample, thirty spectra were taken from five (approximately equidistant) positions along the edge of the coffee ring to compensate for possible inhomogeneity during the air-drying process. On the contrary, only two spectra from each sample were taken during SERS showing the ease and efficiency of the method.

A univariate calibration curve drawn using both Raman approaches showed that it is possible to reduce the detection limit of trenbolone acetate, to the 2ppb-40ppb range recommended by WADA. Consequently, SERS and DCDR have been demonstrated as complementary Raman techniques which if effectively used can contribute to the anti-doping campaign.

Key Words: *Conventional Raman, Surface Enhanced Raman Spectroscopy (SERS), Drop-Coating Deposition Raman (DCDR).*

Silver-Based Nanostructured Surface-Enhanced Raman Spectroscopy Technique for Enhancing Dexamethasone Detection.

Nancy M. Mwenze[1,2,3*,] Zephania Birech[3], Moses Juma [1,2,3], M.S Dhlamini[1,2], Malik Maaza[1,2]

1UNESCO-UNISA Africa Chair in Nanoscience & Nanotechnology Laboratories (U2AC2N), College of Graduate Studies, University of South Africa (UNISA), Muckleneuk Ridge, P.O Box 392, Pretoria, 0003, South Africa
2Nanosciences African Network (NANOAFNET), iThemba LABS-National Research Foundation, P.O Box 722, Somerset West 7129, Western Cape Province, South Africa
3Laser Physics and Spectroscopy Research Group, Department of Physics, University of Nairobi, P.O Box 30197, Nairobi, Kenya

*Corresponding Presenter: *Nancy Mwikali Mwenze*
Email: nancydavid95@gmail.com

Abstract

Abuse and misuse of clinically approved drugs pose a threat to human health, thus, the need for a fast, sensitive, precise, and affordable analytical method to address the drawbacks of conventional techniques for monitoring drug levels. Recently, the surface-enhanced Raman spectroscopy (SERS) technique has emerged as a highly promising analytical tool for fast, sensitive, and specific detection of materials. This is primarily due to its potential for simplified sample preparation, significant signal amplification, and rapid identification of target analytes through distinctive SERS spectra. SERS detection technology possesses inherent advantages over normal Raman spectroscopy, particularly when dealing with complex environmental samples. The conventional Raman spectroscopy technique is limited by its inherent low sensitivity, making it challenging to detect low concentrations of analytes, and this work overcomes this limitation by exploiting the surface plasmon resonance of silver nanostructured metallic surface to amplify Raman signals significantly. This enables the detection of trace amounts of analytes, even down to the single-molecule level. By varying the ablation time in Laser Induced Breakdown Spectrometer (LIBS), we synthesized silver nanoparticles with controlled size and shape to optimize the SERS enhancement effect. Dexamethasone solutions of varying concentrations were prepared, and each concentration was conjugated with the silver nanoparticles. Spectra of the silver, dexamethasone, and conjugated dexamethasone with silver were acquired using a Raman spectrometer (EZRaman- N Portable analyzer system, Enwave Optronics, Inc.) equipped with a 785 nm laser. The spectra were compared highlighting the superior sensitivity and selectivity of SERS for dexamethasone detection, with an enhancement factor of 1.4. Our results demonstrate that compared to the conventional Raman spectroscopy, SERS offers several advantages for the detection of low concentrations of dexamethasone, including increased sensitivity, reduced background interference, improved signal-to-noise ratios, and thus enabling the detection of very low drug levels.

Keywords: SERS, Dexamethasone, Surface Plasmon Resonance, Silver Nanoparticles, LIBS

Biomimicry Highly reflecting material for radiative cooling

N. Botha[1-2], N. Numan[1-2], J.K.Cloete[1-2], B. Machabakacha[1-2], M. Akbari[1-2], R. Morad[1-2], I. Madiba[1-2], Z. Nuru[1-2,3], A. Gibaud [1-2,4], M. Henini [1-2,5], S. Berthier[1-2,6], J. Howell [1-2,7], M. Maaza[1-2]

[1]UNESCO-UNISA Africa Chair in Nanosciences-Nanotechnology, College of Graduate Studies, University of South Africa, Muckleneuk ridge, PO Box 392, Pretoria, South Africa [2]Nanosciences African Network (NANOAFNET), Materials Research Dept., iThemba LABS-National Research Foundation of South Africa, 1 Old Faure Road, Somerset West, Western Cape 7129, PO Box 722, South Africa. [3]Dept. Physics, Adigrat University, Adigrat-Ehiopia [4]IMMM, UMR 6283 CNRS, Bd O. Messiaen, 72085 Le Mans cedex 09, University of Le Maine, Le Mans-France [5]Physics & Astronomy Dept., Nottingham University, NG7 2RD7, UK. [6]Institut des NanoSciences de Paris (Pierre and Marie Curie Paris 6 University and CNRS, France. [7] Physics Dept., Hebrew University of Jerusalem, Israel

Email: bothanandipha9@gmail.com

Abstract

The extreme global warming caused by urban heat island effects, lead to a rapid increase in ambient temperature, unseen hikes in more cooling energy demands, severe indoor and outdoor heat-related human discomfort and elevated urban air pollutions. The rapid overheating of buildings is typically tackled by air-conditioning, heating, and ventilation (HVAC) systems, which accounts for more than half of the total building energy. Conventional HVAC systems rely heavily on vapour compression-based cooling technologies which consume massive fossil energy and emits huge amounts of greenhouse gases. Recently, a promising "sky window" cooling solution in the form of radiative cooling technology which can provide alternative "true" passive cooling for buildings has been highlighted [1,2]. In this study we focussed on the remarkable elevated diffuse reflectivity of naturally available white plant petal in the solar spectrum range and its low diffuse reflectivity in the Infrared. Such an elevated reflectivity was found to be of the order of ~94% comparable to that of standard high reflective materials including ZnO (~92%), TiO2 (~95%), and BaSO4 (~93%). Such a high & low diffuse reflectivity in the Visible & Infrared solar spectrum respectively seem to be correlated to the multi-scale structuring of this petal surface. The observed elevated & low reflectivity in the VIS & NIR spectral regions respectively sustain the bio-mimicking of such a petal's surface for potential radiative cooling applications.
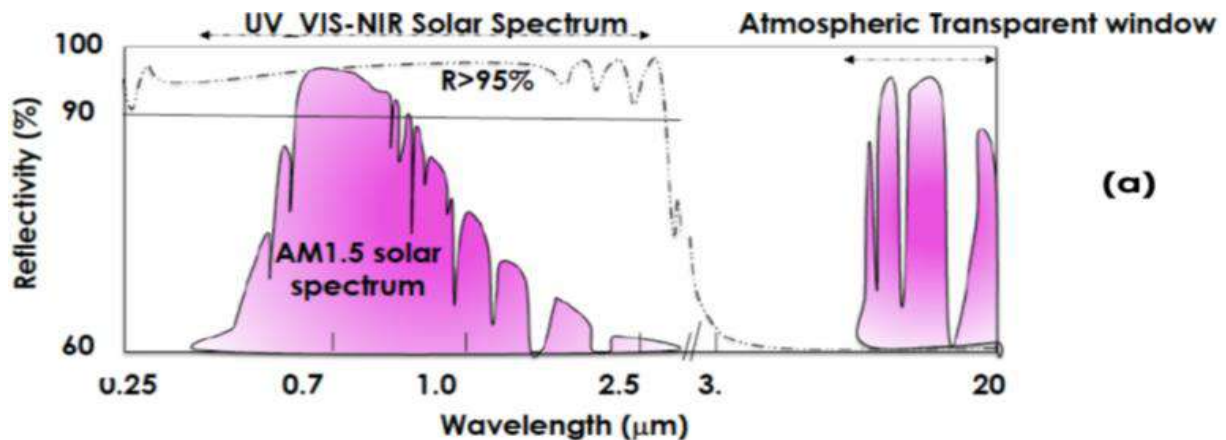
Fig 1. Schematic representation of an optical response of a quasi-ideal Radiative Cooling Material.

[1] Wenxin Li, Yanru Li, Kwok Wei Shah. Solar Energy. 207, 1 2020, 247-269.
[2] Bin Zhao, Mingke Hu, Xianze Ao, Nuo Chen, Gang Pei. Applied Energy. 236, 2019, 489-513.

Development and In-Orbit Calibration of the New-Generation Solar Irradiance Spectrometer

Changchun Institute of Optics, Fine Mechanics and Physics, Chinese Academy of Sciences, China

Authors: Yue Li, Hui Wang

Email: liyue@ciomp.ac.cn

wangh@ciomp.ac.cn

Abstract:

High-precision observation of solar spectral irradiance plays a crucial role in gaining insights into the physical characteristics and activities of the Sun, space weather forecasting, as well as studying Earth's climate and ecology. Within the Earth's atmosphere, solar radiation is absorbed and scattered, particularly in the ultraviolet wavelength range, making it challenging to obtain accurate solar spectral irradiance data. Space-based observations can overcome these atmospheric interferences, providing more precise and comprehensive solar radiation data. Therefore, spaceborne instruments hold a special position in the field of solar spectral irradiance observations. However, the design of space instruments faces numerous constraints, including weight, size, power consumption, and the consideration of thermal regulation. On-orbit calibration of the instrument also presents several challenges.

This paper introduces the Solar Irradiance Spectrometer onboard the Fengyun-3 (05) satellite. The paper describes the principles, structure, and electronic design of the spectrometer. Additionally, the on-orbit calibration approach and a long-term degradation correction method for the instrument are presented. The observation results of the Solar Irradiance Spectrometer demonstrate its excellent spectral resolution in the visible wavelength range, effectively reflecting the detailed structure of solar radiation spectra. Currently, the development of the Fengyun-3(10) Solar Irradiance Spectrometer is underway. After the launch of this satellite, the instrument will enable network observations and further enhance irradiance observation accuracy.

Short Bios:

Yue Li earned his Ph.D. degree from Jilin University in 2012. He is currently a deputy researcher at the Changchun Institute of Optics, Fine Mechanics and Physics, Chinese Academy of Sciences. Dr. Li has over a decade of experience in optical engineering and his team has developed numerous optical instruments for various space missions.

Hui Wang is the deputy director of the International Cooperation Department and also serves as an editor for the journal "Light Science and Application." She has led multiple international cooperation projects, demonstrating her extensive experience in international collaboration.